

***In vivo* role of RIPK1 in the regulation of the murine
intestinal epithelium**

Inaugural-Dissertation

zur

Erlangung des Doktorgrades

Der Mathematisch-Naturwissenschaftlichen Fakultät

der Universität zu Köln

vorgelegt von

Marius Volker Dannappel

aus Bergisch Gladbach

Köln, 2015

Berichterstatter: Prof. Dr. Manolis Pasparakis
Prof. Dr. Carien Niessen

Tag der mündlichen Prüfung: 02.12.2015

Zusammenfassung

Rezeptor-interagierendes Protein Kinase 1 (RIPK1) ist involviert in Signalkaskaden die Zelltod und Entzündungen regulieren. RIPK1 reguliert NF- κ B Aktivierung, interagiert mit RIPK3 um Nekroptose zu steuern und vermittelt Apoptose in einer RIPK1 Kinase Aktivität abhängigen Art und Weise. Das intestinale Epithel ist eine einzellige Schicht, die den luminalen Inhalt von sub-epithelien Immunzellen separiert. Um Gewebemöostase und die intestinale Barriereintegrität zu gewährleisten, muss der Zelltod von intestinalen Epithelzellen streng reguliert sein. Die *in vivo* Funktion von RIPK1 für die Regulierung von Zelltod und Homöostase in Epithelgewebe ist weitgehend unbekannt. Um die Funktion von RIPK1 im intestinalen Epithel zu studieren wurde das Cre-loxP System benutzt um Mäuse zu generieren, die defizitär für RIPK1 spezifisch in intestinalen Epithelzellen sind. Mäuse mit einer IEZ-spezifischen RIPK1 Deletion ($RIPK1^{IEZ-KO}$) zeigten erhöhte IEZ Apoptose begleitet von Villus Atrophie, Krypt Hyperproliferation und eine milde Entzündung im Kolon und Ileum, was zu einem frühzeitigem Tod innerhalb des ersten Lebensmonat führte. Die intestinal Pathologie war teilweise abhängig von TNFR1-vermittelter Signalübertragung aber entwickelte sich unabhängig von der Microbiota und der MyD88-abhängigen Signalübertragung. Epithelzellspezifische Deletion von FADD verhinderte IEZ Apoptose, aber $RIPK1^{IEZ-KO}/FADD^{IEZ-KO}$ Doppelknockout Mäuse zeigten IEZ Nekroptose und entwickelten Colitis ulcerosa. Zusätzliche Deletierung von RIPK3 verhinderte intestinale Entzündung und IEZ Nekroptose, was darauf hindeutet, dass IEZs in $RIPK1^{IEZ-KO}/FADD^{IEZ-KO}$ Mäusen durch RIPK1-unabhängige RIPK3-abhängige Nekroptose starben. Daher besitzt RIPK3-vermittelte Nekroptose in IEZs eine höhere Immunogenizität als FADD-vermittelte Apoptose. RIPK1-defizitäre IEZs zeigten den Abbau von den überlebensfördernden Proteinen TRAF2, cIAP1 und cFLIP, was direkt mit dem Tod von IEZs assoziiert sein könnte.

Zusammenfassend, die Ergebnisse in dieser Arbeit offenbaren eine neue gerüstartige Funktion von RIPK1 für die Regulation von intestinaler Homöostase durch die Verhinderung von FADD-vermittelter Apoptose.

Abstract

Receptor-interacting protein kinase 1 (RIPK1) is involved in signalling pathways regulating cell death and inflammation. RIPK1 regulates NF- κ B activation, interacts with RIPK3 to drive necroptosis and mediates apoptosis in a RIPK1 kinase activity dependent manner. The intestinal epithelium is a single cell layer that separates luminal microbes from sub-epithelial immune cells. To maintain tissue homeostasis and sustain an intact intestinal barrier, cell death of intestinal epithelial cells must be tightly regulated. The *in vivo* role of RIPK1 in regulating epithelial tissue homeostasis and cell death remains largely unknown. To study the function of RIPK1 in the intestinal epithelium, the Cre-loxP system was employed to generate mice that were deficient for RIPK1 specifically in intestinal epithelial cells (IECs). Mice with IEC-specific RIPK1 ablation (RIPK1^{IEC-KO}) exhibited increased IEC apoptosis accompanied by villus atrophy, crypt hyperplasia and very mild inflammation of the colon and the ileum, resulting in premature death within the first month of life. Intestinal pathology was partially dependent on TNFR1 signalling but developed independently of the microbiota and MyD88-dependent signalling. Epithelial specific FADD ablation prevented premature death of RIPK1^{IEC-KO} mice and inhibited IEC apoptosis, but RIPK1^{IEC-KO}/FADD^{IEC-KO} double knockout mice showed IEC necroptosis and developed ulcerating colitis. Additional ablation of RIPK3 prevented intestinal inflammation and IEC necroptosis, indicating that IECs in these mice died by RIPK1-independent RIPK3-dependent necroptosis. Thus in IECs, RIPK3-mediated necroptosis is more immunogenic than FADD-mediated apoptosis. RIPK1-deficient IECs showed degradation of pro-survival proteins TRAF2, cIAP1 and cFLIP, which could be directly associated with death of IECs.

In summary, the results presented in this work reveal a novel scaffolding function of RIPK1 for maintaining intestinal homeostasis by inhibiting FADD-dependent apoptosis of IECs.

Table of content

ZUSAMMENFASSUNG	I
ABSTRACT.....	II
TABLE OF CONTENT	III
LIST OF ABBREVIATIONS.....	VI
ABBREVIATIONS OF UNITS	X
LIST OF FIGURES	XI
LIST OF TABLES.....	XII
1. INTRODUCTION	1
1.1 REGULATED CELL DEATH.....	1
1.1.1 CELL DEATH IN HOMEOSTASIS AND IMMUNITY	1
1.2 RECEPTOR-INTERACTING PROTEIN KINASE 1 (RIPK1).....	3
1.3 DEATH RECEPTOR SIGNALING	5
1.3.1 TNF SIGNALING.....	6
1.3.1.1 NF- κ B activation.....	6
1.3.1.2 TNF induced apoptosis and necroptosis.....	10
1.3.2 APOPTOSIS AND NECROPTOSIS INDUCED BY OTHER DEATH RECEPTORS.....	15
1.4 PATTERN RECOGNITION RECEPTOR (PRR) SIGNALING	16
1.4.1 RIPK1 IN TOLL-LIKE RECEPTOR (TLR) SIGNALING.....	16
1.4.2 RIPK1 IN OTHER PRR SIGNALLING PATHWAYS	19
1.5 INTERFERONS AND NECROSOME FORMATION	20
1.6 ANATOMY OF THE INTESTINAL TRACT	20
1.7 STRUCTURE AND FUNCTION OF THE INTESTINAL EPITHELIUM.....	21
1.8 CELL DEATH AND IMMUNITY IN THE INTESTINAL EPITHELIUM	24
1.9 CRE/LoxP CONDITIONAL GENE TARGETING.....	29
1.10 PROJECT DESCRIPTION	29
2. MATERIAL AND METHODS.....	30
2.1 MATERIAL.....	30
2.1.1 CHEMICALS.....	30
2.1.2 MATERIAL FOR MOUSE WORK	30
2.1.3 MATERIAL FOR HISTOLOGY	30
2.1.4 MATERIAL FOR BIOCHEMISTRY.....	31
2.1.5 MOLECULAR BIOLOGY REAGENTS AND EQUIPMENT	31
2.1.6 LABORATORY EQUIPMENT.....	31
2.1.7 CELL CULTURE	32
2.1.8 SOFTWARE.....	32
2.1.9 BUFFERS AND SOLUTIONS.....	33
2.1.9.1 Washing buffers	33
2.1.9.2 Buffers and solutions for immunostainings	33
2.1.9.3 Preparation of protein extracts	33
2.1.9.4 Buffers and solutions for Western Blot analysis.....	34
2.1.9.5 Buffers for DNA extraction and genotyping PCRs.....	36
2.1.9.6 Buffers for 3D intestinal epithelial cell culture	36
2.2 METHODS	38
2.2.1 ANIMAL HANDLING AND MOUSE EXPERIMENTS.....	38
2.2.1.1 Mouse maintenance.....	38
2.2.1.2 Generation of conditional and full body knockout mice.....	38
2.2.1.3 Generation of inducible conditional knock-out mice.....	39
2.2.1.4 Antibiotic treatment and germ-free mice.....	39
2.2.1.5 Preparation of tissue biopsies.....	40

2.2.1.6	Tissue preparation	40
2.2.1.7	Isolation and FACS analysis of lamina propria immune cells	40
2.2.2	HISTOLOGY	41
2.2.2.1	Preparation of intestinal tissue for histological analysis	41
2.2.2.2	Hematoxylin and Eosin staining	41
2.2.2.3	Periodic acid-Schiff staining of intestinal tissue sections	42
2.2.2.4	Alkaline phosphatase staining	42
2.2.2.5	Immunohistochemistry	42
2.2.3	BIOCHEMICAL ANALYSIS	44
2.2.3.1	Isolation of intestinal epithelial cells (IECs)	44
2.2.3.2	Preparation of protein extracts	44
2.2.3.3	Preparation of cytoplasmic and nuclear protein extracts	45
2.2.3.4	Western Blot analysis	45
2.2.4	MOLECULAR BIOLOGY	47
2.2.4.1	Preparation of genomic DNA	47
2.2.4.2	Genotyping PCRs	48
2.2.4.3	Agarose gel electrophoresis	50
2.2.4.4	RNA extraction	50
2.2.4.5	cDNA synthesis	51
2.2.4.6	Quantitative real time PCR	51
2.2.5	CELL CULTURE	52
2.2.5.1	Isolation and culture of small intestinal organoids	52
2.2.5.2	Tamoxifen-induced deletion of RIPK1 in organoid cultures	53
2.2.5.3	Assessment of cell death in organoids	53
3.	RESULTS	55
3.1	RIPK1 DEFICIENCY IN IECs INDUCES INTESTINAL PATHOLOGY AND EPITHELIAL CELL DEATH	55
3.1.1	GENERATION OF MICE WITH INTESTINAL EPITHELIAL SPECIFIC RIPK1 DEFICIENCY	55
3.1.2	INCREASED IEC APOPTOSIS AND MILD INFLAMMATION IN THE ILEUM OF RIPK1 ^{IEC-KO} MICE	56
3.1.3	INCREASED IEC APOPTOSIS AND MILD INFLAMMATION IN THE COLON OF RIPK1 ^{IEC-KO} MICE	62
3.1.4	PROGRESSIVE PHENOTYPE IN RIPK1 ^{IEC-KO} MICE	67
3.1.5	INDUCIBLE POSTNATAL DELETION OF RIPK1 LEADS TO INTESTINAL PATHOLOGY AND LETHALITY	70
3.2	INTESTINAL PATHOLOGY IN RIPK1^{IEC-KO} MICE DEVELOPS INDEPENDENT OF THE MICROBIOTA	73
3.2.1	ANTIBIOTIC TREATMENT DOES NOT PREVENT DEVELOPMENT OF INTESTINAL DISEASE IN RIPK1 ^{IEC-KO} MICE	73
3.2.2	ANTIBIOTIC TREATMENT DOES NOT PREVENT INTESTINAL PATHOLOGY IN RIPK1 ^{TAMIEC-KO} MICE	74
3.2.3	RIPK1 ^{IEC-KO} MICE DEVELOP INTESTINAL DISEASE INDEPENDENT OF THE MICROBIOTA	75
3.2.4	PHENOTYPE IN RIPK1 ^{IEC-KO} MICE DEVELOPS INDEPENDENTLY OF MYD88-MEDIATED SIGNALING	77
3.3	INTESTINAL PATHOLOGY IN RIPK1^{IEC-KO} MICE PARTIALLY DEPENDS ON TNF SIGNALING	79
3.4	DEATH OF RIPK1^{-/-} IECs DEPENDS ON FADD AND RIPK3 MEDIATED SIGNALING	81
3.4.1	APOPTOSIS IN RIPK1 ^{IEC-KO} MICE DEPENDS ON FADD	81
3.4.2	DEATH OF IECs IN RIPK1 ^{IEC-KO} /FADD ^{IEC-KO} MICE DEPENDS ON RIPK3 MEDIATED NECROPTOSIS	86
3.4.3	DEATH OF RIPK1 ^{-/-} IECs IS INDEPENDENT OF RIPK3	90
3.5	SCAFFOLDING FUNCTION OF RIPK1 PREVENTS THE DEGRADATION OF PRO-SURVIVAL PROTEINS	93
3.5.1	PATHOLOGY IN RIPK1 ^{IEC-KO} MICE IS INDEPENDENT OF NF-κB ACTIVITY	93
3.5.2	RIPK1 PREVENTS DEGRADATION OF PRO-SURVIVAL PROTEINS	95

3.5.3 INCREASED TNF PRODUCTION AS AN AUTOCRINE AMPLIFICATION LOOP CAUSING IEC APOPTOSIS	97
4. DISCUSSION	100
4.1 RIPK1 AS A MASTER REGULATOR OF CELL DEATH.	100
4.2 HOW ARE RIPK1-DEFICIENT IECs SENSITIZED TO FADD-MEDIATED APOPTOSIS?	102
4.3 TRIGGERS OF FADD-DEPENDENT APOPTOSIS IN RIPK1 ^{IEC-KO} MICE	106
4.4 THE ROLE OF RIPK1 IN (INTESTINAL) INFLAMMATION.....	112
4.5 CONCLUDING REMARKS.....	115
REFERENCES	116
ACKNOWLEDGEMENT	139
TEILPUBLIKATION	140
ERKLÄRUNG:	158
CURRICULUM VITAE.....	159
<u>CURRICULUM VITAE</u>	<u>159</u>

List of Abbreviations

ABC	Avidin-Biotin-Complex
ACD	Accidental cell death
BCL-2	B-cell lymphoma 2
BSA	Bovine Serum Albumin
CD	Crohn's Disease
cDNA	complementary DNA
cFLIP	cellular FLICE-like Inhibitory Protein
clAP1/2	Cellular Inhibitor of Apoptosis Protein 1/2
CMV	Cytomegalovirus
CRC	Colorectal Cancer
Cre	Causes recombination
CreER ^{T2}	Causes recombination estrogen receptor
CYLD	Cylindromatosis (Protein)
DAB	Diaminobenzidine
DAMP	Danger Associated Molecular Pattern
DD	Death Domain
DISC	Death-Inducing Signaling Complex
DMEM	Dulbecco's Modified Eagle Medium
DNA	Desoxyribonucleic acid
dNTPs	desoxyribonucleotides
DR	Death Receptor
DTT	Dithiothreitol
ECL	Enhanced Chemiluminescence
EDTA	Ethylene Diamine Tetraacetate
e.g.	for example
FADD	Fas (TNFRSF6)-Associated via Death Domain
FAS	TNF Receptor Superfamily Member 6
FCS	Fetal Calf Serum
GI	Gastrointestinal Tract
H&E	Hematoxylin and Eosin
het	heterozygous
HOIL-1L	Heme-Oxidized IRP2 Ubiquitin Ligase 1 Homolog

HOIP	HOIL-1 Interacting Protein
HRP	Horseradish peroxidase
IBD	Inflammatory Bowel Disease
ID	Intermediate domain
IEC	Intestinal Epithelial Cell
IHC	Immunohistochemistry
IFN- α	Interferon- α
IFN- β	Interferon- β
IFN- γ	Interferon- γ
IL	Interleukin
IKK1	Inhibitor of κ B Kinase 1
IKK2	Inhibitor of κ B Kinase 2
IKK2ca	Inhibitor of κ B Kinase 2 constitutively active
IRF	Interferon Regulatory Factor
KD	kinase dead
IVC	Individually ventilated cages
LoxP	Locus of X-over P1
LUBAC	Linear Ubiquitin Chain Assembly Complex
MAPK	Mitogen-Activated Protein Kinases
MEF	Murine Embryonic Fibroblasts
mEGF	murine epidermal growth factor
MOMP	Mitochondrial Outer Membrane Permeabilization
mRNA	messenger RNA
MyD88	Myeloid Differentiation Primary Response Gene 88
NCCD	Nomenclature Committee on Cell Death
NEMO	Nuclear Factor-kappa B essential modulator
NF- κ B	Nuclear Factor kappa B
NGS	Normal Goat Serum
NP-40	Nonident P40
PAMP	Pathogen Associated Molecular Pattern
PCD	Programmed Cell Death
PCR	Polymerase Chain Reaction
PBS	Phosphate Buffered Saline
PFA	Paraformaldehyde

poly(I:C)	Polyinosinic:polycytidylic acid
PRR	Pattern Recognition Receptor
RCD	Regulated cell death
RHIM	Receptor (TNFRSF)-Interacting Protein Homotypic Interaction Motif
RIPK1	Receptor (TNFRSF)-Interacting Serine-Threonine Protein Kinase 1
RIPK3	Receptor (TNFRSF)-Interacting Serine-Threonine Protein Kinase 3
RNA	Ribonucleic acid
ROS	Reactive Oxygen Species
RT-PCR	Real-Time PCR
SDS	Sodium Dodecyl Sulfate
SHARPIN	SHANK-Associated RH Domain Interacting Protein
SI	Small Intestine
SPF	Specific pathogen free
TA	Transient Amplifying
TAB1	TAK1-Binding Protein 1
TAB2	TAK1-Binding Protein 2
TAK	TGF- β -Activated Kinase 1
TBS	Tris Buffered Saline
TE	Tris EDTA Buffer
Tg	Transgenic
TLR	Toll-Like Receptor
TNF	Tumor Necrosis Factor
TNFR1	TNF Receptor (p55)
TRADD	TNFRSF1A-Associated via Death Domain
TRAF2	TNF Receptor-Associated Factor 2
TRAF5	TNF Receptor-Associated Factor 5
TRAF6	TNF Receptor-Associated Factor 6
TRIF	TIR Domain-Containing Adaptor Inducing IFN- β
UC	Ulcerative Colitis
UPR	Unfolded Protein Response
WT	Wildtype

XIAP	X-linked Inhibitor of Apoptosis
zVAD-fmk	carbobenzoxy-valyl-alanyl-aspartyl-[O-methyl]- fluoromethylketone

Abbreviations of units

cm, μm , nm,	centimetre, micrometre, nanometre
g, mg, μg , ng	gram, milligram, microgram, nanogram
h, min, s	hours, minutes, seconds
kDa	kilodalton
l, ml, μl	litre, millilitre, microlitre
M, mM, μM , nM	molar, millimolar, micromolar, nanomolar
mA	milliampere
mol	mole
rpm	revolutions per minute
V	Volts
W	Watt
$^{\circ}\text{C}$	degree celsius
%	per cent

List of Figures

Figure 1 TNF induced signalling complexes.	12
Figure 2 TLR3 and TLR4 induced signalling pathways.	18
Figure 3 Structure of the small intestinal and colonic epithelium.	23
Figure 4. Conditional deletion of RIPK1 in IECs.	55
Figure 5. RIPK1 ^{IEC-KO} mice develop spontaneous phenotype resulting in premature death.	56
Figure 6. Intestinal pathology and IEC death in RIPK1 ^{IEC-KO} mice.	57
Figure 7. Hyperproliferation and reduced numbers of differentiated epithelial cells in RIPK1 ^{IEC-KO} mice.	58
Figure 8 Increased numbers of apoptotic IECs in RIPK1 ^{IEC-KO} mice.	59
Figure 9 Elevated expression of <i>Tnf</i> and <i>Cxcl1</i> in intestines of 3-week old RIPK1 ^{IEC-KO} mice.	60
Figure 10 Slightly increased leucocyte numbers in the mucosa of 3-week old RIPK1 ^{IEC-KO} mice.	61
Figure 11 Intestinal pathology and IEC apoptosis in the colon of RIPK1 ^{IEC-KO} mice.	62
Figure 12 Hyperproliferation and reduced numbers of differentiated epithelial cells in the colon of RIPK1 ^{IEC-KO} mice.	63
Figure 13 Differential expression of inflammatory cytokines and chemokines in the colon of 3-week old RIPK1 ^{IEC-KO} mice.	64
Figure 14 Increased infiltration of immune cells in the mucosa of RIPK1 ^{IEC-KO} mice.	66
Figure 15. No intestinal pathology in newborn RIPK1 ^{IEC-KO} mice.	67
Figure 16. Intestinal pathology in 1-week old RIPK1 ^{IEC-KO} mice.	68
Figure 17. Acute deletion of RIPK1 results in body weight loss and lethality.	70
Figure 18. Epithelial erosion and IEC apoptosis upon acute deletion of RIPK1.	71
Figure 19. No intestinal pathology in vehicle treated RIPK1 ^{tamIEC-KO} mice and tamoxifen injected VillinCreER ^{T2} mice	72
Figure 20. Antibiotic treatment does not prevent intestinal pathology in RIPK1 ^{IEC-KO} mice	74
Figure 21. Microbiota independent intestinal disease in RIPK1 ^{IEC-KO} mice	76
Figure 22. <i>Myd88</i> independent pathology in RIPK1 ^{IEC-KO} mice.	78
Figure 23. Premature lethality and IEC apoptosis in RIPK1 ^{IEC-KO} mice partially depend on TNFR1-mediated signaling.	80
Figure 24. FADD-dependent IEC apoptosis in the ileum of RIPK1 ^{IEC-KO} mice.	82
Figure 25. Caspase-independent IEC death and ulcerating colitis in RIPK1 ^{IEC-KO} /FADD ^{IEC-KO} mice.	84
Figure 26. Colitis and small intestinal pathology in adult RIPK1 ^{IEC-KO} /FADD ^{IEC-KO} mice.	85
Figure 27. Intestinal pathology in RIPK1 ^{IEC-KO} /FADD ^{IEC-KO} depends on RIPK3.	86
Figure 28. No increased cell death in RIPK1 ^{IEC-KO} /FADD ^{IEC-KO} /Ripk3 ^{-/-} mice.	87
Figure 29. No intestinal pathology in adult RIPK1 ^{IEC-KO} /FADD ^{IEC-KO} /Ripk3 ^{-/-} mice.	88
Figure 30. Increased TNF mRNA levels in the ileum of RIPK1 ^{IEC-KO} /FADD ^{IEC-KO} /Ripk3 ^{-/-} mice.	89
Figure 31. Premature death, cachexia and intestinal pathology in RIPK1 ^{IEC-KO} mice is independent of RIPK3.	91
Figure 32. Apoptosis and Paneth cell loss in RIPK1 ^{IEC-KO} mice is independent of RIPK3.	92
Figure 33. Pathology in RIPK1 ^{IEC-KO} is independent of canonical NF-κB activation.	94
Figure 34. Degradation of cIAP1 and TRAF2 in <i>Ripk1</i> ^{-/-} IECs and RIPK1 ^{tamIEC-KO} organoids.	96
Figure 35. Increased NF-κB activation and <i>Tnf</i> expression in <i>Ripk1</i> ^{-/-} IECs.	97
Figure 36. Increased sensitivity of <i>Ripk1</i> ^{-/-} / <i>Tnfr1</i> ^{-/-} organoids to poly(I:C) and IFN-γ induced death.	98
Figure 37. Intestinal pathology is independent of TRIF-mediated signaling.	99

List of Tables

Table 1: Primary antibodies and conditions for immunohistochemistry	43
Table 2: Secondary antibodies and conditions for immunohistochemistry	44
Table 3: Primary antibodies used for WB analysis.....	47
Table 4: Secondary antibodies used for WB analysis	47
Table 5: Primer-sequences for genotyping PCRs and PCR-amplified fragment sizes.	48
Table 6: PCR programmes for genotyping PCRs	49
Table 7: Taqman probes used for qRT-PCR	52

1. Introduction

1.1 Regulated cell death

The survival of every multicellular organism is inextricably connected to cell death. Throughout life, for the maintenance of tissue homeostasis, cell death is necessary to eliminate damaged and infected cells and to control cell numbers.

Cell death is classified into two gross categories, namely “accidental cell death” (ACD) and “regulated cell death” (RCD). ACD cannot be prevented or modulated, is resistant to pharmacologic interventions and caused by chemical, mechanical or physical insults (Galluzzi et al., 2012). On the other hand, RCD is dependent on an initiating stimulus and engages a molecular machinery to execute death. Therefore, it is amenable to modulation by genetic or pharmacologic means. In a physiological context, for instance during embryonic development, tissue homeostasis or infection and immune responses, RCD is referred to as “programmed cell death” (PCD) (Galluzzi et al., 2015).

In 2012, the Nomenclature Committee on Cell Death (NCCD) proposed a classification of cell death subtypes according to measurable biochemical features such as apoptosis, necroptosis, pyroptosis, autophagic cell death to account for the different forms of cell death, which will be followed throughout this work (Galluzzi et al., 2012).

1.1.1 Cell death in homeostasis and immunity

It is estimated, that every second 10^6 cells die in an adult human body, to keep proliferation and differentiation in balance for organ shaping and homeostasis (Green, Ferguson, Zitvogel, & Kroemer, 2009). These cells die by caspase dependent apoptosis, classically considered as an immunotolerogenic mode of programmed cell death (Green et al., 2009; Poon, Lucas, Rossi, & Ravichandran, 2014). Morphological features of apoptosis are plasma membrane blebbing, cell body shrinkage (pyknosis), nuclear condensation culminating in fragmentation (karyorrhexis) and formation of membrane-bound cell fragments (apoptotic bodies) (Kerr, Wyllie, & Currie, 1972). Fragmented dying cells are rapidly removed by tissue-

resident professional phagocytes (macrophages or dendritic cells) and/or non-professional phagocytes in the neighborhood (Poon et al., 2014). Both, controlled disassembling and rapid removal of apoptotic cells, ensures that no cellular content is released into the extracellular space, thereby preventing the initiation of an inflammatory response (Lamkanfi & Dixit, 2010). Furthermore, apoptotic cells can actively induce the expression of anti-inflammatory cytokines in phagocytes, such as IL-10, transforming growth factor β (TGF- β) and Lactoferrin, which inhibit recruitment of additional macrophages and/or neutrophils (Nagata, Hanayama, & Kawane, 2010; Poon et al., 2014). Impaired clearance of apoptotic cells has been implicated in exacerbated inflammation, atherosclerosis, autoimmunity, cancer and other pathologies (Poon et al., 2014).

Beyond its role during homeostasis, apoptosis is important in the immune response during infection. Upon sensing the presence of an invading pathogen, the immune system activates signaling pathways that promote pro-inflammatory and anti-microbial gene expression to counteract the infection. In addition, proteins regulating cell survival and cell death are expressed. In various infection models, induction of apoptosis in infected cells was shown to reduce pathogen replication and dissemination (Lamkanfi & Dixit, 2010). Apoptosis can be induced by different means. Through binding of death receptor ligands (DRLs) to their widely expressed specific death receptors (DRs 1-6) on the cell surface, death receptor mediated or “extrinsic apoptosis” is induced. In contrast to this, the death-inducing stimulus can emanate from the cytoplasm by mitochondrial cytochrome c release, leading to “intrinsic apoptosis”, or by pattern recognition receptors (PRRs). One important protein involved in signal transduction and regulation of cell death in response to DR and PRR stimulation is receptor-interacting protein kinase 1 (RIPK1).

For a long time, apoptosis was considered to be the only form of RCD, whereas necrosis was categorized as an ACD modality in response to physiochemical stress. Morphologically, necrotic cell death is characterized by organelle swelling and loss of plasma membrane integrity (Festjens, Vanden Berghe, & Vandenabeele, 2006; Krysko, Vanden Berghe, D'Herde, & Vandenabeele, 2008; Vanden Berghe et al., 2010). The rupture of the cell

membrane results in an uncontrolled release of intracellular “danger-associated molecular patterns” (DAMPs) including heat-shock protein 70 (HSP70), DNA-binding protein high mobility group box 1 (HMGB1) and DNA fragments, which have potent pro-inflammatory capabilities (Kono & Rock, 2008; Krysko et al., 2008; Lamkanfi & Dixit, 2010). Therefore, in contrast to immunotolerogenic apoptotic cell death, necrosis is considered as an immunogenic mode of cell death.

Recent findings implicated necrosis in various pathologic conditions like ischemia-reperfusion (I/R) and traumatic injury, Amyotrophic lateral sclerosis (ALS), Huntington’s disease, systemic inflammation, atherosclerosis, microbial as well as viral infections and others (W. Zhou & Yuan, 2014). In 1988 it was discovered, that stimulation with tumor necrosis factor (TNF) could induce necrotic cell death in some cell lines (Laster, 1988). Further studies revealed necrosis not to be accidental, but rather a regulated form of cell death that engages a molecular machinery. After the discovery that the chemical compound necrostatin-1 can inhibit DR-induced necrosis, the new definition “necroptosis” was introduced to describe regulated necrosis (Degterev et al., 2005; Vandenabeele, Declercq, Van Herreweghe, & Vanden Berghe, 2010). In addition to DR signaling, necroptosis can be induced by stimulation of various PRRs and interferon alpha/beta receptor 1 (IFNAR1) (Kaiser et al., 2013; Robinson et al., 2012; Thapa et al., 2011). Downstream of DRs and PRRs, receptor-interacting protein kinase 3 (RIPK3) and RIPK1, the latter one constituting the molecular target of necrostatin-1, are essential for DR induced necroptosis (Cho et al., 2009; Degterev et al., 2008; He et al., 2009; Holler, 2000; Holler et al., 2000; D. W. Zhang et al., 2009).

1.2 Receptor-interacting protein kinase 1 (RIPK1)

RIPK1 was discovered in 1995 as an interaction partner of the death receptor Fas (CD95) and is constitutively expressed in many tissues (Stanger, Leder, Lee, Kim, & Seed, 1995). Human RIPK1 is a 671 aa protein with a predicted molecular weight of 76 kDa encoded by the *rip1* gene located on chromosome 6 (Hsu, Huang, Shu, Baichwal, & Goeddel, 1996). Murine RIPK1 consists of 656 aa and shares 68% homology with human RIPK1 with the highest similarity in the death domain (Hsu, Huang, et al., 1996; Stanger et al., 1995).

RIPK1 is one of seven known members of the RIP kinase family, classified as serine/threonine kinases due to a conserved kinase domain present in all identified RIP kinases (Festjens, Vanden Berghe, Cornelis, & Vandenabeele, 2007; D. Zhang, Lin, & Han, 2010).

RIPK1 consists of three domains; a N-terminal kinase domain, an intermediate domain (ID) and a C-terminal death domain (DD). The kinase domain enables RIPK1 to autophosphorylate, which is required for RIPK1 mediated necroptosis but not for TNF induced NF- κ B activation (Hsu, Huang, et al., 1996; Newton et al., 2014; Polykratis et al., 2014; Ting, Pimentel-Muinos, & Seed, 1996). At residue aspartic acid 324 (Asp324) the ID domain harbors a caspase-8 cleavage site. Cleavage of RIPK1 at this site shuts off NF- κ B activation, inhibits necroptosis and promotes apoptosis during DR induced caspase-8 activation and RIG-I mediated antiviral responses (Lin, Devin, Rodriguez, & Liu, 1999; Rajput et al., 2011). Upon TNF signaling, Lysine 377 (K377) located in the ID of RIPK1 is ubiquitinated by Lys63-linked ubiquitin chains and this modification seems to be important for RIPK1 mediated NF- κ B activation (Ea, Deng, Xia, Pineda, & Chen, 2006; H. Li, Kobayashi, Blonska, You, & Lin, 2006). In addition, a receptor-interacting protein homotypic interaction motif (RHIM), that is responsible for the interaction of proteins containing this particular protein-protein binding motif, is present in the ID. The RHIM domain is required for the interaction of RIPK1 with RIPK3, TIR-domain-containing adaptor-inducing IFN β (TRIF) and DNA-dependent activator of IRFs (DAI) (Kaiser & Offermann, 2005; X. Sun, Yin, Starovasnik, Fairbrother, & Dixit, 2002; Upton, Kaiser, & Mocarski, 2008). A DD enabling its interaction with death receptors, TNFR1-associated death domain protein (TRADD) and FAS-associated death domain (FADD) can be found at the C-terminus of RIPK1 (Park et al., 2007). Via its DD-mediated interactions RIPK1 is involved in the assembly of intracellular signaling complexes that initiate downstream signaling to induce pro-inflammatory and pro-survival gene expression or trigger apoptosis or necroptosis.

Ever since its discovery, RIPK1 has been implicated in the regulation of cell death, as its overexpression caused spontaneous death in baby hamster kidney cells (Stanger et al., 1995). Mice with full body ablation of RIPK1 were born at the expected Mendelian ratios but died within 3 days after birth due to

massive cell death of adipose lineages and T-cells in lymphoid tissues (Kelliher et al., 1998).

RIPK1 is involved in genotoxic stress induced NF- κ B activation mediated by the NEMO PIDDosome, a complex that contains p53-induced protein with a death domain (PIDD), RIP1, NEMO and IKK2 (Janssens, Tinel, Lippens, & Tschopp, 2005). In a second pathway, RIPK1 and NEMO induce cytokine production and caspase-8 activation upon extensive DNA damage sensed by ataxia telangiectasia mutated (ATM) kinase (Biton & Ashkenazi, 2011).

Furthermore, a direct role of RIPK1 as a repressor of gene transcription in the nucleus downstream of epidermal growth factor receptor (EGFR) has been reported (Ramnarain et al., 2008). However, most studies on RIPK1 focused on its cytoplasmic role in signal transduction and regulation of cell death. The mechanisms of RIPK1 mediated signaling pathways are described in the following chapters.

1.3 Death receptor signaling

The tumor necrosis factor (TNF) ligand superfamily and their cognate receptors are important regulators of inflammatory responses and cell death in response to infection and tissue injury. Members of the TNF receptor superfamily are expressed differentially in different cell types. The death receptors (DR), a subgroup of the TNF receptor superfamily, are characterized by a cytoplasmic DD motif. Upon ligand binding to its receptor, the DR's DD recruits DD containing adapter proteins forming a receptor associated signaling complex to initiate downstream signaling cascades resulting in cell death or inflammatory gene expression.

In humans, six different death receptors have been identified: Tumor necrosis factor superfamily member 1a, (*Tnfrsf1a*) (TNFR1) is activated by TNF and lymphotoxin α (LT α), tumor necrosis factor receptor superfamily member 6 (*Tnfrsf6*) (Fas or CD95) is activated by Fas ligand (FasL or CD95L), DR3 (*Tnfrsf25*) is activated by TL1A, TNF-related apoptosis-inducing ligand receptor 1 and 2 (TRAILR1 and TRAILR2) are bound by TRAIL (Apo2) and finally, DR6 is activated by amyloid precursor protein (APP) (Silke & Hartland,

2013; Wilson, Dixit, & Ashkenazi, 2009). DR 3 and DR6 may not efficiently induce cell death (Wajant, 2003). Mice express homologs of all human DRs except TRAILRs. Instead, murine TRAILR is a single ortholog of human TRAILR1 and TRAILR2.

1.3.1 TNF signaling

1.3.1.1 NF- κ B activation

TNF exerts its pro-inflammatory and anti-apoptotic functions by activating canonical transcription factor NF- κ B, c-Jun N-terminal kinase (JNK) and p38 mitogen-activated protein kinases (MAPK). TNF ligation to TNFR1 initiates receptor trimerization and subsequent recruitment of adaptor proteins TRADD and RIPK1 to TNFR1 via DD interactions. However, the mechanisms coordinating DD interactions between TNFR1, TRADD and RIPK1 are not fully understood (Hayden & Ghosh, 2012; Hsu, Huang, et al., 1996). TRADD recruits the E3 ubiquitin ligases TNFR-associated factor 2 (TRAF2) and TRAF5 via TRAF binding domain interactions (Hsu, Huang, et al., 1996; Hsu, Shu, Pan, & Goeddel, 1996; Hsu, Xiong, & Goeddel, 1995). TRAF2 binds the E3 ligases cellular inhibitors of apoptosis (cIAP1 and cIAP2) and recruits them to the TNFR1 complex (Rothe, Pan, Henzel, Ayres, & Goeddel, 1995; Shu, Takeuchi, & Goeddel, 1996). The TRAF2-cIAP1/2 axis including E3 ligase activity of cIAP1 are required for the efficient recruitment of the linear ubiquitin chain assembly complex (LUBAC), consisting of haem-oxidized IRP2 ubiquitin ligase-1 (HOIL-1L), HOIL-1 interacting protein (HOIP) and SHANK-associated RH domain-interacting protein (SHARPIN) (Haas et al., 2009). This complex, when associated to the receptor, is termed 'complex I' (Figure 1). To mediate downstream signaling, cIAPs modify Lys377 of RIPK1 by adding K63-linked poly-ubiquitin chains (Mahoney et al., 2008). This modification provides a scaffolding platform for the further recruited proteins transforming growth factor β activated kinase (TAK1), TAK1 binding protein 1 and 2 (TAB1/TAB2), I κ B kinase 1 and 2 (IKK1/IKK2) and NF- κ B essential modulator (NEMO) (Hayden & Ghosh, 2012). RIPK1 K63-ubiquitin chain mediated proximity of TAB1/TAB2/TAK1 and IKK1/IKK2/NEMO complexes induces trans-auto-phosphorylation of TAK1. Activated TAK1 initiates MAPK kinase activation and phosphorylates IKK2. Nuclear factor of kappa light polypeptide gene

enhancer in B-cells (NF- κ B) inhibitor alpha (I κ B α) is phosphorylated by IKK2, and thereby targeted for ubiquitination and proteasomal degradation. The canonical NF- κ B heterodimer p65:p50 is then released and translocates to the nucleus, where it induces target gene expression (Figure 1) (Hayden & Ghosh, 2012).

Addition of K48-, K63-linked and linear ubiquitin chains to different members of receptor-associated 'complex I' are thought to be important for efficient signal transduction and modulation. Upon TNF stimulation, RIPK1 and NEMO are modified with linear ubiquitin chains added by LUBAC. These are believed to stabilize complex I as well as to support efficient recruitment of NEMO, due to its high binding affinity for linear ubiquitin chains (Mollah et al., 2007; Tokunaga et al., 2009). Accordingly, cells or mice deficient in HOIL-1 and HOIP or carrying mutations in *Sharpin* (chronic proliferative dermatitis mutation; cpdm) showed reduced I κ B α phosphorylation after TNF stimulation (Gerlach et al., 2011; Ikeda et al., 2011; Tokunaga et al., 2011).

The importance RIPK1 and its modification with K63-linked ubiquitin chains for NF- κ B activation remain controversial to date (Hayden & Ghosh, 2014; Ofengeim & Yuan, 2013). Initially, RIPK1 was reported to be essential for NF- κ B activation (Ea et al., 2006; Hsu, Huang, et al., 1996; Kelliher et al., 1998; H. Li et al., 2006). RIPK1 deficient B-cells failed to activate NF- κ B in response to murine and human TNF as demonstrated by electrophoretic mobility shift assay (EMSA) (Kelliher et al., 1998). The importance of RIPK1 for NF- κ B activation was attributed to TNF induced K63-linked polyubiquitination of K377, because mutating this residue abolished the recruitment of TAK- and IKK-complexes to complex I as well as I κ B α phosphorylation after TNF stimulation (Ea et al., 2006; H. Li et al., 2006).

In contrast, a different study reported ubiquitinated RIPK1 and no defects in I κ B α phosphorylation upon TNF stimulation of cells expressing a mutated ubiquitin, which cannot be linked using residue K63 (Xu, Skaug, Zeng, & Chen, 2009). From these results, an ubiquitin-dependent but K63-polyubiquitination independent mechanism for TNF-induced IKK activation was concluded (Xu et al., 2009). A more recent study reported normal NF- κ B activation in multiple cell types isolated from RIPK1 deficient mice and

suggested a cell type specific function of RIPK1 for NF- κ B activation (Wong et al., 2010).

Although the exact role of RIPK1 for NF- κ B activation remains elusive, TRADD is required for full TNF-induced NF- κ B activation (Ermolaeva et al., 2008; Pobezinskaya et al., 2008). TRADD deficient mouse embryonic fibroblasts (MEFs) and bone marrow-derived macrophages (BMDMs) showed reduced I κ B α phosphorylation and no ubiquitination of RIPK1 after TNF stimulation (Ermolaeva et al., 2008; Pobezinskaya et al., 2008). Other proteins of complex I, such as cIAP1 and cIAP2 were shown to be likewise important for NF- κ B activation (Mahoney et al., 2008). *Traf2*^{-/-} cells show slightly reduced NF- κ B activation in response to TNF, whereas TRAF2/5 double knockout cells are completely defective in IKK activation, suggesting redundant functions of TRAF2 and TRAF5 in the context of NF- κ B activation (Tada et al., 2001; Yeh et al., 1997).

NF- κ B target genes include pro-inflammatory genes, e.g. *Tnf*, *Il6*, anti-apoptotic gene *Cflar*, encoding Cellular FLICE (FADD-like IL-1 β -converting enzyme)-inhibitory protein (cFLIP), and negative regulators of canonical NF- κ B signaling, A20 and cylindromatosis (CYLD). Both, A20 and CYLD, are deubiquitylating enzymes that can interact with RIPK1. CYLD is capable of removing K63-ubiquitin chains from RIPK1, thereby promoting the dissociation of complex I and triggering the formation of a death inducing cytosolic complex (DISC) (Hitomi et al., 2008; Moquin, McQuade, & Chan, 2013; O'Donnell, Legarda-Addison, Skountzos, Yeh, & Ting, 2007; Wright et al., 2007). On the other hand, A20 has dual ubiquitin editing properties on RIPK1. First, the N-terminal deubiquitylase domain of A20 removes K63-polyubiquitin chains from RIPK1, and second, a C-terminal zinc finger domain catalyzes K48-linked polyubiquitination of RIPK1, thereby targeting RIPK1 for proteasomal degradation (Wertz & Dixit, 2008).

Some proteins of the canonical NF- κ B pathway downstream of TNFR1 function as negative regulators in the non-canonical NF- κ B pathway, which usually is activated by ligands of a subset of the TNF ligand superfamily including BAFF, TWEAK or CD40L (Darding & Meier, 2012). In unstimulated

cells, NF- κ B inducing kinase (NIK) is modified with K48-linked ubiquitin chains and thus targeted for proteasomal degradation by a TRAF2-TRAF3-cIAP1/2 complex. In order to induce ubiquitination of NIK, TRAF3 directly binds to NIK and recruits TRAF2. TRAF2 then recruits cIAP1/2, which in turn attaches K-48 linked ubiquitin chains to NIK. Consequently, non-canonical NF- κ B is not active at steady state (Vallabhapurapu et al., 2008; Zarnegar et al., 2008). Upon stimulation and subsequent receptor ligation, the TRAF2-TRAF3-cIAP1/2 complex is recruited to the receptor. Depending on the activated receptor and the cellular context, either TRAF3 is ubiquitinated by cIAPs and subsequently degraded, or TRAF2 and cIAP1/2 are degraded. In both cases, NIK is stabilized and phosphorylates IKK1. Active IKK1 forms homodimers, which in turn phosphorylate p100, thereby inducing its partial degradation and the generation of a p52 cleavage fragment. p52 dimerizes with RelB, the dimer translocates to the nucleus and induces target gene expression. Beside receptor stimulation, deletion of cIAPs or TRAF2 can result in activation of non-canonical NF- κ B signaling (Vallabhapurapu et al., 2008; Zarnegar et al., 2008).

1.3.1.2 TNF induced apoptosis and necroptosis

In addition to anti-apoptotic signaling mediated via complex I formation and NF- κ B activation, TNF signaling can induce the formation of death inducing cytosolic complexes (DISC) complex IIa, complex IIb and complex IIc (also called the necrosome) resulting in apoptotic (complex IIa and IIb) or necroptotic cell death (complex IIc/necrosome) (Figure 1) (Pasparakis & Vandenabeele, 2015).

Destabilization of complex I results in the formation of complex IIa by association of TRADD with FADD via DD interaction and subsequent recruitment of caspase-8 by FADD through the death effector domain (DED) (Kelliher et al., 1998; Micheau & Tschopp, 2003; L. Wang, Du, & Wang, 2008). An alternative apoptosis inducing complex, called complex IIb, consisting of RIPK1, RIPK3, FADD and caspase-8 can form as well (Figure 1) (Pasparakis & Vandenabeele, 2015; L. Wang et al., 2008; Wilson et al., 2009). In both complexes FADD recruits two procaspase-8 molecules that dimerize. Procaspase-8 dimers undergo a conformational change resulting in autocatalytic cleavage and the generation of p43/p41, p30 and other caspase-8 cleavage fragments. In a second cleavage step, p43/p41 and p30 fragments are processed to p10 and p18 fragments that form a fully catalytic active caspase-8 heterotetramer (Medema, Scaffidi, et al., 1997; Medema, Toes, et al., 1997). Active caspase-8 in turn cleaves and thereby activates effector caspases-3, -6 and -7 as well as BH3 interacting domain (Zheng et al.) death agonist. Bid mediates the release of mitochondrial proteins, thus inducing apoptosome formation and procaspase-9 activation in an indirect manner. Active caspase-9 in turn activates effector caspases, thereby providing an amplification loop for induction of apoptosis in cells with low levels of DISC components (Wilson et al., 2009). Effector caspases further activate cytoplasmic endonucleases, which degrade nuclear material, and proteases for the degradation of cytoskeletal proteins causing morphological features observed in apoptotic cells (Elmore, 2007).

The third death-inducing complex downstream of TNF, complex IIc, is composed of RIPK1, RIPK3 and mixed lineage kinase domain like (MLKL) (Pasparakis & Vandenabeele, 2015). According to the current model, RIPK1 autophosphorylation alters the conformation of RIPK1 and allows a RHIM

mediated interaction with RIPK3 (Chan, Luz, & Moriwaki, 2015). The RIPK1-RIPK3 heterodimer recruits additional RIPK3 molecules to form a large RIPK3-RIPK3 amyloid complex leading to RIPK3 autophosphorylation (Cho et al., 2009; He et al., 2009; J. Li et al., 2012; D. W. Zhang et al., 2009). Dimerization or oligomerization as well as phosphorylation of at least one RIPK3 molecule within the complex at Ser232 (Ser227 in human RIPK3) is essential for the recruitment of MLKL to the necrosome complex (W. Chen et al., 2013; J. Li et al., 2012; McQuade, Cho, & Chan, 2013; Orozco et al., 2014; Wu et al., 2014). RIPK3 phosphorylates MLKL at Ser345, Ser347, Ser352 and Thr349 (Thr357 and Ser358 in human MLKL). This leads to the exposure of the 4-helical bundle domain of MLKL, stimulating its oligomerization and subsequent translocation to the plasma membrane (Cai et al., 2014; X. Chen et al., 2014; Dondelinger et al., 2014; Murphy et al., 2013; L. Sun et al., 2012; H. Wang et al., 2014; Xie et al., 2013). Although the precise mechanism of necroptosis through MLKL function is not entirely clear, two models have been proposed so far: first, disruption of cell membrane by MLKL results in influx of Ca^{2+} and Na^{+} and second, MLKL was shown to directly disrupt membrane integrity by binding to membrane phospholipids via its 4-helical bundle domain (Cai et al., 2014; X. Chen et al., 2014; Dondelinger et al., 2014; Su et al., 2014; H. Wang et al., 2014).

The final cellular outcome of TNFR1 induced signaling is regulated through different ways. First, NF- κ B activation induces the expression of anti-apoptotic proteins such as cFLIP, a catalytically inactive homolog of caspase-8. The two predominant isoforms of cFLIP, cFLIP_L and cFLIP_S both can form heterodimers with caspase-8. cFLIP_L has a similar domain architecture as caspase-8, but lacks a catalytic cysteine residue (Darding & Meier, 2012). Caspase-8-cFLIP_L heterodimers allow partial caspase-8 enzymatic activity but not caspase-8 autocatalytic cleavage to inhibit the generation of the apoptosis inducing p18/p10 caspase-8 fragments (Pop et al., 2011; Scaffidi, Kirchhoff, Krammer, & Peter, 1999; Wachter et al., 2004). On the other hand, cFLIP_S only contains the DED and dimerization with caspase-8 completely inhibits the enzymatic activity of caspase-8 (Kavuri et al., 2011).

cFLIP_L is a negative regulator of complex IIa mediated apoptosis, which is induced by stimulating cells with TNF and protein synthesis inhibitor cyclohexamide (Chx) (L. Wang et al., 2008). TNF stimulation of Panc-1 cells in which FLIP is knocked down mimicked the combinatory stimulation of TNF and Chx (L. Wang et al., 2008). Furthermore, overexpression of cFLIP protected cells from TNF and Chx induced apoptosis (L. Wang et al., 2008). Apoptosis mediated by complex IIa occurs independent of RIPK1 or its kinase activity, since knockdown of RIPK1 or addition of Nec-1 did not protect cells from TNF and Chx induced apoptosis (Holler et al., 2000; L. Wang et al., 2008). In fact, RIPK1 deficient fibroblasts and lymphocytes were highly sensitive to TNF induced apoptosis (Kelliher et al., 1998; H. Zhang et al., 2011). Another study reported no difference in viability of primary and immortalized RIPK1 deficient MEFs in response to TNF compared to WT MEFs (Wong et al., 2010). Interestingly, *Ripk1*^{-/-} MEFs were sensitized to TNF/Chx-induced apoptosis, arguing for a pro-survival role of RIPK1 in TNF/Chx-induced complex IIa mediated apoptosis (Wong et al., 2010).

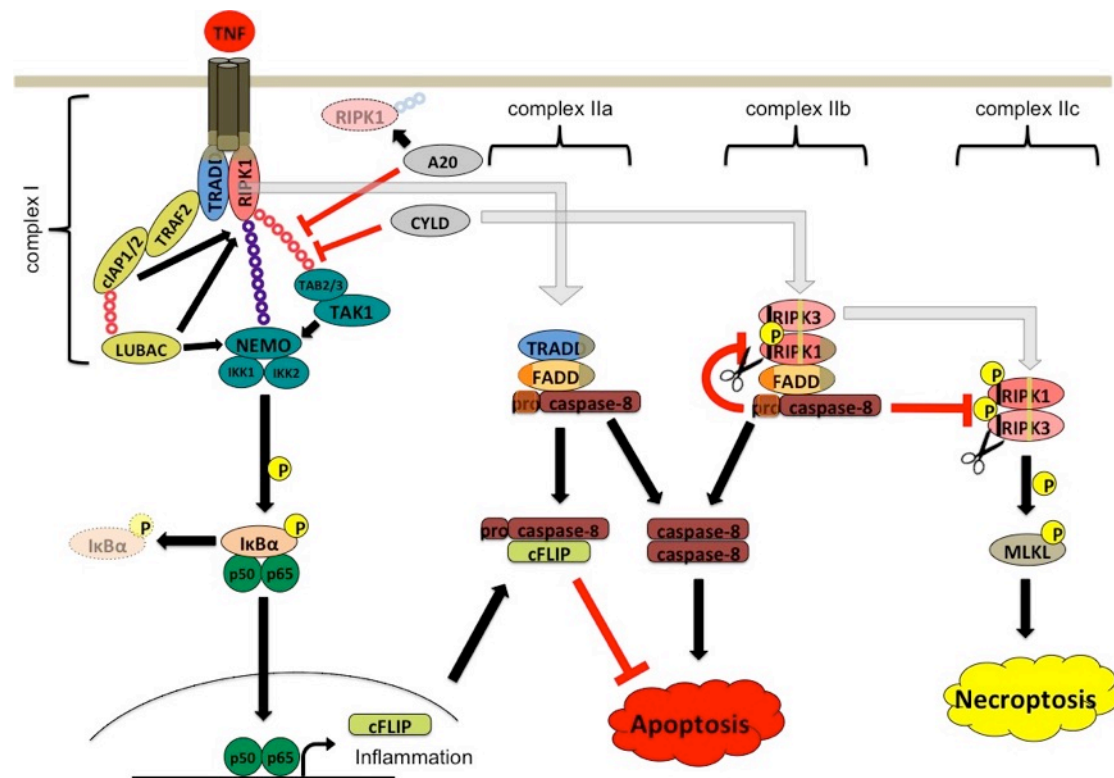


Figure 1 TNF induced signalling complexes.

Upon binding to its cognate receptor, TNF is capable to induce distinct intracellular signalling pathways. TNF ligation results in assembly of a receptor-associated complex I, which mediates downstream NF-κB activation for pro-survival and pro-inflammatory gene transcription. Apoptosis can be induced by the formation of death inducing complex IIa composed of TRADD, FADD and caspase-8, which is negatively regulated by cFLIP. Destabilization of complex I by deubiquitination of RIPK1 leads to the assembly of a RIPK1, RIPK3, FADD and caspase-8 containing apoptosis inducing cytosolic complex IIb. In complex IIa and

IIb FADD recruits dimerizing pro-caspase-8 molecules, which are activated by autocatalytic cleavage to induce apoptosis. When caspase-8 activity is blocked, RIPK1 and RIPK3 are no longer cleaved by caspase-8 within complex IIb, stabilize and auto-phosphorylate. Phosphorylated RIPK3 phosphorylates MLKL, which then executes necroptosis. **For details see text.**

K63-linked ubiquitination chains are represented by red rings and linear ubiquitination chains by purple rings; Brown insets in TRADD and FADD represent DDs, orange insets in FADD and pro-caspase-8 depict DEDs. Yellow and black stripes in RIPK1 and RIPK3 represent RHIMs and caspase-8 cleavage sites respectively.

Abbreviations: cIAP1/2, cellular inhibitors of apoptosis 1/2; CYLD, cylindromatosis; FADD, Fas-associated via death domain; IKK1/2, inhibitor of κ B kinase 1/2; LUBAC, linear ubiquitin chain assembly complex, MLKL, mixed lineage kinase domain-like; NEMO, NF- κ B essential modifier; P, phosphorylation; RIPK1/3, receptor interacting protein kinase 1/3; TAB2/3, TGF-beta activated kinase 1 binding protein 2/3; TAK1, TGF-beta activated kinase 1; TNF, tumor necrosis factor; TNFR1, TNF receptor 1; TRADD, TNF receptor associated death domain; TRAF2, TNF receptor-associated factor 2.

On the other hand, complex IIb mediated apoptosis is induced upon stimulation of cells with TNF and Smac mimetics (SM), a synthetic IAPs antagonist that induces autoubiquitination and proteasomal degradation of cIAP1 and cIAP2 (Bertrand et al., 2008; Gaither et al., 2007; L. Li et al., 2004; Petersen, Peyton, Minna, & Wang, 2010; Petersen et al., 2007; E. Varfolomeev et al., 2007; Vince et al., 2007). A complex with similar components, called the “riposome”, can form upon loss of cIAPs upon TLR3 stimulation or genotoxic stress independent of death receptor stimulation (Feoktistova et al., 2011; Tenev et al., 2011). TAK1, NEMO or Pellino deficient cells are also sensitized to TNF-induced complex IIb-mediated apoptosis (Pasparakis & Vandenabeele, 2015). Apoptosis induced by complex IIb is dependent on RIPK1 and its kinase activity as it can efficiently be inhibited by RIPK1 deletion or addition of Nec1 (Arslan & Scheidereit, 2011; Bertrand et al., 2008; Dondelinger et al., 2013; Gaither et al., 2007; Geserick et al., 2009; Petersen et al., 2007; L. Wang et al., 2008; Wong et al., 2010).

Destabilization of complex I by deubiquitination or impaired K63-linked or linear ubiquitination of RIPK1 is believed to favor the formation of death-inducing complex IIb and/or complex IIc. For instance, disabled K63-linked ubiquitination of RIPK1 by cIAPs upon SM treatment favors complex IIb formation and apoptosis (Bertrand et al., 2008; L. Wang et al., 2008). The importance of IAPs for prevention of RIPK1-mediated inflammation and cell death is underscored by the finding, that deletion of RIPK3 or one allele of RIPK1 partially rescues the embryonic lethality of *ciap1^{-/-} xiap^{-/-}* or *ciap1^{-/-} ciap2^{-/-}* mice (Moulin et al., 2012). Furthermore, cells expressing mutated

RIPK1, where the addition of ubiquitin chains to K377 is prevented, were highly sensitive to TNF-induced apoptosis (O'Donnell et al., 2007).

In addition, mutation of SHARPIN or HOIL-1 deficiency renders cells sensitive to TNF induced RIPK1 kinase activity dependent apoptosis and necroptosis (Gerlach et al., 2011; Ikeda et al., 2011; Tokunaga et al., 2011). Chronic proliferative dermatitis mice (*cpdm*) carry a mutation in the *Sharpin* gene and develop spontaneous inflammation of the skin, primarily caused by TNFR1-induced RIPK1 kinase activity and TRADD dependent apoptosis (Berger et al., 2014; Gijbels et al., 1996; Kumari et al., 2014; Seymour et al., 2007).

In contrast to the findings described above, other studies reported ubiquitinated RIPK1 in complex II, suggesting that deubiquitination of RIPK1 is not essential for the induction of cell death (Cho et al., 2009; Lamothe, Lai, Xie, Schneider, & Darnay, 2013; Moquin et al., 2013).

In both, complex IIa and IIb, execution of extrinsic apoptosis depends on FADD and caspase-8. Full body ablation of either FADD or caspase-8 resulted in early embryonic lethality due to extensive RIPK3-dependent necroptosis, demonstrating that FADD and caspase-8 suppress necroptosis *in vivo* (Kaiser et al., 2011; Oberst et al., 2011; E. E. Varfolomeev et al., 1998; Yeh et al., 1998; H. Zhang et al., 2011; J. Zhang, Cado, Chen, Kabra, & Winoto, 1998). Caspase-8 suppresses necroptosis by cleaving RIPK1 and RIPK3, while the C-terminal RIPK1 cleavage fragment inhibits TNF-induced NF- κ B activation and promotes apoptosis (Feng, Ma, Yang, & Wu, 2006; Feng et al., 2007; J. W. Kim, Choi, & Joe, 2000; Lin et al., 1999; Martinon, Holler, Richard, & Tschopp, 2000). Apoptosis mediated by complex IIa or IIb can be blocked by addition of pan-caspase inhibitor zVAD-fmk, which sensitizes cells to necroptotic cell death. Since Nec1 efficiently blocks necroptosis downstream of TNFR1, TNF-induced necroptosis is RIPK1 kinase activity dependent (Cho et al., 2009; He et al., 2009; D. W. Zhang et al., 2009).

In addition to RIPK1 and RIPK3, CYLD is another substrate of caspase-8 capable of promoting necroptosis. Mutation of the caspase-8 cleavage site of CYLD sensitized cells to TNF-induced necroptosis (O'Donnell et al., 2011). Furthermore, knockdown or deletion of CYLD protected against TNF/Smac

mimetics induced apoptosis as well as RIPK1-mediated necroptosis (Hitomi et al., 2008; Moquin et al., 2013; L. Wang et al., 2008). Since in *Cyld*^{-/-} cells RIPK1 and RIPK3 ubiquitination was greatly enhanced, it was suggested that CYLD exerts its pro-necrotic function by deubiquitinating RIPK1 and RIPK3 within the necrosome rather than acting in complex I (Moquin et al., 2013).

1.3.2 Apoptosis and necroptosis induced by other death receptors

Fas/CD95 (tumor necrosis factor receptor superfamily member 6; TNFRSF6) and TRAIL receptor (in humans TRAILR1 and TRAILR2) are members of the DR family that can induce apoptosis after stimulation with their specific ligands CD95L (or agonistic antibodies) or TRAIL/Apo2L respectively (Lavrik & Krammer, 2012; Wilson et al., 2009). Fas ligation induces receptor oligomerization and formation of a membrane associated DISC composed of FADD, procaspase-8 and cFLIP_L (Muzio et al., 1996; Scaffidi et al., 1999; Sprick et al., 2002). Stimulation outcome is determined by the stoichiometry of forming procaspase-8 and cFLIP homo- or heterodimers and their processing. Induction of apoptosis is correlated to the amount of generated p43/p41 caspase-8 cleavage fragments, whereas induction of non-apoptotic pathways, namely NF-κB activation, depends on the amount of p43-FLIP cleavage fragments (Neumann et al., 2010). Although apoptosis occurs independent of RIPK1, upon loss of IAPs and/or caspase inhibition Fas can induce RIPK1 kinase dependent necroptosis (Geserick et al., 2009; Holler et al., 2000).

RIPK1 has been implicated in Fas induced cytokine and chemokine production via activation of NF-κB (Cullen et al., 2013). Furthermore, in Fas stimulated Jurkat cells, RIPK1 is required for NF-κB activation but is dispensable for ERK and JNK activation (Kreuz et al., 2004).

A DISC with a similar composition is formed upon TRAIL stimulation. In contrast to the membrane associated Fas DISC, the TRAIL DISC is internalized by the endosome (Sprick et al., 2002; X. D. Zhang, Franco, Nguyen, Gray, & Hersey, 2000). Beside apoptosis, TRAIL can also induce the formation a secondary cytosolic complex that is devoid of TRAILR but contains FADD, caspase-8, TRAF2 and NEMO (E. Varfolomeev et al., 2005). The formation of this secondary complex requires caspase-8 activity and results in NF-κB and MAPK activation. Within this complex, RIPK1 is required

for efficient IKK and p38 activation but is dispensable for JNK activation (E. Varfolomeev et al., 2005).

1.4 Pattern Recognition Receptor (PRR) signaling

Recognition of invading pathogens and the initiation of a proper innate immune response are critical for host defense. Pattern recognition receptors (PRR) are part of the innate immune system and activated by molecular structures shared by many pathogens, called pathogen-associated molecular pattern (PAMPs), as well as in response to cellular stress and DAMPs. Signaling via PRR initiates an inflammatory response to fight the infection, alerts the adaptive immune system and can induce the death of infected cells to prevent pathogen dissemination. The PRR family includes Toll-like receptors (TLRs), C-type lectin receptors (CLRs), NOD-like receptors (NLRs), RIG-I like receptors (RLRs) and others (Kawai & Akira, 2011).

1.4.1 RIPK1 in Toll-like receptor (TLR) signaling

TLRs are transmembrane proteins consisting of a leucine-rich repeat (LRR) ectodomain for recognition of PAMPs; a transmembrane domain; and an intracellular Toll-interleukin 1 (IL-1) receptor (TIR) domain for signal transduction (Kawai & Akira, 2010). Until now, 12 and 10 TLRs have been identified in mice and humans, respectively.

TLRs detect distinct PAMPs derived from bacteria, mycobacteria, viruses, fungi and parasites. TLR3 is activated by virus derived double-stranded RNA or its synthetic analog poly(I:C), internalized and translocated to the endosome (Alexopoulou, Holt, Medzhitov, & Flavell, 2001; Oshiumi, Matsumoto, Funami, Akazawa, & Seya, 2003; Yamamoto et al., 2003; Yamamoto, Sato, Hemmi, et al., 2002; Yamamoto, Sato, Mori, et al., 2002). TLR4 detects lipopolysaccharides, an outer membrane component of gram-negative bacteria, as well as gram-positive bacterial derived cytolysins (Hoshino et al., 1999; Poltorak et al., 1998; Qureshi et al., 1999).

Except TLR3, all TLRs use TIR-domain containing myeloid differentiation primary response 88 (MyD88) as an adaptor protein to initiate downstream signaling resulting in NF- κ B- and MAPK-mediated pro-inflammatory gene expression. TLR3 exclusively, and TLR4 as an additional signaling arm, utilize

TIR-domain-containing adapter-inducing interferon- β (TRIF) to induce cytokine expression through interferon regulatory factor 3/7 (IRF) and NF- κ B activation as well as cell death (Kawai & Akira, 2010).

To activate NF- κ B, TRIF interacts with RIPK1 via RHIM domain interaction and TRAF6 via a TRAF6 binding domain (Cusson-Hermance, Khurana, Lee, Fitzgerald, & Kelliher, 2005; Meylan et al., 2004). TRADD and the E3 ligase Pellino1 are recruited to RIPK1, and the latter one attaches K63-ubiquitin chains to RIPK1, thereby providing a platform for recruitment and activation of the TAK and canonical IKK complex to mediate MAPK and NF- κ B activation (Cusson-Hermance et al., 2005).

The TRIF-dependent signaling arm downstream of TLR3 and TLR4 is capable to induce apoptosis and necroptosis in order to eliminate infected host cells (Lamkanfi & Dixit, 2010). A preassembled complex called "Ripoptosome" containing TRIF, RIPK1, RIPK3, FADD, caspase-8, caspase-10 and cFLIP can induce apoptosis and necroptosis in some cell lines after TLR3 stimulation upon loss of IAPs, although the necessity for a direct interaction with TLR3 remains elusive (Feoktistova et al., 2011; Tenev et al., 2011). RIPK1 is the core component of the Ripoptosome and its kinase activity is required for apoptosis and necroptosis, whereas the type of cell death induced depends on the ratio of cFLIP isoforms within the complex (Feoktistova et al., 2011; Tenev et al., 2011). More recently, the sequential assembly of a similar machinery, additionally containing TRADD and TRAF2, directly to TLR3 in the presence of cIAPs was demonstrated. This TLR3-induced apoptosis is RIPK1 dependent and negatively regulated by the TRADD-TRAF2-cIAPs complex (Estornes et al., 2012). Likewise to TLR3, also TLR4 stimulation was reported to induce TRIF-dependent apoptosis through the downstream effectors RIPK1, FADD and caspase-8 (Ma, Temkin, Liu, & Pope, 2005; Ruckdeschel et al., 2004).

When caspase-8 activity is inhibited, TLR3 or TLR4 stimulation can induce RIPK3 mediated, TRIF- and RIPK1 kinase activity dependent necroptosis (He, Liang, Shao, & Wang, 2011; Kaiser et al., 2013; Polykratis et al., 2014). However, also RIPK1-independent necroptosis downstream of TLR3 has been reported, presumably mediated via a direct RHIM-mediated interaction between TRIF and RIPK3 (He et al., 2011; Kaiser et al., 2013). In contrast to

RIPK1, TRIF does not contain a kinase domain suggesting different mechanisms of RIPK3 activation by RIPK1 and TRIF (Chan et al., 2015). RIPK3 was shown to compete with RIPK1 for binding to the RHIM domain in TRIF and therefore RIPK3 can prevent TRIF/RIPK1 dependent NF- κ B activation (Meylan et al., 2004). In addition, TRIF was identified as a substrate for caspase-8 and its cleavage inhibited NF- κ B activation. However if cleavage of TRIF suppresses necroptosis is not known (Rebsamen, Meylan, Curran, & Tschopp, 2008). In summary, similar to TNFR1 signaling, TLR3/TLR4 signaling can have three distinct cellular outcomes; NF- κ B activation; apoptosis and necroptosis. However, the hierarchy of RHIM interactions between TRIF, RIPK1 and RIPK3 to determine cell fate are not known (Kaiser et al., 2013).

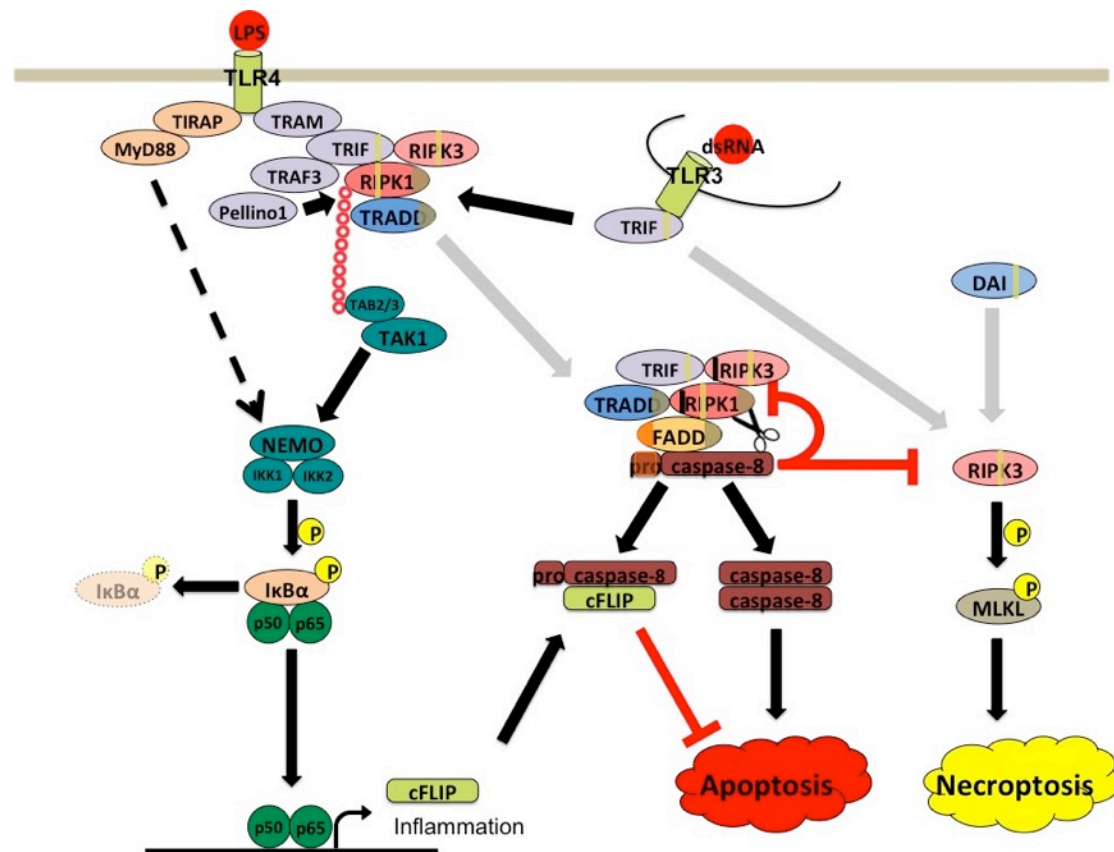


Figure 2 TLR3 and TLR4 induced signalling pathways.

LPS binding to TLR4 induces MyD88-dependent NF- κ B activation. TLR3- and TLR4-induced TRIF dependent NF- κ B activation requires RIPK1 TRADD, TRAF3 and Pellino1. Pellino1 modifies RIPK1 with K63-linked polyubiquitination chains (red rings) providing a scaffold for downstream NF- κ B activation. RIPK3 can negatively regulate TRIF-dependent NF- κ B activation. An apoptosis inducing complex containing TRIF, TRADD, RIPK1, RIPK3, FADD and caspase-8 can form after TLR3 and TLR4 stimulation. When caspase-8 activity is inhibited, TLR3 stimulation can induce RIPK1-dependent as well as RIPK1-independent RIPK3 and MLKL-mediated necroptosis. DAI can directly interact with RIPK3 via a RHIM interaction to induce necroptosis. For details see text.

Yellow stripes in TRIF, RIPK1 and RIPK3 represent RHIMs. Brown insets in RIPK1 and TRADD depict DDs. Black stripes in RIPK1 and RIPK3 represent caspase-8 cleavage sites. Orange insets in FADD and procaspase-8 illustrate DEDs.

Abbreviations: DAI, DNA-dependent activator of IRFs; FADD, Fas-associated via death domain; IKK1/2, inhibitor of κ B kinase 1/2; MLKL, mixed lineage kinase domain-like; MyD88, myeloid differentiation primary response gene 88; NEMO, NF- κ B essential modifier; P, phosphorylation; RIPK1/3, receptor interacting protein kinase 1/3; TAB2/3, TGF-beta activated kinase 1 binding protein 2/3; TAK1, TGF-beta activated kinase 1; TIRAP, TIR-domain containing adaptor protein; TNF, tumor necrosis factor; TNFR1, TNF receptor 1; TRADD, TNF receptor associated death domain; TRAF3, TNF receptor-associated factor 3; TRAM, TRIF-related adaptor molecule.

1.4.2 RIPK1 in other PRR signalling pathways

In addition to TLRs, viral nucleic acids sensing retinoic acid inducible gene I (RIG-I) and DNA-dependent activator of IFN-regulatory factors (DAI) also utilized RIPK1/RIPK3 for downstream signalling (Chan et al., 2015; Christofferson, Li, & Yuan, 2014).

Upon detection of viral RNA with its DExD/H-box RNA helicase domain, RIG-I recruits mitochondrial antiviral signalling (MAVS) via its caspase recruitment domains (CARD) domains. Subsequently, a mitochondrial complex containing RIPK1, FADD, TRADD, caspase-8 among other proteins is assembled to activate the downstream IKK complex for NF- κ B and IRF activation (Christofferson et al., 2014). The activity of the signaling complex is modulated indirectly by RIPK1 and its posttranslational modifications. Ubiquitination of RIPK1 at K377 is required for efficient virus-induced activation of IRF3 and NF- κ B. Caspase-8 negatively regulates the RIG-I response by cleaving RIPK1 at Asp324 to generate a 38 kDA fragment that mitigates IRF activation. The recruitment of caspase-8 to the RIG-I complex depends on the presence of RIPK1 and for its cleavage RIPK1 needs to be modified with polyubiquitin chains (Rajput et al., 2011).

DAI induces type I IFNs, NF- κ B activation and necroptotic cell death in response to double stranded viral DNA via RHIM interactions with RIPK1 and RIPK3. Both, RIPK1 and RIPK3, are required for full activation of NF- κ B, whereas necroptosis induced by DAI is independent of RIPK1 but requires RIPK3 (Rebsamen et al., 2009; Upton, Kaiser, & Mocarski, 2010, 2012).

1.5 Interferons and necrosome formation

Type I (predominantly α/β) and type II (γ) interferons (IFN) are pleiotropic cytokines with antiviral and immune-modulatory functions. While IFN α and β bind to IFN-I receptor, a heterodimer of two IFN- α receptor proteins (IFNAR1 and IFNAR2), IFN- γ signals through its heterodimeric receptor composed of IFN- γ receptor 1 (IFNGR1) and 2 (IFNGR2). Ligand binding activates several signaling pathways including NF- κ B, Phosphatidylinositol-4,5-bisphosphate 3-kinases (PI3Ks) and Janus-kinase (JAK)-signal transducers and activators of transcription (STAT)-pathway to induce the expression of target genes (Stark, Kerr, Williams, Silverman, & Schreiber, 1998). Type I and II IFNs activated protein kinase R (PKR) was proposed to induce necrosome formation in the absence of FADD or caspase activity (Robinson et al., 2012; Thapa et al., 2011; Thapa et al., 2013). PKR mediates the phosphorylation of RIPK1 and thereby induces RIPK1-RIPK3-dependent necroptosis, which under steady state conditions is licensed by binding of phosphorylated FADD to RIPK1 (Thapa et al., 2013). However, a recent study demonstrated no defects in IFN- γ induced necroptosis in PKR deficient macrophages (McComb et al., 2014). Moreover, TNF, LPS and poly(I:C) triggered necroptosis in macrophages depends on IFNAR1-IFN-stimulated gene factor 3 (ISGF3) signaling, indicating the requirement of an autocrine loop of IFN α and β for the execution of RIPK1-RIPK3 dependent necroptosis (McComb et al., 2014).

1.6 Anatomy of the intestinal tract

The intestinal tract is divided into the small intestine and the large intestine, also called colon. The small intestine stretches from the pylorus to the ileocaecal valve, and is subdivided (from cranial to caudal) into the duodenum, jejunum and the ileum. The colon starts at the caecum, followed by the ascending colon, descending colon, and the rectum. The primary function of the intestinal tract is the digestion of food, absorption of nutrients, reabsorption of water, whereas the latter mainly occurring in the colon.

The gastrointestinal wall is composed of the serosa/adventitia, muscularis externa, submucosa and the mucosa (from the outside to the inside), separating the intestinal lumen from the abdominal and pelvic cavity. The

serosa or adventitia consists of connective tissue and squamous epithelium to reduce frictional forces for surrounding organs during peristaltic movements. Within the serosa/adventitia lies the muscularis externa, which is formed by two smooth muscle layers, the outer longitudinal and inner circular muscle, both responsible for peristalsis, the unidirectional transport of luminal content towards the anus. The underlying submucosa is a layer of connective tissue containing blood vessels, lymphatic vessels and nerves branching into the muscularis externa and mucosa. The mucosa is the innermost layer and can be divided into three different parts: First, the muscularis mucosa, a smooth muscle layer separating the mucosa and the submucosa, second, the lamina propria, a layer of connective tissue containing nerve endings, capillaries, lymph nodes and vast numbers of immune cells, and third, the intestinal epithelium.

1.7 Structure and function of the intestinal epithelium

The intestinal epithelium is a monolayer of polarized epithelial cells that provide a physical and biochemical border separating the mucosal immune cells from the contents of the lumen. Instead of being a passive nutrient-absorbing barrier, intestinal epithelial cells (IECs) perform diverse functions crucial for homeostasis, such as mediating selective transport, regulating barrier integrity, influencing microbial colonization, sampling the luminal microenvironment for antigens as well as beneficial and pathogenic microbes and fulfilling immunomodulatory functions. Moreover, IECs do not only function in an intrinsic fashion, but are part of a coordinated relationship between subepithelial immune cells and the intestinal microbiota (Maloy & Powrie, 2011).

To keep this delicate system at balance, different regions of the intestinal epithelium evolved different anatomical architectures and highly specialized epithelial cells types, adapted to the distinct physiological functions. The small intestine is organized into the crypts of Lieberkühn, epithelial invaginations into the underlying connective tissue that harbor pluripotent intestinal stem cells as well as transient amplifying (TA) cells, and epithelial protrusions into the lumen, called villi, which drastically increase the surface area for nutrient absorption. In contrast, the colon lacks villi and has a flat surface epithelium

but shares the organisation into stem cell and TA cell compartments (Figure 3) (van der Flier & Clevers, 2009). The intestinal epithelium has the highest turnover rate of all tissues in adult mammals with IECs being renewed every 4 to 5 days (van der Flier & Clevers, 2009). Self-renewal is orchestrated by Lgr5 expressing stem cells, also called crypt base columnar cells (CBC), residing at the bottom of the crypts, which divide asymmetrically once per 24 h (Barker et al., 2007; Cheng & Leblond, 1974). They give rise to one stem cell residing in the crypt and a transient amplifying (TA) cell that migrates upwards to the crypt/villus border while it undergoes 4 to 5 rounds of cell division. During this time, IEC progenitors start to differentiate and reach the villus border after 2 days as mature epithelial cells, whereas they continue to migrate upwards the crypt-villus axis. The cell fate and proliferative capacity of differentiating progenitor cells is determined by the activity or repression of various signaling pathways, such as Wnt-, Notch-, bone morphogenetic protein (BMP)- and Hedgehog signaling (Barker, Bartfeld, & Clevers, 2010; Crosnier, Stamatakis, & Lewis, 2006; van der Flier & Clevers, 2009). In general, differentiated intestinal epithelial cells can be divided into two groups, absorptive and secretory cell lineages. Absorptive enterocytes are the most prevalent cell type in the intestinal epithelium and account for more than 80% of all IECs. They have an apical brush border and are responsible for uptake and transport of nutrients across the epithelium (van der Flier & Clevers, 2009). Enteroendocrine cells belong to the secretory lineages, make up less than 1% of IECs and are scattered throughout the epithelium. They coordinate and modulate gut function by secreting hormones, such as gastrin, motilin or cholecystokinin. Goblet cells are the most prominent secretory cell lineage in the intestinal epithelium and their occurrence increases from the duodenum (4%) to the descending colon (16%) (van der Flier & Clevers, 2009). They produce secretory mucus glycoproteins (mucins), trefoil factor peptides (TFF) and other proteins that are the major components of the upper and lower mucus layer. The mucus layer provides protection against mechanical forces that emerge during movement of luminal content and importantly, limit or completely prevent microbial colonization in the outer and inner mucus layer respectively (Y. S. Kim & Ho, 2010). Paneth cells secrete antimicrobial peptides (AMP), for instance lysozyme P and α -defensins, into the lumen of

the small intestinal crypts to keep them free of microbes. As these AMPs diffuse into the mucus layer, they help to shape the composition of the residential microbiota and prevent infections by pathogens (Bevins & Salzman, 2011; Brandl, Plitas, Schnabl, DeMatteo, & Pamer, 2007; Cash, Whitham, Behrendt, & Hooper, 2006; Mukherjee, Vaishnava, & Hooper, 2008; Salzman, Ghosh, Huttner, Paterson, & Bevins, 2003). During differentiation, Paneth cells escape upward migration and instead, move to the bottom of the crypt where they reside. With a life expectancy of 6 to 8 weeks, they are the most long-lived differentiated cell lineage within the intestinal epithelium (Barker et al., 2010).

Except for Paneth cells, differentiated cells continuously migrate upwards along the crypt-villus axis until they reach the tip of the villus after 3-5 days (Barker et al., 2010; van der Flier & Clevers, 2009). Here they detach and are exfoliated into the lumen. Although shedding cells show morphological features of apoptosis, it was shown that IEC death induced by loss of cell contacts, called anoikis, is a caspase independent process (Eisenhoffer et al., 2012; Hall, Coates, Ansari, & Hopwood, 1994; Shibahara et al., 1995). However, the precise mechanisms regulating anoikis are unknown (Vereecke, Beyaert, & van Loo, 2011).

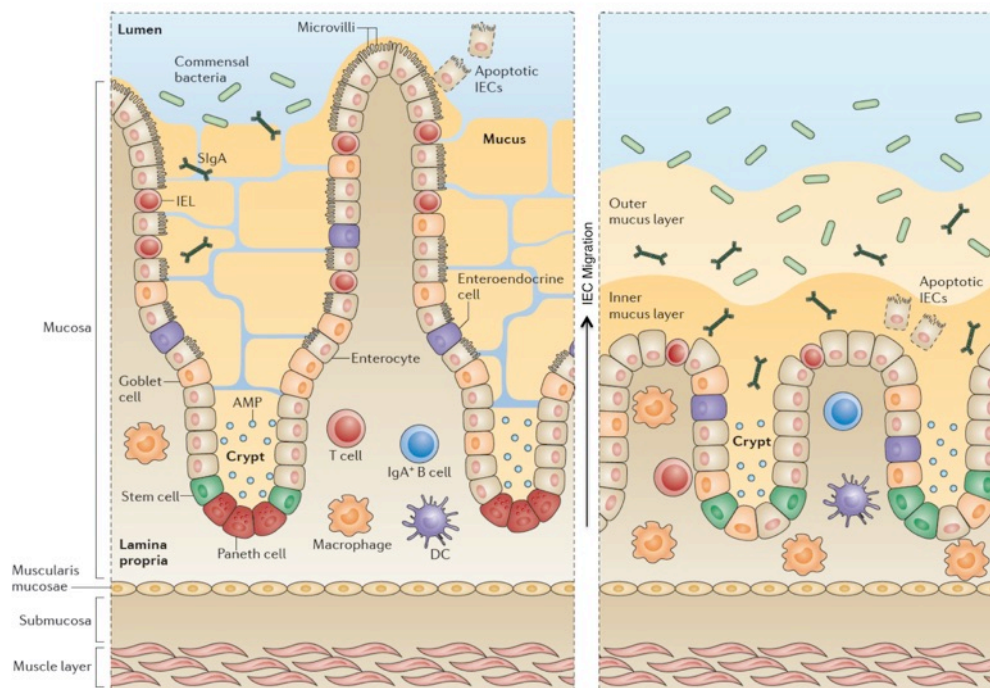


Figure 3 Structure of the small intestinal and colonic epithelium.

The intestinal epithelium forms a monolayer of polarized epithelial cells covered with mucus and separates luminal contents and immune cells in the lamina propria. In the small intestine (SI) (left) and colon (right)

epithelial invaginations called crypts contain rapidly proliferating stem cells and progenitor cells. Small intestinal crypts are additionally populated by Paneth cells, which secrete anti-microbial peptides (AMP) and contribute to the maintenance of the stem cell niche. Epithelial protrusions in the SI called villi, harbour differentiated intestinal epithelial cell lineages, which include nutrient absorbing enterocytes, hormone secreting enteroendocrine cells and mucus secreting goblet cells. Mucus enriched in AMPs and secretory IgA (SIgA) prevents close contact between commensals or pathogens with intestinal epithelial cells. Abbreviations: DC, dendritic cell; IEL, intraepithelial lymphocyte. **Modified from (Mowat & Agace, 2014).**

1.8 Cell death and immunity in the intestinal epithelium

The ratio between proliferation, differentiation and cell death within the intestinal epithelium has to be tightly regulated. Increased proliferation or defects in the execution of cell death are associated with the development of colorectal cancer (CRC) (Grivennikov, Greten, & Karin, 2010). On the other hand, excessive or uncontrolled cell death might result in compromised barrier integrity. This would allow an uncontrolled translocation of immunoreactive luminal antigens into the lamina propria and a direct contact with mucosal immune cells triggering an inflammatory response. Indeed, increased cell death and dysregulated barrier function has been implicated in the aetiology and pathology of inflammatory bowel disease (IBD) and its two major clinical forms, Crohn's Disease (CD) and Ulcerative Colitis (UC) (Maloy & Powrie, 2011; Peterson & Artis, 2014; Roda et al., 2010). However, signaling pathways that regulate epithelial cell death are also involved in the maintenance of intestinal homeostasis and consequently need to be tightly balanced.

IECs express various PPR such as TLRs, NLRs, RIG-I like receptors, on their basolateral and apical membranes (Takeuchi & Akira, 2010). Therefore, IECs show basal levels of NF- κ B activation with protective effects including epithelial cell proliferation, IgA production, barrier stability and antimicrobial responses, but without inducing an inflammatory response (Abreu, 2010; Rakoff-Nahoum, Hao, & Medzhitov, 2006; Rakoff-Nahoum, Paglino, Eslami-Varzaneh, Edberg, & Medzhitov, 2004).

The importance of TLR- and MyD88 dependent signaling is demonstrated by studies with knockout mice in experimental colitis. For instance, *Myd88*^{-/-}, *Tlr2*^{-/-} as well as *Tlr4*^{-/-} mice showed more severe intestinal pathology and

increased mortality in response to DSS induced colitis (Rakoff-Nahoum et al., 2004).

During homeostatic conditions, TLR4 is expressed at low levels in IECs and located at the apical side (Abreu et al., 2001; Fukata et al., 2007; Lavelle et al., 2010). However, patients with IBD showed increased *Tlr4* mRNA levels, which are suspected to cause increased sensitivity towards the microbiota and induce epithelial cell death (Abreu et al., 2001; Cario, 2013; Cario & Podolsky, 2000; Frolova, Drastich, Rossmann, Klimesova, & Tlaskalova-Hogenova, 2008; Hausmann et al., 2002). In line with this, TLR4 was shown to contribute to necrotizing enterocolitis (NEC) by inducing enterocyte apoptosis as well as inhibiting enterocyte migration and proliferation. Accordingly, TLR4 deficiency protected newborn mice from NEC, although the molecular mechanisms of TLR4 mediated IEC death remain elusive (Hackam, Afrazi, Good, & Sodhi, 2013; Leaphart et al., 2007; Sodhi et al., 2010). In the context of intestinal infection models, full body TLR4 deficiency is associated with impaired clearance after infection with *Salmonella typhimurium* or *Escherichia Coli*, although both studies focused on the importance of TLR4 induced cytokine production by subepithelial immune cells to fight the infection (Vazquez-Torres et al., 2004; Weiss, Raupach, Takeda, Akira, & Zychlinsky, 2004).

TLR3 is expressed at low levels in IECs of lactating mice and expression levels increase strongly during postnatal development (Pott & Hornef, 2012). Infection of mice with rotavirus or injection of its synthetic analog polyinosinic-polycytidylic acid (poly(I:C)) induced TLR3-TRIF dependent IEC apoptosis, villus shortening and antiviral gene response (McAllister et al., 2013; Pott & Hornef, 2012; A. Sato et al., 2006; R. Zhou, Wei, Sun, & Tian, 2007). However, a different study reported that IFN- β production in response to rotavirus infection is mediated by RIG-I-MAVS signaling and independent of TLR3 and TRIF (Broquet, Hirata, McAllister, & Kagnoff, 2011).

Beside its protective effect, aberrant TLR3 and TLR4 mediated signaling can induce IEC death and thereby contribute to intestinal pathology, although the molecular mechanisms of IEC death in the different models remain unknown.

Death receptor ligands, in particular TNF, are potent regulators of cell death and inflammatory responses. In the intestinal tract the main sources of TNF are macrophages, Th17 cells and IECs (Nazli et al., 2010; Sanchez-Munoz, Dominguez-Lopez, & Yamamoto-Furusho, 2008; Taylor, Dzus, & Colgan, 1998; Zachrisson, Neopikhanov, Samali, & Uribe, 2001). IECs express TNFR1 and therefore can respond to TNF by promoting inflammation and cell survival or undergo cell death (Lau et al., 2011; Strater & Moller, 2000). Intraperitoneal injection of TNF into wildtype mice caused villi shortening due to exfoliation of dying epithelial cells. However, TNF injection did not cause intestinal inflammation, presumably because of TNF-induced rearrangements of cell junctions (Marchiando et al., 2011; Marchiando et al., 2010; McAllister et al., 2013; Piguet, Vesin, Guo, Donati, & Barazzone, 1998; Williams et al., 2013). On the other hand, overexpression of TNF induces transmural intestinal inflammation primarily mediated by TNF responsiveness of bone marrow and parenchymal cells (Armaka et al., 2008; Kontoyiannis, Pasparakis, Pizarro, Cominelli, & Kollias, 1999). Moreover, intestinal epithelial specific overexpression of TNF induces a similar intestinal pathology, however IECs are not the initiating responders to TNF causing intestinal inflammation (Roulis, Armaka, Manoloukos, Apostolaki, & Kollias, 2011). TNF is considered as a major driver of pathogenesis in IBD, since patients show increased levels of TNF in areas with disease manifestation (Arijs et al., 2009; Braegger, Nicholls, Murch, Stephens, & MacDonald, 1992; Breese et al., 1994; Komatsu et al., 2001; MacDonald, Hutchings, Choy, Murch, & Cooke, 1990; Reimund et al., 1996). Furthermore, anti-TNF treatment is used as an effective therapy for IBD (Hanauer et al., 2002; Hanauer et al., 2006; Sandborn et al., 2007; Sandborn et al., 2001). Finally, an IBD susceptibility locus encompassing the *Tnf* gene has been identified in genome wide association studies (GWAS) (Dechairo et al., 2001; Hampe et al., 1999; Rioux et al., 2000).

Many genes known for their contribution to intestinal homeostasis, such as *Nod2*, *Tlr4*, *Atg16l* and *Tnfaip3*, have been identified as susceptibility loci for IBD development (Kaser, Zeissig, & Blumberg, 2010; Pott & Hornef, 2012). Some of these susceptibility genes exert their function at least partially via

NF- κ B signaling. Genetic studies in mice demonstrated the importance of intestinal epithelial NF- κ B signaling for the maintenance of homeostasis. For instance, mice with intestinal epithelial specific ablation of TAK1, NEMO or both, IKK1 and IKK2 show excessive IEC apoptosis and develop spontaneous colitis (Kajino-Sakamoto et al., 2008; Nenci et al., 2007). NEMO-deficient IECs died by TNF-induced apoptosis that result in compromised barrier integrity. Subsequently, bacteria are able to translocate into the mucosa where they activate immune cells. Activated immune cells in turn trigger colitis. Consequently, blocking TNF- or MyD88-dependent signaling protected NEMO^{IEC-KO} mice from developing colitis (Nenci et al., 2007). The death of NEMO-deficient IECs can only partially be attributed to canonical (p65-dependent) NF- κ B activation, since mice with IEC-specific deletion of p65 do not phenocopy NEMO^{IEC-KO} mice. These mice show slightly elevated levels of IEC death and intestinal disease with low penetrance but increased susceptibility to DSS induced colitis (Steinbrecher, Harmel-Laws, Sitcheran, & Baldwin, 2008). In addition, interference with the cell death machinery regulating extrinsic apoptosis can cause intestinal pathology as well. Intestinal epithelial cell specific deletion of cFLIP results in embryonic lethality, suggesting an important role for cFLIP during gut development (Wittkopf et al., 2013). Induced deletion of cFLIP in IECs of adult mice resulted in rapid mortality as a consequence of massive epithelial cell apoptosis and intestinal inflammation. cFLIP-deficient IECs were highly susceptible to TNF- and FAS-induced RIPK3-independent apoptosis, supporting a role of cFLIP as negative regulator of caspase-8 activity (Wittkopf et al., 2013). Inhibition of extrinsic apoptosis by intestinal epithelial specific caspase-8 or FADD ablation caused spontaneous caspase-independent death of IECs. Interestingly, although functionally dependent on each other, FADD deficiency triggers colitis, enteritis and Paneth cell death, whereas mice lacking caspase-8 develop enteritis accompanied by Paneth cell loss, but no colitis (Gunther et al., 2011; Welz et al., 2011). The reason for this phenotypic difference is unknown, but could be attributed to additional functions of FADD in controlling intestinal homeostasis. Development of colitis but not enteritis and Paneth cell death in FADD^{IEC-KO} mice depends on TNF, the microbiota and was ameliorated by additional deletion of CYLD (Welz et al., 2011). Caspase-8 deficiency

sensitized IECs to TNF, poly(I:C) and LPS induced death resulting in death of mice (Gunther et al., 2015). Interestingly, LPS induced death by triggering TNF production in non-epithelial cells rather than directly acting on IECs to induce TLR4 mediated signaling in IECs (Gunther et al., 2015). Both, FADD and caspase-8 deficient IECs died by RIPK3 dependent necroptosis, indicating an important role of FADD and caspase-8 as negative regulators of necroptosis *in vivo*.

As described in the previous chapters, RIPK1 is a constituent of the same death-inducing complexes. Nevertheless, its role in the intestinal epithelium is remains unknown.

In summary, signaling pathways controlling intestinal homeostasis require a tight regulation and dysfunction is associated with intestinal pathology. Although extrinsic apoptosis or necroptosis *per se* are not required for gut development and epithelial renewal, a functional cell death machinery is necessary to prevent excessive epithelial death and inflammatory disorders. However, the detailed mechanisms regulating cell death or survival require further investigation.

1.9 Cre/LoxP conditional gene targeting

Cell type specific analysis of gene function in mice can be achieved using Cre/LoxP mediated recombination for conditional genes. Furthermore, Cre/LoxP mediated recombination allows the study the function of genes essential for embryonic development. In order to generate a conditional knockout allele, two specific 34 bp DNA sequences, called “LoxP” sites, are inserted in the same orientation to flank the desired gene locus or particular exons of interests. An allele carrying LoxP sites is called ‘floxed’ (FL) and mice carrying conditional alleles referred to as “floxed” mice. These floxed mice are crossed to mice expressing a bacteriophage P1-derived Cre recombinase under the control of a tissue specific promoter. Only in Cre expressing cells, LoxP sites are recognized and recombined by Cre, resulting in the excision of the floxed DNA fragment and an inactivation of the gene of interest.

1.10 Project description

The intestinal epithelium is a monolayer of cells with an exceptional high homeostatic cell turnover in highly balanced and complex processes to ensure barrier integrity. Several signaling pathways, such as NF- κ B, are implicated in maintaining homeostasis. Excessive IEC death, for instance caused by disturbance of these pathways, can result in compromised barrier integrity, allowing a direct interaction between luminal antigens and sub-epithelial immune cells resulting in intestinal inflammation.

RIPK1 serves as a central signaling node in cytokine and PRR signaling pathways at the crossroad to induce pro-survival signaling or apoptosis as well as necroptosis. However, the function of RIPK1 *in vivo* in epithelial tissues remains largely unknown. In this study, Cre/LoxP conditional gene targeting was employed to generate mice with intestinal epithelial cell specific ablation of RIPK1, enabling to investigate the function of RIPK1 specifically in intestinal epithelial cells *in vivo*.

2. Material and Methods

2.1 Material

2.1.1 Chemicals

Chemicals and compounds were purchased from AppliChem (Darmstadt, Germany), Corning (Corning, NY, United States), DAKO (Santa Clara, CA, United States), GE Healthcare (Chalfont St Giles, Great Britain), Merck (Darmstadt, Germany), Qiagen (Hilden, Germany), Roche (Basel, Switzerland), Roth (Karlsruhe, Germany), Sigma Aldrich (München, Germany), ThermoFisher Scientific (Waltham, MA, United States), VWR (Radnor, PA, United States).

2.1.2 Material for mouse work

Syringes, Braun

Injection needles, Braun

Ampicillin, ICN Biomedicals

Ciprofloxacin, Fluka

Meronem, AstraZeneca

Neomycin, Sigma

Vancomycin, Eberth

Tamoxifen, Sigma

Dimethylsulfoxid, PAN Biotech GmbH

Cornoil, Sigma

2.1.3 Material for histology

Tissue retriever 2100, PickCell

Tissue processor, Leica TP1020

Rotary Microtome, Leica RM2255

Modular tissue embedding center, Leica EG1150 and Leica EG1150C

Microscope, Leica DM5500B

ABC Kit Vectastain Elite (Vector, PK 6100)

Avidin/Biotin Blocking Kit (Vector, SP-2001)

Liquid DAB Substrate Chromogen System (DakoCytomation, Code K3466 and Vector, ImPACT™ DAB SK-4105)

Normal goat serum, Vector Laboratories

Entellan, Merck

Glass slides, Menzel

Cover slides, Menzel

2.1.4 Material for biochemistry

Homogenizer Precellys 24, PeqLab

2 ml tubes for homogenisation, PeqLab

1,4 mm Zirconium oxide beads for tissue homogenisation, PeqLab

Gel casting system and SDS-Page system, Biorad

Power supply, Biorad

Protease Inhibitor Cocktail complete mini EDTA free, Roche

Phosphatase inhibitor, PhosphoStop, Roche

Bradford reagent, Biorad

Protein Marker PeqGold Protein Marker V, PeqLab

PVDF membranes Immobilon-P, Millipore

Films Hyperfilm ECL, Amersham

Super RX, Fujifilm

2.1.5 Molecular biology reagents and equipment

Trizol reagent, Invitrogen

RNA extraction RNeasy mini kit, Qiagen

RNase-free DNase set Qiagen

Super scriptIII cDNA synthesis Kit, Invitrogen

RT Cycler ABI HT 7900 Cycler, Applied Biosystems

Power SYBR® Green PCR Master Mix, Applied Biosystems

TaqMan® Gene Expression Master Mix, Applied Biosystems

MicroAmp® Optical Adhesive Film, Applied Biosystems

MicroAmp™ Optical 384-Well Reaction Plate, Applied Biosystems

2.1.6 Laboratory equipment

Centrifuges, Eppendorf and Haereus

Thermomixer, Eppendorf

PCR-cyclers, Biorad DNA Engine, Biometra and Eppendorf

DNA ladder, PeqLab
Primers, Invitrogen and Metabion
Bio Photometer, Eppendorf
NanoDrop ND8100, PeqLab

2.1.7 Cell culture

Plastic ware for cell culture from BD Falcon, Millipore, TPP, Corning Tubes
Eppendorf 1,5 ml and 2 ml reaction tubes
Advanced DMEM/F12, Gibco
DPBS, Gibco
Fetal Calf Serum, PAN
100x Penicillin (10000 U/ml)/Streptomycin (10000 µg/ml), Gibco
100x L-Glutamine (200 mM), Gibco
HEPES (1 M), Invitrogen
B27, Invitrogen
N2, Invitrogen
N-Acetylcysteine, Sigma-Aldrich
R-Spondin, RandD Systems
Noggin, Peprotech
mEGF, Invitrogen Biosource
Matrigel, Corning
4-Hydroxytamoxifen, Sigma
Ethanol, VWR
TNF, University of Ghent
Poly(I:C), Amersham
hIFN-β, peprotech
mIFN-γ, Immunotools
zVAD-fmk, Enzo

2.1.8 Software

Photoshop CS3, Leica microscopy Software Leica application suite, Prism
Graph, Microsoft Office., FACSDiva, FlowJo

2.1.9 Buffers and solutions

2.1.9.1 Washing buffers

PBS (1x) pH 7,3

NaCl	137 mM
KCl	2.7 mM
Na ₂ HPO ₄ -7H ₂ O	4.3 mM
KH ₂ PO ₄	1.4 mM

TBS (1x) pH 7,5

Tris-Base	24.2 g
NaCl	80g

2.1.9.2 Buffers and solutions for immunostainings

Endogenous peroxidase blocking buffer (for IHC)

NaCitrate	0.04 M
Na ₂ HPO ₄	0.121 M
NaN ₃	0.03 M
H ₂ O ₂	3% (v/v)

Antigen retrieval buffer, Citrate buffer, pH 6.0

NaCitrate	10 mM
Tween-20	0.05% (v/v)

Antigen retrieval buffer, TEX Protease K buffer, pH 8.0 (for protease mediated antigen retrieval)

Tris-Base	50 mM
EDTA	1 mM
Triton X-100	0.5% (v/v)

2.1.9.3 Preparation of protein extracts

High salt RIPA lysis buffer

HEPES (pH 7.6)	20 mM
NaCl	350 mM

MgCl ₂	1 mM
EDTA	0.5 mM
EGTA	0.1 mM
Glycerol	20% (v/v)

1% Nonident P-40, Protease inhibitor and Phosphatase inhibitors were added prior to use.

Cytoplasmic and nuclear protein extraction buffers

Buffer A (hypotonic lysis buffer)

HEPES (pH 7.6)	10 mM
KCl	10 mM
MgCl ₂	2 mM
EDTA	0.1 mM

Protease inhibitor and Phosphatase inhibitors were added prior to use.

After swelling 0.8% (v/v) Nonident P-40 was added.

Buffer C (high salt nuclear lysis buffer)

HEPES (pH 7.8)	50 mM
KCl	50 mM
NaCl	300 mM
EDTA	0.1 mM
Glycerol	10% (v/v)

Protease inhibitor and Phosphatase inhibitors were added prior to use.

2.1.9.4 Buffers and solutions for Western Blot analysis

Tris-glycine electrophoresis buffer

Tris-Base	25 mM
Glycine	250 mM
SDS	0.1% (w/v)

SDS-polyacrylamide gel

10% resolving gel (for 20 ml)

H ₂ O	7.9 ml
30% acrylamide mix	6.7 ml
1.5 M Tris (pH 8.8)	5.0 ml

10% (w/v) SDS	0.2 ml
10% (w/v) APS	0.2 ml
TEMED	0.012 ml

5% stacking gel (for 10 ml)

H ₂ O	6.8 ml
30% acrylamide mix	1.7 ml
1 M Tris (pH 6.8)	1.25 ml
10% (w/v) SDS	0.1 ml
10% (w/v) APS	0.1 ml
TEMED	0.01 ml

Transfer buffer (for semidry and wet transfer)

Tris-Base	25 mM
Glycine	192 mM
Methanol, pH 8.3	20% (v/v)

Blocking buffer

Tween-20	0.1% (v/v)
nonfat dry milk	5% (w/v)
in PBS	

Primary and secondary antibody dilution buffer

Tween-20	0.1% (v/v)
Nonfat dry milk or BSA	5% (w/v)
in TBS	

5x Laemmli loading buffer

Tris-HCl (pH 6.8)	250 mM
SDS	10% (w/v)
Glycerol	50% (v/v)
Bromphenolblue	0.01%
β-Mercaptoethanol	10%

2.1.9.5 Buffers for DNA extraction and genotyping PCRs

Tail lysis buffer

Tris-HCl (pH 8.5)	100 mM
EDTA	5 mM
NaCl	200 mM
SDS	0.2% (w/v)

0.1 mg Proteinase K (10 mg/ml in 50 mM Tris, pH 8.0) per 100 µl lysis buffer was added prior to use.

TE buffer

Tris-HCl (pH 8)	10 mM
EDTA (pH 8)	1 mM

10x TAG buffer

Tris-Base (pH 8.5)	200 mM
KCl	500 mM

TAE buffer (25x) for 10 l

Tris-Base (pH 8.5)	1210 g
EDTA (pH 8.0)	500 ml of 0.5 M solution
Acetic acid	285.5 ml

2.1.9.6 Buffers for 3D intestinal epithelial cell culture**Complete medium without growth factors (CM-GF)**

Advanced DMEM/F12	500 ml
Glutamax 100x	5 ml
HEPES (1M)	5 ml
Pen/Strep	5 ml

Complete medium with growth factors (CM+GF)

CM-GF	50 ml
B27 (50x)	1 ml
N2 (100x)	0.5 ml
n-Acetylcysteine	0.125 ml (of 500 mM stock)

ENR (EGF, Noggin, R-Spondin)

CM+GF	78 μ l
EGF	2 μ l (of 500 μ g/ml stock)
Noggin	10 μ l (of 100 μ g/ml stock)
R-Spondin	10 μ l (of 100 μ g/ml stock)

2.2 Methods

2.2.1 Animal handling and mouse experiments

2.2.1.1 Mouse maintenance

Mice were maintained in a conventional animal facility in individually ventilated cages (IVC) in a specific pathogen free (SPF) mouse facility in the Institute for Genetics and the CECAD Research Center at the University of Cologne. Mice were kept under a 12 hours light/dark cycle, given acidified water and a regular chow diet (Teklad Global Rodent 2018, Harlan) *ad libitum*.

For breeding, male and female mice were placed together into one cage at a minimum age of eight weeks. Litters marked with an eartag at 2-weeks of age and tail biopsies were taken at the same age for isolation of genomic DNA and genotyping. Litters were weaned with an age of three weeks.

Care of all mice was within institutional animal care committee guidelines. Animal procedures were conducted in accordance with European, national and institutional guidelines. All protocols were approved by local government authorities (Landesamt für Natur, Umwelt und Verbraucherschutz Nordrhein-Westfalen, Germany). Animals requiring medical attention were provided with appropriate care and excluded from the experiments described. No other exclusion criteria existed.

Germ-free mice were produced by embryonic transfer into the gnotobiotic facilities at the University of Ulm and of the Hannover Medical School.

2.2.1.2 Generation of conditional and full body knockout mice

To generate mice with a deletion of RIPK1 specifically in the intestinal epithelium (RIPK1^{IEC-KO} mice), *Ripk1^{fl/fl}* mice were crossed with villin Cre transgenic mice (Madison et al., 2002). *Ripk1^{fl/fl}* mice were generated as described in 3.1 and backcrossed in a C57BL/6 background for 10 generations. RIPK1^{IEC-KO} mice were crossed to *Fadd^{fl/fl}* mice (Mc Guire et al., 2010), *Myd88^{-/-}* mice (Adachi et al., 1998), *Tnfr1^{-/-}* mice (Pfeffer et al., 1993), *Trif^{fl/fl}* mice (Dannappel et al., 2014), R26IKK2ca^{sfl/sfl} (Sasaki et al., 2006) or *Ripk3^{-/-}* mice (Newton, Sun, & Dixit, 2004) to generate double or triple deficient mice. All mice were analysed at 3 weeks of age unless otherwise

indicated. For all experiments littermates not carrying the villin Cre transgene were used as control mice.

2.2.1.3 Generation of inducible conditional knock-out mice

To generate mice with a tamoxifen-inducible conditional RIPK1 allele in the intestinal epithelium, *Ripk1^{fl/fl}* mice were bred with VillinCreER^{T2} transgenics (el Marjou et al., 2004). VillinCreER^{T2} recombinase activity was induced by three daily intraperitoneal injections of 1 mg tamoxifen dissolved in DMSO/cornoil in 100 µl total volume. Vehicle-treated control mice received three daily intraperitoneal injections of DMSO in cornoil. Littermates only carrying loxP flanked *Ripk1* alleles served as control mice for all experiments.

2.2.1.4 Antibiotic treatment and germ-free mice

For depletion of the intestinal microbiota, RIPK1^{IEC-KO} mice were treated with two different mixtures of broad spectrum antibiotics supplied through the drinking water starting from embryonic day (E)17.5. To achieve efficient microbiota depletion, two different antibiotic mixtures were applied. One antibiotics regimen consisted of a mixture containing 1g/l ampicillin, 1 g/l neomycin, 0.5 g/l ciprofloxacin and 0.5 g/l meronem and was administered until weaning. After weaning, ciprofloxacin was replaced by 0.5 g/l vancomycin. The second antibiotic cocktail consisted of 1 g/l ampicillin, 1 g/l metronidazole, 0.2 g/l ciprofloxacin and 0.5 g/l vancomycin. As neither the overall physiological response nor the tissue pathology differed between the two regimens, mouse groups receiving either antibiotic mixture were analyzed together and data from individual experiments were pooled.

For antibiotic treatment of VillinCreER^{T2}/*Ripk1^{fl/fl}* mice, 1g/l ampicillin, 1 g/l neomycin, 0.5 g/l meronem and 0.5 g/l vancomycin was given for 4 weeks prior administration of tamoxifen (see 2.2.1.3).

In all cases, drinking water with antibiotics was exchanged every second day and mice were transferred into a new cage. In order to check the efficiency of microbiota depletion, homogenized feces (10 mg feces in 100 µl in LB medium) were plated on agar plates in serial dilutions.

Germ-free mice were generated by embryonic transfer into the gnotobiotic facilities at the University of Ulm and of the Hannover Medical School. Survival of germ-free RIPK1^{IEC-KO} mice was monitored at the Hannover Medical School by daily inspection. Mice were sacrificed and dissected when medical attention was required.

2.2.1.5 Preparation of tissue biopsies

Mice were euthanized by cervical dislocation or decapitation.

2.2.1.6 Tissue preparation

After euthanasia, the abdominal cavity was opened by a longitudinal incision. The colon and small intestine were removed by one cut near the anus and a second cut after the pylorus. The intestine was washed in PBS, mesentery, fat and luminal content were removed. A small piece of about 5 mm length from the distal colon and ileum was collected for RNA extraction. For histological examination, the remaining colon and ileum were cut open longitudinally and rolled up lengthwise with the help of injection needles to form a so called "swiss-rolls".

2.2.1.7 Isolation and FACS analysis of lamina propria immune cells

Immune cells of the colon and lamina propria were isolated as described previously (Klose et al., 2013). In brief, the mice were euthanized and the colon and/or small intestine were collected as described in sections 2.2.1.5 and 2.2.1.6. The intestines were washed in ice-cold PBS, remaining fat and Peyer's Patches were removed, and the intestines were opened longitudinally. To remove epithelial cells, intestines were incubated in 1xHBSS containing 5 mM EDTA and 10 mM HEPES at 37°C for 15 min under agitation. The supernatant was removed and this procedure was repeated twice. Afterwards, the tissue was chopped into pieces and incubated in HBSS supplemented with 4% FCS, Dispasell (0.15 mg ml⁻¹; Roche), Collagenase D (0.4 mg ml⁻¹; Roche) and DNaseI (0.5 mg ml⁻¹; Sigma Aldrich) in order to digest the tissue. Isolated immune cells were purified by Percoll gradient centrifugation (GE Healthcare LifeScience). Isolated immune cells were incubated with CD16/CD132 antibody (BD Biosciences) for 15 min to block Fc

receptors. In order to so stain for the individual immune cell subpopulations, the cells were incubated with the following antibodies for 30 min on ice: CD3e (145-2C11), CD11b (M1/70), CD45.2 (104), Ly6G (1A8), B220 (RA3-6B2), F4/80 (BM8) (BD Biosciences). Afterwards, stained immune cells were analyzed with a BD FACS Canto I (BD Biosciences) using FACSDiva software. Experiments were analyzed with FlowJo software (Tristar). Isolation of lamina propria immune cells was performed by/under supervision of Dr. Christina Eftychi.

2.2.2 Histology

2.2.2.1 Preparation of intestinal tissue for histological analysis

For histological examination the tissue was transferred into histology cassettes and fixed in 4% paraformaldehyde overnight at 4°C. For dehydration the samples were passed through increasing concentrations of ethanol (2 h for each in 30% (v/v), 50% (v/v), 70% (v/v), 96% (v/v) and 2 times in 100% (v/v) ethanol). Subsequently, samples were incubated twice for 2 h in xylol and then transferred to liquid paraffin for embedding in paraffin blocks. The tissue was sectioned at 3-4 µm thickness, mounted on glass slides and dried overnight at 37°C.

2.2.2.2 Hematoxylin and Eosin staining

For deparaffinisation tissue sections were placed in xylol for 20 min. Rehydration was performed by placing the slides in descending series of ethanol solutions for 2 min each (100% (v/v), 96% (v/v), 75% (v/v) ethanol) and washed for 5 min in tap water. The sections were stained in Meyer's Hematoxylin for 1 min, differentiated in tepid water for 10 sec, incubated in tap water for 15 min to develop blue staining and washed for 1 min in deionised water. The slides were placed in Eosin staining solution for 1 min. To remove excessive staining the slides were washed in tap water for 7 times. The samples were placed for 1 min each in 75% (v/v), 96% (v/v) and 100% (v/v) ethanol and then cleared in xylol for dehydration and preservation. Finally, coverslips were mounted with Entellan.

2.2.2.3 Periodic acid-Schiff staining of intestinal tissue sections

For periodic acid-Schiff (PAS) staining, slides were deparaffinized, rehydrated and washed as described in section 2.2.2.2 (H&E staining procedure). Tissue sections were treated with periodic acid for 5 min and washed two times for 5 min in tap water, followed by incubation in Schiff's reagent for 5 to 10 min. Chromogen formation was monitored under the microscope and the reaction was stopped by washing the slides in running tap water for 10 min. Nuclei were counterstained with Meyer's Hematoxylin for 1 min. Samples were washed, dehydrated and mounted as described above (see 2.2.2.2).

2.2.2.4 Alkaline phosphatase staining

Staining for alkaline phosphatase was performed with Vector® Red Alkaline Phosphatase Substrate Kit I (Cat. No. SK-5100) according to manufacturer's instructions. Tissue sections were deparaffinised and rehydrated as described under H&E staining procedure (see 2.2.2.2). Samples were rinsed with 20x TBS. To visualize the presence of alkaline phosphates, 1 drop of Vulcan Fast Red Chromogen was added to 2.5 ml Vulcan Red buffer, mixed well, added to the slides and incubated for 15 min. Formation of the reaction product was followed under the microscope and reaction was stopped after a sufficient staining intensity was observed by washing the slides for 1 min in deionised water. Nuclei were counterstained with Meyer's Hematoxylin for 1 min. Samples were washed, dehydrated and mounted as described above (see 2.2.2.2).

2.2.2.5 Immunohistochemistry

For immunohistochemical (IHC) stainings, tissue sections were deparaffinised and rehydrated in ascending concentrations of ethanol as described in section 2.2.2.2. Endogenous peroxidase activity was blocked by incubation of samples for 15 min at room temperature with endogenous peroxidase blocking buffer. Thereafter slides were washed 3 times for 5 min in tap water. Antigen unmasking was performed either by heat induced antigen retrieval in citrate buffer for 20 min at 120°C in a pressure steam cooking device or by Proteinase K digestion with 10 µg/ml Proteinase K in TEX buffer for 10 min at room temperature. Afterwards the samples were washed three times for 5 min

in PBS. In order to block unspecific background, sections were incubated either in PBS with 10% (v/v) normal goat serum (NGS), 0.3% (v/v) Triton X-100 and Avidin or in PBS supplemented with 1% (w/v) bovine serum albumin (BSA), 10% NGS, 0.2% (v/v) cold fish skin gelatine, 0.3% (v/v) Triton X-100 and Avidin for 1 h at room temperature. Primary antibodies were diluted in PBS with 0.2% (v/v) cold fish skin gelatine and Biotin and incubated on the sections overnight at 4°C. Samples were washed three times for 5 min in PBS with 0.5% (v/v) Tween-20. Thereafter secondary antibodies were incubated on the slides for 1 h at room temperature diluted in PBS with 10% (v/v) NGS or 1% (w/v) BSA, 10% (v/v) NGS, 0.2% (v/v) cold fish skin gelatine and 0.3% (v/v) Triton X-100. After washing three times for 5 min with PBS, 0.5% (v/v) Tween-20 an Avidin-Biotin-HRP complex (ABC Kit) was applied to the slides for 30 min at room temperature. After washing in PBS, 0.5% Tween-20 the staining was developed by exposing the sections to DAB chromogen. Formation of precipitate was followed under the microscope and when a sufficient signal intensity was reached, the reaction was stopped by washing the slides in PBS. To ensure equal staining conditions incubation times with DAB were equal for all corresponding samples. Nuclei were counterstained with Hematoxylin for 1 min and subsequently dehydrated in descending concentrations of ethanol, cleared in xylol and mounted in Entellan.

Table 1: Primary antibodies and conditions for immunohistochemistry

Antigen	Company	Clone	Host	Dilution
B220	homemade	RA3 6B2	rat	1:1000
cleaved caspase-3	Cell signalling	9661	rabbit	1:1000
CD3	Abcam	ab5690	rabbit	1:200
CD45	BD Bioscience	30-F11	rat	1:500
F4/80	homemade	BM8	rat	1:200
Gr1	BD Pharmingen	1A8	rat	1:500
Ki67	DAKO	TEC-3	rat	1:1000
Lysozyme	DAKO	EC 3.2.1.17	rabbit	1:2000

Table 2: Secondary antibodies and conditions for immunohistochemistry

Antigen	Company	Clone	Host	Dilution
biotinylated rat IgG	DAKO	E0468	rabbit	1:1000
Biotinylated rabbit IgG	Perkin Elmer	NEF813	goat	1:1000

2.2.3 Biochemical analysis

2.2.3.1 Isolation of intestinal epithelial cells (IECs)

In order to isolate IECs mice were euthanized, the colon and the small intestine were removed and transferred into ice-cold PBS as described above (see section 2.2.1.6). The isolation procedure for IECs was described previously in (Ukena et al., 2007). Briefly, colon and small intestine were opened longitudinally and luminal content was removed by washing in cold PBS. Intestinal tissue was incubated in a 50 ml Falcon tube with 10 mM DTT in PBS for 10 min at 37°C and 180 rpm to remove mucus and debris. After washing in PBS, the colon/small intestines were transferred into new Falcon tubes and incubated in 1x HANK's salt solution (HBSS) supplemented for 15 min at 37°C and 180 rpm. To efficiently detach IECs and crypts from the underlying tissue, the tubes were vortexed at full speed for 1 min. Afterwards the remaining colon/ small intestines was removed with a forceps and IECs were harvested by centrifugation for 10 min at 1200 rpm. The supernatant was removed, the pellets were resuspended in 1-3 ml PBS and transferred into Eppendorf tubes. IECs were centrifuged for 1 min at 13000 rpm, the supernatant was discarded and isolated IECs were frozen in liquid nitrogen or directly processed for extraction of proteins or RNA.

2.2.3.2 Preparation of protein extracts

For total protein extraction from colonic or small intestinal IECs, cells were lysed for 30 min on ice in high salt RIPA buffer supplemented with protease- and phosphatase inhibitors. During incubation on ice cells were inverted repetitively. Afterwards protein samples were centrifuged for 20 min at 13000 rpm and 4°C to pellet cell debris. The supernatant was collected and protein concentration was determined.

2.2.3.3 Preparation of cytoplasmic and nuclear protein extracts

To prepare cytoplasmic and nuclear protein fractions, pelleted IECs were resuspended in an appropriate amount of hypotonic buffer A and incubated on ice for 10 min. Afterwards NP-40 was added to a final concentration of 0.8% (v/v) and incubated for 5 min on ice to lyse the plasma membrane. The cytoplasmic protein fraction was separated from nuclei by centrifugation at 13000 rpm for 1 min at 4°C. The supernatant containing cytoplasmic proteins was transferred into a new Eppendorf tube and frozen away. The pellet containing nuclei was washed twice in buffer A without NP-40 to remove remaining cytoplasmic extracts and detergent. In order to lyse the nuclei, the pellet was resuspended in an appropriate volume of buffer C and incubated on ice for 30 min. Afterwards, samples were centrifuged for 10 min at 13000 rpm at 4°C and the supernatant with nuclear proteins was collected into a new tube and frozen away. The protein concentration of cytoplasmic and nuclear fractions was determined.

2.2.3.4 Western Blot analysis

Protein extracts were boiled for 10 min in 1x Laemmli buffer to denature proteins and reduce disulfide bonds. Proteins were separated according to size on 10% SDS-polyacrylamid gels (SDS-PAGE). Electrophoresis was performed under denaturing conditions in Tris-Glycine electrophoresis buffer. After sufficient separation was achieved, proteins were transferred to PVDF membranes by semidry or wet transfer. PVDF membranes were activated by incubation in 100% (v/v) methanol for 5 min and subsequently placed in transfer buffer. Two Whatman papers (3 mm) were soaked in transfer buffer and SDS gels were equilibrated in transfer buffer for 5 to 15 min. The following bottom to top assembly was used for both semidry and wet transfer: A sheet of Whatman paper was covered by the SDS gel, followed by the PVDF membrane and another piece of Whatman paper on the top. For efficient semidry transfer of proteins to the PVDF membrane 1 mA current was applied per cm² membrane for 2 h. Wet transfer was performed with 120 mA current per membrane for 2 h or with 30 mA current per membrane for overnight transfer. After protein transfer the membranes were washed in PBS

for 5 min on a shaker. Equal loading, efficiency and quality of protein transfer were checked by Ponceau S staining. In order to de-stain membranes, they were washed in PBS with 0.5% (v/v) Tween-20 until Ponceau S staining disappeared. To reduce unspecific binding of antibodies, membranes were incubated with PBS supplemented with 5% (w/v) non-fat dry milk, 0.5% (v/v) Tween-20 for 1 h under agitation. Primary antibodies were diluted in PBS with 5% (w/v) BSA, 0.1% (v/v) Tween-20, 0.001% NaN₃ and incubated on the membrane overnight at 4°C under constant agitation. Membranes were washed three times for 5 min in PBS with 0.1% (v/v) Tween-20 and incubated with HRP-conjugated secondary antibody diluted in PBS with 5% (w/v) non-fat dry milk and 0.1% (v/v) Tween-20 for 1 h at room temperature under agitation. Afterwards membranes were washed three times for 5 min in PBS with 0.1% (w/v) Tween-20. Protein bands were visualized using commercial ECL, ECL Pico or ECL Femto with varying exposure times to chemiluminescent films depending on the individual band intensities. Exposed films were developed and fixed in AGFA developer solution and AGFA fixation solution respectively.

Table 3: Primary antibodies used for WB analysis

Antigen	Company	Clone	Host	Dilution
β -Actin	Santa Cruz	I19	goat	1:5000
cFLIP	Alexis	ADI-AAP-440-E	rabbit	1:1000
clAP1	Enzo	ALX-803-335-C100	rat	1:1000
Cre				
c-Rel	Santa Cruz	sc-71	rabbit	1:1000
HDAC1	HDAC1	sc-7872	rabbit	1:1000
p50/p105	NCI BRB	NR1157	rabbit	1:20000
p65	Santa Cruz	sc-372	rabbit	1:1000
p100/52	NCI BRB	NR1495	rabbit	1:20000
RelB	Cell Signaling	4922	rabbit	1:1000
RIPK1	BD Bioscience	610459	mouse	1:1000
RIPK3	Enzo	ADI-905-242-100	rabbit	1:1000
TRAF2	Santa Cruz	sc-876	rabbit	1:1000
α -Tubulin	Sigma	B-5-1-2	mouse monoclonal	1:5000

Table 4: Secondary antibodies used for WB analysis

Antigen	Company	Clone	Host	Dilution
Rabbit IgG-HRP	GE Healthcare	NA934V	goat	1:5000/ 1:10000
Mouse IgG-HRP	GE Healthcare	NA9310V	sheep	1:5000/ 1:10000
Goat IgG HRP	Jackson Lab	705-035-003	donkey	1:5000
Rat IgG-HRP	Jackson Lab	112-035-003	goat	1:5000

2.2.4 Molecular Biology

2.2.4.1 Preparation of genomic DNA

Tail biopsies were digested in 200 μ l tail lysis buffer supplemented with 10 mg/ml Proteinase K for a least 2 h at 56°C. For precipitation of DNA 200 μ l isopropanol were added and the tube was inverted several times. The tube was centrifuged for 2 min at 13000 rpm, the supernatant discarded and 200 μ l 70% (v/v) ethanol were added to wash the DNA. The sample was centrifuged

again for 2 min at 13000 rpm, the supernatant discarded and the pellet air-dried for 20 min. Finally, the DNA pellet was resuspended in 200 μ l Tris-EDTA buffer and used for genotyping PCRs.

2.2.4.2 Genotyping PCRs

Genotyping was performed by using 2 μ l genomic tail DNA for Polymerase-chain-reaction (PCR) based genotyping per reaction. For one reaction 2 μ l genomic tail DNA were mixed with 12.5 μ l ready-to-use Mastermix (VWR), 2 μ l of 3 μ M primer mix and 10.5 μ l H₂O. Annealing and elongation temperatures depend on the primer sets used for individual PCRs (see Table 5 and Table 6). 10 μ l of the PCR reaction products were separated on 2% (w/v) agarose gels.

Table 5: Primer-sequences for genotyping PCRs and PCR-amplified fragment sizes. WT: wildtype; Tg: transgene; FL: floxed; KO: knock-out; DEL: deleted

Typing for	Primer sequence (5' □3')	Band size
villin Cre	ACA GGC ACT AAG GGA GCC AAT G AT TGCA GGT CAG AAA GAG GTC ACA G GTT CTT GCG AAC CTC ATC ACT C	WT: 900 bp Tg: 350 bp
villin CreER^{T2}	CAA GCC TGG CTC GAC GGC C CGC GAA CAT CTT CAG GTT CT	Tg: 300 bp
Ripk1 floxed	CAT GGC TGC AAA CAC CTA AAC GTT ACA ACA TGC AAA TCA AC	WT: 320 bp FL: 380 bp
Ripk1 deleted	GAGGAAGACATCACTGAAGA CAGAGGGCTGGATCTGGTGG	KO: 230 bp
Myd88	GAG CAG GCT GAG TGC AAA CTT GGT CTG AGC CTC TAC ACC CTT CTC TTC TCC ACA ATC GCC TTC TAT CGC CTT CTT GAC GAG	WT: 1000 bp KO: 1000 bp (2 PCRs)
Tnfr1	AGA AAT GTC CCA GGT GGA GAT CTC GGC TGC AGT CCA CGC ACT GG ATT CGC CAA TGA CAA GAC GCT GG	WT: 120 bp KO: 300 bp
Fadd	TCA CCG TTG CTC TTT GTC TAC GTA ATC TCT GTA GGG AGC CCT CTA GCG CAT AGG ATG ATC AGA	WT: 208 bp FL: 280 bp DEL: 331 bp
Ripk3	CGC TTT AGA AGC CTT CAG GTT GAC GCC TGC CCA TCA GCA ACT C CCA GAG GCC ACT TGT GTA GCG	WT: 320 bp KO: 485 bp

Table 6: PCR programmes for genotyping PCRs

Typing for	PCR program		Cycles
	Temperature	Time	
villin Cre	94°C	3 min	35
	94°C	1 min	
	67°C		
	72°C		
	72°C	5 min	
Ripk1 floxed	94°C	2 min	35
	94°C	30 sec	
	60°C	30 sec	
	72°C	30 sec	
	72°C	5 min	
Ripk1 deleted	94°C	2 min	35
	94°C	30 sec	
	60°C	30 sec	
	72°C	30 sec	
	72°C	5 min	
Myd88	94°C	3 min	35
	94°C	30 sec	
	67°C	1 min	
	72°C	1 min	
	72°C	5 min	
Tnfr1	94°C	2 min	30
	94°C	1 min	
	61°C	30 sec	
	72°C	30 sec	
	72°C	2 min	
Fadd	94°C	3 min	34
	94°C	30 sec	
	55°C	30 sec	
	72°C	30 sec	
	72°C	3 min	

Table 6 continued			
<i>Ripk3</i>	94°C	4 min	30
	94°C	1 min	
	60°C	30 sec	
	72°C	1 min	
	72°C	10 min	

2.2.4.3 Agarose gel electrophoresis

Agarose gel electrophoresis was performed to separate PCR-amplified DNA fragments according to size. 2% (w/v) agarose was dissolved by boiling in 1x TAE buffer and 0.5 mg/ml Ethidiumbromide were added. Gels were run in 1x TAE buffer for 20 to 40 min at 120 to 140 mV.

2.2.4.4 RNA extraction

For RNA extraction from whole colon/small intestinal tissue or IECs, samples were homogenized in 1 ml Trizol reagent (Invitrogen) and incubated for 20 min at room temperature for complete cell lysis. Samples were centrifuged for 10 min at 13000 rpm to pellet cell debris. The supernatant was transferred into a new tube and incubated for 5 min at room temperature. To extract nucleic acids 200 µl chloroform per 1 ml Trizol were added and samples were mixed vigorously for 15 sec followed by 5 min incubation at room temperature. The samples were centrifuged for 15 min at 13000 rpm to separate aqueous and organic phase. Afterwards the upper aqueous phase was transferred into a new tube containing an equal volume of 70% (v/v) ethanol and mixed gently. The samples were loaded on Quiagen RNeasy columns. For binding of nucleic acids to the filter of the column, the columns were centrifuged for 1 min at 9000 rpm. For washing 500 µl washing buffer (provided by manufacturer) was added and the column was subsequently centrifuged at 9000 rpm for 30 sec. In order to digest genomic DNA RNase-free DNase diluted in RDD buffer (provided by manufacturer) was added to the column and incubated for 30 min at room temperature. Afterwards the column was washed twice as described and RNA was eluted in nuclease free H₂O by centrifugation for 2 min at 13000 rpm. To check for possible genomic DNA contamination, equal volumes of RNA were subjected to β-Actin PCR (see

section 2.2.4.3). Finally, the concentration and purity of extracted RNA were assessed by photometric analysis using NanoDrop.

2.2.4.5 cDNA synthesis

In order to synthesize cDNA, the Superscript III kit (Invitrogen) was used according to manufacturer's instructions. For 10 μ l final reaction volume, 1 μ g RNA was mixed with 1 μ l of 50 ng/ μ L random hexamer primers and 1 μ l of 10 mM dNTPs. The reaction mixture was first incubated at 65°C for 5 min to allow primers to anneal to mRNA and subsequently cooled on ice for a few minutes. Meanwhile, 10 μ l cDNA reaction mix containing 2 μ l 10x RT-reaction buffer, 4 μ l 25 mM MgCl₂, 2 μ l 0.1 M DTT, 1 μ l RNase OUT (40 U/ μ l) and 1 μ l of SuperScript III polymerase (200 U/ μ L) were prepared and added to the samples. Reverse transcription was performed in a PCR cycler using the following program: 10 min at 25°C, 50 min at 50°C for cDNA synthesis and 5 min at 85°C heat-inactivation. To digest the RNA 1 μ l RNaseH was added to the reaction and the samples were incubated for 20 min at 37°C. The cDNA reaction mix was diluted 10-fold in nuclease-free water and 1 μ l of cDNA was used for an actin-PCR to check successful cDNA synthesis.

2.2.4.6 Quantitative real time PCR

Gene expression was quantified by performing probe-based Taqman quantitative real time PCR (qRT-PCR). All samples were run in two technical replicates. qRT-PCR was performed in a final volume of 10 μ l, consisting of 2 μ l cDNA, 5 μ l Mastermix (Applied Biosystems), 0.5 μ l primer-probe mix (Applied Biosystems) and 2.5 μ l nuclease-free water. All reactions were carried out in 384-well plates. The following PCR program was performed: 10 min at 95°C for the activation of the polymerase, followed by 40 amplification cycles each with 10 sec at 95°C and 1 min at 60°C each.

The comparative $\Delta\Delta$ CT or Δ CT was used to determine RNA expression levels of the genes of interest. For the $\Delta\Delta$ CT method, the CT value of the endogenous reference gene (TATA box binding protein) was subtracted from the CT values of the target gene to obtain the Δ CT value for each duplicate. Relative quantification was performed by calculation of the $\Delta\Delta$ CT value.

Table 7: Taqman probes used for qRT-PCR

Gene	Taqman probe
<i>Ccl2</i>	Mm00441242_m1
<i>Ccl5</i>	Mm01302428_m1
<i>Cxcl1</i>	Mm00433859_m1
<i>Il-1b</i>	Mm00434228_m1
<i>Il-12a, p35</i>	Mm00434165_m1
<i>Tnf</i>	Mm00443258_m1
<i>Tbp</i>	Mm00446973_m1

2.2.5 Cell culture

2.2.5.1 Isolation and culture of small intestinal organoids

Small intestinal crypts were isolated and grown to organoids as previously described (T. Sato et al., 2009). Mice were sacrificed and the small intestine isolated as described in sections 2.2.1.5 and 2.2.1.6 respectively. To remove luminal content the small intestine was cut open longitudinally and was washed in PBS. The intestine was placed on a petri dish and cut opened up with tweezers making sure the mucosal side was facing upwards. A smoothed coverslip was used to carefully scrape off the villi. After a short washing in PBS the intestine was chopped into 2 to 4 mm pieces and transferred into a 50 ml Falcon tube. To wash the intestinal tissue 10 ml PBS were added, pieces were pipetted up and down, were allowed to settle down and the supernatant aspirated. Washing was repeated 15 to 20 times until the supernatant was clear. Afterwards the pieces of intestine were incubated in PBS containing 2 mM EDTA for 30 min at 4°C under agitation to release the crypts from the underlying tissue. Intestinal fragments were allowed to settle and the supernatant was aspirated. To isolate and collect intestinal crypts, 10 ml PBS supplemented with 10 (w/v) FCS were added to the intestinal tissue and mixed vigorously. The supernatant was aspirated and passed through a 70 µM cell strainer. The flow through containing small intestinal crypts was collected and this procedure was repeated three more times. Crypt fractions 3 and 4 were centrifuged for 5 min at 800 rpm. The supernatant was removed, the pellets were resuspended in 5 ml CM-GF and centrifuged for 5 min at 600

rpm to remove single cells. The culture of the isolated crypt fractions was performed in a lamin-rich Matrigel, shown to support small intestinal growth. An adequate amount of crypts was resuspended in 200 μ l matrigel and 50 μ l matrigel drops with crypts were seeded out per well in a 24-well plate. Matrigel was allowed to polymerize for 10 min at 37°C and 500 μ l CM+GF with 5 μ l ENR were added to the crypts. In order to prevent anoikis, 1 μ l of 10 mM ROCK inhibitor (Y27632) (Sigma) was added to the crypt culture for the first 3 days.

For the passage of crypt cultures the matrigel was gently detached from the the well with a 1000 μ l pipet tip and transferred into a 15 ml Falcon tube. IN order to mechanically rupture the crypts, the medium containing the crypts and the matrigel was passed through a 23 gauge syringe several times. The crypt fragments were centrifuged for 5 min at 600 rpm at 4°C, the supernatant was aspirated and crypts were resuspended in an appropriate volume of matrigel. For culturing in 24-well plates, 50 μ l matrigel was seeded per well, 20 μ l matrigel were used per well in a 48-well plate and 10 μ l matrigel per well for culturing organoids in a 96-well plate. After incubation for a few minutes at 37°C, 500 μ l, 200 μ l or 100 μ l CM+GF supplemented with 1 μ l ENR per 100 μ l medium was added to the corresponding wells.

2.2.5.2 Tamoxifen-induced deletion of RIPK1 in organoid cultures

For tamoxifen-induced *in vitro* deletion of RIPK1 in crypt cultures organoids from VillinCreER^{T2}/*Ripk1*^{fl/fl} mice were isolated as described in 2.2.5.1. Organoids were maintained in culture for at least 4 passages before the deletion of RIPK1 was induced. The cultures were seeded and grown in DMEM/F12 without phenol red for 24 to 36 h. In order to delete RIPK1, 100 nM 4-hydroxytamoxifen (4-OHT) dissolved in ethanol or for mock treatment, an equal amount of ethanol was added to the culture medium. After 20 to 24 h the 4-OHT containing medium was replaced by fresh culture medium and organoids were kept in culture for further analysis as indicated.

2.2.5.3 Assessment of cell death in organoids

In order to quantify cell death in organoids by propidium iodide (PI) uptake, organoids were cultured and RIPK1 was deleted by addition of 4-OHT as

described above (2.2.5.1 and 2.2.5.2). To harvest the crypts for analysis, the medium was removed from the wells and 300 μ l TrypLE™ solution (Life Technologies) per well were added. Organoids were carefully detached with a 1000 μ l pipet tip and transferred into an Eppendorf tube. For mechanic break up, the organoids were passed 2 times through a syringe with a 23 G injection needle and incubated for 5 min at 37 °C. 800 μ l PBS with 2% FCS were added to the culture to stop further digestion and the samples were centrifuged for 5 min at 500 rpm. Subsequently, organoids were resuspended in 200 μ l PBS supplemented with 2% FCS and propidium iodide was added to a final concentration of 1 μ g/ml immediately before FACS analysis. Cell death was determined by quantification of PI-positive cells as acquired with a FACSCalibur FACS analyser.

3. Results

3.1 RIPK1 deficiency in IECs induces intestinal pathology and epithelial cell death

3.1.1 Generation of mice with intestinal epithelial specific RIPK1 deficiency

To investigate the role of RIPK1 in the murine intestinal epithelium, mice lacking RIPK1 specifically in the cells of the intestinal epithelium were generated. Therefore *Ripk1^{fl/fl}* mice (Dannappel et al., 2014) were crossed to mice that express Cre recombinase under control of the intestinal epithelial cell (IEC) specific villin promoter (el Marjou et al., 2004). In these mice, the third exon of the *Ripk1* alleles is excised by Cre recombinase only in IECs. The resulting mice (from here on called 'RIPK1^{IEC-KO} mice') are deficient for RIPK1 specifically in IECs.

Successful deletion of RIPK1 in colonic and small intestinal IECs was confirmed by Western Blot (Figure 4).

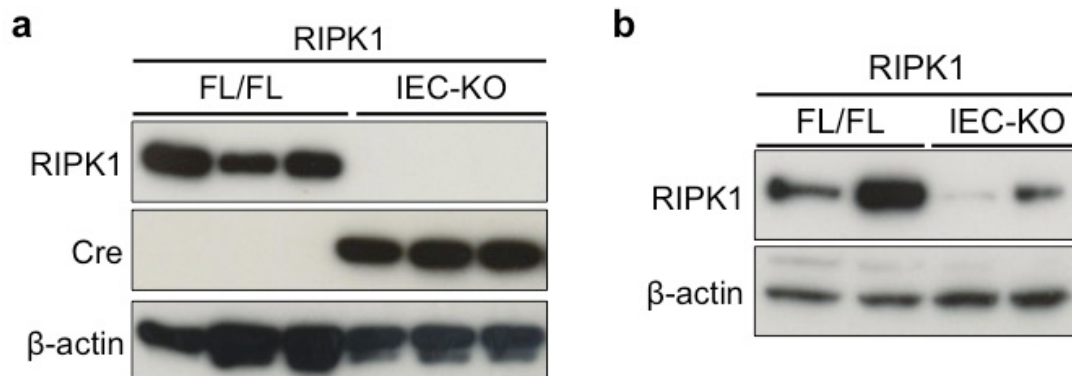


Figure 4. Conditional deletion of RIPK1 in IECs.

Whole cell protein extracts from primary (a) small intestinal and (b) colonic IECs from *Ripk1^{fl/fl}* mice (FL/FL) and RIPK1^{IEC-KO} mice (IEC-KO) were analysed by immunoblot with the indicated antibodies.

3.1.2 Increased IEC apoptosis and mild inflammation in the ileum of RIPK1^{IEC-KO} mice

RIPK1^{IEC-KO} mice were born at expected Mendelian ratios (Figure 5a), however grew slower and had significantly reduced body weight at 3 weeks of age compared to their *Ripk1^{fl/fl}* littermates (Figure 5b). These mice showed signs of cachexia, which became apparent at 2 weeks of age (data not shown). All RIPK1^{IEC-KO} mice died prematurely before reaching an age of 28 days (Figure 5c), showing that RIPK1^{IEC-KO} mice develop a severe spontaneous phenotype and that intestinal RIPK1 has an important role in maintaining intestinal homeostasis.

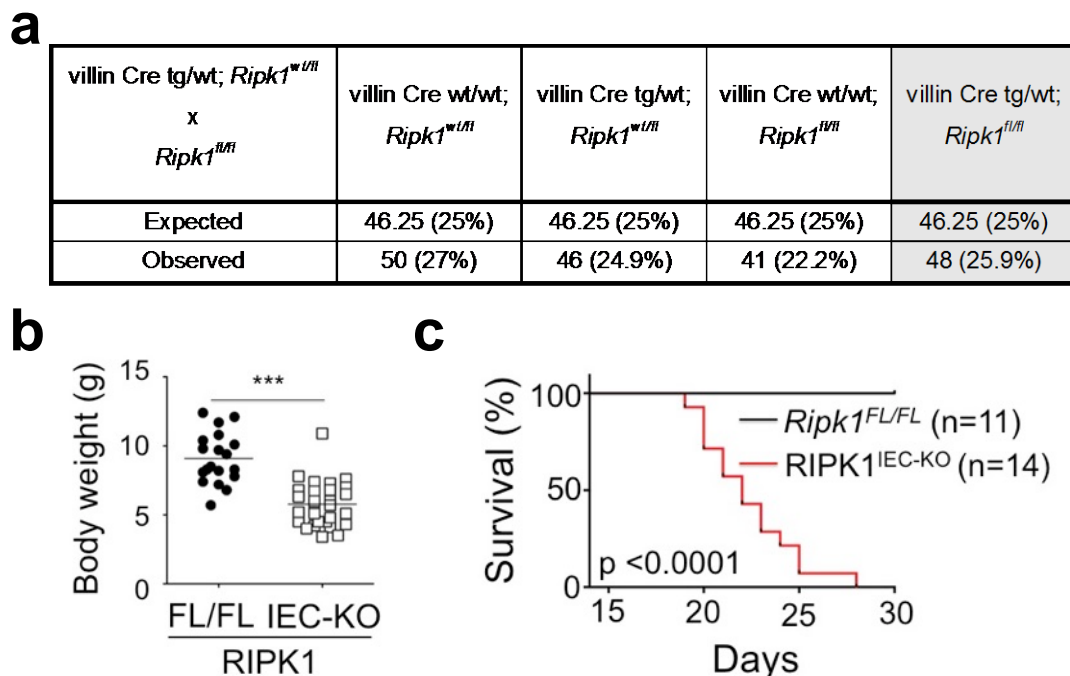


Figure 5. RIPK1^{IEC-KO} mice develop spontaneous phenotype resulting in premature death.

(a) Table showing expected and observed absolute number and possibilities of offspring with the indicated genotype resulting from breeding villin Cre tg/wt; *Ripk1^{wt/fl}* mice with villinCre wt/wt; *Ripk1^{fl/fl}* mice. (b) Body weight of *Ripk1^{fl/fl}* (FL/FL) and RIPK1^{IEC-KO} mice (IEC-KO) mice at 3 weeks of age. (c) Kaplan-Meier survival curve for *Ripk1^{fl/fl}* and RIPK1^{IEC-KO} mice. * $P \leq 0.05$, ** $P \leq 0.01$, *** $P \leq 0.005$

Histological analysis of Hematoxylin and Eosin (H&E) stained ileal sections from 3 week-old RIPK1^{IEC-KO} mice revealed an almost complete loss of villus structures throughout the ileum (Figure 6 red line). Numerous cells with morphological features of dying cells such as fragmented nucleus were identified in the lumen of the crypts and within the epithelium, indicating that *Ripk1^{-/-}* IECs undergo cell death (Figure 6 black arrows). Crypts were

elongated compared to *Ripk1^{fl/fl}* mice suggesting hyperproliferation in intestines of $RIPK1^{IEC-KO}$ mice (Figure 6 black line). Staining against Ki67, a marker for proliferative cells, confirmed increased numbers of proliferating IECs in $RIPK1^{IEC-KO}$ mice and expansion of the transient amplifying (TA) cell compartment (Figure 7). PAS staining against glycosylated mucus-proteins secreted by goblet cells and staining against alkaline phosphatase (AP) expressed by mature enterocytes on small intestinal sections of $RIPK1^{IEC-KO}$ mice showed reduced numbers of goblet cells and mature enterocytes respectively (Figure 7). In addition, lysozyme staining revealed reduced numbers of Paneth cells in $RIPK1^{IEC-KO}$ mice compared to *Ripk1^{fl/fl}* mice (Figure 7).

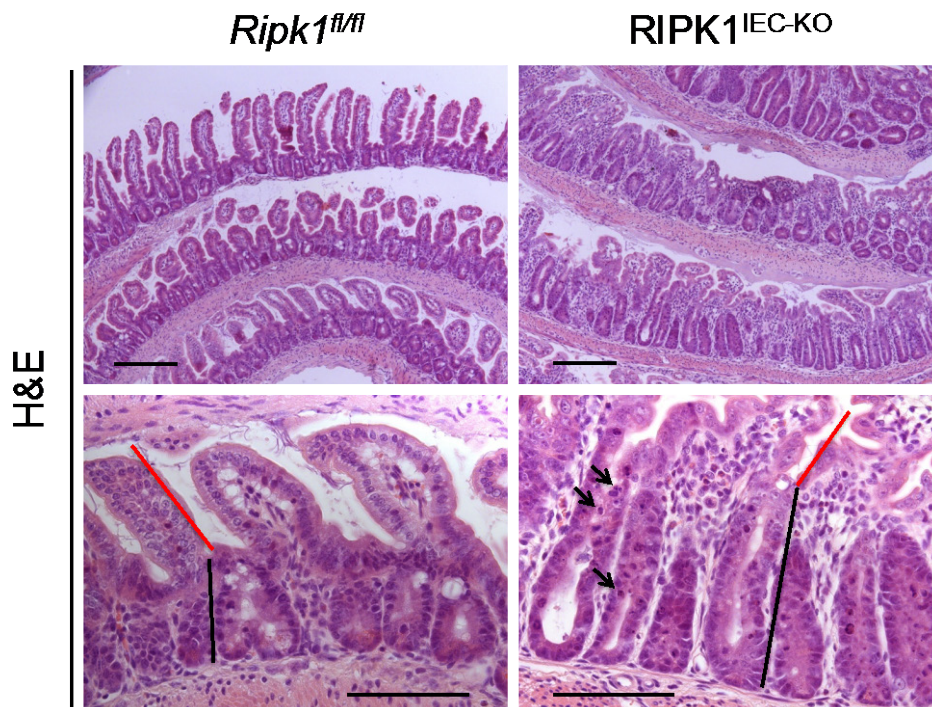


Figure 6. Intestinal pathology and IEC death in $RIPK1^{IEC-KO}$ mice.

Representative images of haematoxylin and eosin stained ileal sections from 3-week old *Ripk1^{fl/fl}* mice and $RIPK1^{IEC-KO}$ mice. Red line depicts villus length. Black line represents crypt length. Black arrows indicate dead epithelial cells. Scale bars: 100 μ m.

As described above, ileal H&E sections of 3-week old $RIPK1^{IEC-KO}$ mice showed increased incidence of dying intestinal epithelial cells. In order to determine the type of epithelial death, IHC against cleaved caspase-3 (CC3) was done.

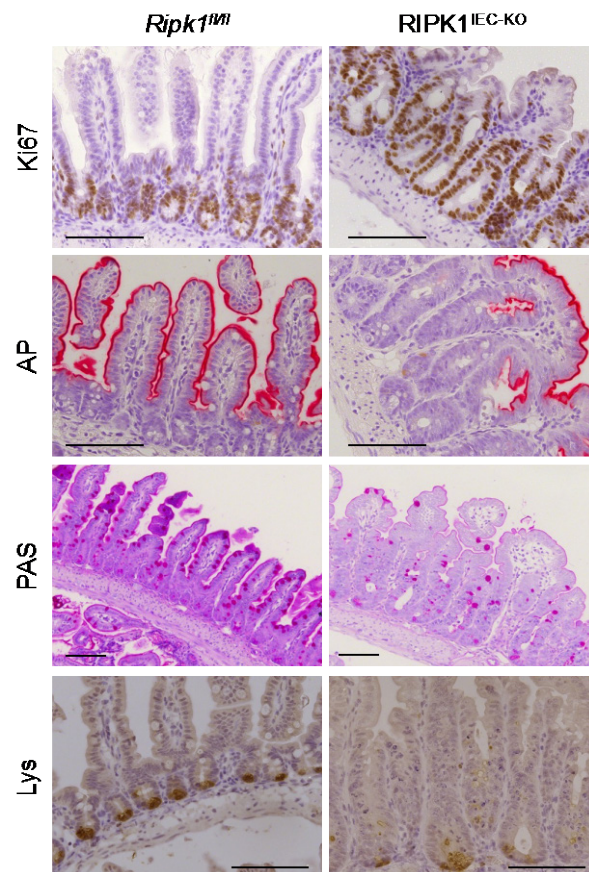


Figure 7. Hyperproliferation and reduced numbers of differentiated epithelial cells in RIPK1^{IEC-KO} mice.

Representative images of small intestinal swiss rolls from 3-week old *Ripk1^{fl/fl}* and RIPK1^{IEC-KO} mice stained for alkaline phosphatase (AP), Periodic acid-Schiff (PAS), immunostained for Ki67 and lysozyme and counterstained with haematoxylin. Scale bars: 100 μ m.

As shown in Figure 8, RIPK1^{IEC-KO} mice showed high numbers of dying epithelial cells that were positive for cleaved caspase-3, indicating that RIPK1 deficiency sensitized IECs to apoptosis. Apoptosis of *Ripk1^{-/-}* IECs occurred mainly in the crypts and the TA cell compartment of the intestinal epithelium, indicating that primarily undifferentiated progenitor cells underwent apoptosis. Quantification of cell death revealed that 50% of all crypts in the ileum of RIPK1^{IEC-KO} mice harboured apoptotic IECs (Figure 8). In average, every crypt in RIPK1^{IEC-KO} harbored two apoptotic cells, emphasizing the massive extent of cell death observed in this phenotype (Figure 8). Taken together, these results show that RIPK1^{IEC-KO} mice develop a severe spontaneous phenotype characterised by extensive apoptosis of IECs, villus atrophy, reduced numbers of differentiated cells, epithelial hyperproliferation and premature lethality.

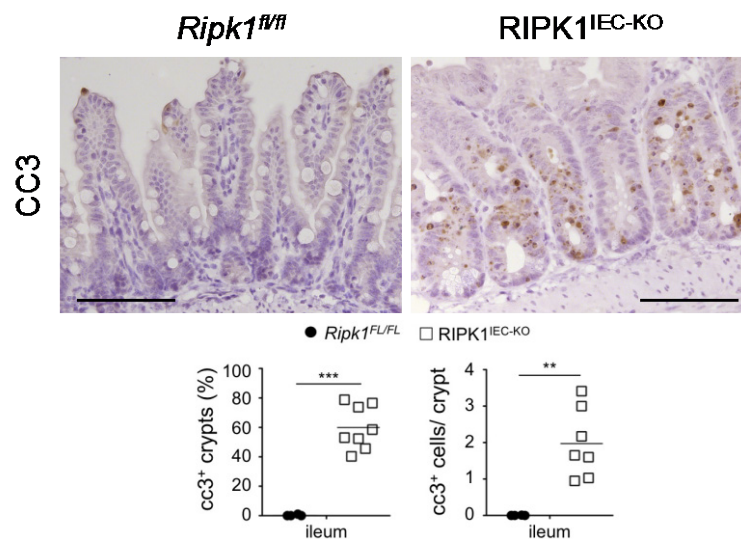


Figure 8 Increased numbers of apoptotic IECs in *RIPK1^{IEC-KO}* mice.

(a) Immunohistochemical staining for CC3 and haematoxylin counterstaining of small intestinal sections from 3-week old *Ripk1^{fl/fl}* and *RIPK1^{IEC-KO}* mice. Scale bars: 100 μ m. (b) Quantification of crypts containing CC3-positive cells and the number of CC3-positive cells per crypt in the ileum of 3-week old *Ripk1^{fl/fl}* and *RIPK1^{IEC-KO}* mice. * $P \leq 0.05$, ** $P \leq 0.01$, *** $P \leq 0.005$

To check if increased epithelial death triggers an inflammatory response, quantitative real time PCR (qRT-PCR) was employed to monitor expression levels of inflammatory cytokines and chemokines in whole small intestinal tissue isolated from *RIPK1^{IEC-KO}* mice and their *Ripk1^{fl/fl}* littermates. Messenger RNA (mRNA) levels of *Tnf*, an important pro inflammatory cytokine, and *Cxcl1*, a chemoattractant for neutrophils were statistically significantly increased in *RIPK1^{IEC-KO}* compared to their floxed littermates (Figure 9). Other cytokines, *Il1b* and *Il12a*, showed no difference in expression levels between *RIPK1^{IEC-KO}* mice and *Ripk1^{fl/fl}* mice. Furthermore, expression of chemokines *Ccl2* and *Ccl5* was not different between *RIPK1^{IEC-KO}* and *Ripk1^{fl/fl}* mice (Figure 9). To further elucidate the immune response in the intestines of 3-week old *RIPK1^{IEC-KO}* mice, immunostainings allowing identification of different immune cell lineages were performed on tissue sections. Furthermore, immune cells were isolated from the small intestinal lamina propria, immunostained for different immune cell lineages and subsequently analysed with FACS. Immunostaining for $CD45^+$ cells, a marker for immune cells with hematopoietic origin, revealed that the overall number of immune cells is slightly increased in *RIPK1^{IEC-KO}* mice (Figure 10).

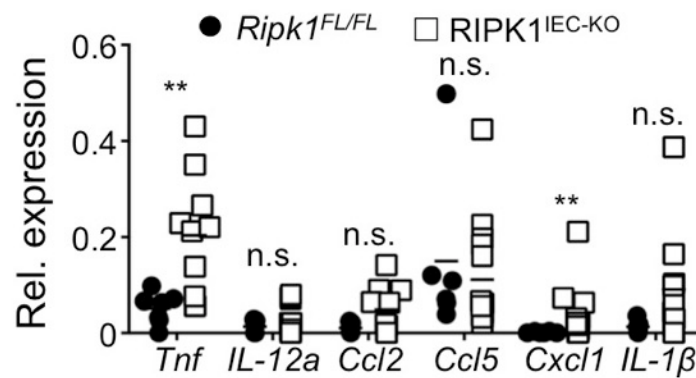


Figure 9 Elevated expression of *Tnf* and *Cxcl1* in intestines of 3-week old RIPK1^{IEC-KO} mice.

qRT-PCR analysis of inflammatory cytokine and chemokine mRNA expression levels in whole small intestinal tissue from 3-week old *Ripk1*^{fl/fl} and RIPK1^{IEC-KO} mice.

n.s. not significant. *P≤0.05, **P≤0.01, ***P≤0.005

In more detail, a few Gr1 positive granulocytes scattered throughout the lamina propria of RIPK1^{IEC-KO} mice were detected, and the number of F4/80 positive macrophages did not differ between RIPK1^{IEC-KO} and control mice (Figure 10). IHC for cells of the adaptive immune response revealed no visually detectable changes in B220 positive B-cell and CD3 positive T-cell numbers in RIPK1^{IEC-KO} mice and compared to their floxed littermates (Figure 10). FACS analysis of immune cells isolated from the lamina propria allowed a more quantitative comparison of immune cell numbers in RIPK1^{IEC-KO} and *Ripk1*^{fl/fl} mice. The total number of CD45⁺ leucocytes was slightly increased in RIPK1^{IEC-KO} mice compared to *Ripk1*^{fl/fl} mice, although this change was not statistically significant (Figure 10). Analysis of the composition of the CD45⁺ leucocyte population revealed significantly increased numbers of Gr1⁺ granulocytes in the small intestine of RIPK1^{IEC-KO} mice compared to control mice (Figure 10). The numbers of CD11b^{hi} F4/80⁺ Ly6G⁻ macrophages and CD3⁺ T-cells did not differ between RIPK1^{IEC-KO} and *Ripk1*^{fl/fl} mice (Figure 10). Finally, the total numbers of B220 positive B-cells were significantly reduced in RIPK1^{IEC-KO} mice compared to littermate controls. Taken together, these results show that ablation of RIPK1 in the small intestine causes a severe spontaneous phenotype, characterized by extensive intestinal epithelial cell apoptosis, hyperproliferation and a mild inflammatory response.

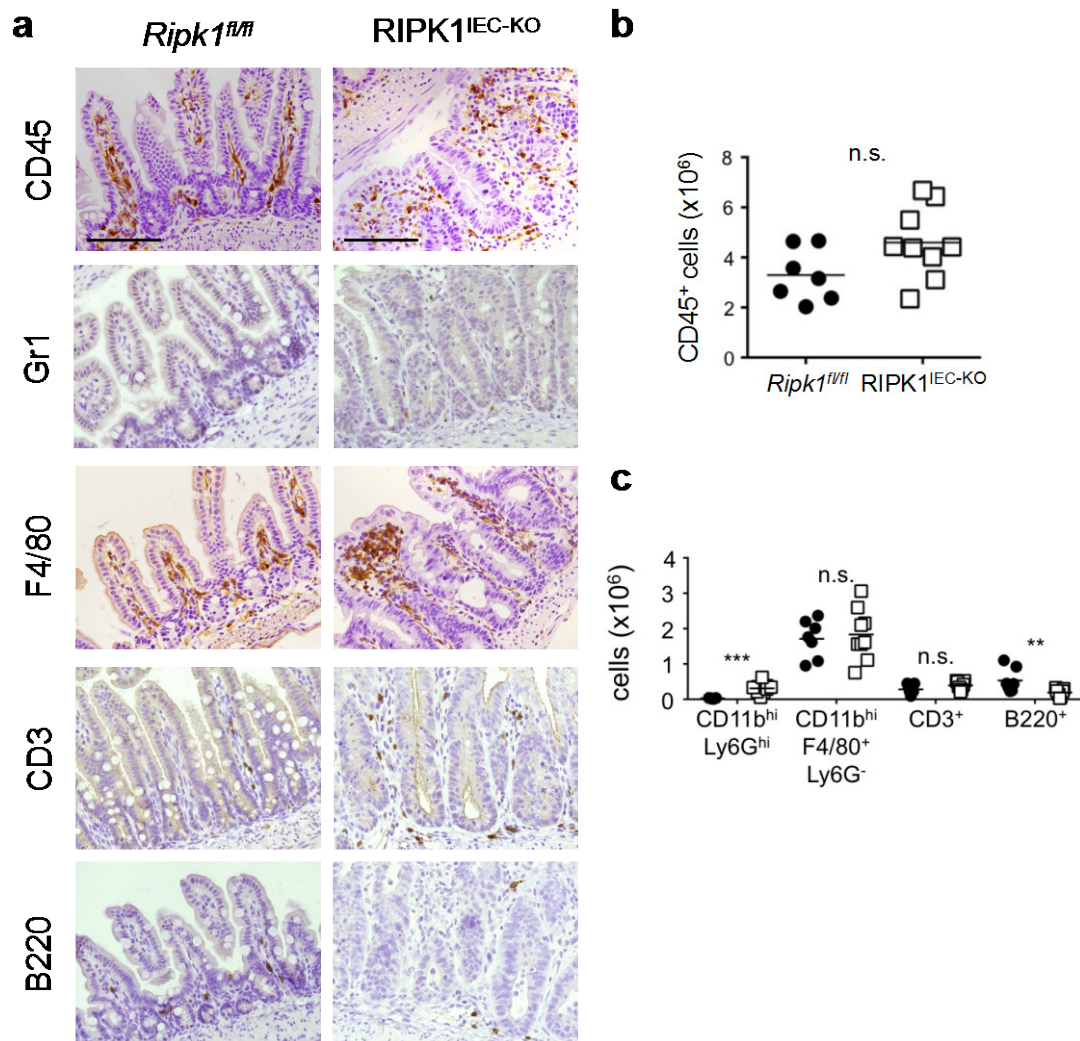


Figure 10 Slightly increased leucocyte numbers in the mucosa of 3-week old RIPK1^{IEC-KO} mice.

(a) Ileal swiss rolls from 3-week old *Ripk1^{fl/fl}* and RIPK1^{IEC-KO} mice were immunostained for CD45, Gr1, F4/80, CD3, B220 and counterstained with haematoxylin. Scale bars: 100 μ m (b) Lamina propria immune cells were isolated from 3-week old *Ripk1^{fl/fl}* and RIPK1^{IEC-KO} mice, immunostained for CD45 and analysed by FACS. (c) Lamina propria immune cells were isolated from 3-week old *Ripk1^{fl/fl}* and RIPK1^{IEC-KO} mice, immunostained for CD11b Ly6G (neutrophils), CD11b F4/80 Ly6G (macrophages), CD3 (T-cells) and B220 (B-cells) and analysed by flow cytometry. Isolation and immunostaining of lamina propria immune cells in (b) and (c) was done by Dr. Christina Eftchi. n.s. not significant. * $P \leq 0.05$, ** $P \leq 0.01$, *** $P \leq 0.005$

3.1.3 Increased IEC apoptosis and mild inflammation in the colon of RIPK1^{IEC-KO} mice

To investigate the colon pathology of RIPK1^{IEC-KO} mice, H&E sections of colons from 3-week-old RIPK1^{IEC-KO} mice were examined. In the proximal colon, RIPK1^{IEC-KO} mice showed increased cellularity in the lamina propria, elongated crypts and high numbers of cells with morphological features of dying cells within the epithelium and the lumen of the crypts (Figure 11).

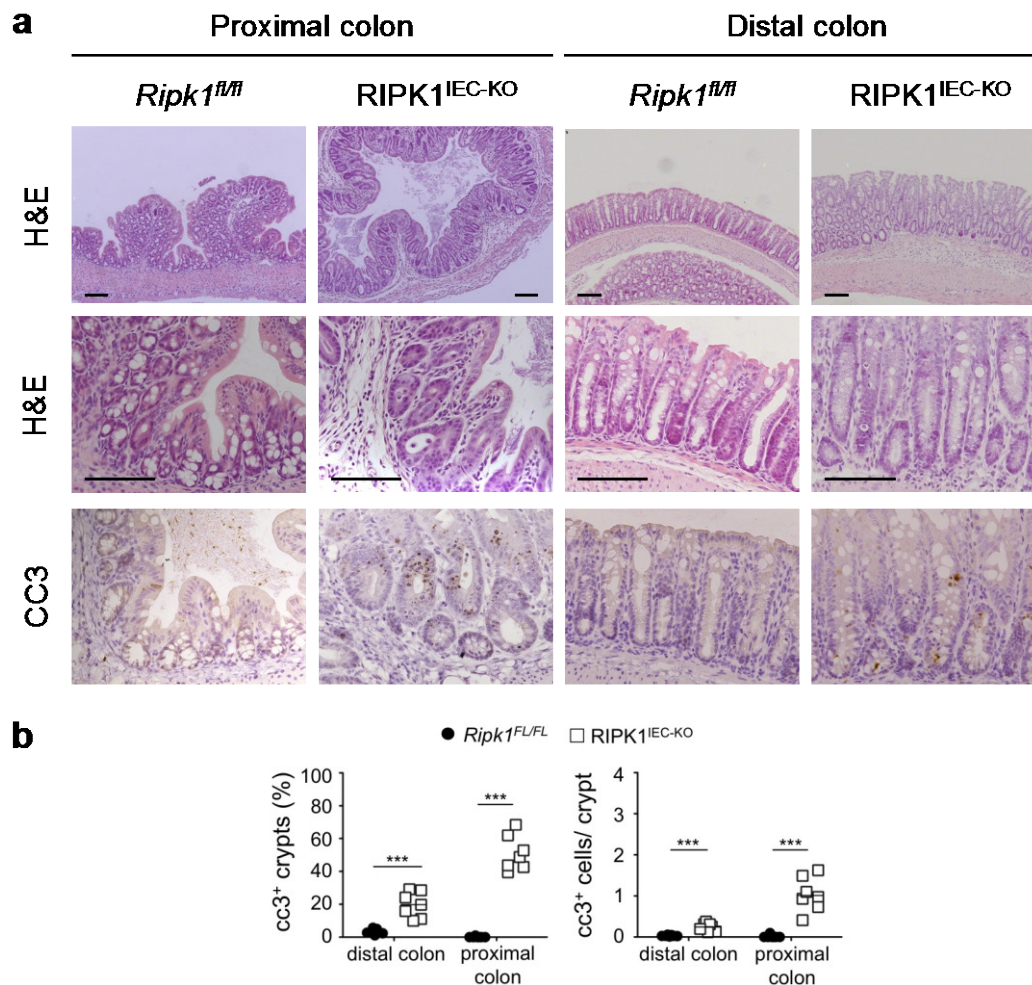


Figure 11 Intestinal pathology and IEC apoptosis in the colon of RIPK1^{IEC-KO} mice.

(a) Histological analysis of colonic swiss rolls from 3-week old RIPK1^{IEC-KO} mice stained with H&E or immunostained for CC3. Scale bars: 100 μ m. **(b)** Quantification of CC3-staining for the distal and proximal colon of 3-week old *Ripk1^{fl/fl}* and RIPK1^{IEC-KO} mice. n.s. not significant. * $P \leq 0.05$, ** $P \leq 0.01$, *** $P \leq 0.005$

IHC against CC3 indicated that death of IECs was apoptotic (Figure 11). Extensive IEC apoptosis was affecting 50% of the crypts in the proximal colon with each crypt harbouring one apoptotic epithelial cell in average (Figure 11).

Ki-67 staining revealed increased numbers of proliferating cells, suggesting a hyperproliferating epithelium in the proximal colon. RIPK1^{IEC-KO} mice had reduced numbers of goblet cells and mature enterocytes compared to control mice as shown by staining for PAS and AP respectively (Figure 12).

In the distal colon the phenotype was less severe compared to the proximal colon. Crypts were only slightly elongated compared to *Ripk1^{fl/fl}* mice and few scattered dying IECs were detected within the epithelium and (Figure 11). Staining against CC3 showed that these cells died by apoptosis, although the extent of cell death was less pronounced compared to the proximal colon and the ileum (Figure 11). As already indicated by H&E sections, Ki-67 staining confirmed that the number of proliferating cells was only slightly increased in RIPK1^{IEC-KO} mice compared to *Ripk1^{fl/fl}* mice (Figure 12). Similar to the ileum and the proximal colon, goblet cell numbers were reduced in the distal colon of RIPK1^{IEC-KO} mice compared to their floxed littermates (Figure 12).

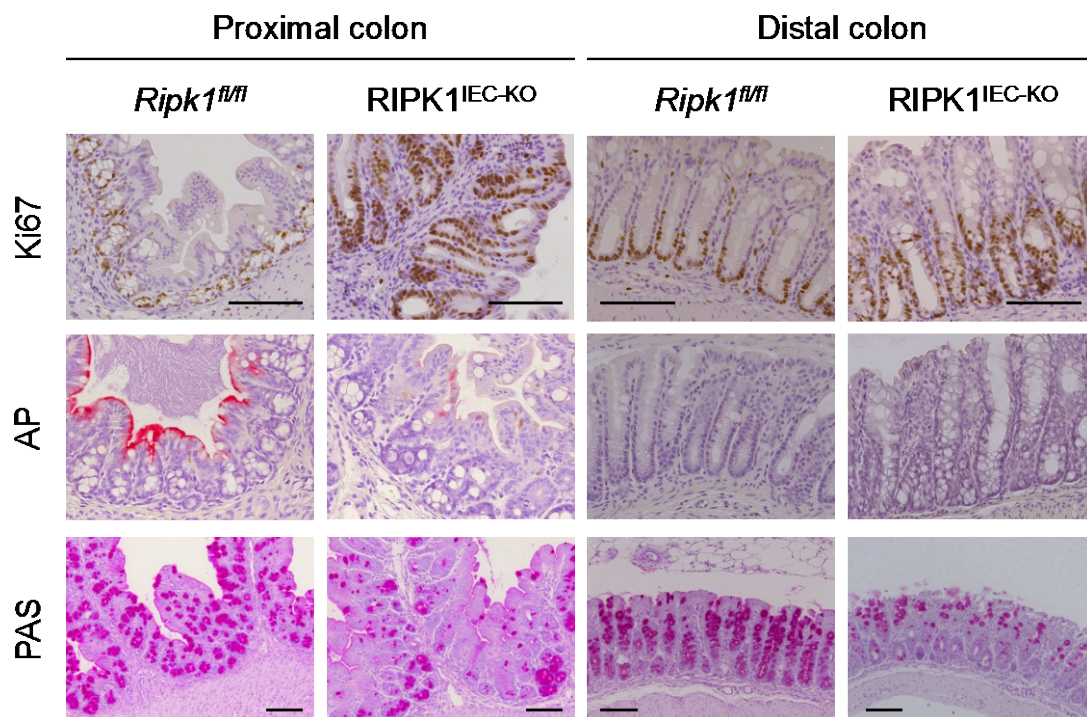


Figure 12 Hyperproliferation and reduced numbers of differentiated epithelial cells in the colon of RIPK1^{IEC-KO} mice.

Representative images of colon swiss rolls from 3-week old RIPK1^{IEC-KO} mice stained stained for AP, PAS, immunostained for Ki67 and counterstained with haematoxylin. Scale bars: 100 μ m.

To assess whether RIPK1^{IEC-KO} mice suffered from colitis, qRT-PCR was performed using whole colon tissue isolated from 3-week old RIPK1^{IEC-KO} and control mice. Messenger RNA levels for *Tnf*, *Ccl5*, *Cxcl1* and *Il1b* were significantly increased in RIPK1^{IEC-KO} mice compared to *Ripk1^{fl/fl}* mice (Figure 13). Expression levels of cytokine *Il12a* and chemokine *Ccl2* did not differ between 3-week old RIPK1^{IEC-KO} and *Ripk1^{fl/fl}* mice (Figure 13).

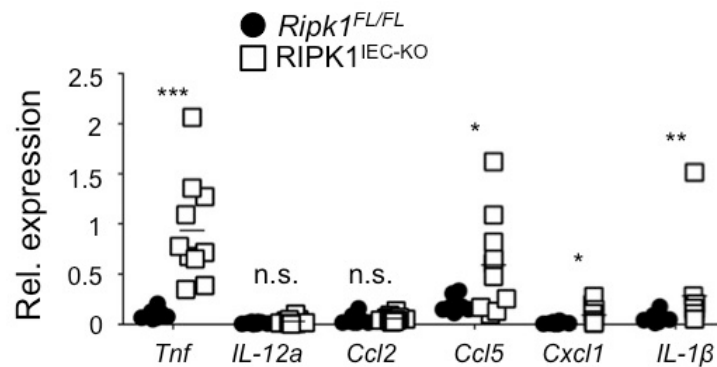


Figure 13 Differential expression of inflammatory cytokines and chemokines in the colon of 3-week old RIPK1^{IEC-KO} mice.

qRT-PCR analysis of inflammatory cytokine and chemokine expression levels in whole colonic tissue from 3-week old *Ripk1^{fl/fl}* and RIPK1^{IEC-KO} mice.

n.s. not significant. *P≤0.05, **P≤0.01, ***P≤0.005

In order to assess the composition of immune cells in the colon of RIPK1^{IEC-KO} mice, IHC against the different immune cell lineages was performed. Staining against CD45 showed that the overall number of immune cells was increased in the proximal but not in the distal colon (Figure 14). Gr1 positive granulocytes were only rarely detected in the lamina propria of RIPK1^{IEC-KO} mice (Figure 14). IHC indicated that the number of B220 positive B-cells did not differ between RIPK1^{IEC-KO} and *Ripk1^{fl/fl}* mice, however an increase in CD3 positive T-cells was detected in the proximal colon, but not the distal colon of RIPK1^{IEC-KO} mice when compared to control mice (Figure 14). For a direct quantitative comparison of leucocyte numbers, immune cells of the lamina propria were isolated from 3-week old RIPK1^{IEC-KO} mice and their *Ripk1^{fl/fl}* littermates, immunostained and subsequently analysed with FACS. The total number of CD45⁺ leucocytes in the lamina propria was significantly increased in RIPK1^{IEC-KO} mice compared to control mice (Figure 14). This increase was mainly due to significantly increased numbers of CD11b^{hi} Ly6G^{hi} neutrophils and CD3⁺ T-cells in RIPK1^{IEC-KO} mice. No differences in the numbers of

CD11b^{hi} F4/80⁺ Ly6G⁻ macrophages and B220⁺ B-cells were detected between RIPK1^{IEC-KO} mice and *Ripk1*^{fl/fl} mice (Figure 14). Taken together, these data show that RIPK1^{IEC-KO} mice develop a severe spontaneous phenotype in the proximal colon associated with extensive IEC apoptosis, hyperproliferation and mild inflammation characterized by moderately increased *mRNA* levels of a number of cytokines and chemokines as well as mild leucocyte infiltrations. In contrast to this, a comparable mild phenotype was observed in the distal part of the colon.

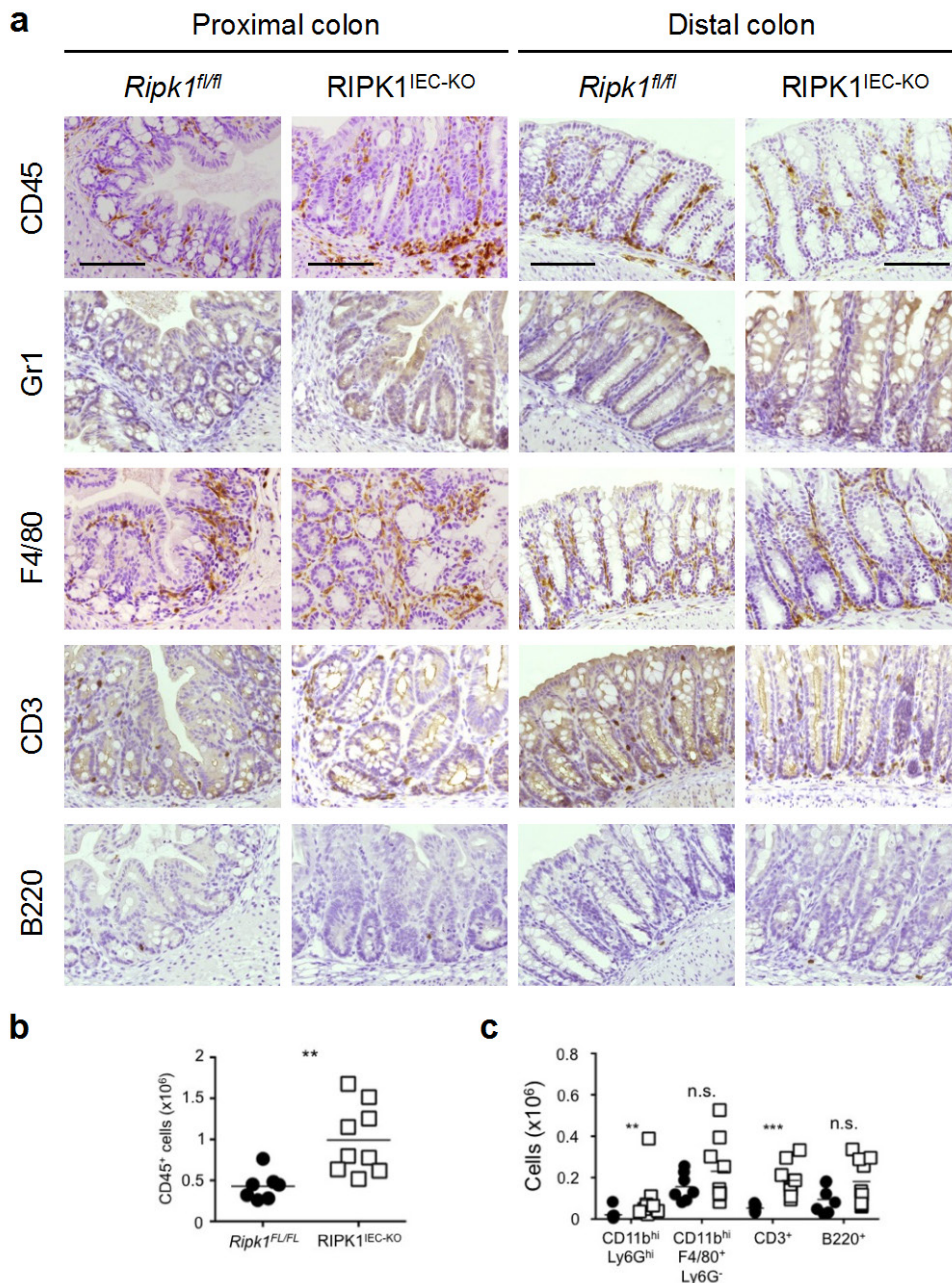


Figure 14 Increased infiltration of immune cells in the mucosa of RIPK1^{IEC-KO} mice.

(a) Colon swiss rolls from 3-week old *Ripk1^{fl/fl}* and RIPK1^{IEC-KO} mice were immunostained for CD45, Gr1, F4/80, CD3, B220 and counterstained with haematoxylin. Scale bars: 100 μ m (b) Colonic lamina propria immune cells were isolated from 3-week old *Ripk1^{fl/fl}* and RIPK1^{IEC-KO} mice, immunostained for CD45 and analysed by FACS. (c) Colonic lamina propria immune cells were isolated from 3-week old *Ripk1^{fl/fl}* and RIPK1^{IEC-KO} mice, immunostained for CD11b Ly6G (neutrophils), CD11b F4/80 Ly6G (macrophages), CD3 (T-cells) and B220 (B-cells) and analysed by flow cytometry. Isolation, immunostaining and FACS of lamina propria immune cells in (b) and (c) was done by Dr. Christina Eftychi. n.s. not significant. * $P \leq 0.05$, ** $P \leq 0.01$, *** $P \leq 0.005$

3.1.4 Progressive phenotype in RIPK1^{IEC-KO} mice

To investigate the development of the intestinal phenotype in RIPK1^{IEC-KO} mice, newborn and 7-day old RIPK1^{IEC-KO} mice were analysed. Newborn RIPK1^{IEC-KO} mice were macroscopically indistinguishable from their floxed littermates and exhibited a largely normal histopathology (data not shown and Figure 15a). Few apoptotic epithelial cells were found in the small intestine and the colon of newborn RIPK1^{IEC-KO} mice (Figure 15a). No difference in numbers of proliferating epithelial cells were detected, and numbers of CD45⁺ leucocytes did not differ between RIPK1^{IEC-KO} and *Ripk1*^{fl/fl} mice in both the ileum and colon (Figure 15a). qRT-PCR revealed that mRNA levels of the tested cytokines and chemokines, except for *Ccl5*, were not significantly up- or downregulated in RIPK1^{IEC-KO} mice compared to control mice (Figure 15).

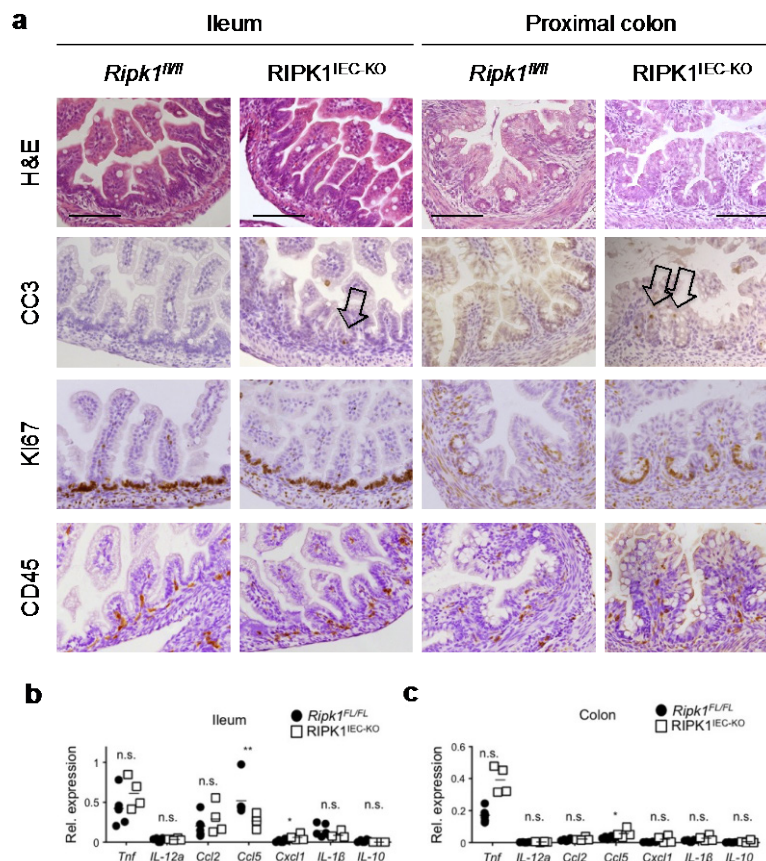


Figure 15. No intestinal pathology in newborn RIPK1^{IEC-KO} mice.

(a) Representative images of intestinal sections from newborn *Ripk1*^{fl/fl} and RIPK1^{IEC-KO} mice stained with H&E or immunostained for CC3, Ki67 and CD45. Scale bars: 100 μm. (b,c) qRT-PCR analysis of ileal (b) and colonic (c) whole tissue for mRNA expression levels of cytokines and chemokines in RIPK1^{IEC-KO} mice compared to *Ripk1*^{fl/fl} mice. n.s. not significant. *P≤0.05, **P≤0.01, ***P≤0.005

At 7 days of age, H&E stained sections of RIPK1^{IEC-KO} mice showed local loss of villus structures in the small intestine, elongated crypts and dying epithelial cells in both colon and small intestine (Figure 16a). IHC against CC3 revealed increased numbers of apoptotic cells in colon and small intestine of RIPK1^{IEC-KO} mice compared to floxed littermates (Figure 16a).

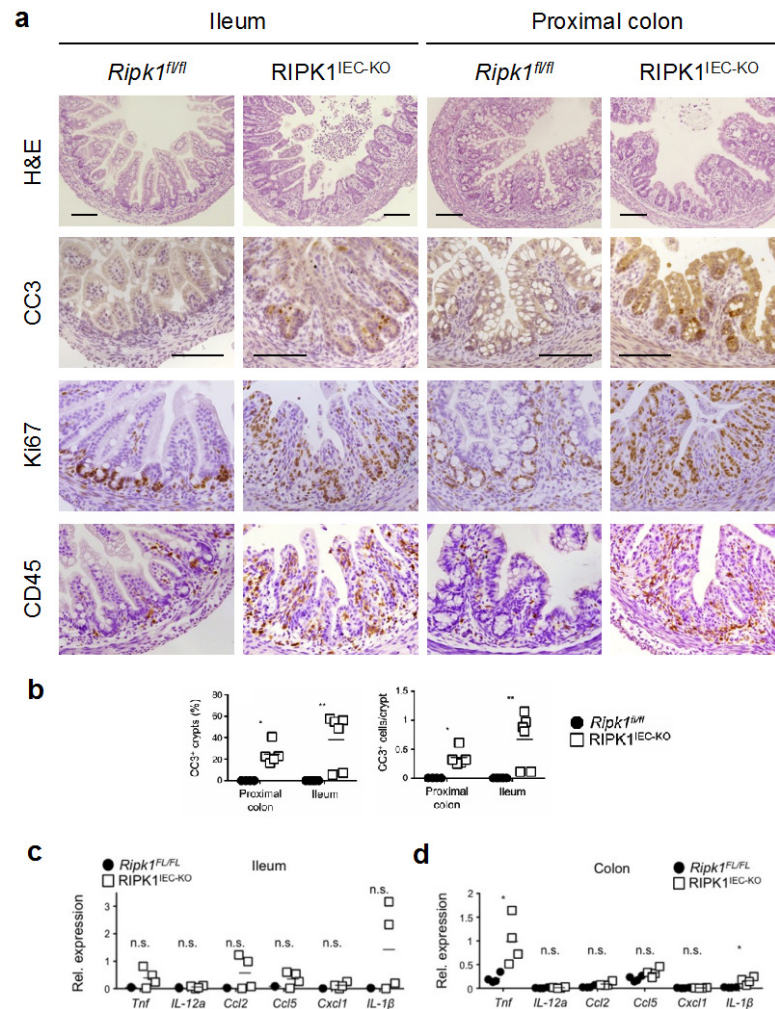


Figure 16. Intestinal pathology in 1-week old RIPK1^{IEC-KO} mice.

(a) Representative images of intestinal sections from 1-week old *Ripk1^{fl/fl}* and RIPK1^{IEC-KO} mice stained with H&E or immunostained for CC3, Ki67 or CD45. Scale bars: 100 μm (b) Quantification of crypts containing CC3⁺ cells and the number of CC3⁺ cells per crypts in 1-week-old *Ripk1^{fl/fl}* and RIPK1^{IEC-KO} mice. (c, d) qRT-PCR for mRNA expression levels of inflammatory cytokines and chemokines in ileal (b) and colonic (c) tissue from 1-week old *Ripk1^{fl/fl}* and RIPK1^{IEC-KO} mice. n.s. not significant. *P≤0.05, **P≤0.01, ***P≤0.005

Tissue section stainings as well as quantification of cell death revealed an intermediate stage between the extent of apoptosis observed in RIPK1^{IEC-KO} mice at 1 day and 3 weeks of age (Figure 16a, b). This indicates a

progressive exacerbation of the phenotype with age. Increased numbers of proliferating epithelial cells, a moderate increase in CD45+ leucocytes in the lamina propria accompanied by a moderate increase in *Tnf* and *Il1b* mRNA levels was observed in 1-week old RIPK1^{IEC-KO} mice (Figure 16a, c, d). These results suggest that the phenotype caused by RIPK1 ablation develops progressively after birth and hyperproliferation as well as mild inflammation in the colon and the small intestine occur in response to IEC apoptosis.

3.1.5 Inducible postnatal deletion of RIPK1 leads to intestinal pathology and lethality

To exclude potential developmental defects caused by IEC specific deletion of RIPK1 during embryogenesis, a tamoxifen-inducible mouse model was used (Marjou et al., 2004). In this transgenic mouse line, called *villin-CreER^{T2}*, Cre recombinase is fused to a mutated ligand-binding domain of the human estrogen receptor and expressed under the control of the IEC specific villin promoter (el Marjou et al., 2004).

Deletion of RIPK1 was achieved by three daily intraperitoneal (i.p.) injections of 1 mg tamoxifen and mice were sacrificed 24 h after the last tamoxifen injection (from here on referred to as 'RIPK1^{tamIEC-KO}') (Figure 17a). Efficient deletion of RIPK1 upon tamoxifen injections was confirmed by Western Blot analysis (Figure 17b). Acute depletion of RIPK1 caused a severe spontaneous intestinal pathology accompanied by 20% body weight loss and death of RIPK1^{tamIEC-KO} mice (Figure 17c, d). Histological analysis revealed that RIPK1^{tamIEC-KO} mice but not tamoxifen treated *Ripk1^{fl/fl}* littermates showed massive epithelial erosion, goblet cell loss and IEC apoptosis in the colon and the small intestine (Figure 18).

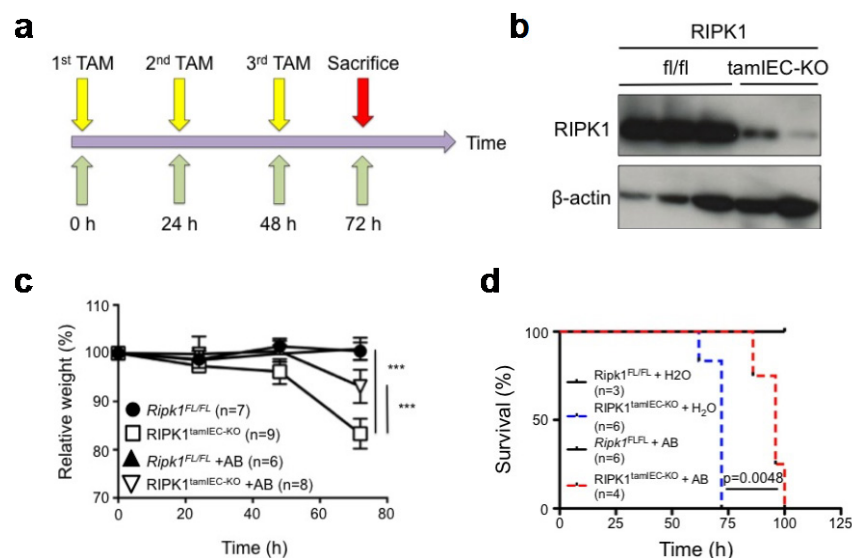


Figure 17. Acute deletion of RIPK1 results in body weight loss and lethality.

(a) Mice received three daily i.p. injections of 1 mg tamoxifen and were sacrificed 24h after the last injection. (b) Immunoblot analysis of small intestinal IEC protein extracts isolated from *Ripk1^{fl/fl}* mice and RIPK1^{tamIEC-KO} mice 24 h after the last tamoxifen injection. (c,d) Body weight (c) and Kaplan-Meier survival curve (d) of tamoxifen-injected *Ripk1^{fl/fl}* and RIPK1^{tamIEC-KO} mice receiving normal drinking water or antibiotics. 0h marks the timepoint of the first tamoxifen injection. h, hours AB, antibiotics. n.s. not significant. *P \leq 0.05, **P \leq 0.01, ***P \leq 0.005

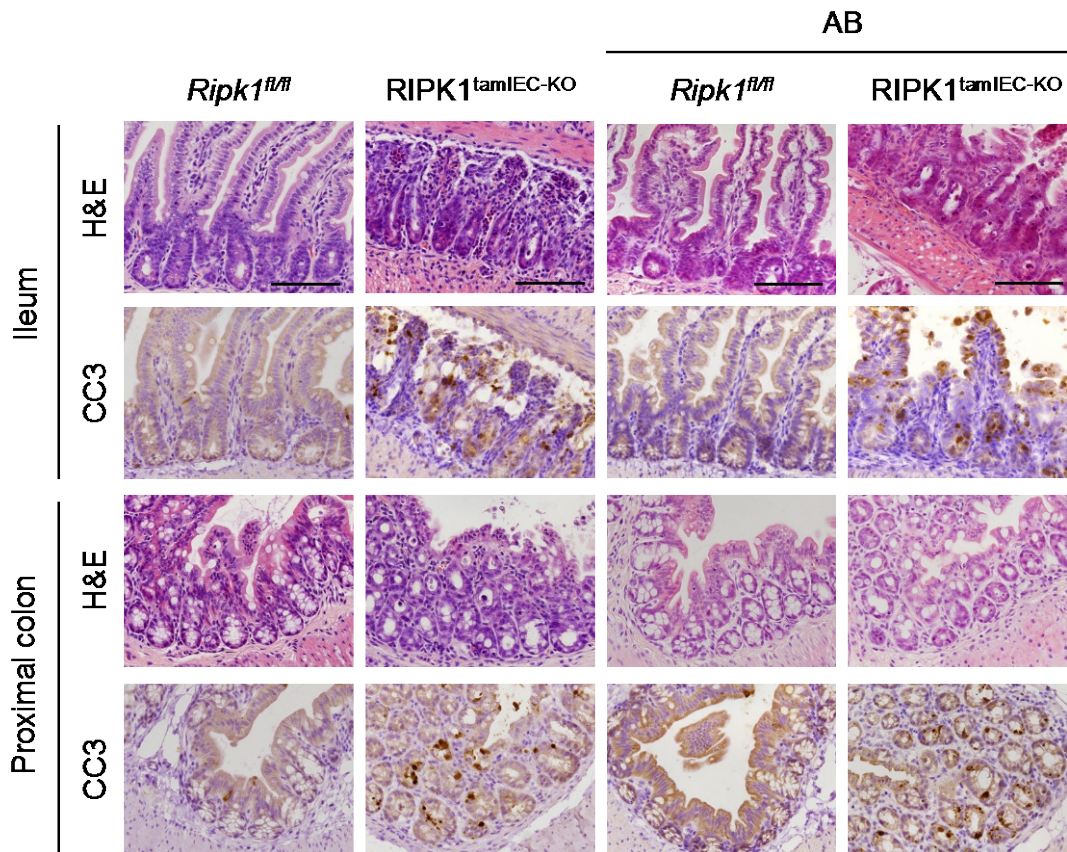


Figure 18. Epithelial erosion and IEC apoptosis upon acute deletion of RIPK1. Representative H&E stained or CC3 immunostained histological images from colonic and ileal swiss rolls of tamoxifen-treated *Ripk1^{fl/fl}* and *RIPK1^{tamIEC-KO}* mice receiving antibiotics (AB) or normal drinking water. Scale bars: 100 μ m

Importantly, vehicle treated *RIPK1^{tamIEC-KO}* mice as well as tamoxifen injected *villin-CreER^{T2}* mice did not develop intestinal pathology and increased IEC apoptosis, indicating that IEC apoptosis was specifically induced after deletion of RIPK1 (Figure 19a-d). These results demonstrate an important epithelial cell-intrinsic role of RIPK1 in preventing IEC apoptosis and maintaining intestinal homeostasis.

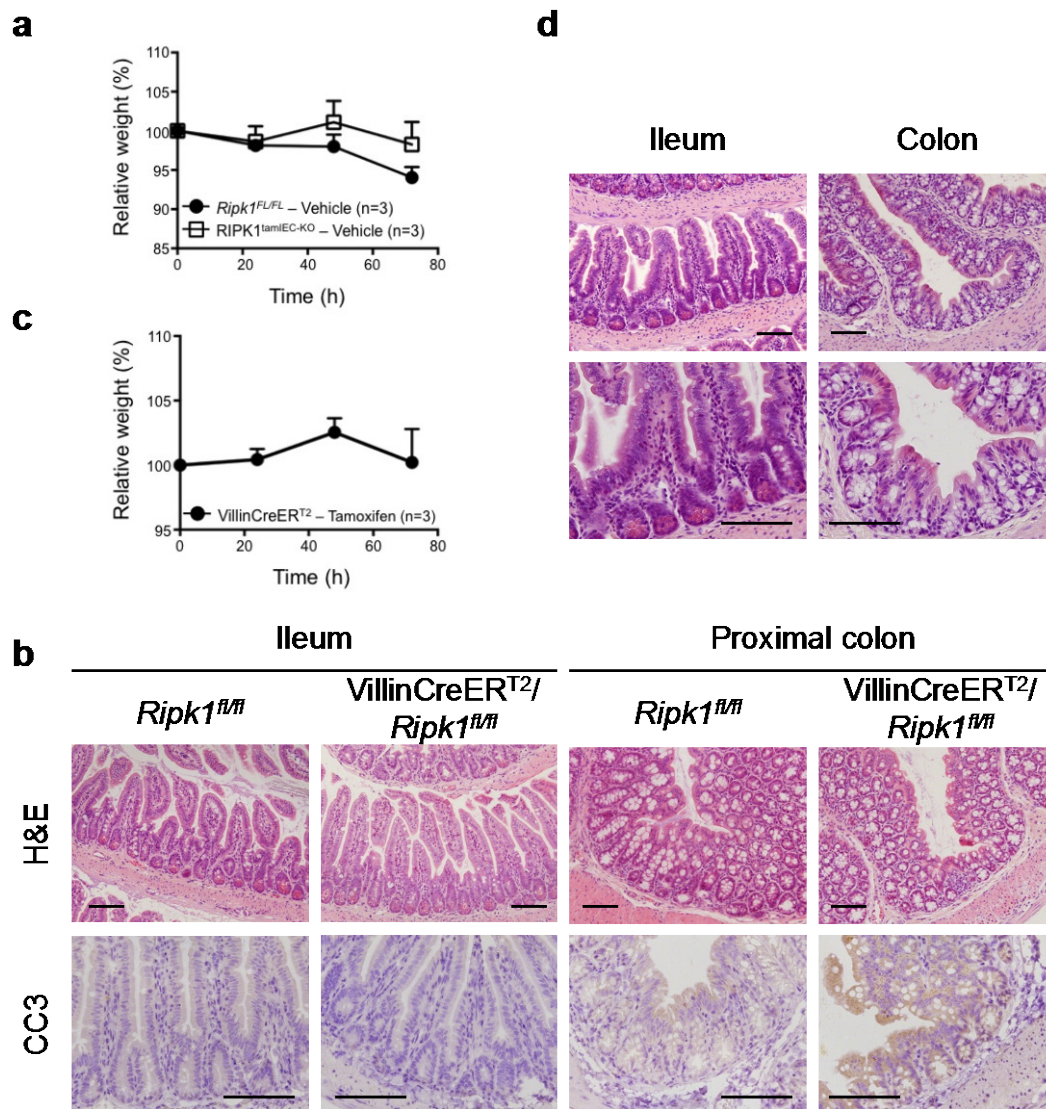


Figure 19. No intestinal pathology in vehicle treated *RIPK1*^{tamIEC-KO} mice and tamoxifen injected *VillinCreER*^{T2} mice
(a) Body weight of vehicle-treated *Ripk1*^{fl/fl} and *RIPK1*^{tamIEC-KO} mice. **(b)** Representative H&E stained colonic and ileal swiss rolls from vehicle-treated *Ripk1*^{fl/fl} and *RIPK1*^{tamIEC-KO} mice. Scale bars: 100 μ m. **(c)** Body weight of tamoxifen-injected *VillinCreER*^{T2} mice. **(d)** H&E stained colonic ileal swiss rolls from tamoxifen-injected *VillinCreER*^{T2} mice. Scale bars: 100 μ m.

3.2 Intestinal pathology in RIPK1^{IEC-KO} mice develops independent of the microbiota

3.2.1 Antibiotic treatment does not prevent development of intestinal disease in RIPK1^{IEC-KO} mice

The microbiota regulates intestinal homeostasis and contributes to intestinal inflammation in IBD patients as well as in genetic mouse models of IBD (Maloy & Powrie, 2011). In order to check if microbial derived signaling contributes to the phenotype observed in the RIPK1^{IEC-KO} mice, mice were treated with broad-spectrum antibiotics in the drinking water from E17.5 until 21 days of age to diminish microbial colonization of the gastrointestinal tract. At 3 weeks of age, antibiotic treated RIPK1^{IEC-KO} mice showed signs of wasting syndrome and had significantly reduced body weight compared to antibiotics receiving floxed littermates (Figure 20a). Although wasting occurred, the survival of AB treated SPF-housed RIPK1^{IEC-KO} mice was slightly prolonged compared to conventional SPF-housed RIPK1^{IEC-KO} mice (Figure 20b). Histological examination of H&E stained sections and immunostaining against CC3 showed that antibiotic treated RIPK1^{IEC-KO} mice developed intestinal pathology and showed extensive IEC apoptosis similar to conventional housed RIPK1^{IEC-KO} mice, suggesting that the microbiota does not contribute to the intestinal pathology observed in RIPK1^{IEC-KO} mice (Figure 20c).

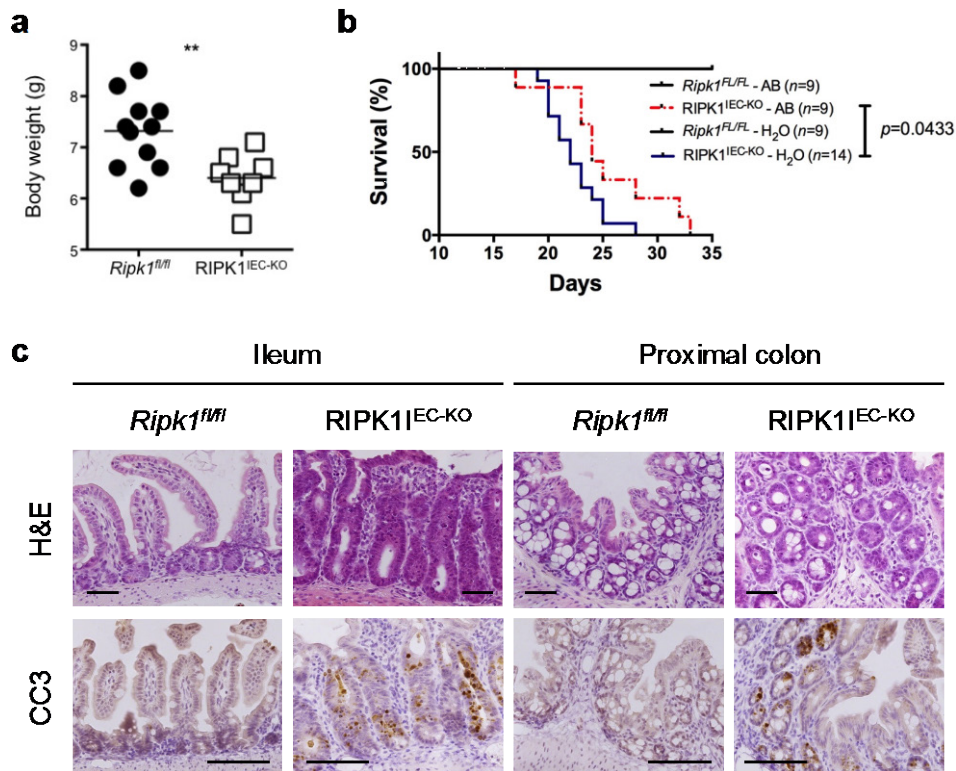


Figure 20. Antibiotic treatment does not prevent intestinal pathology in RIPK1^{IEC-KO} mice

(a) Body weight of 3-week old *Ripk1^{fl/fl}* and RIPK1^{IEC-KO} mice receiving antibiotics in the drinking water. (b) Kaplan-Meier survival curve of *Ripk1^{fl/fl}* and RIPK1^{IEC-KO} mice with normal water and antibiotics in the drinking water (data for conventional *Ripk1^{fl/fl}* and RIPK1^{IEC-KO} mice taken from Fig5c). (c) Representative images of intestinal sections from 3-week old antibiotic treated *Ripk1^{fl/fl}* and RIPK1^{IEC-KO} mice stained with H&E or immunostained against CC3. Scale bars: 100 μ m. n.s. not significant. * $P \leq 0.05$, ** $P \leq 0.01$, *** $P \leq 0.005$

3.2.2 Antibiotic treatment does not prevent intestinal pathology in RIPK1^{tamIEC-KO} mice

In order to investigate if the microbiota contributes to intestinal pathology induced upon acute deletion of RIPK1 (RIPK1^{tamIEC-KO} mice), cohorts of mice were treated with antibiotics in the drinking water for 4 weeks prior to deletion of RIPK1. Microbiota depletion significantly reduced body weight loss in RIPK1^{tamIEC-KO} mice and prolonged survival compared to conventional housed RIPK1^{tamIEC-KO} mice (Figure 17c, d). However, neither intestinal pathology nor the extent of cell death was ameliorated but rather delayed in antibiotic treated RIPK1^{tamIEC-KO} mice (Figure 18). In line with the results from the antibiotic treated conditional RIPK1 knockout mice, diminishing the microbiota had a mild effect on the macroscopic appearance of the mice but had no effect on the intestinal pathology.

3.2.3 RIPK1^{IEC-KO} mice develop intestinal disease independent of the microbiota

To unequivocally address the role of microbial induced signaling in RIPK1^{IEC-KO} mice, germfree RIPK1^{IEC-KO} mice were generated in the gnotobiotic facilities of the Universities of Ulm and Hannover. At 3-weeks of age, germfree RIPK1^{IEC-KO} mice had significantly reduced body weight compared to germfree *Ripk1*^{fl/fl} littermates (Figure 21a). Despite wasting, some germfree RIPK1^{IEC-KO} mice showed prolonged survival compared to SPF housed RIPK1^{IEC-KO} mice survived up to 16 weeks of age (Figure 21b).

Histological examination of H&E stained sections from colon and ileum of 3-week old mice revealed that germfree RIPK1^{IEC-KO} mice developed intestinal pathology (Figure 21c). To directly compare tissue damage between SPF housed and germfree RIPK1^{IEC-KO} mice, H&E stained sections were subjected to a blindfolded semi-quantitative composite scoring system addressing intestinal pathology (Adolph et al., 2013). In the colon, germfree RIPK1^{IEC-KO} mice exhibit tissue damage to the same extent as SPF housed RIPK1^{IEC-KO} mice, whereas in the ileum pathology is slightly but significantly ameliorated in germfree RIPK1^{IEC-KO} mice (Figure 21d). IHC for CC3 showed that germfree RIPK1^{IEC-KO} mice were not protected against apoptosis of IECs in the colon and the ileum. Quantification of cell death revealed that numbers of apoptotic IECs were significantly increased in the distal colon of germfree RIPK1^{IEC-KO} mice but did not differ in the proximal colon and the ileum compared to SPF RIPK1^{IEC-KO} mice (Figure 21e).

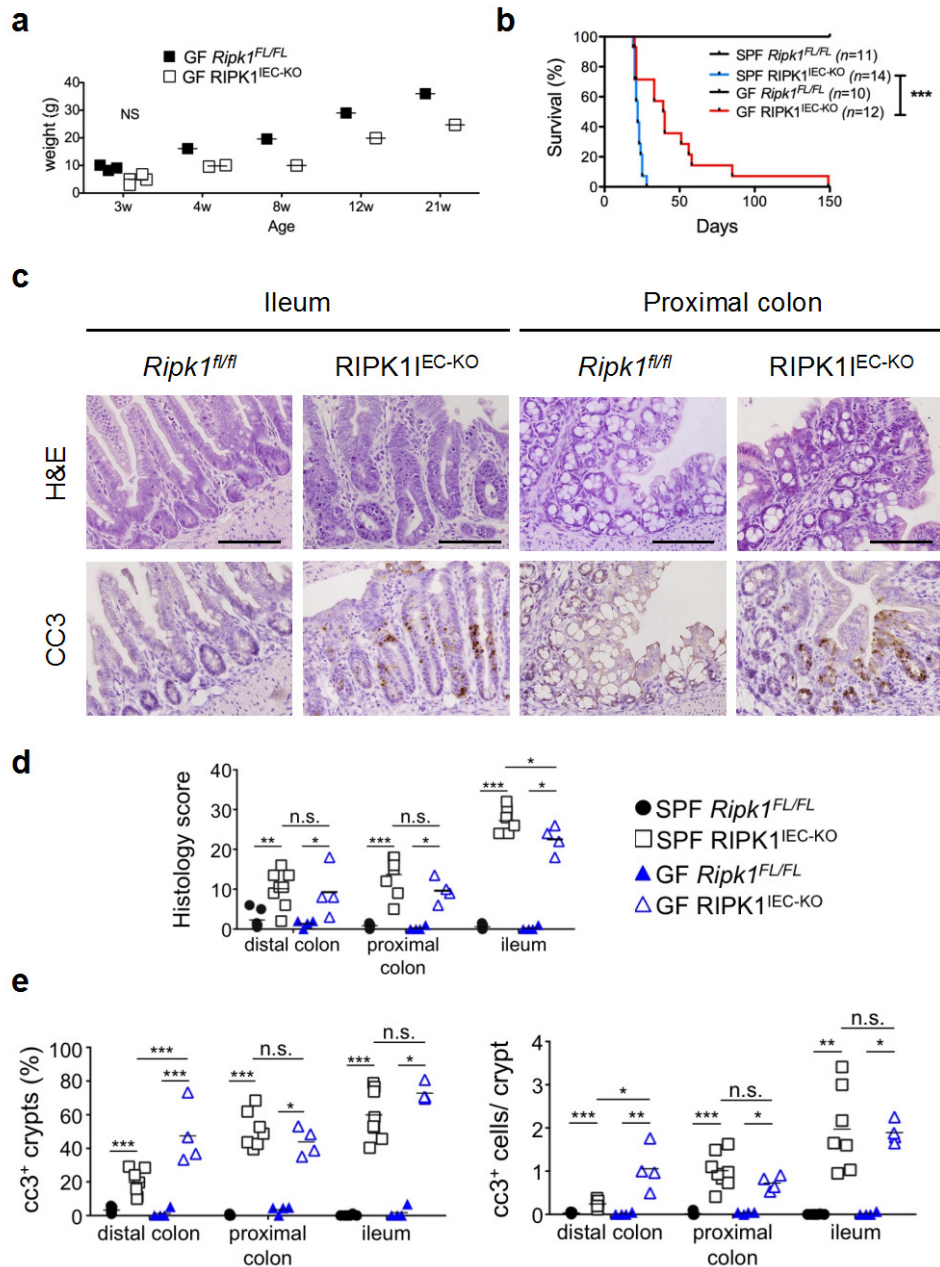


Figure 21. Microbiota independent intestinal disease in RIPK1^{IEC-KO} mice
(a) Body weight of germ-free *Ripk1*^{fl/fl} and RIPK1^{IEC-KO} mice at different ages. **(b)** Kaplan-Meier survival curve of SPF-housed germ-free *Ripk1*^{fl/fl} and RIPK1^{IEC-KO} mice. Survival data of SPF-housed *Ripk1*^{fl/fl} and RIPK1^{IEC-KO} mice taken from Fig.5c) **(c)** Representative images of intestinal sections from 3-week old germ-free *Ripk1*^{fl/fl} and RIPK1^{IEC-KO} mice stained with H&E or immunostained for CC3. Scale bars: 100 μ m. **(d)** Quantification of intestinal pathology observed in SPF-housed and germ-free RIPK1^{IEC-KO} mice at 3-week of age. Histology scoring was performed by Dr. Katerina Vlantis. **(e)** Quantification of crypts containing CC3-positive cells and the number of CC3-positive cells per crypt in the colon and small intestine of 3-week old SPF-housed and germ-free *Ripk1*^{fl/fl} and RIPK1^{IEC-KO} mice. Data for SPF-housed *Ripk1*^{fl/fl} and RIPK1^{IEC-KO} mice were taken from Figure 8b and 11b. n.s. not significant. *P \leq 0.05, **P \leq 0.01, ***P \leq 0.005

3.2.4 Phenotype in RIPK1^{IEC-KO} mice develops independently of Myd88-mediated signaling

RIPK1 is a signaling adapter protein involved in bacterial induced toll-like receptor (TLR) signaling. To investigate a potential contribution of TLR-signaling to *Ripk1*^{-/-} IEC apoptosis and intestinal disease of RIPK1^{IEC-KO} mice, RIPK1^{IEC-KO} mice were crossed with *Myd88* full body knockout mice, to generate mice, with ablation of RIPK1 specifically in the intestinal epithelium and MYD88 in all cells of the mice (Adachi et al., 1998). Full body MYD88 deficiency did not prevent severe wasting and premature death of RIPK1^{IEC-KO} mice (Figure 22a and data not shown). Analysis of H&E stained sections revealed that 3 week old RIPK1^{IEC-KO}/*Myd88*^{-/-} mice developed intestinal pathology in the colon and the ileum (Figure 22b). CC3 staining showed high numbers of apoptotic IECs in the colon and ileum. Except for the distal colon, where more apoptotic cells were found, IEC apoptosis occurred to the same extent as observed in RIPK1^{IEC-KO} mice (Figure 22b, c). These results suggest, that microbiota induced TLR signaling does not trigger cell death in *Ripk1*^{-/-} IECs and does not contribute to the pathology observed in RIPK1^{IEC-KO} mice.

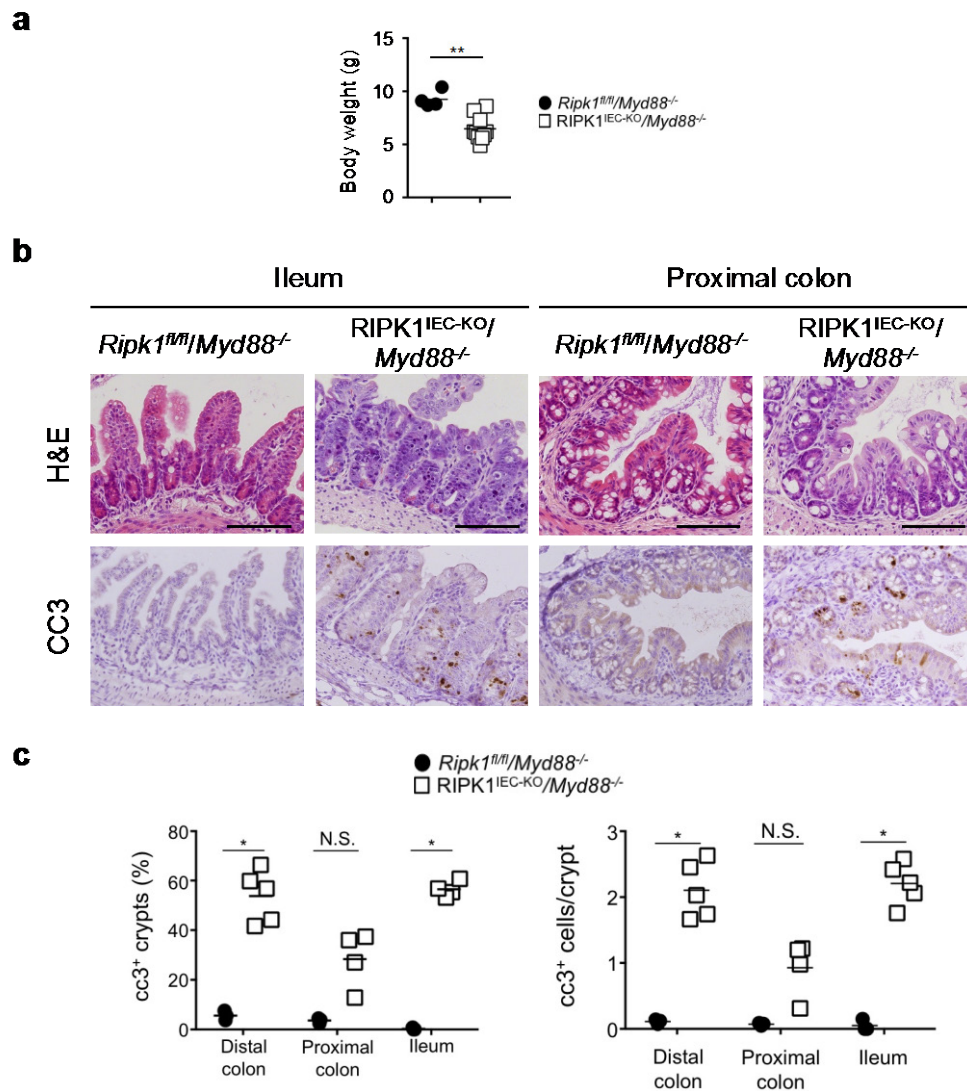


Figure 22. *Myd88* independent pathology in *RIPK1^{IEC-KO}* mice

(a) Body weight of 3-week old *Ripk1^{fl/fl}/Myd88^{-/-}* and *RIPK1^{IEC-KO}/Myd88^{-/-}* mice. (b) Representative images from intestinal sections from 3-week old *Ripk1^{fl/fl}/Myd88^{-/-}* and *RIPK1^{IEC-KO}/Myd88^{-/-}* mice stained with H&E or immunostained for CC3. Scale bars: 100 μ m (c) Quantification of crypts containing CC3-positive cells and the number of CC3-positive cells per crypt in the colon and small intestine of 3-week old *Ripk1^{fl/fl}/Myd88^{-/-}* and *RIPK1^{IEC-KO}/Myd88^{-/-}* mice. n.s. not significant. * $P \leq 0.05$, ** $P \leq 0.01$, *** $P \leq 0.005$

3.3 Intestinal pathology in RIPK1^{IEC-KO} mice partially depends on TNF signaling

RIPK1 is an important signaling node downstream of TNFR1, which can induce cell death as well as cell survival. To address whether TNFR1 mediated signaling is involved in the development of the intestinal pathology and apoptosis observed in RIPK1^{IEC-KO} mice, RIPK1^{IEC-KO} mice were crossed with *Tnfr1* (*Tnfrsf1a*) full body knockout mice (Pfeffer et al., 1993). Resulting RIPK1^{IEC-KO}/*Tnfr1*^{-/-} mice were deficient for RIPK1 specifically in IECs and lacked TNFR1 in all cells of the mice. RIPK1^{IEC-KO}/*Tnfr1*^{-/-} mice were partially protected from cachexia and 50% of the mice survived until 3 months of age (Figure 23a, b), indicating that severe wasting and premature death of RIPK1^{IEC-KO} mice depends on TNFR1 mediated signaling. Histological examination of H&E stained sections from 3-week old RIPK1^{IEC-KO}/*Tnfr1*^{-/-} mice revealed partial protection from villus atrophy in the ileum, a less severe reduction of goblet cells in colon and small intestine as well as reduced numbers of epithelial cells in the epithelium with morphological features of dying cells (Figure 23c). Immunohistochemistry for CC3 and quantification of cell death revealed reduced numbers of apoptotic IECs in the ileum as well as proximal colon of RIPK1^{IEC-KO}/*Tnfr1*^{-/-} mice and increased IEC apoptosis in the distal colon compared to RIPK1^{IEC-KO} mice (Figure 23c, d). These results suggest that TNFR1 mediated signaling contributes to intestinal pathology and cell death in RIPK1^{IEC-KO} mice, but also TNFR1-independent signaling appears to be involved.

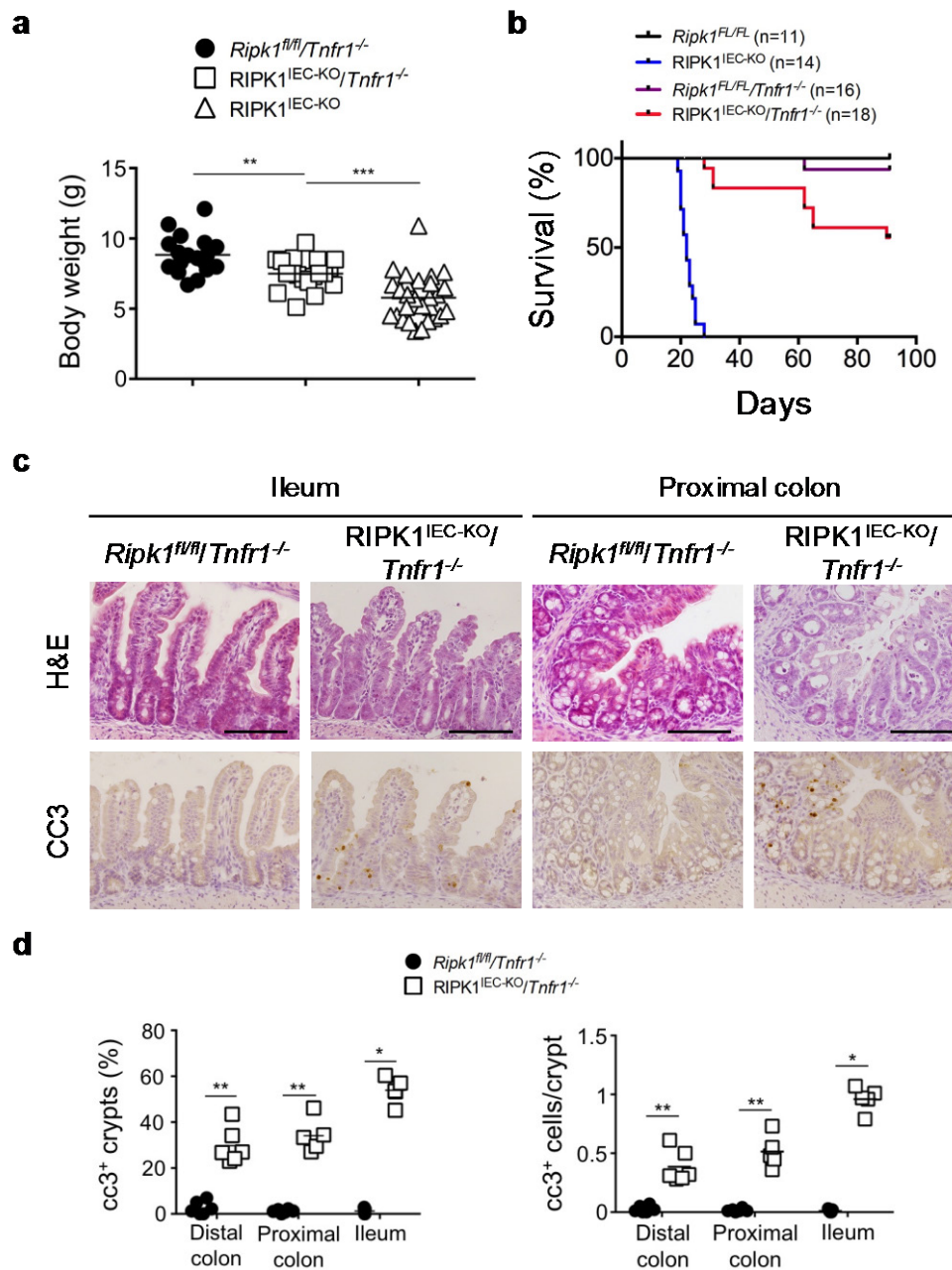


Figure 23. Premature lethality and IEC apoptosis in *RIPK1^{IEC-KO}* mice partially depend on TNFR1-mediated signaling.

(a) Body weight of 3-week old *RIPK1^{IEC-KO}* mice, *Ripk1^{fl/fl}/Tnfr1^{-/-}* and *RIPK1^{IEC-KO}/Tnfr1^{-/-}* mice. Data for *RIPK1^{IEC-KO}* mice were taken from Figure 5b. (b) Kaplan-Meier survival curve for *RIPK1^{IEC-KO}*, *Ripk1^{fl/fl}/Tnfr1^{-/-}* and *RIPK1^{IEC-KO}/Tnfr1^{-/-}* mice. Survival data of *RIPK1^{IEC-KO}* mice was taken from Figure 5c. (c) Representative images from intestinal sections from 3-week old *Ripk1^{fl/fl}/Tnfr1^{-/-}* and *RIPK1^{IEC-KO}/Tnfr1^{-/-}* mice were stained with H&E or immunostained for CC3. Scale bars: 100 μ m (d) Quantification of crypts containing CC3-positive cells and the number of CC3-positive cells per crypt in the colon and ileum of 3-week old *Ripk1^{fl/fl}/Tnfr1^{-/-}* and *RIPK1^{IEC-KO}/Tnfr1^{-/-}* mice. n.s. not significant. * $P \leq 0.05$, ** $P \leq 0.01$, *** $P \leq 0.001$

3.4 Death of *Ripk1*^{-/-} IECs depends on FADD and RIPK3 mediated signaling

3.4.1 Apoptosis in RIPK1^{IEC-KO} mice depends on FADD

Execution of extrinsic apoptosis is mediated by FADD and caspase-8 (Boldin, Goncharov, Goltsev, & Wallach, 1996; Chinnaiyan, O'Rourke, Tewari, & Dixit, 1995; Muzio et al., 1996). FADD integrates upstream signals with its DD and binds to caspase-8 via its DED, inducing caspase-8 dimerization that triggers its autocatalytic activity resulting in the execution of apoptosis (Muzio et al., 1996; Muzio, Stockwell, Stennicke, Salvesen, & Dixit, 1998). To assess if *Ripk1*^{-/-} IECs die by FADD-caspase-8 dependent apoptosis, RIPK1^{IEC-KO} mice were crossed to *Fadd*^{f/f} mice (Mc Guire et al., 2010). Resulting RIPK1^{IEC-KO}/FADD^{IEC-KO} mice, that were deficient for RIPK1 and FADD specifically in IECs, had only slightly reduced body weight at 3 weeks of age and a normal life span (Figure 24a, b). In contrast to this, RIPK1^{IEC-KO}/FADD^{hetIEC-KO} littermate mice had reduced body weight and died prematurely similar to RIPK1^{IEC-KO} mice, indicating that wasting and premature death of RIPK1^{IEC-KO} mice is caused by FADD mediated processes (Figure 24a, b). Analysis of H&E stained ileal sections revealed that 3-week old RIPK1^{IEC-KO}/FADD^{IEC-KO} mice did not develop similar intestinal pathology as observed in RIPK1^{IEC-KO} mice, whereas their RIPK1^{IEC-KO}/FADD^{hetIEC-KO} littermates did (Figure 24c). Staining for lysozyme indicated that Paneth cell loss in RIPK1^{IEC-KO}/FADD^{IEC-KO} mice persisted (Figure 24c). Furthermore, RIPK1^{IEC-KO}/FADD^{IEC-KO} mice had slightly increased numbers of immune cells in the ileal lamina propria as shown by immunohistochemical staining for CD45 (Figure 24c). Importantly, CC3 staining showed significantly reduced numbers of apoptotic IECs in the ileum of RIPK1^{IEC-KO}/FADD^{IEC-KO} mice (Figure 24c, d), indicating that *Ripk1*^{-/-} IECs died by FADD dependent apoptosis. However, many dying CC3 negative IECs were detected, suggesting that these died a caspase-independent death (Figure 24c inset, arrow). In conclusion, these results show that small intestinal pathology in RIPK1^{IEC-KO} mice is caused by FADD-dependent IEC apoptosis. The additional epithelial specific ablation of FADD prevents IECs apoptosis, but triggers non-apoptotic death of IECs and a pathology reminiscent of the phenotype described for FADD^{IEC-KO} mice (Welz et al., 2011).

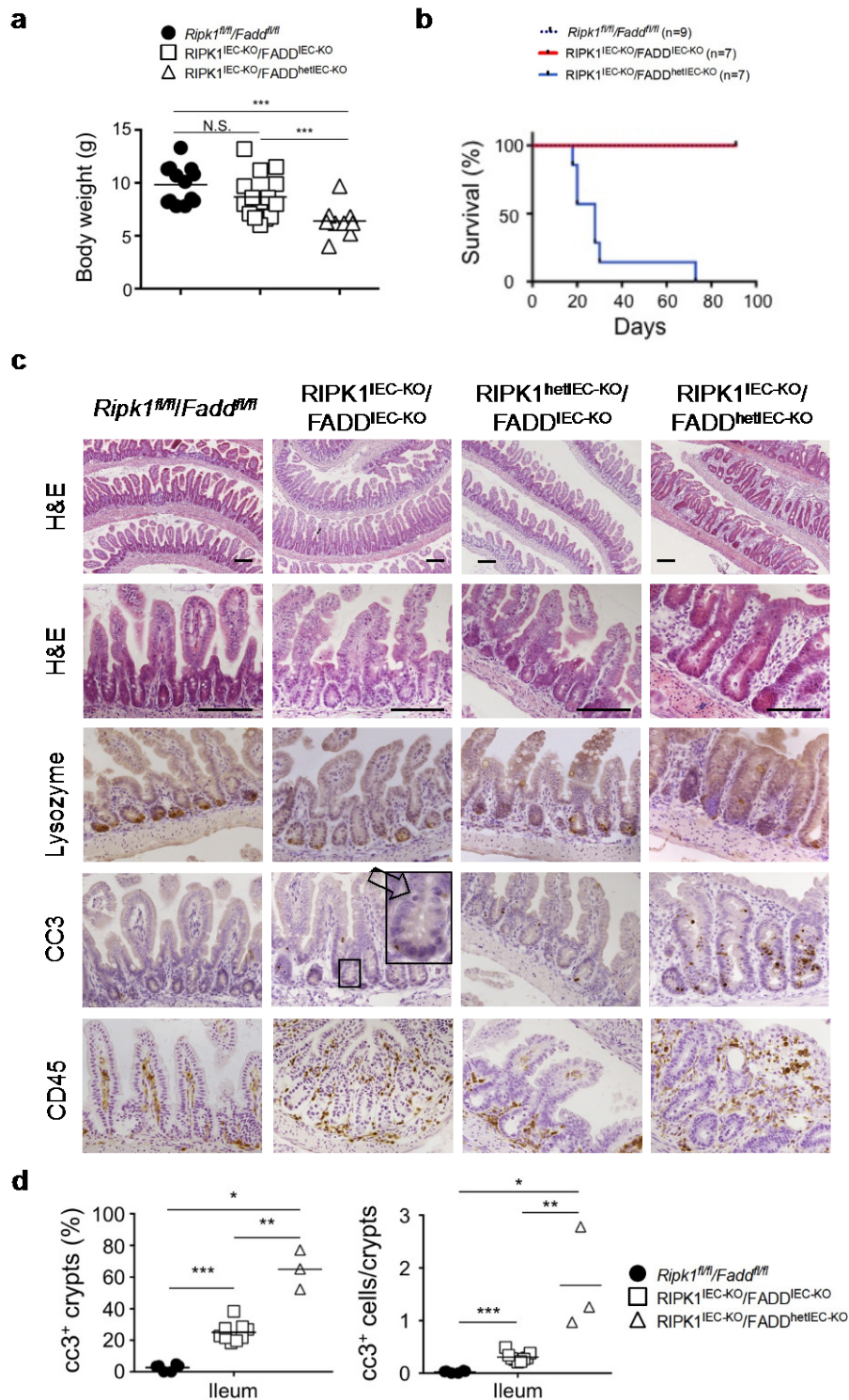


Figure 24. FADD-dependent IEC apoptosis in the ileum of $RIPK1^{IEC-KO}$ mice. (a) Body weight of 3-week old *Ripk1^{fl/fl}/Fadd^{fl/fl}*, *RIPK1^{IEC-KO}/FADD^{hetIEC-KO}* and *RIPK1^{IEC-KO}/FADD^{IEC-KO}* mice. (b) Kaplan-Meier survival curve of mice with the indicated genotypes. (c) Representative images of ileal sections from mice with the indicated genotypes stained with H&E or immunostained for Lysozyme, CC3 and CD45. Scale bars: 100 μ m (d) Quantification of crypts containing CC3-positive cells and the number of CC3-positive cells per crypt in the ileum of 3-week old *Ripk1^{fl/fl}/Fadd^{fl/fl}*, *RIPK1^{IEC-KO}/FADD^{hetIEC-KO}* and *RIPK1^{IEC-KO}/FADD^{IEC-KO}* mice. n.s. not significant. * $P \leq 0.05$, ** $P \leq 0.01$, *** $P \leq 0.005$

To understand the role of FADD in the context of the colonic RIPK1^{IEC-KO} phenotype, 3-week old RIPK1^{IEC-KO}/FADD^{IEC-KO} mice were analysed. Similar to the ileum, ablation of FADD in RIPK1-deficient IECs significantly reduced the extent of pathology and the number of CC3 positive cells in the proximal colon when compared to RIPK1^{IEC-KO}/FADD^{hetIEC-KO} or RIPK1^{IEC-KO} mice (Figure 25). In stark contrast to RIPK1^{IEC-KO} mice, where the distal colon was only mildly affected, 3-week old RIPK1^{IEC-KO}/FADD^{IEC-KO} mice showed an aggravated pathology in this region (Figure 25). Examination of H&E stained colon sections revealed that 8 out of 14 RIPK1^{IEC-KO}/FADD^{IEC-KO} mice showed areas with epithelial erosion and elevated numbers of infiltrating immune cells at 3 weeks of age in the distal to medial colon, which have never been observed in RIPK1^{IEC-KO} mice (n=18) (Figure 25). This was further supported by staining for CD45, which revealed increased numbers of immune cells in the distal colon of RIPK1^{IEC-KO}/FADD^{IEC-KO} mice (Figure 25). As described for the ileum and proximal colon, few CC3 positive dying cells were detected but high numbers of dying CC3 negative cells were found in the epithelium and lumen of the crypts of RIPK1^{IEC-KO}/FADD^{IEC-KO} mice (Figure 25a magnified inset with arrow, b).

Adult RIPK1^{IEC-KO}/FADD^{IEC-KO} mice had similar body weight like their floxed littermates (data not shown). Analysis of H&E stained ileal sections from 13-week old RIPK1^{IEC-KO}/FADD^{IEC-KO} mice revealed villus shortening, loss of goblet and Paneth cells and crypt elongation, which were not observed in *Ripk1^{fl/fl}/Fadd^{fl/fl}* mice. Few dying cells but no gross aberrant morphological changes were observed in the proximal colon of 13-week old RIPK1^{IEC-KO}/FADD^{IEC-KO} mice (Figure 26). In the distal colon many dying IECs were found in the epithelium and the presence of ulcers were detected in adult RIPK1^{IEC-KO}/FADD^{IEC-KO} mice (Figure 26).

Taken together, these data show that IECs in RIPK1^{IEC-KO} mice die by FADD dependent apoptosis and additional IEC specific deletion of FADD protects *Ripk1^{-/-}* IECs from undergoing apoptosis, however sensitizes IECs to a caspase-independent death.

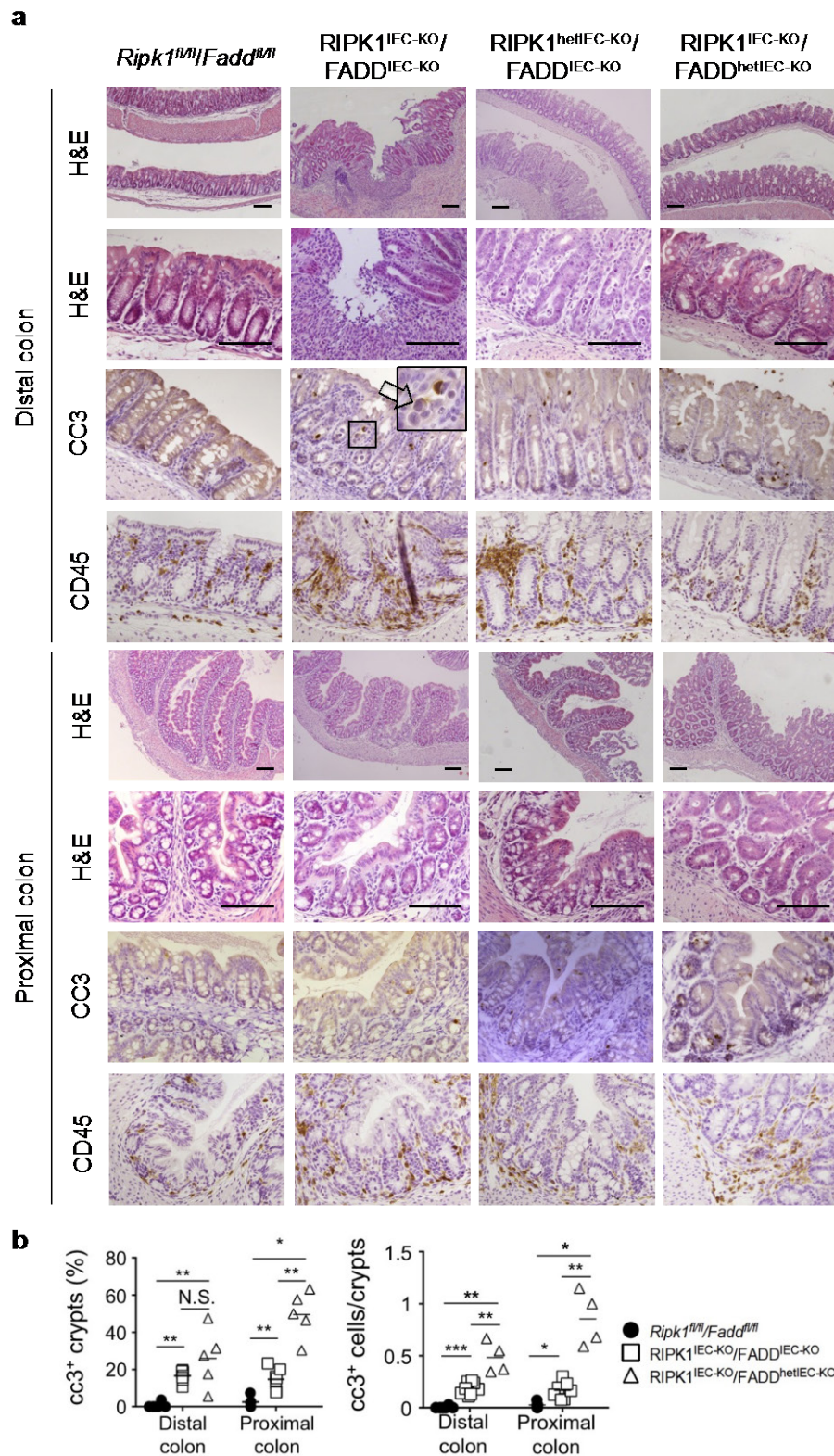


Figure 25. Caspase-independent IEC death and ulcerating colitis in $RIPK1^{IEC-KO}/FADD^{IEC-KO}$ mice.

(a) Representative images from H&E stained and CC3 or CD45 immunostained colon swiss rolls from 3-week old mice with the indicated genotypes. Scale bars: 100 μ m (d) Quantification of crypts containing CC3-positive cells and the number of CC3-positive cells per crypt in the distal and proximal colon from 3-week old $Ripk1^{fl/fl}/Fadd^{fl/fl}$, $RIPK1^{IEC-KO}/FADD^{hetIEC-KO}$ and $RIPK1^{IEC-KO}/FADD^{IEC-KO}$ mice. n.s. not significant. * $P \leq 0.05$, ** $P \leq 0.01$, *** $P \leq 0.005$

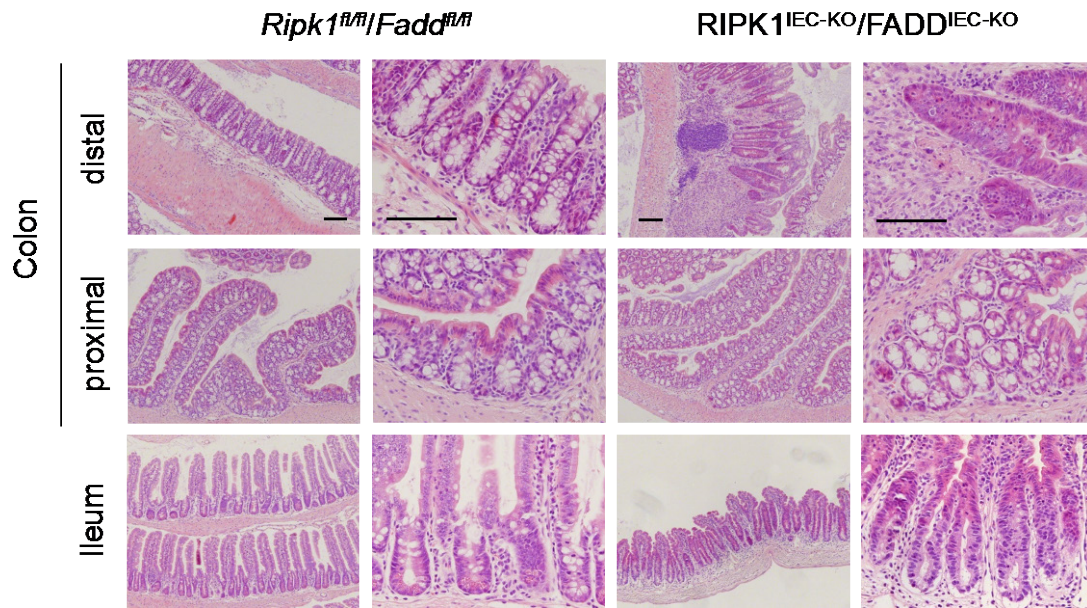


Figure 26. Colitis and small intestinal pathology in adult $RIPK1^{IEC-KO}/FADD^{IEC-KO}$ mice.

Histological analysis of H&E stained colonic and ileal sections from adult $Ripk1^{fl/fl}/Fadd^{fl/fl}$ and $RIPK1^{IEC-KO}/FADD^{IEC-KO}$ mice. Scale bars: 100 μ m.

3.4.2 Death of IECs in $RIPK1^{IEC-KO}/FADD^{IEC-KO}$ mice depends on RIPK3 mediated necroptosis

RIPK3 and its kinase activity have been shown to be crucial for the execution of TNF-induced necroptosis (Cho et al., 2009; He et al., 2009; D. W. Zhang et al., 2009). Murine RIPK3 deficiency does not result in a significant phenotypic effect, enabling to study the role of RIPK3 and necroptosis in various infection and disease models (Newton et al., 2004; Vanden Berghe, Linkermann, Jouan-Lanhouet, Walczak, & Vandenabeele, 2014). In the context of intestinal epithelial specific FADD deficiency, RIPK3 was reported to be an essential mediator non-apoptotic death of IECs (Welz et al., 2011). Given the striking phenotypic similarities between $FADD^{IEC-KO}$ and $RIPK1^{IEC-KO}/FADD^{IEC-KO}$ mice, it could be possible that pathology in $RIPK1^{IEC-KO}/FADD^{IEC-KO}$ mice depends on RIPK3 dependent death. To investigate the role of RIPK3 in RIPK1- and FADD-double deficient IECs, $RIPK1^{IEC-KO}/FADD^{IEC-KO}$ mice were crossed to $Ripk3^{-/-}$ mice (Newton et al., 2004).

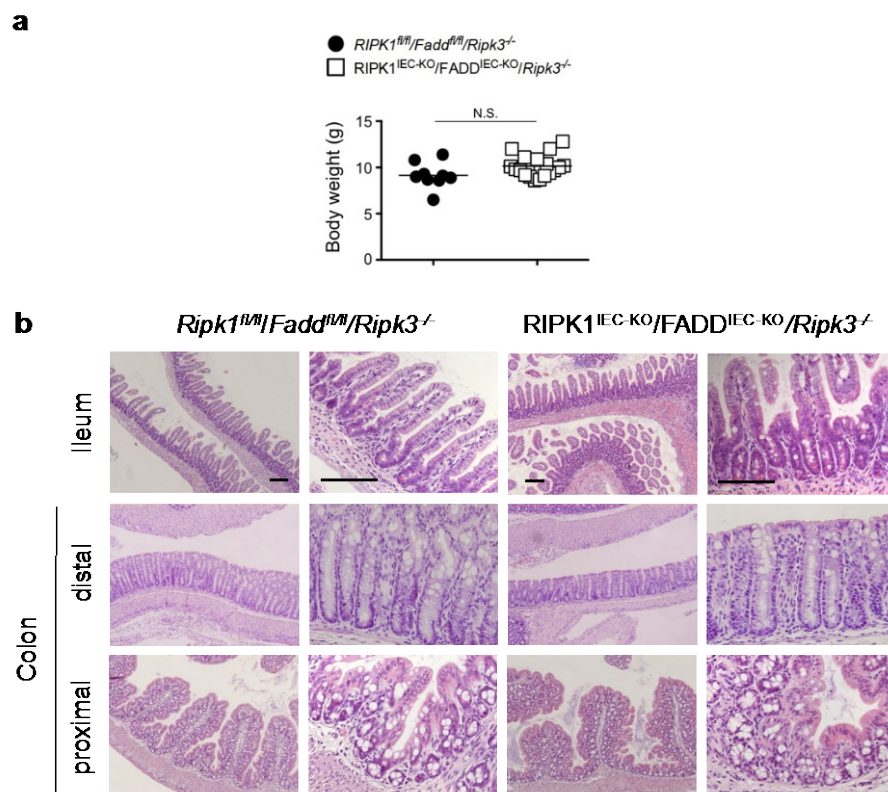


Figure 27. Intestinal pathology in $RIPK1^{IEC-KO}/FADD^{IEC-KO}$ depends on RIPK3. (a) Body weight of 3-week old $RIPK1^{IEC-KO}/FADD^{IEC-KO}/Ripk3^{-/-}$ and $Ripk1^{fl/fl}/Fadd^{fl/fl}/Ripk3^{-/-}$ mice. (b) Representative histological images from H&E stained ileal and colonic sections from 3-week old $RIPK1^{IEC-KO}/FADD^{IEC-KO}/Ripk3^{-/-}$ and $Ripk1^{fl/fl}/Fadd^{fl/fl}/Ripk3^{-/-}$ mice. Scale bars: 100 μ m. n.s. not significant.

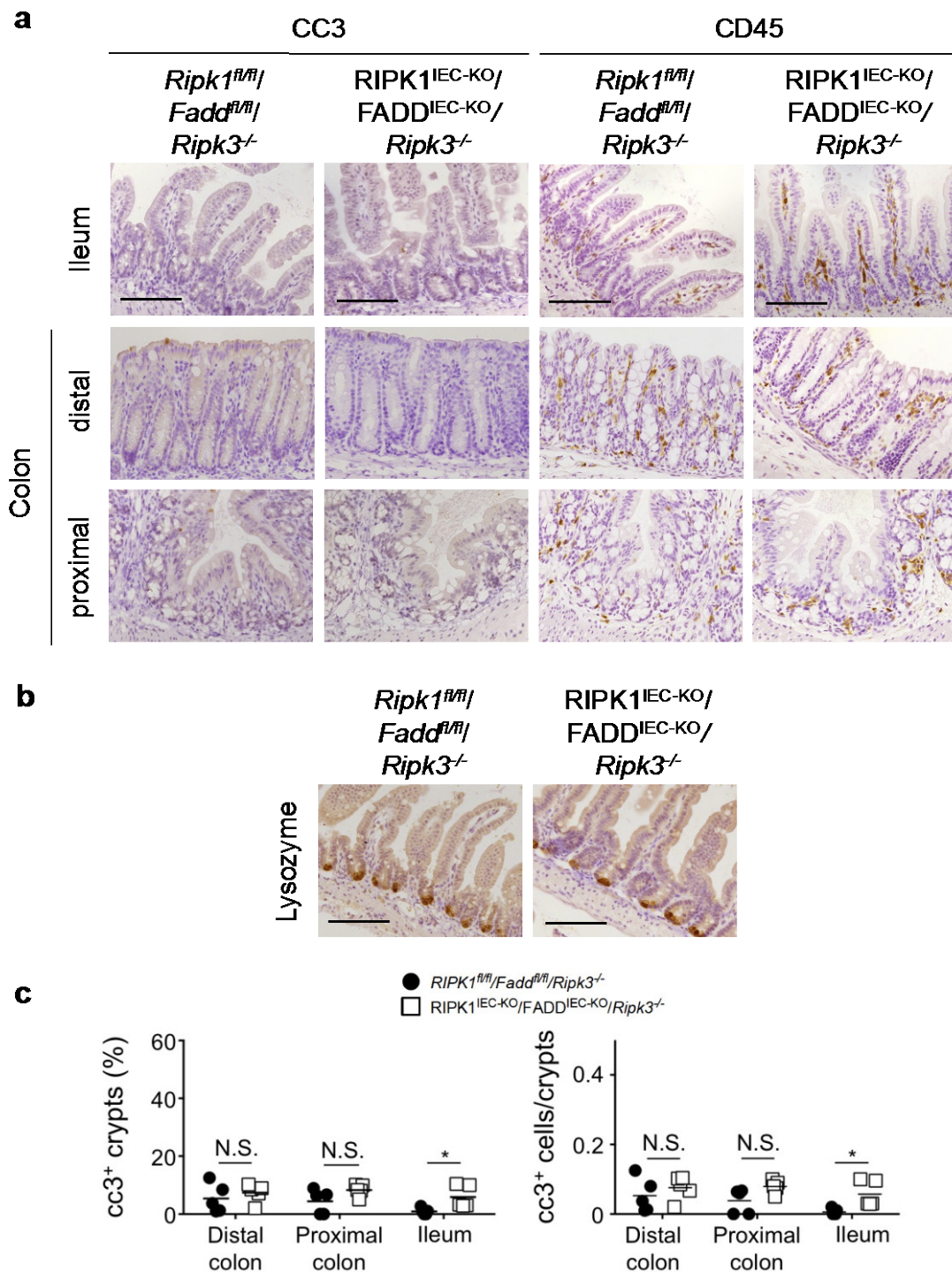


Figure 28. No increased cell death in RIPK1^{IEC-KO}/FADD^{IEC-KO}/*Ripk3^{-/-}* mice.
(a) Representative images from CC3 and CD45 immunostained colonic and ileal swiss rolls from 3-week old *Ripk1^{fl/fl}/Fadd^{fl/fl}/Ripk3^{-/-}* and RIPK1^{IEC-KO}/FADD^{IEC-KO}/*Ripk3^{-/-}* mice. Scale bars: 100 μ m. **(b)** Immunostaining of ileal sections from 3-week old *Ripk1^{fl/fl}/Fadd^{fl/fl}/Ripk3^{-/-}* and RIPK1^{IEC-KO}/FADD^{IEC-KO}/*Ripk3^{-/-}* mice for lysozyme. Scale bars: 100 μ m. **(c)** Quantification of crypts containing CC3-positive cells and the number of CC3-positive cells per crypt in the ileum, distal and proximal colon of 3-week old *Ripk1^{fl/fl}/Fadd^{fl/fl}/Ripk3^{-/-}* and RIPK1^{IEC-KO}/FADD^{IEC-KO}/*Ripk3^{-/-}* mice. n.s. not significant. * $P \leq 0.05$, ** $P \leq 0.01$, *** $P \leq 0.005$

RIPK1^{IEC-KO}/FADD^{IEC-KO}/Ripk3^{-/-} mice were born at expected mendelian ratios, RIPK1^{IEC-KO}/FADD^{IEC-KO}/Ripk3^{-/-} mice had normal body weight and a normal life span (Figure 27a). Histological examination of H&E stained swiss rolls of ileal and colonic sections from 3-week old triple knockout mice did not show signs of any pathology and were indistinguishable from their littermate controls (Figure 27b). Intestinal epithelial apoptosis was not increased in the colon and only slightly increased in the small intestine of RIPK1^{IEC-KO}/FADD^{IEC-KO}/Ripk3^{-/-} mice compared to control *Ripk1^{fl/fl}/Fadd^{fl/fl}/Ripk3^{-/-}* mice, although in the ileum it reached statistical significance (Figure 28a, c). Furthermore, no CC3 negative dying cells were detected in the colon and the ileum (Figure 28a), indicating that caspase-independent cell death in RIPK1^{IEC-KO}/FADD^{IEC-KO} mice is RIPK3-dependent. The numbers of CD45 positive immune cells in the lamina propria of triple knockout mice was similar to control mice, suggesting that colitis and enteritis in RIPK1^{IEC-KO}/FADD^{IEC-KO} mice was a consequence of RIPK3 dependent death of IECs (Figure 28a).

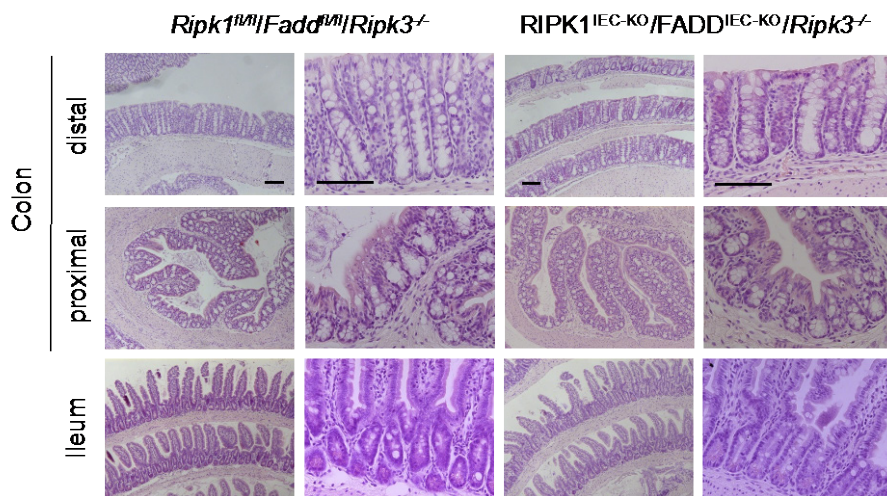


Figure 29. No intestinal pathology in adult RIPK1^{IEC-KO}/FADD^{IEC-KO}/Ripk3^{-/-} mice. Histological analysis of H&E stained colonic and ileal sections from 13-week old RIPK1^{IEC-KO}/FADD^{IEC-KO}/Ripk3^{-/-} mice and *Ripk1^{fl/fl}/Fadd^{fl/fl}/Ripk3^{-/-}* mice. Scale bars: 100 μ m.

Colonic and ileal H&E stained sections from 13-week old RIPK1^{IEC-KO}/FADD^{IEC-KO}/Ripk3^{-/-} mice were indistinguishable from *Ripk1^{fl/fl}/Fadd^{fl/fl}/Ripk3^{-/-}* littermates (Figure 29). Despite the lack of intestinal pathology in RIPK1^{IEC-KO}/FADD^{IEC-KO}/Ripk3^{-/-} mice, 3-week old triple knockout mice displayed slightly increased levels of *Tnf*, *Il1b*, *Ccl5* and *Il10* as shown by qRT-PCR analysis of whole small intestinal tissue (Figure 30).

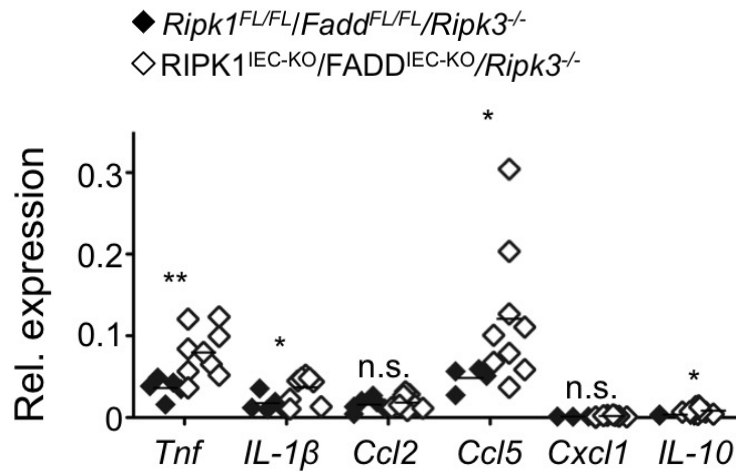


Figure 30. Increased TNF mRNA levels in the ileum of *RIPK1^{IEC-KO}/FADD^{IEC-KO}/Ripk3^{-/-}* mice.

qRT-PCR analysis of mRNA expression levels for inflammatory cytokines and chemokines of whole ileal tissue from 3-week old *Ripk1^{fl/fl}/Fadd^{fl/fl}/Ripk3^{-/-}* and *RIPK1^{IEC-KO}/FADD^{IEC-KO}/Ripk3^{-/-}* mice. n.s. not significant. * $P \leq 0.05$, ** $P \leq 0.01$, *** $P \leq 0.005$

3.4.3 Death of *Ripk1*^{-/-} IECs is independent of RIPK3

As described previously, *Ripk1*^{-/-} IECs died by FADD dependent apoptosis, and in IECs with additional deletion of FADD the mode of death switched to RIPK3-dependent necroptosis. These results suggest that RIPK3 alone might not be a major driver of apoptosis and pathology in RIPK1^{IEC-KO} mice. To investigate a potential role of RIPK3 in the apoptosis observed in IECs of RIPK1^{IEC-KO} mice, RIPK1^{IEC-KO} mice were crossed to *Ripk3*^{-/-} mice (Newton et al., 2004). RIPK1^{IEC-KO}/*Ripk3*^{-/-} mice showed significant reduction of body weight compared to their *Ripk1*^{fl/fl}/*Ripk3*^{-/-} littermates and died prematurely (Figure 31a, b). Histological examination of H&E stained ileal and colonic sections revealed that RIPK1^{IEC-KO}/*Ripk3*^{-/-} mice developed intestinal pathology reminiscent of RIPK1^{IEC-KO} mice (Figure 31c). Furthermore, RIPK1^{IEC-KO}/*Ripk3*^{-/-} mice exhibited Paneth cell loss and IEC apoptosis to the same extent as RIPK1^{IEC-KO} mice did, indicating that apoptosis in *Ripk1*^{-/-} IECs is independent of RIPK3 and RIPK3-mediated necroptosis is not a primary pathway triggering death of IECs and pathology in RIPK1^{IEC-KO} mice (Figure 32).

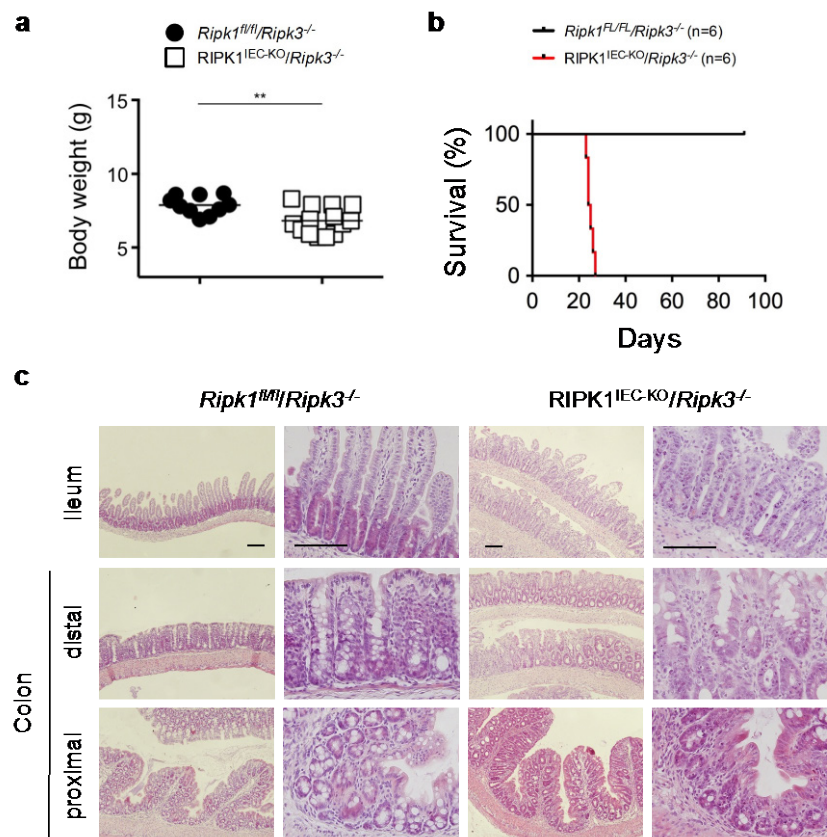


Figure 31. Premature death, cachexia and intestinal pathology in $RIPK1^{IEC-KO}$ mice is independent of RIPK3.

(a) Body weight of 3-week old *Ripk1^{fl/fl}/Ripk3^{-/-}* and *RIPK1^{IEC-KO}/Ripk3^{-/-}* mice. (b) Kaplan-Meier survival curve of *Ripk1^{fl/fl}/Ripk3^{-/-}* and *RIPK1^{IEC-KO}/Ripk3^{-/-}* mice. (c) Histological analysis of H&E stained colonic and ileal sections from 3-week old *Ripk1^{fl/fl}/Ripk3^{-/-}* and *RIPK1^{IEC-KO}/Ripk3^{-/-}* mice. Scale bars: 100 μ m. * $P \leq 0.05$, ** $P \leq 0.01$, *** $P \leq 0.005$

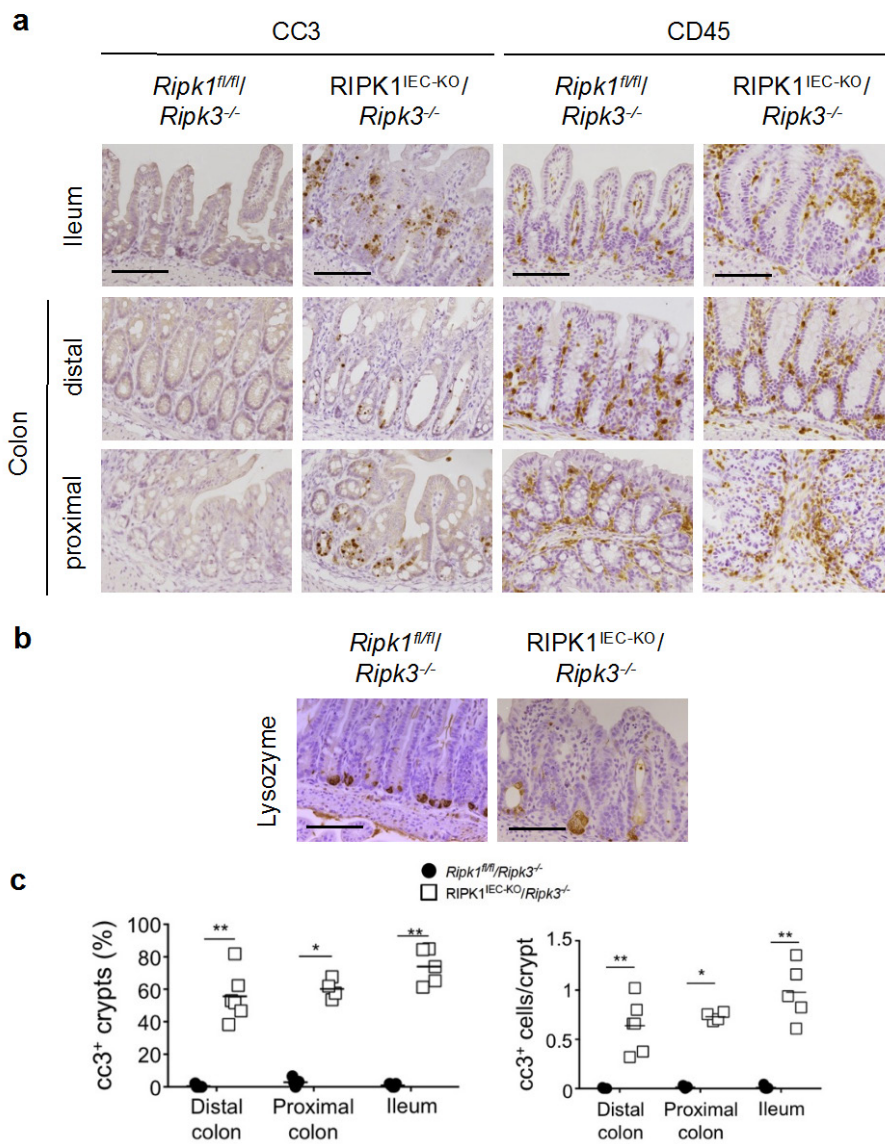


Figure 32. Apoptosis and Paneth cell loss in RIPK1^{IEC-KO} mice is independent of RIPK3.

(a, b) Representative images from (a) CC3, CD45 and (b) lysozyme immunostained colonic and ileal swiss rolls from 3-week old *Ripk1^{fl/fl}/Ripk3^{-/-}* and RIPK1^{IEC-KO}/*Ripk3^{-/-}* mice. Scale bars: 100 μ m. (c) Quantification of crypts containing CC3-positive cells and the number of CC3-positive cells per crypt in the ileum, distal and proximal colon of 3-week old *Ripk1^{fl/fl}/Ripk3^{-/-}* and RIPK1^{IEC-KO}/*Ripk3^{-/-}* mice. * $P \leq 0.05$, ** $P \leq 0.01$, *** $P \leq 0.005$

3.5 Scaffolding function of RIPK1 prevents the degradation of pro-survival proteins

3.5.1 Pathology in RIPK1^{IEC-KO} mice is independent of NF- κ B activity

The *in vivo* results presented above revealed an important cell intrinsic function of RIPK1 to protect IECs from apoptosis. The role of RIPK1 in NF- κ B activation is controversial and possibly cell type specific (Gentle et al., 2011; Kelliher et al., 1998; Wong et al., 2010). Given the fact that RIPK1 deficiency, but not loss of RIPK1 kinase activity, triggered IEC apoptosis, it could be possible that *Ripk1*^{-/-} IECs are sensitized to apoptosis due to the loss of RIPK1 scaffolding function for NF- κ B activation (Polykratis et al., 2014). On the other hand, mice lacking p65 or IKK2 specifically in IECs do not develop spontaneous pathology (Egan et al., 2004; Steinbrecher et al., 2008). Furthermore, mice deficient for NEMO in IECs develop spontaneous colitis but survive to adulthood (Nenci et al., 2007). To address if impaired NF- κ B activation caused apoptosis of *Ripk1*^{-/-} IECs, RIPK1^{IEC-KO} mice were crossed to mice carrying a stop floxed constitutively active IKK2 transgene (IKK2ca) (Sasaki et al., 2006). Heterozygous IEC specific expression of the IKK2ca transgene was reported to show sustained NF- κ B activation in intestinal epithelial cells (Vlantis et al., 2011). RIPK1^{IEC-KO}/IKK2ca^{IEChet} mice were born at expected mendelian ratios, but had slightly reduced body weight compared to their floxed littermates and died prematurely (Figure 33a and data not shown). In line with this, RIPK1^{IEC-KO}/IKK2ca^{IEChet} mice were not protected from IEC apoptosis and intestinal pathology (Figure 33b). Compared to RIPK1^{IEC-KO} mice, the pathology was aggravated in colons of RIPK1^{IEC-KO}/IKK2ca^{IEChet} mice. Colonic crypts were showing more severe hyperproliferation than in RIPK1^{IEC-KO} mice and local accumulations of immune cells were present, which were not observed in RIPK1^{IEC-KO} mice (Figure 33b). These results suggest that *Ripk1*^{-/-} IECs are not sensitized to apoptosis by reduced NF- κ B activity.

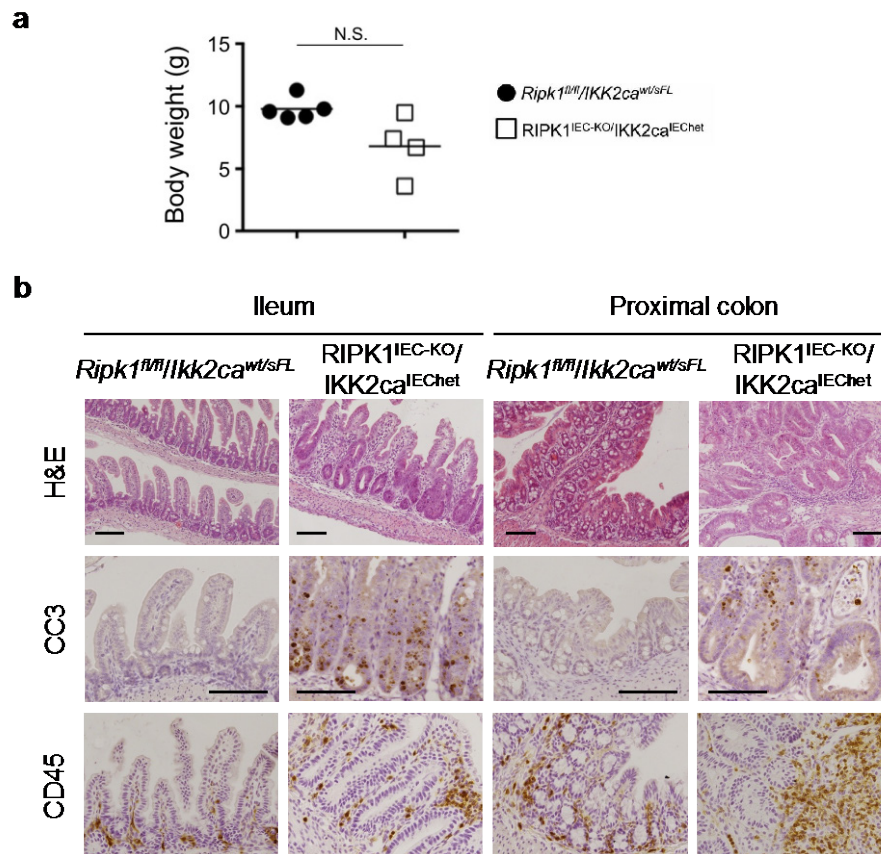


Figure 33. Pathology in $RIPK1^{IEC-KO}$ is independent of canonical NF- κ B activation.

(a) Body weight of 3-week old $RIPK1^{IEC-KO}/IKK2ca^{IEChet}$ and *Ripk1^{fl/fl}/Ikk2ca^{wt/fl}* mice. (b) Representative histological images of H&E stained, CC3 and CD45 immunostained colonic and ileal sections from 3-week old *Ripk1^{fl/fl}/Ikk2ca^{wt/fl}* and $RIPK1^{IEC-KO}/IKK2ca^{IEChet}$ mice. Scale bars: 100 μ m. n.s. not significant. * $P \leq 0.05$, ** $P \leq 0.01$, *** $P \leq 0.005$

3.5.2 RIPK1 prevents degradation of pro-survival proteins

Previous studies showed that TNF stimulation of *Ripk1*^{-/-} MEFs induced degradation of TRAF2 as well as cIAP1 and subsequent stabilization of NIK resulting in non-canonical NF-κB activation as shown by p110 processing to p52 (Gentle et al., 2011; J. Y. Kim et al., 2011). Furthermore the authors showed cleavage of cFLIP and caspase-8 activation in RIPK1 deficient MEFs upon TNF stimulation culminating in death of *Ripk1*^{-/-} MEFs (Gentle et al., 2011; J. Y. Kim et al., 2011). Therefore it could be possible that RIPK1 deficiency sensitizes IECs to apoptosis by impaired stability of pro-survival proteins. Indeed, western blot analysis of IECs showed that protein levels of cIAP1 and TRAF2 were reduced in RIPK1^{IEC-KO} mice compared to *Ripk1*^{fl/fl} mice (Figure 34b), suggesting that RIPK1 might control their stability thereby promoting IEC survival. Since the mRNA levels of *Birc2* (cIAP1) and *Cflip* (cFLIP) were not reduced *Ripk1*^{-/-} IECs compared to *Ripk1*^{fl/fl} IECs (Figure 34a), it is likely that posttranslational mechanisms induced the degradation of cIAP1 and TRAF2 in *Ripk1*^{-/-} IECs. Consistent with previous studies, TNF stimulation of *Ripk1*^{-/-} MEFs induced rapid degradation of cIAP1, TRAF2 and TRADD (data not shown).

To assess whether degradation of proteins involved in TNFR1 signaling complex 1 could be occur in the absence of RIPK1 in intestinal epithelial cells *in vitro*, the intestinal organoid culture system was employed (T. Sato et al., 2009). Intestinal crypts isolated from RIPK1^{IEC-KO} mice did not form organoids and died within 48 hours after isolation, whereas organoids from *Ripk1*^{fl/fl} mice could be maintained in culture (data not shown). This shows that RIPK1 deficiency also caused IEC death *in vitro*. In order to obtain RIPK1 deficient organoids, intestinal organoids from RIPK1^{tamIEC-KO} mice were cultured and deletion of RIPK1 was induced by adding 4-hydroxytamoxifen (4-OHT) to the culture medium for 24 hours (see 2.2.5.1 and 2.2.5.2). This treatment was sufficient to induce efficient deletion of RIPK1 (Figure 34c). 48 h after adding 4-OHT, RIPK1^{tamIEC-KO} organoids showed reduced protein levels of cIAP1, TRAF2 and cFLIP, whereas Cre negative *Ripk1*^{fl/fl} organoids did not (Figure 34c). In addition, RIPK1^{tamIEC-KO} organoids died 48 h after administration of 4-OHT as shown by photography and FACS analysis of the change of PI

positive organoids (Figure 34d, e). These results suggest that the degradation of pro-survival protein might contribute to the death of *Ripk1*^{-/-} IECs.

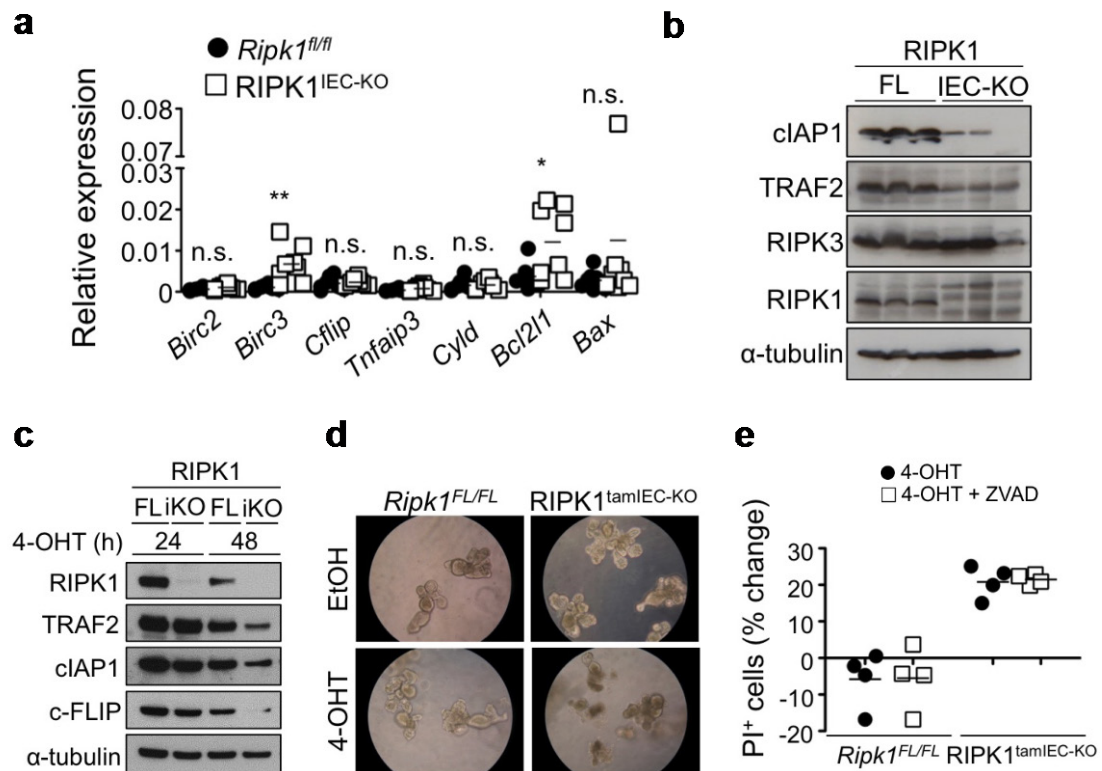


Figure 34. Degradation of cIAP1 and TRAF2 in *Ripk1*^{-/-} IECs and RIPK1^{tamIEC-KO} organoids.

(a) qRT-PCR analysis for mRNA expression levels of pro-survival and pro-apoptotic genes in intestinal epithelial cells isolated from 3-week *Ripk1*^{fl/fl} and RIPK1^{IEC-KO} mice. (b) Immunoblot analysis of small intestinal IECs from 3-week old *Ripk1*^{fl/fl} and RIPK1^{IEC-KO} mice for the indicated antibodies. Animals were sacrificed and IEC were isolated by Marius Dannappel. Dr. Chun Kim performed immunoblot analysis of IEC extracts. (c) Immunoblot analysis of *Ripk1*^{fl/fl} (FL) and RIPK1^{tamIEC-KO} (iKO) organoids after 48 h treatment with 4-hydroxytamoxifen (4-OHT) with the indicated antibodies. Organoid culture was performed by Marius Dannappel and Dr. Chun Kim performed immunoblot analysis of organoid lysates. (d) Representative images depicting *Ripk1*^{fl/fl} and RIPK1^{tamIEC-KO} organoids 48 h after treatment with 4-OHT for 20 h. Original magnification, x400. (e) FACS analysis of PI-stained cells from *Ripk1*^{fl/fl} and RIPK1^{tamIEC-KO} organoids 43 h after 4-OHT treatment in the presence or absence of zVAD. Organoid cell culture was done by Marius Dannappel and PI-staining and FACS analysis was performed by Dr. Katerina Vlantis. *P≤0.05, **P≤0.01, ***P≤0.005

3.5.3 Increased TNF production as an autocrine amplification loop causing IEC apoptosis

Previous studies have shown that deletion of cIAP1/2 using SMAC (also known as DIABLO) mimetics induced the activation of canonical and non-canonical NF- κ B signalling resulting in the expression of TNF and other cytokines (E. Varfolomeev et al., 2007). Since *Ripk1*^{-/-} IECs and organoids showed degradation of cIAP1 (Figure 34b, c), it might be possible that cIAP1 degradation results in NF- κ B activation and subsequent TNF expression which induces death of IECs or organoids in an autocrine manner. In order to test this hypothesis, IECs from RIPK1^{IEC-KO} and *Ripk1*^{fl/fl} mice were isolated, cytoplasmic and nuclear fractions prepared and analyzed by immunoblot. The

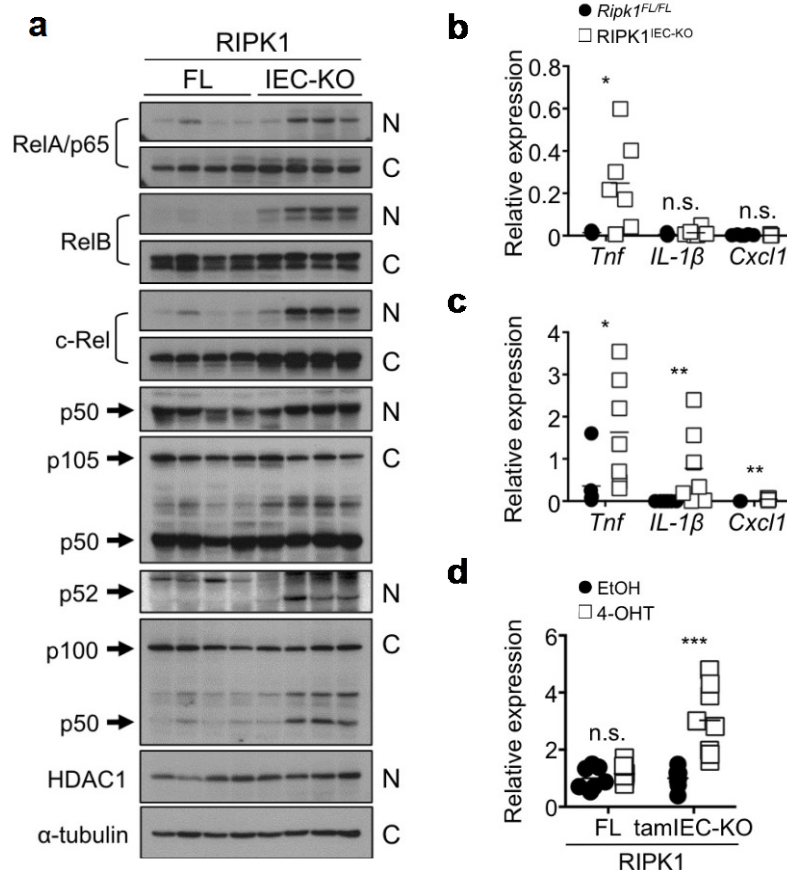


Figure 35. Increased NF- κ B activation and *Tnf* expression in *Ripk1*^{-/-} IECs.

(a) Immunoblot analysis of nuclear- and cytoplasmic fractions prepared from IECs isolated from 3-week old *Ripk1*^{fl/fl} and RIPK1^{IEC-KO} mice probed with the indicated antibodies. Mice were sacrificed and IEC isolated by Marius Dannappel. Dr. Chun Kim prepared nuclear and cytoplasmic fractions and performed immunoblot analysis. (b, c) qRT-PCR analysis of mRNA expression levels of *Tnf*, *Il1b* and *Cxcl1* in IECs from small intestine (b) and colon (c) of 3-week old *Ripk1*^{fl/fl} and RIPK1^{IEC-KO} mice. qRT-PCR in (c) was pipetted by Dr. Teresa Corona. (d) qRT-PCR analysis for *Tnf* expression levels in *Ripk1*^{fl/fl} and RIPK1^{tamIEC-KO} mice 30 h after 4-OHT or EtOH removal. N, nuclear, C, cytoplasmic, EtOH, ethanol, 4-OHT, 4-hydroxytamoxifen *P < 0.05, **P < 0.01, ***P < 0.005

nuclear fraction of RIPK1-deficient IECs showed p65, RelB and c-Rel as well as processed p50 and p52, indicating increased NF- κ B activity compared to *Ripk1^{fl/fl}* mice, where only p50 was detected in the nuclear fraction (Figure 35a).

Consistent with this hypothesis, qPCR analysis using IECs from RIPK1^{IEC-KO} and *Ripk1^{fl/fl}* mice revealed significantly increased expression levels of TNF in the colon and small intestine of RIPK1^{IEC-KO} mice and elevated *I11b* mRNA levels in the colon (Figure 35b, c). Furthermore, deletion of RIPK1 by 4-OHT treatment in RIPK1^{tamIEC-KO} organoids led to increased expression levels of TNF within 30h after the removal of 4-OHT that was not observed in vehicle-treated control organoids (Figure 35d).

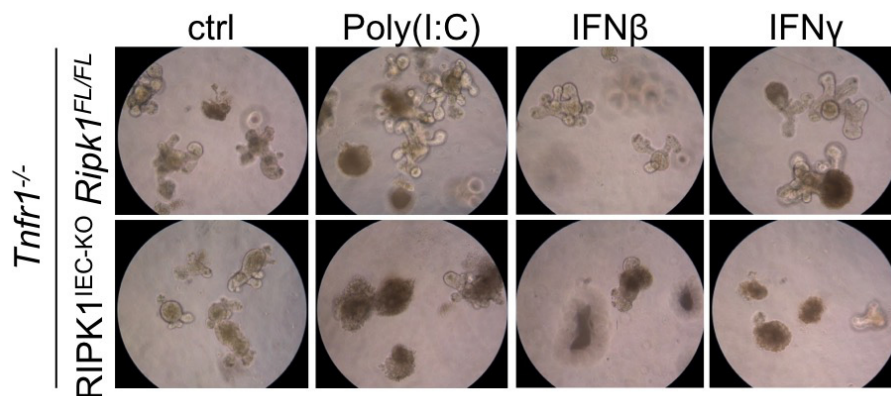


Figure 36. Increased sensitivity of *Ripk1^{-/-}/Tnfr1^{-/-}* organoids to poly(I:C) and IFN-induced death.

Representative images of organoids isolated from RIPK1^{IEC-KO}/*Tnfr1^{-/-}* and *Ripk1^{fl/fl}/Tnfr1^{-/-}* mice taken 16 h after stimulation with poly(I:C), IFN- β and IFN- γ . Experiments were performed by Marius Dannappel and Dr. Katerina Vlantis. Ctrl, control, IFN, interferon. Original magnification, x400.

As described above, intestinal crypts isolated from RIPK1^{IEC-KO} mice failed to form organoids *in vitro*. Interestingly, intestinal crypts from RIPK1^{IEC-KO}/*Tnfr1^{-/-}* mice could be grown to organoids and maintained in culture for a few weeks, although they did not grow as well as control organoids from *Ripk1^{fl/fl}/Tnfr1^{-/-}* mice (Figure 36). This is in line with the idea that TNF produced by *Ripk1^{-/-}* IECs induced death in autocrine manner. Nevertheless, organoids from RIPK1^{IEC-KO}/*Tnfr1^{-/-}* mice were highly sensitive to polyinosinic:polycytidylic acid (poly(I:C)), interferon- β (IFN- β) and IFN- γ induced death (Figure 36). Therefore, it is possible that TIR-domain-containing adaptor-inducing interferon- β (TRIF)- and IFN-dependent signaling pathways also contribute to the death of *Ripk1^{-/-}* IECs and to the pathology in RIPK1^{IEC-KO} mice. To assess

the effect of TRIF-mediated signaling pathways in the context of pathology and IEC death in RIPK1^{IEC-KO} mice, RIPK1^{IEC-KO} mice were crossed to *Trif*^{fl/fl} mice (Dannappel et al., 2014). RIPK1^{IEC-KO}/TRIF^{IEC-KO} mice showed similar body weight reduction and premature lethality like RIPK1^{IEC-KO} mice did (Figure 37a and data not shown). In line with this, intestinal pathology and cell death was not ameliorated compared to RIPK1^{IEC-KO} mice, indicating that, if at all, TRIF-mediated signaling plays, if at all, only a minor role in the development of the *in vivo* pathology exhibited by RIPK1^{IEC-KO} mice (Figure 37b).

Taken together, these result show that RIPK1 controls stability of TNFR1 complex 1 proteins, thereby promoting survival of IECs. Furthermore, RIPK1 deficiency is associated with increased canonical and non-canonical NF-κB activity, resulting in increased TNF expression that triggers death of *Ripk1*^{-/-} IECs in an autocrine manner.

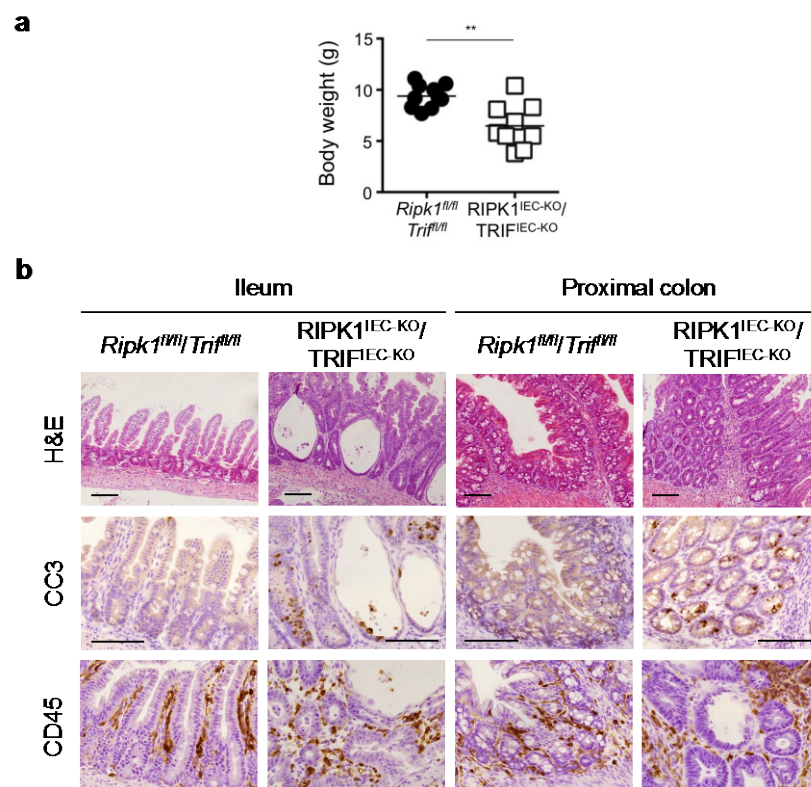


Figure 37. Intestinal pathology is independent of TRIF-mediated signaling. (a) Body weight of 3-week old *Ripk1*^{fl/fl}/*Trif*^{fl/fl} and RIPK1^{IEC-KO}/TRIF^{IEC-KO} mice. (b) Representative histological images of H&E stained, CC3 and CD45 immunostained colonic and ileal sections from 3-week old *Ripk1*^{fl/fl}/*Trif*^{fl/fl} and RIPK1^{IEC-KO}/TRIF^{IEC-KO} mice. Scale bars: 100 μm. *P≤0.05, **P≤0.01, ***P≤0.005

4. Discussion

4.1 RIPK1 as a master regulator of cell death.

Cell death and inflammation are crucial processes to control viability and homeostasis of an organism, and dysfunction of either may be of pathological outcome. RIPK1 serves as an essential signaling node regulating inflammation, apoptosis and necroptosis in response to various stimuli such as TNF and some TLR-ligands, and thus, must be tightly controlled for the maintenance of tissue homeostasis. Indeed, mice with homozygous deletion of RIPK1 show excessive cell death and inflammation in several tissues and die shortly after birth (Kelliher et al., 1998).

Here we set to investigate the role of RIPK1 specifically in IECs and to circumvent early postnatal lethality of *Ripk1*^{-/-} mice, we generated conditional RIPK1 knockout mice lacking RIPK1 specifically in IECs. RIPK1^{IEC-KO} mice have a cachectic appearance, die prematurely and show massive IEC apoptosis (Figure 5-Figure 12). Additional deletion of FADD protected IECs from succumbing to apoptosis but sensitized RIPK1 and FADD double-deficient IECs to caspase-3 independent RIPK3-driven cell death (Figure 24, Figure 25). RIPK3 deficiency did not protect RIPK1^{IEC-KO} mice from developing intestinal pathology (Figure 31, Figure 32), but rescued IEC death and inflammation in RIPK1^{IEC-KO}/FADD^{IEC-KO} mice (Figure 24, Figure 25). Therefore, similar to FADD^{IEC-KO} mice (Welz et al., 2011), IECs of RIPK1^{IEC-KO}/FADD^{IEC-KO} mice die by necroptosis, whereas RIPK3-driven necroptosis is no major contributor to the pathology in RIPK1^{IEC-KO} mice. Thus, in this work, we could demonstrate an important cell-intrinsic role of RIPK1 for the maintenance of intestinal epithelial homeostasis by inhibiting FADD-dependent apoptosis of IECs. Furthermore, this work provides evidence for the *in vivo* relevance of RIPK1-independent RIPK3-dependent necroptosis, which drives the phenotype in RIPK1^{IEC-KO}/FADD^{IEC-KO} mice and most likely in FADD^{IEC-KO} mice (Welz et al., 2011). Similarly, intestinal pathology in FADD^{IEC-KO} mice could not be prevented by expressing kinase-dead RIPK1 in IECs, providing further evidence for the *in vivo* importance of RIPK1-kinase activity independent RIPK3-dependent necroptosis (Dannappel et al., 2014).

The role of RIPK1 in IECs as an inhibitor of apoptosis is distinct to the role of RIPK1 in other tissues. For instance in the skin, RIPK1-deficiency caused skin inflammation and sensitized keratinocytes to FADD-dependent apoptosis as well as RIPK3-MLKL-dependent necroptosis (Dannappel et al., 2014). FADD deficiency did not protect against but delayed skin inflammation in RIPK1^{E-KO} mice. In turn, these results suggest that the early postnatal skin inflammation and death observed in FADD^{E-KO} mice depend on RIPK1 (Bonnet et al., 2011; Dannappel et al., 2014). Thus, RIPK1 has a tissue specific function to maintain homeostasis in epithelial tissues. Similar to the skin, hematopoietic specific deletion of RIPK1 in mice caused apoptosis and RIPK3-dependent necroptosis in hematopoietic cells resulting in death of the mice (Roderick et al., 2014). In addition, two recent publications demonstrated a contribution of both concurrent pathways, FADD-caspase-8-mediated apoptosis and RIPK3-MLKL-dependent necroptosis to the early postnatal death of *Ripk1*^{-/-} mice, as neither ablation of FADD/caspase-8 nor RIPK3/MLKL alone could prevent lethality of RIPK1-null mice (Dillon et al., 2014; Kaiser et al., 2014; Rickard et al., 2014; H. Zhang et al., 2011). However, *Ripk1*^{-/-}/*Caspase-8*^{-/-}/*Ripk3*^{-/-} and *Ripk1*^{-/-}/*Fadd*^{-/-}/*Ripk3*^{-/-} mice, in which extrinsic apoptosis and necroptosis are blocked, survive until adulthood without an aberrant gross morphology, although while aging, they develop acute lymphoproliferative syndrome (ALPS) (Dillon et al., 2014; Rickard et al., 2014). Taken together, these genetic studies suggest that RIPK1 ensures the maintenance of health in an organism in a cell-type specific manner, by inhibiting both apoptotic and necroptotic cell death.

One important remaining question is, why RIPK1-deficiency sensitizes IECs to apoptosis, whereas in other tissues such as skin, thymus or liver, both apoptosis and necroptosis occur (Dannappel et al., 2014; Rickard et al., 2014). It was proposed that RIPK3 expression levels correlate with a cell's ability to undergo necroptosis (He et al., 2009). However, primary RIPK1-deficient IECs have comparably higher RIPK3 protein levels as epidermal extracts from RIPK1^{E-KO} mice (Dannappel et al., 2014), thus, the sensitivity towards necroptosis is probably independent of RIPK3 protein levels. Maybe the reason for sensitization to the type of cell death in the context of RIPK1-

deficiency lies, first, in the nature of the cell death trigger (discussed below), and/or second, in a yet to be identified cell-intrinsic characteristic(s) of IECs. Future work is required to address this question.

In addition to its pro-survival function, RIPK1 has death-inducing capacities. Full body deletion of caspase-8 or FADD results in embryonic lethality at E10.5 due to failed vascularization of the yolk sac, which is fully rescued by additional ablation of RIPK3 (Dillon et al., 2012; Kaiser et al., 2011; Oberst et al., 2011; Sakamaki et al., 2002; E. E. Varfolomeev et al., 1998; Yeh et al., 1998). Interestingly, ablation of RIPK1 rescues the embryonic lethality of FADD and caspase-8 deficient mice, however these mice succumb postnatally as RIPK1-deficient mice do (Dillon et al., 2014; Kaiser et al., 2014; H. Zhang et al., 2011). The embryonic lethality of *fadd*^{-/-} and *caspase-8*^{-/-} mice is TNFR1-dependent, thus RIPK1 promotes lethality in FADD and caspase-8 deficient mice by mediating TNF-induced RIPK3-dependent necroptosis (Dillon et al., 2014).

In summary, RIPK1 is a key regulator of cell death and inflammation endowed with anti-apoptotic and anti-necroptotic as well as pro-necroptotic functions, which are most likely dependent on the cellular context and on the cell type specific manner.

4.2 How are RIPK1-deficient IECs sensitized to FADD-mediated apoptosis?

It is well known that RIPK1 deficient lymphocytes and MEFs are sensitized to TNF-induced caspase-8 mediated apoptosis (Feoktistova et al., 2011; Kelliher et al., 1998; Lee, Shank, Cusson, & Kelliher, 2004; Oberst et al., 2011; Tenev et al., 2011; H. Zhang et al., 2011). Since RIPK1 kinase dead MEFs or BMDMs are not sensitized to TNF-induced apoptosis and mice expressing a kinase-inactive RIPK1 (*Ripk1*^{D138N} mice) do not show a spontaneous phenotype, the increased sensitivity to cell death and the survival promoting function of RIPK1 in IECs is independent of its kinase activity (Lee et al., 2004; Newton et al., 2014; Polykratis et al., 2014). RIPK1-deficient IECs do

not show impaired, but rather increased nuclear translocation of the active NF- κ B subunits. In addition, heterozygous IEC-specific expression of a constitutively active IKK2 did not ameliorate the extent of apoptosis in RIPK1-deficient IECs. Instead, intestinal pathology was rather aggravated compared to RIPK1^{IEC-KO} mice, which might be partially attributed to the very mild inflammation observed in IKK2ca^{IEChet} mice (Vlantis et al., 2011). Finally, mRNA levels of pro-survival genes, some of them NF- κ B target genes, were not reduced in RIPK1-deficient IECs. All together, these results suggest that the role of RIPK1 in prevention of FADD-dependent apoptosis in IECs is independent of its role in NF- κ B signaling and that RIPK1 is not required for NF- κ B activation in IECs. In line with this result, another recent publication demonstrated unaffected I κ B α phosphorylation and NF- κ B target gene expression in response to TNF in organoids with induced deletion of RIPK1 (Takahashi et al., 2014).

RIPK1 has been shown to be important for the stability of cIAP1 and TRAF2 within the TNFR1-associated signaling complex (Gentle et al., 2011; J. Y. Kim et al., 2011). TNF stimulation of *Ripk1*^{-/-} MEFs induced the degradation of cIAP1, TRAF2 and cFLIP_L, resulting in NIK stabilization and subsequent non-canonical NF- κ B activation as well as caspase-8 dependent apoptosis (Gentle et al., 2011; J. Y. Kim et al., 2011). Furthermore, loss of IAPs alone (by treatment with compound A or BV6) was sufficient for the stabilization of NIK and to activate canonical and non-canonical NF- κ B pathways resulting in *de novo* TNF production inducing a positive feedback amplification and cell death in various cancer cell lines (E. Varfolomeev et al., 2007; Vince et al., 2007). Degradation of cIAP1, cFLIP_L and TRAF2, NIK stabilization, canonical as well as non-canonical NF- κ B activation and increased TNF production was observed in IECs isolated from RIPK1^{IEC-KO} mice and RIPK1-deficient organoids (Figure 34, Figure 35) (Takahashi et al., 2014). However, if the non-canonical NF- κ B pathway contributes to the phenotype observed in RIPK1^{IEC-KO} mice is not known and needs to be addressed. In the case of RIPK1-null mice, additional ablation of NIK did not rescue the early postnatal lethality, arguing against a physiological relevance of non-canonical NF- κ B activation in the context of RIPK1-deficiency (Dillon et al., 2014). Therefore, in accordance with the inhibitory function of RIPK1 in FADD-caspase-8

mediated apoptosis, the degradation of pro-survival proteins cIAP1, TRAF2 and cFLIP_L might be directly connected to caspase-8 dependent cell death.

Except mammalian XIAP, cellular inhibitors of apoptosis family members are not able to directly inhibit the catalytic activity of caspases (Eckelman & Salvesen, 2006; Eckelman, Salvesen, & Scott, 2006). In case of cIAP1 and cIAP2, it was proposed that they modify caspase-3 and -7 with K48-linked ubiquitination chains to promote their proteosomal degradation (Choi et al., 2009). Aside from regulating effector-caspases, an important pro-survival function of cIAP1 and cIAP2 is attributed to their ability to promote NF- κ B pathway mediated pro-survival protein expression and to inhibit RIPK1 kinase activity (complex IIb-) dependent apoptosis (Bertrand et al., 2008; Mahoney et al., 2008; Petersen et al., 2007; E. Varfolomeev et al., 2007; Vince et al., 2007; L. Wang et al., 2008). Both, impaired NF- κ B activation and prevention of complex IIb-formation, cannot be attributed to *Ripk1*^{-/-} IECs. Thus it is possible that death of RIPK1-deficient cells is not caused by loss of cIAP1, or second, cIAP1 has another, so far unappreciated pro-survival.

Another possibility is that death of RIPK1-deficient IECs is caused by the loss of TRAF2. Interestingly, *Traf2*^{-/-} MEFs exhibit a very similar response upon TNF stimulation as *Ripk1*^{-/-} MEFs do, however they do not show degradation of cIAP1, indirectly arguing against the loss of cIAP1 as cause of death in RIPK1-deficient MEFs (Gentle et al., 2011). In the same study the authors could demonstrate that the degradation of TRAF2 is responsible for the increased sensitivity of *Ripk1*^{-/-} MEFs to TNF (Gentle et al., 2011). In both, RIPK1- and TRAF2-deficient MEFs, TNF stimulation induced proteasome dependent cFLIP_L destabilization, suggesting that, either TNF induces cFLIP_L degradation or, cFLIP_L is constantly degraded and reappears through a RIPK1- and TRAF2-dependent mechanism (Gentle et al., 2011). Reduced cFLIP_L levels in turn, could change the stoichiometry within the TNFR1 DISC allowing uncontrolled caspase-8 dimerization and subsequent activation resulting in apoptotic cell death. Similar to MEFs and IECs, primary *Ripk1*^{-/-} keratinocytes showed low levels of TRAF2 degradation in response to TNF stimulation, whereas cIAP1 protein levels were already very low in unstimulated cells (Dannappel et al., 2014). In response to TNF, *Ripk1*^{-/-} keratinocytes died by apoptosis in vitro (Dannappel et al., 2014). Presumably,

degradation of TRAF2 and cIAP1 is a common mechanism explaining the increased sensitivity of RIPK1-deficient cells to TNF-induced apoptosis. These degradation processes may also attribute for the very similar phenotype of *Traf2*^{-/-} mice in a C57BL/6 background and for *Ripk1*^{-/-} mice and might be causative for the sensitization for cell death (Kelliher et al., 1998; Yeh et al., 1997). In a BALB/C background, *Traf2*^{-/-} mice exhibited a phenotype reminiscent to RIPK1^{IEC-KO} mice, characterized by premature lethality within 3 weeks after birth and TNF-dependent intestinal epithelial cell apoptosis (Piao et al., 2011). Therefore, it could be possible that RIPK1 acts upstream of TRAF2 to prevent IEC apoptosis. The really interesting new gene (RING) domain and cIAP1/2 interaction motif (CIM) of TRAF2 were shown to confer resistance to TNF-induced cell death (Vince et al., 2009; L. Zhang, Blackwell, Shi, & Habelhah, 2010). TRAF2 RING domain mutant cells exhibited normal NF- κ B activation in response to TNF, therefore its pro-survival function must be independent of NF- κ B activation (Vince et al., 2009). A potential mechanism, by which the RING domain of TRAF2 could promote survival, is by modifying the large catalytic domain of caspase-8 with K-48 linked ubiquitin chains upon caspase-8 autoprocessing and thereby triggering its proteasomal degradation (Gonzalvez et al., 2012). Like this, TRAF2 could increase the cell's threshold to undergo extrinsic apoptosis (Gonzalvez et al., 2012). It is unknown how the CIM domain of TRAF2 promotes survival, however, one possibility could be a role for cIAPs in the regulation of caspase-8 activity.

The molecular mechanism, by which RIPK1 stabilizes TRAF2 remains elusive for the moment (Gentle et al., 2011). One possibility is that RIPK1 prevents the modification of TRAF2 and cIAP1 with ubiquitin chains in a direct or indirect kinase activity independent manner, which would target them for degradation. However supporting experimental evidence is pending at the moment. Overexpression systems in a RIPK1-deficient and RIPK1-mutant background would help to address these questions and to unravel the molecular mechanism TNF-induced apoptosis in the absence of RIPK1 and TRAF2.

4.3 Triggers of FADD-dependent apoptosis in RIPK1^{IEC-KO} mice

Ablation of RIPK1 in IECs disables RIPK1-dependent processes that are required to protect IECs from undergoing FADD-dependent apoptosis. IEC apoptosis still occurs in the intestines of germ-free RIPK1^{IEC-KO} mice (Figure 21), thus the signals triggering apoptosis in *Ripk1*^{-/-} IECs are independent of the microbiota and are most likely host organism derived. In order to understand the function of RIPK1 in regulating cell death in different signalling pathways, it is necessary to identify triggers that cause death in RIPK1-deficient IECs, but not in healthy IECs under physiological conditions.

Signalling via RIPK1 can be stimulated by death receptor ligands TNF, Fas, TRAIL to induce apoptosis and, under particular conditions, also necroptosis (Weinlich & Green, 2014). Full body ablation of TNFR1 partly protected RIPK1^{IEC-KO} mice from severe wasting, prevented premature lethality and significantly reduced the extent of IEC apoptosis in the colon and small intestine of RIPK1^{IEC-KO} mice (Figure 23) (Takahashi et al., 2014). Interestingly, primary *Ripk1*^{-/-} IECs expressed increased levels of TNF (Figure 35). Similarly, tamoxifen-inducible deletion of RIPK1 in organoids resulted in increased TNF expression and subsequent death of organoids (Figure 35). Therefore, TNF is largely responsible for triggering IEC apoptosis and intestinal pathology and in RIPK1^{IEC-KO} mice and, furthermore, RIPK1-deficient IECs are one important source of TNF, which triggers apoptosis in an autocrine manner.

In other models, RIPK1-deficiency caused pathologies that differentially depend on TNF-signalling. For instance, in RIPK1^{E-KO} mice, TNFR1 deficiency reduced keratinocyte necroptosis and delayed the onset of skin inflammation, but could not completely prevent it (Dannappel et al., 2014). In RIPK1-null mice in a C57BL/6 background, TNFR1 deficiency did not protect against early postnatal lethality and systemic inflammation, however rescued the colonic and small intestinal phenotype of *Ripk1*^{-/-} mice (Rickard et al., 2014). On a mixed C57BL/6 129/Sv caspase-11-deficient background, TNFR1 deletion prolonged survival of *Ripk1*^{-/-} mice up to 12 days (Cusson, Oikemus,

Kilpatrick, Cunningham, & Kelliher, 2002; Dillon et al., 2014). The reason for the phenotypic differences observed in RIPK1-null mice in the different genetic backgrounds is unknown.

Beside the importance of TNF-induced signalling in the context of the RIPK1^{IEC-KO} mice phenotype, apoptotic IECs were still observed in RIPK1^{IEC-KO}/*Tnfr1*^{-/-} mice, suggesting that also TNFR1-independent signalling pathways contribute to cell death in RIPK1^{IEC-KO} mice. Possibly, other death receptor ligands, such as Fas or TRAIL induce *Ripk1*^{-/-} IEC apoptosis. However, combined deletion of TNF and FasL was not able to prevent postnatal death of RIPK1-deficient mice (Rickard et al., 2014). Binding of FasL or TRAIL to their cognate receptors, leads to direct recruitment of FADD via DD interactions, thereby triggering the assembly of a membrane-associated DISC for the induction of apoptosis. RIPK1 was shown to be dispensable for FasL-induced apoptosis and only had a minor cytoprotective role in TRAIL-induced apoptosis (Geserick et al., 2009; Holler et al., 2000; E. Varfolomeev et al., 2005). Therefore, it is unlikely that FasL or TRAIL contribute to the intestinal pathology in RIPK1^{IEC-KO} mice.

During bacterial or viral infections, PAMPs are detected by PRRs such as TLR3 and TLR4 and activate host-defence pathways to mount an adequate immune response. Dependent on the cellular context, TLR3/TLR4 stimulation can induce TRIF RHIM interaction-dependent apoptosis and necroptosis (Kaiser & Offermann, 2005). Therefore, it is conceivable, that TLR3/TLR4-induced signalling triggers apoptosis of RIPK1-deficient IECs. However, IEC-specific TRIF ablation did not ameliorate severe wasting, premature lethality and intestinal cell death of RIPK1^{IEC-KO} mice, indicating that TRIF-mediated signalling is not involved in apoptosis of RIPK1-deficient IECs (Figure 37). Interestingly, in contrast to *Ripk1*^{-/-} organoids, *Ripk1*^{-/-}/*Tnfr1*^{-/-} organoids grew in culture for a limited period of time, but were highly sensitive to Poly(I:C), IFN- β and IFN- γ induced cell death (Figure 36). Therefore, TRIF- and/or IFN-mediated pathways might contribute to IEC death together with TNFR1 in a redundant fashion. This possibility is supported by the fact that the survival of *Ripk1*^{-/-}/*Tnfr1*^{-/-}/*Trif*^{-/-} mice is significantly extended beyond those of *Ripk1*^{-/-}

Tnfr1^{-/-} and *Ripk1*^{-/-}/*Trif*^{-/-} mice (Dillon et al., 2014). In the skin, TRIF-deficiency slightly ameliorated the extent of skin inflammation in RIPK1^{E-KO} mice (Dannappel et al., 2014). Although the effect of TRIF-ablation on the extent of keratinocyte apoptosis and necroptosis was not evaluated in this work, TRIF and TNFR1 double deficiency might provide further protection from skin pathology in RIPK1^{E-KO} mice. On the other hand, in both models RIPK3-mediated necroptosis is an important driver of the phenotype, and TRIF deletion maybe disables a TRIF-RIPK3 RHIM-mediated interaction that causes necroptosis in the absence of RIPK1. In this case, given the RIPK3-independency of the intestinal phenotype, TNFR1-TRIF double deficiency would not give any further protection compared to TNFR1 deficiency. However, this needs to be addressed with a genetic approach requiring the generation of triple mutant animals.

Similar to TNFR1 and TRIF-double deficiency, *Ripk1*^{-/-}/*Tnfr1*^{-/-}/*Ifnar*^{-/-} mice had a survival advantage compared to *Ripk1*^{-/-}/*Tnfr1*^{-/-} and *Ripk1*^{-/-}/*Ifnar*^{-/-} mice (Dillon et al., 2014). *In vitro* studies revealed that *Ripk1*^{-/-} MEFs are sensitized to type I IFN-induced death, that depends on RIPK3 and MLKL (Dillon et al., 2014; Kaiser et al., 2014). As RIPK3-dependent necroptotic death plays no major role in RIPK1-deficient IECs, it is unlikely that deletion of IFNAR would ameliorate cell death in RIPK1^{IEC-KO} mice, although experimental evidence is required to assess this possibility.

Given the importance of RIPK1 in the described signalling pathways regulating cell death and cytokine production, it is not surprising that RIPK1 is linked to bacterial and viral infections. Several studies emphasized the importance of RIPK1 and/or RIPK3 mediated cell death pathways during infection scenarios. In order to successfully disseminate and infect another host, many viruses counteract host's cell death machinery. For instance, vaccinia virus expresses B13R/Spi2, a potent inhibitor of caspase-1 and caspase-8. Infected cells are sensitized to RIPK1/RIPK3 dependent necroptosis induced by increased TNF expression after pathogen encounter in different tissues. In line with this, VV infected *Ripk3*^{-/-} mice showed reduced cell death and inflammation and finally succumbed to the infection due to uncontrolled spreading of the pathogen (Chan et al., 2003; Cho et al., 2009).

Likewise *Ripk1*^{D138N} mice showed impaired control of vaccinia virus replication, underlining the importance of RIPK1/RIPK3-mediated necroptosis for the host's antiviral response (Polykratis et al., 2014). However, if infections with VV cause or prevent RIPK1/RIPK3-dependent necroptosis in healthy IECs is unknown.

Murine cytomegalovirus (MCMV) encodes viral inhibitor of caspase-8 activation (vICA) and viral inhibitor of RIP activation (vIRA) to block both, apoptotic and necroptotic cell death (Brune, Menard, Heesemann, & Koszinowski, 2001; Mack, Sickmann, Lembo, & Brune, 2008; Rebsamen et al., 2009; Upton et al., 2008). vIRA harbors two RHIM-domains and can prevent death of infected host cells by binding to RIPK1 and RIPK3 to prevent DAI induced necroptosis and NF- κ B activation. Mutating the RHIM of vIRA abolished the virulence of MCMV due to increased host cell necroptosis, which was restored in *Dai*^{-/-} and *Ripk3*^{-/-} mice (Upton et al., 2012). In rare cases, cytomegalovirus infection can cause ileitis and colitis in immunocompetent patients, although it remains elusive if CMV interferes or hijacks the RIPK1/RIPK3-dependent cell death machinery in infected IECs (Tejedor Cerdena et al., 2011). In the described examples, the diverse roles of RIPK1 during infections were examined mainly in immune cells and the possibility of bacterial and viral induced apoptosis/necroptosis in IECs remain elusive. A recent publication demonstrated that poly(I:C) directly triggers a TLR3-TRIF-caspase-8 pathway to induce IEC apoptosis and IEC shedding (McAllister et al., 2013). Although not evaluated in this specific experimental setting, it is likely that RIPK1 is a mediator of TLR3-TRIF induced apoptosis in IECs, as reported for other cell types (Estornes et al., 2012). Upon blocking extrinsic apoptosis, as in Caspase-8^{IEC-KO} mice, intraperitoneal injection of Poly(I:C), induced RIPK1 kinase-dependent RIPK3-dependent IEC necroptosis, providing further evidence for a physiological role of RIPK1 in the regulation of TLR3-induced cell death in IECs. However, the contribution of RIPK1 in IEC-specific viral infection models still needs to be addressed.

Several recent studies revealed, that bacterial infections can induce RIPK1 and/or RIPK3 dependent cell death. For instance, *Salmonella enterica* serovar Typhimurium can induce macrophage death by triggering type I IFN

production that culminates in autocrine RIPK1- and RIPK3-dependent macrophage necroptosis to evade host's innate immune system (Robinson et al., 2012). In a similar way and in contrast to VV and MCMV infections, *Mycobacterium tuberculosis* uses TNF-induced host cell RIPK1/RIPK3-dependent necroptosis for its own dissemination into the extracellular space (Chan et al., 2015). The primary etiological agent of periodontitis, *Porphyromonas gingivalis*, which is also associated with atherosclerosis, was shown to specifically cleave RIPK1 in infected human aortic endothelial cells with a lysine-specific Kgp protease to prevent activation of the host cell death machinery (Madrigal, Barth, Papadopoulos, & Genco, 2012). Finally, in specific infection scenarios, RIPK1 can have dual functions. First, macrophages infected with *Yersinia pestis*, the causative agent of "black death", are removed by RIPK1 kinase-dependent caspase-8 mediated apoptosis and second, both, RIPK1 and caspase-8 are required for TNF, IL-6, IL-18 production and caspase-1 activation in *Y. pestis* infected macrophages (Grobner et al., 2007; Philip et al., 2014; Weng et al., 2014). Although these studies suggest differential roles for RIPK1 during bacterial infections, most of the studies focused on the role of immune cells during infections. Many pathogens, for instance *Helicobacter pylori*, *Clostridium difficile*, *Cryptosporidium parvum*, *Shigella dysenteriae* and enterohemorrhagic *Escherichia coli* (EHEC) were shown to induce IEC apoptosis *in vitro* and/or *in vivo*, however the molecular mechanism of cell death was investigated in these studies (Keenan, Sharpnack, Collins, Formal, & O'Brien, 1986; Wada, Mori, & Iwanaga, 1997; Wagner et al., 1997). Nevertheless, it has been reported that gastrointestinal attaching and effacing (A/E) pathogens, such as enteropathogenic *Escherichia coli* (EPEC), *Shigella* and *Salmonella* express a type III secretion system effector NleB1, which directly interacts with death domain proteins FADD, RIPK1 and TRADD to antagonize DR-induced apoptosis of in 293T cells (S. Li et al., 2013; Pearson et al., 2013). Therefore, although experimental evidence is missing so far, it is possible that RIPK1-regulated cell death in IECs is involved in bacterial infections.

Beside its role in RIPK1 in the described pathways, RIPK1 is suggested to be involved in other cell survival/proliferation pathways, such as insulin-like

growth factor 1 receptor (IGF-1R) or epidermal growth factor receptor (EGFR)-mediated signalling (Lin, Yang, Wang, & Liu, 2006; Ramnarain et al., 2008). However, if RIPK1 has a role in regulating cell survival or cell death within these pathways and if this is relevant for RIPK1-deficient IECs is unknown and needs to be addressed.

Upon DNA damage, a signalling platform called the PIDDosome forms, that among others, contains NEMO and RIPK1 and signals through either cell survival or caspase-2 mediated apoptosis. Within the PIDDosome, RIPK1 negatively regulates DNA-damage induced apoptosis by promoting NF- κ B activation (Tinel et al., 2007). During excessive DNA damage induced by etoposide, an inhibitor of topoisomerases, ATM stimulates two sequential NF- κ B activation pathways via NEMO and RIPK1 in cancer cells to induce feedforward autocrine TNF-signaling in order to eliminate affected cells and alert neighbouring cells (Biton & Ashkenazi, 2011). RIPK1 regulates genotoxic stress induced apoptosis in a kinase activity dependent and DR-independent manner within a cytosolic platform called “Ripoptosome” (Tenev et al., 2011). Within the Ripoptosome, the levels of cFLIP_L and cFLIP_S determine cell fate between apoptosis and RIPK3-dependent necroptosis by regulating caspase-8 activity (Feoktistova et al., 2011). Although the mode of death may have different consequences relevant for some pathophysiological conditions, it is rather unlikely that genotoxic stress is a trigger of apoptosis in *Ripk1*^{-/-} IECs.

In summary, autocrine TNF is the major inducer of IEC apoptosis in the colon and ileum of RIPK1^{IEC-KO} mice. However, beside TNF, other triggers of FADD-dependent apoptosis in RIPK1-deficient IECs exist, that still need to be identified to understand how RIPK1 regulates intestinal homeostasis. In addition, many studies revealed that RIPK1-regulated cell death pathways not only regulate homeostasis, but also are important during pathophysiological conditions such as infections and for executing appropriate host immune responses to protect the organism.

4.4 The role of RIPK1 in (intestinal) inflammation

Except for *Tnf* and *Cxcl1*, expression of cytokines and chemokines was only slightly upregulated in the colon and ileum of RIPK1^{IEC-KO} mice on mRNA levels (Figure 9, Figure 13). Although, the overall number of leucocytes and in particular CD11b^{hi} Ly6G^{hi} neutrophils, which are usually the first cells recruited to a site of inflammation, were differentially increased in the lamina propria of RIPK1^{IEC-KO} intestines, on histological sections they showed a dispersed staining pattern and were not found in focal spots (Figure 10, Figure 14). Ulcers were not detectable in none of the examined H&E stained sections from colon and ileum derived from RIPK1^{IEC-KO} mice (Figure 6). Thus, despite extensive epithelial cell apoptosis, RIPK1^{IEC-KO} mice develop only very mild inflammation in the colon and the ileum. IEC apoptosis, intestinal pathology and premature death of RIPK1^{IEC-KO} mice were independent of commensal bacteria and MyD88-mediated signalling (Figure 17, Figure 18, Figure 20- Figure 22). Noteworthy, another publication reported a partial dependency of severe wasting, premature lethality and inflammation in RIPK1^{IEC-KO} mice on the microbiota and MyD88-dependent signalling (Takahashi et al., 2014). However, in this study, a detailed characterization of colitis/iliitis in both has so far not been provided, and similar to our results, double-knockout mice still showed IEC apoptosis. The reason for the discrepancies in the macroscopic state and survival of RIPK1^{IEC-KO} mice between both studies are unknown. Nevertheless, since antibiotic treatment ameliorated wasting and prolonged the survival of RIPK1^{IEC-KO} (Figure 20) (Takahashi et al., 2014) as well as of RIPK1^{tamIEC-KO} (Figure 17, Figure 18) and low numbers of germ-free RIPK1^{IEC-KO} mice survived up to 22 weeks (Figure 21a, b), it is possible that the depletion or absence of the microbiota has a beneficial effect for the overall constitution and survival of the mice without affecting IEC death and intestinal pathology.

The phenotype of RIPK1^{IEC-KO} mice is in stark contrast to other murine intestinal models of (extrinsically-induced) intestinal cell death such as NEMO^{IEC-KO} mice or FADD^{IEC-KO} mice, which have less dying IECs compared to RIPK1^{IEC-KO} mice, but develop ulcerating colitis already at 3 weeks of age

(Nenci et al., 2007; Welz et al., 2011)(unpublished data). In both cases, colitis depends on commensals inducing MyD88-dependent signalling, however death of IECs is only reduced but not abrogated (Nenci et al., 2007; Welz et al., 2011)(unpublished data). In line with this, previous reports showed, that IECs express low levels of TLR4 and LPS-induced death of IECs in mice depends on TNF produced by non-epithelial cells in response to LPS sensing (Gunther et al., 2015; Williams et al., 2013). Thus, most likely commensal-induced TLR4-MyD88-mediated signalling does not directly induce IEC death in $RIPK1^{IEC-KO}$, $FADD^{IEC-KO}$ and $NEMO^{IEC-KO}$ mice. In the case of the latter two, according to the current model, a compromised barrier integrity, caused by IEC death, allows the translocation of bacterial antigens in to the bowel wall, where they activate mucosal immune cells and thereby induce cytokine production, which drives the inflammatory phenotype. Increased abundance of inflammatory cytokines such as TNF in turn, induces death of more IECs triggering a feedforward loop sustaining and promoting disease development.

Within the intestinal epithelium, dead cells are removed mainly by cell shedding, whereas the contribution of phagocytosis is under debate, thus controlled proliferation and regulation of cell adhesion- and tight junction proteins is necessary for proper barrier integrity. As $RIPK1^{IEC-KO}$ mice do not show ulcerating colitis (and ileitis), one may speculate that despite extensive cell death, the intestinal epithelial barrier integrity remains intact. This would provide an explanation why MyD88 ablation, and thus sensing of bacteria in the lamina propria, does not have an impact on the pathology in these mice. However, if a compromised barrier is the cause or the consequence of intestinal inflammation remains a question at the moment. Recently, it was demonstrated that mice with IEC specific ablation of claudin-7, a constituent of epithelial tight junctions, primarily had a leaky intestinal barrier, which was followed by inflammation of the colon, suggesting that a compromised barrier might be sufficient to cause colitis (Tanaka et al., 2015). Similarly, $Caspase-8^{IEC-KO}$ mice, an intestinal cell death model for RIPK3-dependent IEC necroptosis, showed breakdown of epithelial barrier upon poly(I:C) injection that most likely contributes to lethal systemic spreading of intestinal microbes (Gunther et al., 2015). It remains to be shown, if the expression of

constituents regulating proliferation, cell adhesion and epithelial tight- and gap junctions differs between RIPK1^{IEC-KO} mice and other mouse models, or is regulated differentially by other means.

Another possibility, which could account for the different pathology in the RIPK1^{IEC-KO}-, NEMO^{IEC-KO}-, FADD^{IEC-KO}- and Caspase-8^{IEC-KO} mice, is the mode of cell death of IECs. Historically, apoptosis is considered as an immunotolerogenic or “silent” mode of cell death during which the dying cells are orderly disassembled by phagocytes to limit the amount of released DAMPs. In contrast, unregulated necrosis/necroptosis are considered as immunogenic, due to the uncontrolled release of DAMPs into the neighbourhood. Accordingly, in RIPK1^{IEC-KO} mice, with predominantly apoptotic IECs, no or only a mild inflammation would be expected. In contrast, in RIPK1^{IEC-KO}/FADD^{IEC-KO} the dominant mode of death switched to RIPK3-dependent necroptosis, that is immunogenic, resulting in colitis with presence of ulcers in 50% of the analysed mice (Figure 25).

In other intestinal cell death models, such as NEMO^{IEC-KO} mice, IKK1/2^{IEC-KO} mice and TAK1^{IEC-KO} mice, apoptosis is the main driver of the phenotype, however, mice develop severe colitis (Kajino-Sakamoto et al., 2008; Nenci et al., 2007). However, it should be considered that in these models impaired NF-κB and MAPK activation may also contribute to the observed phenotypes. Although a possible a role of necroptosis needs to be addressed in these models, they demonstrate that apoptotic IEC death is able to trigger intestinal inflammation. Since the molecular mechanisms initiating apoptosis differ in RIPK1^{IEC-KO} mice on the one, and NEMO^{IEC-KO} on the other hand, it could be possible that the mode of apoptosis has an influence on the immunogenicity itself or indirectly via the products that are exposed on the cell surface or secreted by dying cells. For instance it was shown that a small difference in the combination of molecules exposed during death of cells, can determine if the dying cell is recognised as immunogenic or not (Obeid et al., 2007). As mentioned, the immunogenic potential of necrotic/necroptotic death is attributed to the release of DAMPs, subdivided further into molecules with non-inflammatory functions in living cells with immunomodulatory properties such as HMGB1, uric acid, ATP and second, alarmins and molecules with

cytokine-like functions, for instance IL-1 α , IL-1 β or IL-33 (Kaczmarek, Vandenameele, & Krysko, 2013). In the plasma of *Ripk1*^{-/-} mice increased levels of IL-33 but not HMGB1 were detected, and this increase was independent of caspase-8 but dependent on RIPK3 and MLKL, thus seems to be specific for necroptosis (Rickard et al., 2014). IL-33 is of special interest, since it is a chromatin-associated protein constitutively expressed by epithelial cells and usually inactivated by effector caspases during apoptosis (Luthi et al., 2009; Palmer & Gabay, 2011). However, if levels of IL-33 or another yet to be identified DAMP differ before the onset of inflammation and may account for the phenotypic difference in RIPK1^{IEC-KO} mice and RIPK1^{IEC-KO}/FADD^{IEC-KO} as well as other intestinal cell death models remains to be shown.

In summary, it is not clear if a different mode of cell death and/or differences in the barrier regulation account for the phenotypic differences in regard to inflammation that are observed in RIPK1^{IEC-KO} mice and other models.

4.5 Concluding Remarks

The data presented in this work unravels RIPK1 as an important regulator of intestinal homeostasis that prevents FADD-dependent apoptosis during homeostatic conditions. Further studies are required to decipher the molecular mechanisms of RIPK1-regulated cell death downstream of TNF and other signalling pathways. This might provide important insights to understand the pathogenesis of human diseases such as IBD. Although the pathogenic role of TNF in IBD is not fully understood, anti-TNF therapy is successfully used in IBD patients. There is increasing evidence that apoptosis and necroptosis contributes to the pathology in IBD and thus, specific targeting of components of cell death effectors may provide novel therapeutic opportunities.

References

- Abreu, M. T. (2010). Toll-like receptor signalling in the intestinal epithelium: how bacterial recognition shapes intestinal function. *Nat Rev Immunol*, *10*(2), 131-144. doi: 10.1038/nri2707
- Abreu, M. T., Vora, P., Faure, E., Thomas, L. S., Arnold, E. T., & Arditi, M. (2001). Decreased expression of Toll-like receptor-4 and MD-2 correlates with intestinal epithelial cell protection against dysregulated proinflammatory gene expression in response to bacterial lipopolysaccharide. *J Immunol*, *167*(3), 1609-1616.
- Adachi, O., Kawai, T., Takeda, K., Matsumoto, M., Tsutsui, H., Sakagami, M., . . . Akira, S. (1998). Targeted disruption of the MyD88 gene results in loss of IL-1- and IL-18-mediated function. *Immunity*, *9*(1), 143-150.
- Adolph, T. E., Tomczak, M. F., Niederreiter, L., Ko, H. J., Bock, J., Martinez-Naves, E., . . . Blumberg, R. S. (2013). Paneth cells as a site of origin for intestinal inflammation. *Nature*, *503*(7475), 272-276. doi: 10.1038/nature12599
- Alexopoulou, L., Holt, A. C., Medzhitov, R., & Flavell, R. A. (2001). Recognition of double-stranded RNA and activation of NF-kappaB by Toll-like receptor 3. *Nature*, *413*(6857), 732-738. doi: 10.1038/35099560
- Arijs, I., De Hertogh, G., Lemaire, K., Quintens, R., Van Lommel, L., Van Steen, K., . . . Rutgeerts, P. (2009). Mucosal gene expression of antimicrobial peptides in inflammatory bowel disease before and after first infliximab treatment. *PLoS One*, *4*(11), e7984. doi: 10.1371/journal.pone.0007984
- Armaka, M., Apostolaki, M., Jacques, P., Kontoyiannis, D. L., Elewaut, D., & Kollias, G. (2008). Mesenchymal cell targeting by TNF as a common pathogenic principle in chronic inflammatory joint and intestinal diseases. *J Exp Med*, *205*(2), 331-337. doi: 10.1084/jem.20070906
- Arslan, S. C., & Scheidereit, C. (2011). The prevalence of TNFalpha-induced necrosis over apoptosis is determined by TAK1-RIP1 interplay. *PLoS One*, *6*(10), e26069. doi: 10.1371/journal.pone.0026069
- Barker, N., Bartfeld, S., & Clevers, H. (2010). Tissue-resident adult stem cell populations of rapidly self-renewing organs. *Cell Stem Cell*, *7*(6), 656-670. doi: 10.1016/j.stem.2010.11.016
- Barker, N., van Es, J. H., Kuipers, J., Kujala, P., van den Born, M., Cozijnsen, M., . . . Clevers, H. (2007). Identification of stem cells in small intestine and colon by marker gene Lgr5. *Nature*, *449*(7165), 1003-1007. doi: 10.1038/nature06196
- Berger, S. B., Kasparcova, V., Hoffman, S., Swift, B., Dare, L., Schaeffer, M., . . . Gough, P. J. (2014). Cutting Edge: RIP1 kinase activity is dispensable for normal development but is a key regulator of inflammation in SHARPIN-deficient mice. *J Immunol*, *192*(12), 5476-5480. doi: 10.4049/jimmunol.1400499
- Bertrand, M. J., Milutinovic, S., Dickson, K. M., Ho, W. C., Boudreault, A., Durkin, J., . . . Barker, P. A. (2008). cIAP1 and cIAP2 facilitate cancer cell survival by functioning as E3 ligases that promote RIP1 ubiquitination. *Mol Cell*, *30*(6), 689-700. doi: 10.1016/j.molcel.2008.05.014

- Bevins, C. L., & Salzman, N. H. (2011). Paneth cells, antimicrobial peptides and maintenance of intestinal homeostasis. *Nat Rev Microbiol*, *9*(5), 356-368. doi: 10.1038/nrmicro2546
- Biton, S., & Ashkenazi, A. (2011). NEMO and RIP1 control cell fate in response to extensive DNA damage via TNF-alpha feedforward signaling. *Cell*, *145*(1), 92-103. doi: 10.1016/j.cell.2011.02.023
- Boldin, M. P., Goncharov, T. M., Goltsev, Y. V., & Wallach, D. (1996). Involvement of MACH, a novel MORT1/FADD-interacting protease, in Fas/APO-1- and TNF receptor-induced cell death. *Cell*, *85*(6), 803-815.
- Bonnet, M. C., Preukschat, D., Welz, P. S., van Loo, G., Ermolaeva, M. A., Bloch, W., . . . Pasparakis, M. (2011). The adaptor protein FADD protects epidermal keratinocytes from necroptosis in vivo and prevents skin inflammation. *Immunity*, *35*(4), 572-582. doi: 10.1016/j.immuni.2011.08.014
- Braegger, C. P., Nicholls, S., Murch, S. H., Stephens, S., & MacDonald, T. T. (1992). Tumour necrosis factor alpha in stool as a marker of intestinal inflammation. *Lancet*, *339*(8785), 89-91.
- Brandl, K., Plitas, G., Schnabl, B., DeMatteo, R. P., & Pamer, E. G. (2007). MyD88-mediated signals induce the bactericidal lectin RegIII gamma and protect mice against intestinal *Listeria monocytogenes* infection. *J Exp Med*, *204*(8), 1891-1900. doi: 10.1084/jem.20070563
- Breese, E. J., Michie, C. A., Nicholls, S. W., Murch, S. H., Williams, C. B., Domizio, P., . . . MacDonald, T. T. (1994). Tumor necrosis factor alpha-producing cells in the intestinal mucosa of children with inflammatory bowel disease. *Gastroenterology*, *106*(6), 1455-1466.
- Broquet, A. H., Hirata, Y., McAllister, C. S., & Kagnoff, M. F. (2011). RIG-I/MDA5/MAVS are required to signal a protective IFN response in rotavirus-infected intestinal epithelium. *J Immunol*, *186*(3), 1618-1626. doi: 10.4049/jimmunol.1002862
- Brune, W., Menard, C., Heesemann, J., & Koszinowski, U. H. (2001). A ribonucleotide reductase homolog of cytomegalovirus and endothelial cell tropism. *Science*, *291*(5502), 303-305. doi: 10.1126/science.291.5502.303
- Cai, Z., Jitkaew, S., Zhao, J., Chiang, H. C., Choksi, S., Liu, J., . . . Liu, Z. G. (2014). Plasma membrane translocation of trimerized MLKL protein is required for TNF-induced necroptosis. *Nat Cell Biol*, *16*(1), 55-65. doi: 10.1038/ncb2883
- Cario, E. (2013). The human TLR4 variant D299G mediates inflammation-associated cancer progression in the intestinal epithelium. *Oncoimmunology*, *2*(7), e24890. doi: 10.4161/onci.24890
- Cario, E., & Podolsky, D. K. (2000). Differential alteration in intestinal epithelial cell expression of toll-like receptor 3 (TLR3) and TLR4 in inflammatory bowel disease. *Infect Immun*, *68*(12), 7010-7017.
- Cash, H. L., Whitham, C. V., Behrendt, C. L., & Hooper, L. V. (2006). Symbiotic bacteria direct expression of an intestinal bactericidal lectin. *Science*, *313*(5790), 1126-1130. doi: 10.1126/science.1127119
- Chan, F. K., Luz, N. F., & Moriwaki, K. (2015). Programmed necrosis in the cross talk of cell death and inflammation. *Annu Rev Immunol*, *33*, 79-106. doi: 10.1146/annurev-immunol-032414-112248

- Chan, F. K., Shisler, J., Bixby, J. G., Felices, M., Zheng, L., Appel, M., . . . Lenardo, M. J. (2003). A role for tumor necrosis factor receptor-2 and receptor-interacting protein in programmed necrosis and antiviral responses. *J Biol Chem*, *278*(51), 51613-51621. doi: 10.1074/jbc.M305633200
- Chen, W., Zhou, Z., Li, L., Zhong, C. Q., Zheng, X., Wu, X., . . . Han, J. (2013). Diverse sequence determinants control human and mouse receptor interacting protein 3 (RIP3) and mixed lineage kinase domain-like (MLKL) interaction in necroptotic signaling. *J Biol Chem*, *288*(23), 16247-16261. doi: 10.1074/jbc.M112.435545
- Chen, X., Li, W., Ren, J., Huang, D., He, W. T., Song, Y., . . . Han, J. (2014). Translocation of mixed lineage kinase domain-like protein to plasma membrane leads to necrotic cell death. *Cell Res*, *24*(1), 105-121. doi: 10.1038/cr.2013.171
- Cheng, H., & Leblond, C. P. (1974). Origin, differentiation and renewal of the four main epithelial cell types in the mouse small intestine. I. Columnar cell. *Am J Anat*, *141*(4), 461-479. doi: 10.1002/aja.1001410403
- Chinnaiyan, A. M., O'Rourke, K., Tewari, M., & Dixit, V. M. (1995). FADD, a novel death domain-containing protein, interacts with the death domain of Fas and initiates apoptosis. *Cell*, *81*(4), 505-512.
- Cho, Y. S., Challa, S., Moquin, D., Genga, R., Ray, T. D., Guildford, M., & Chan, F. K. (2009). Phosphorylation-driven assembly of the RIP1-RIP3 complex regulates programmed necrosis and virus-induced inflammation. *Cell*, *137*(6), 1112-1123. doi: 10.1016/j.cell.2009.05.037
- Choi, Y. E., Butterworth, M., Malladi, S., Duckett, C. S., Cohen, G. M., & Bratton, S. B. (2009). The E3 ubiquitin ligase cIAP1 binds and ubiquitinates caspase-3 and -7 via unique mechanisms at distinct steps in their processing. *J Biol Chem*, *284*(19), 12772-12782. doi: 10.1074/jbc.M807550200
- Christofferson, D. E., Li, Y., & Yuan, J. (2014). Control of life-or-death decisions by RIP1 kinase. *Annu Rev Physiol*, *76*, 129-150. doi: 10.1146/annurev-physiol-021113-170259
- Crosnier, C., Stamatakis, D., & Lewis, J. (2006). Organizing cell renewal in the intestine: stem cells, signals and combinatorial control. *Nat Rev Genet*, *7*(5), 349-359. doi: 10.1038/nrg1840
- Cullen, S. P., Henry, C. M., Kearney, C. J., Logue, S. E., Feoktistova, M., Tynan, G. A., . . . Martin, S. J. (2013). Fas/CD95-induced chemokines can serve as "find-me" signals for apoptotic cells. *Mol Cell*, *49*(6), 1034-1048. doi: 10.1016/j.molcel.2013.01.025
- Cusson, N., Oikemus, S., Kilpatrick, E. D., Cunningham, L., & Kelliher, M. (2002). The Death Domain Kinase RIP Protects Thymocytes from Tumor Necrosis Factor Receptor Type 2-induced Cell Death. *Journal of Experimental Medicine*, *196*(1), 15-26. doi: 10.1084/jem.20011470
- Cusson-Hermance, N., Khurana, S., Lee, T. H., Fitzgerald, K. A., & Kelliher, M. A. (2005). Rip1 mediates the Trif-dependent toll-like receptor 3- and 4-induced NF- κ B activation but does not contribute to interferon regulatory factor 3 activation. *J Biol Chem*, *280*(44), 36560-36566. doi: 10.1074/jbc.M506831200
- Dannappel, M., Vlantis, K., Kumari, S., Polykratis, A., Kim, C., Wachsmuth, L., . . . Pasparakis, M. (2014). RIPK1 maintains epithelial homeostasis by

- inhibiting apoptosis and necroptosis. *Nature*, 513(7516), 90-94. doi: 10.1038/nature13608
- Darding, M., & Meier, P. (2012). IAPs: guardians of RIPK1. *Cell Death Differ*, 19(1), 58-66. doi: 10.1038/cdd.2011.163
- Dechairo, B., Dimon, C., van Heel, D., Mackay, I., Edwards, M., Scambler, P., . . . Carey, A. (2001). Replication and extension studies of inflammatory bowel disease susceptibility regions confirm linkage to chromosome 6p (IBD3). *Eur J Hum Genet*, 9(8), 627-633. doi: 10.1038/sj.ejhg.5200687
- Degterev, A., Hitomi, J., Germscheid, M., Ch'en, I. L., Korkina, O., Teng, X., . . . Yuan, J. (2008). Identification of RIP1 kinase as a specific cellular target of necrostatins. *Nat Chem Biol*, 4(5), 313-321. doi: 10.1038/nchembio.83
- Degterev, A., Huang, Z., Boyce, M., Li, Y., Jagtap, P., Mizushima, N., . . . Yuan, J. (2005). Chemical inhibitor of nonapoptotic cell death with therapeutic potential for ischemic brain injury. *Nat Chem Biol*, 1(2), 112-119. doi: 10.1038/nchembio711
- Dillon, C. P., Oberst, A., Weinlich, R., Janke, L. J., Kang, T. B., Ben-Moshe, T., . . . Green, D. R. (2012). Survival function of the FADD-CASPASE-8-cFLIP(L) complex. *Cell Rep*, 1(5), 401-407. doi: 10.1016/j.celrep.2012.03.010
- Dillon, C. P., Weinlich, R., Rodriguez, D. A., Cripps, J. G., Quarato, G., Gurung, P., . . . Green, D. R. (2014). RIPK1 blocks early postnatal lethality mediated by caspase-8 and RIPK3. *Cell*, 157(5), 1189-1202. doi: 10.1016/j.cell.2014.04.018
- Dondelinger, Y., Aguilera, M. A., Goossens, V., Dubuisson, C., Grootjans, S., Dejardin, E., . . . Bertrand, M. J. (2013). RIPK3 contributes to TNFR1-mediated RIPK1 kinase-dependent apoptosis in conditions of cIAP1/2 depletion or TAK1 kinase inhibition. *Cell Death Differ*, 20(10), 1381-1392. doi: 10.1038/cdd.2013.94
- Dondelinger, Y., Declercq, W., Montessuit, S., Roelandt, R., Goncalves, A., Bruggeman, I., . . . Vandenabeele, P. (2014). MLKL compromises plasma membrane integrity by binding to phosphatidylinositol phosphates. *Cell Rep*, 7(4), 971-981. doi: 10.1016/j.celrep.2014.04.026
- Ea, C. K., Deng, L., Xia, Z. P., Pineda, G., & Chen, Z. J. (2006). Activation of IKK by TNFalpha requires site-specific ubiquitination of RIP1 and polyubiquitin binding by NEMO. *Mol Cell*, 22(2), 245-257. doi: 10.1016/j.molcel.2006.03.026
- Eckelman, B. P., & Salvesen, G. S. (2006). The human anti-apoptotic proteins cIAP1 and cIAP2 bind but do not inhibit caspases. *J Biol Chem*, 281(6), 3254-3260. doi: 10.1074/jbc.M510863200
- Eckelman, B. P., Salvesen, G. S., & Scott, F. L. (2006). Human inhibitor of apoptosis proteins: why XIAP is the black sheep of the family. *EMBO Rep*, 7(10), 988-994. doi: 10.1038/sj.embor.7400795
- Egan, L. J., Eckmann, L., Greten, F. R., Chae, S., Li, Z. W., Myhre, G. M., . . . Kagnoff, M. F. (2004). I kappa B-kinase beta-dependent NF-kappa B activation provides radioprotection to the intestinal epithelium. *Proc Natl Acad Sci U S A*, 101(8), 2452-2457.
- Eisenhoffer, G. T., Loftus, P. D., Yoshigi, M., Otsuna, H., Chien, C. B., Morcos, P. A., & Rosenblatt, J. (2012). Crowding induces live cell

- extrusion to maintain homeostatic cell numbers in epithelia. *Nature*, 484(7395), 546-549. doi: 10.1038/nature10999
- el Marjou, F., Janssen, K. P., Chang, B. H., Li, M., Hindie, V., Chan, L., . . . Robine, S. (2004). Tissue-specific and inducible Cre-mediated recombination in the gut epithelium. *Genesis*, 39(3), 186-193. doi: 10.1002/gene.20042
- Elmore, S. (2007). Apoptosis: a review of programmed cell death. *Toxicol Pathol*, 35(4), 495-516. doi: 10.1080/01926230701320337
- Ermolaeva, M. A., Michallet, M. C., Papadopoulou, N., Utermohlen, O., Kranidioti, K., Kollias, G., . . . Pasparakis, M. (2008). Function of TRADD in tumor necrosis factor receptor 1 signaling and in TRIF-dependent inflammatory responses. *Nat Immunol*, 9(9), 1037-1046. doi: 10.1038/ni.1638
- Estornes, Y., Toscano, F., Virard, F., Jacquemin, G., Pierrot, A., Vanbervliet, B., . . . Lebecque, S. (2012). dsRNA induces apoptosis through an atypical death complex associating TLR3 to caspase-8. *Cell Death Differ*, 19(9), 1482-1494. doi: 10.1038/cdd.2012.22
- Feng, S., Ma, L., Yang, Y., & Wu, M. (2006). Truncated RIP3 (tRIP3) acts upstream of FADD to induce apoptosis in the human hepatocellular carcinoma cell line QGY-7703. *Biochem Biophys Res Commun*, 347(3), 558-565. doi: 10.1016/j.bbrc.2006.06.118
- Feng, S., Yang, Y., Mei, Y., Ma, L., Zhu, D. E., Hoti, N., . . . Wu, M. (2007). Cleavage of RIP3 inactivates its caspase-independent apoptosis pathway by removal of kinase domain. *Cell Signal*, 19(10), 2056-2067. doi: 10.1016/j.cellsig.2007.05.016
- Feoktistova, M., Geserick, P., Kellert, B., Dimitrova, D. P., Langlais, C., Hupe, M., . . . Leverkus, M. (2011). cIAPs block Ripoptosome formation, a RIP1/caspase-8 containing intracellular cell death complex differentially regulated by cFLIP isoforms. *Mol Cell*, 43(3), 449-463. doi: 10.1016/j.molcel.2011.06.011
- Festjens, N., Vanden Berghe, T., Cornelis, S., & Vandenabeele, P. (2007). RIP1, a kinase on the crossroads of a cell's decision to live or die. *Cell Death Differ*, 14(3), 400-410. doi: 10.1038/sj.cdd.4402085
- Festjens, N., Vanden Berghe, T., & Vandenabeele, P. (2006). Necrosis, a well-orchestrated form of cell demise: signalling cascades, important mediators and concomitant immune response. *Biochim Biophys Acta*, 1757(9-10), 1371-1387. doi: 10.1016/j.bbabi.2006.06.014
- Frolova, L., Drastich, P., Rossmann, P., Klimesova, K., & Tlaskalova-Hogenova, H. (2008). Expression of Toll-like receptor 2 (TLR2), TLR4, and CD14 in biopsy samples of patients with inflammatory bowel diseases: upregulated expression of TLR2 in terminal ileum of patients with ulcerative colitis. *J Histochem Cytochem*, 56(3), 267-274. doi: 10.1369/jhc.7A7303.2007
- Gaither, A., Porter, D., Yao, Y., Borawski, J., Yang, G., Donovan, J., . . . Zawel, L. (2007). A Smac mimetic rescue screen reveals roles for inhibitor of apoptosis proteins in tumor necrosis factor- α signaling. *Cancer Res*, 67(24), 11493-11498. doi: 10.1158/0008-5472.CAN-07-5173
- Galluzzi, L., Bravo-San Pedro, J. M., Vitale, I., Aaronson, S. A., Abrams, J. M., Adam, D., . . . Kroemer, G. (2015). Essential versus accessory

- aspects of cell death: recommendations of the NCCD 2015. *Cell Death Differ*, 22(1), 58-73. doi: 10.1038/cdd.2014.137
- Galluzzi, L., Vitale, I., Abrams, J. M., Alnemri, E. S., Baehrecke, E. H., Blagosklonny, M. V., . . . Kroemer, G. (2012). Molecular definitions of cell death subroutines: recommendations of the Nomenclature Committee on Cell Death 2012. *Cell Death Differ*, 19(1), 107-120. doi: 10.1038/cdd.2011.96
- Gentle, I. E., Wong, W. W., Evans, J. M., Bankovacki, A., Cook, W. D., Khan, N. R., . . . Vaux, D. L. (2011). In TNF-stimulated cells, RIPK1 promotes cell survival by stabilizing TRAF2 and cIAP1, which limits induction of non-canonical NF-kappaB and activation of caspase-8. *J Biol Chem*, 286(15), 13282-13291. doi: 10.1074/jbc.M110.216226
- Gerlach, B., Cordier, S. M., Schmukle, A. C., Emmerich, C. H., Rieser, E., Haas, T. L., . . . Walczak, H. (2011). Linear ubiquitination prevents inflammation and regulates immune signalling. *Nature*, 471(7340), 591-596. doi: 10.1038/nature09816
- Geserick, P., Hupe, M., Moulin, M., Wong, W. W., Feoktistova, M., Kellert, B., . . . Leverkus, M. (2009). Cellular IAPs inhibit a cryptic CD95-induced cell death by limiting RIP1 kinase recruitment. *J Cell Biol*, 187(7), 1037-1054. doi: 10.1083/jcb.200904158
- Gijbels, M. J., Zurcher, C., Kraal, G., Elliott, G. R., HogenEsch, H., Schijff, G., . . . Bruijnzeel, P. L. (1996). Pathogenesis of skin lesions in mice with chronic proliferative dermatitis (cpdm/cpdm). *Am J Pathol*, 148(3), 941-950.
- Gonzalvez, F., Lawrence, D., Yang, B., Yee, S., Pitti, R., Marsters, S., . . . Ashkenazi, A. (2012). TRAF2 Sets a threshold for extrinsic apoptosis by tagging caspase-8 with a ubiquitin shutoff timer. *Mol Cell*, 48(6), 888-899. doi: 10.1016/j.molcel.2012.09.031
- Green, D. R., Ferguson, T., Zitvogel, L., & Kroemer, G. (2009). Immunogenic and tolerogenic cell death. *Nat Rev Immunol*, 9(5), 353-363. doi: 10.1038/nri2545
- Grivennikov, S. I., Greten, F. R., & Karin, M. (2010). Immunity, inflammation, and cancer. *Cell*, 140(6), 883-899. doi: 10.1016/j.cell.2010.01.025
- Grobner, S., Adkins, I., Schulz, S., Richter, K., Borgmann, S., Wesselborg, S., . . . Autenrieth, I. B. (2007). Catalytically active Yersinia outer protein P induces cleavage of RIP and caspase-8 at the level of the DISC independently of death receptors in dendritic cells. *Apoptosis*, 12(10), 1813-1825. doi: 10.1007/s10495-007-0100-x
- Gunther, C., Buchen, B., He, G. W., Hornef, M., Torow, N., Neumann, H., . . . Becker, C. (2015). Caspase-8 controls the gut response to microbial challenges by Tnf-alpha-dependent and independent pathways. *Gut*, 64(4), 601-610. doi: 10.1136/gutjnl-2014-307226
- Gunther, C., Martini, E., Wittkopf, N., Amann, K., Weigmann, B., Neumann, H., . . . Becker, C. (2011). Caspase-8 regulates TNF-alpha-induced epithelial necroptosis and terminal ileitis. *Nature*, 477(7364), 335-339. doi: 10.1038/nature10400
- Haas, T. L., Emmerich, C. H., Gerlach, B., Schmukle, A. C., Cordier, S. M., Rieser, E., . . . Walczak, H. (2009). Recruitment of the linear ubiquitin chain assembly complex stabilizes the TNF-R1 signaling complex and

- is required for TNF-mediated gene induction. *Mol Cell*, 36(5), 831-844. doi: 10.1016/j.molcel.2009.10.013
- Hackam, D. J., Afrazi, A., Good, M., & Sodhi, C. P. (2013). Innate immune signaling in the pathogenesis of necrotizing enterocolitis. *Clin Dev Immunol*, 2013, 475415. doi: 10.1155/2013/475415
- Hall, P. A., Coates, P. J., Ansari, B., & Hopwood, D. (1994). Regulation of cell number in the mammalian gastrointestinal tract: the importance of apoptosis. *J Cell Sci*, 107 (Pt 12), 3569-3577.
- Hampe, J., Shaw, S. H., Saiz, R., Leysens, N., Lantermann, A., Mascheretti, S., . . . Schreiber, S. (1999). Linkage of inflammatory bowel disease to human chromosome 6p. *Am J Hum Genet*, 65(6), 1647-1655. doi: 10.1086/302677
- Hanauer, S. B., Feagan, B. G., Lichtenstein, G. R., Mayer, L. F., Schreiber, S., Colombel, J. F., . . . Group, A. I. S. (2002). Maintenance infliximab for Crohn's disease: the ACCENT I randomised trial. *Lancet*, 359(9317), 1541-1549. doi: 10.1016/S0140-6736(02)08512-4
- Hanauer, S. B., Sandborn, W. J., Rutgeerts, P., Fedorak, R. N., Lukas, M., MacIntosh, D., . . . Pollack, P. (2006). Human anti-tumor necrosis factor monoclonal antibody (adalimumab) in Crohn's disease: the CLASSIC-I trial. *Gastroenterology*, 130(2), 323-333; quiz 591. doi: 10.1053/j.gastro.2005.11.030
- Hausmann, M., Kiessling, S., Mestermann, S., Webb, G., Spottl, T., Andus, T., . . . Rogler, G. (2002). Toll-like receptors 2 and 4 are up-regulated during intestinal inflammation. *Gastroenterology*, 122(7), 1987-2000.
- Hayden, M. S., & Ghosh, S. (2012). NF-kappaB, the first quarter-century: remarkable progress and outstanding questions. *Genes Dev*, 26(3), 203-234. doi: 10.1101/gad.183434.111
- Hayden, M. S., & Ghosh, S. (2014). Regulation of NF-kappaB by TNF family cytokines. *Semin Immunol*, 26(3), 253-266. doi: 10.1016/j.smim.2014.05.004
- He, S., Liang, Y., Shao, F., & Wang, X. (2011). Toll-like receptors activate programmed necrosis in macrophages through a receptor-interacting kinase-3-mediated pathway. *Proc Natl Acad Sci U S A*, 108(50), 20054-20059. doi: 10.1073/pnas.1116302108
- He, S., Wang, L., Miao, L., Wang, T., Du, F., Zhao, L., & Wang, X. (2009). Receptor interacting protein kinase-3 determines cellular necrotic response to TNF-alpha. *Cell*, 137(6), 1100-1111. doi: 10.1016/j.cell.2009.05.021
- Hitomi, J., Christofferson, D. E., Ng, A., Yao, J., Degterev, A., Xavier, R. J., & Yuan, J. (2008). Identification of a molecular signaling network that regulates a cellular necrotic cell death pathway. *Cell*, 135(7), 1311-1323. doi: 10.1016/j.cell.2008.10.044
- Holler, N. (2000). <ni1200_489-Holler-2000.pdf>.
- Holler, N., Zaru, R., Micheau, O., Thome, M., Attinger, A., Valitutti, S., . . . Tschopp, J. (2000). Fas triggers an alternative, caspase-8-independent cell death pathway using the kinase RIP as effector molecule. *Nat Immunol*, 1(6), 489-495. doi: 10.1038/82732
- Hoshino, K., Takeuchi, O., Kawai, T., Sanjo, H., Ogawa, T., Takeda, Y., . . . Akira, S. (1999). Cutting edge: Toll-like receptor 4 (TLR4)-deficient

- mice are hyporesponsive to lipopolysaccharide: evidence for TLR4 as the Lps gene product. *J Immunol*, 162(7), 3749-3752.
- Hsu, H., Huang, J., Shu, H. B., Baichwal, V., & Goeddel, D. V. (1996). TNF-dependent recruitment of the protein kinase RIP to the TNF receptor-1 signaling complex. *Immunity*, 4(4), 387-396.
- Hsu, H., Shu, H. B., Pan, M. G., & Goeddel, D. V. (1996). TRADD-TRAF2 and TRADD-FADD interactions define two distinct TNF receptor 1 signal transduction pathways. *Cell*, 84(2), 299-308.
- Hsu, H., Xiong, J., & Goeddel, D. V. (1995). The TNF receptor 1-associated protein TRADD signals cell death and NF-kappa B activation. *Cell*, 81(4), 495-504.
- Ikeda, F., Deribe, Y. L., Skanland, S. S., Stieglitz, B., Grabbe, C., Franz-Wachtel, M., . . . Dikic, I. (2011). SHARPIN forms a linear ubiquitin ligase complex regulating NF-kappaB activity and apoptosis. *Nature*, 471(7340), 637-641. doi: 10.1038/nature09814
- Janssens, S., Tinel, A., Lippens, S., & Tschopp, J. (2005). PIDD mediates NF-kappaB activation in response to DNA damage. *Cell*, 123(6), 1079-1092. doi: 10.1016/j.cell.2005.09.036
- Kaczmarek, A., Vandenabeele, P., & Krysko, D. V. (2013). Necroptosis: the release of damage-associated molecular patterns and its physiological relevance. *Immunity*, 38(2), 209-223. doi: 10.1016/j.immuni.2013.02.003
- Kaiser, W. J., Daley-Bauer, L. P., Thapa, R. J., Mandal, P., Berger, S. B., Huang, C., . . . Mocarski, E. S. (2014). RIP1 suppresses innate immune necrotic as well as apoptotic cell death during mammalian parturition. *Proc Natl Acad Sci U S A*, 111(21), 7753-7758. doi: 10.1073/pnas.1401857111
- Kaiser, W. J., & Offermann, M. K. (2005). Apoptosis Induced by the Toll-Like Receptor Adaptor TRIF Is Dependent on Its Receptor Interacting Protein Homotypic Interaction Motif. *The Journal of Immunology*, 174(8), 4942-4952. doi: 10.4049/jimmunol.174.8.4942
- Kaiser, W. J., Sridharan, H., Huang, C., Mandal, P., Upton, J. W., Gough, P. J., . . . Mocarski, E. S. (2013). Toll-like receptor 3-mediated necrosis via TRIF, RIP3, and MLKL. *J Biol Chem*, 288(43), 31268-31279. doi: 10.1074/jbc.M113.462341
- Kaiser, W. J., Upton, J. W., Long, A. B., Livingston-Rosanoff, D., Daley-Bauer, L. P., Hakem, R., . . . Mocarski, E. S. (2011). RIP3 mediates the embryonic lethality of caspase-8-deficient mice. *Nature*, 471(7338), 368-372. doi: 10.1038/nature09857
- Kajino-Sakamoto, R., Inagaki, M., Lippert, E., Akira, S., Robine, S., Matsumoto, K., . . . Ninomiya-Tsuji, J. (2008). Enterocyte-Derived TAK1 Signaling Prevents Epithelium Apoptosis and the Development of Ileitis and Colitis. *The Journal of Immunology*, 181(2), 1143-1152. doi: 10.4049/jimmunol.181.2.1143
- Kaser, A., Zeissig, S., & Blumberg, R. S. (2010). Inflammatory bowel disease. *Annu Rev Immunol*, 28, 573-621. doi: 10.1146/annurev-immunol-030409-101225
- Kavuri, S. M., Geserick, P., Berg, D., Dimitrova, D. P., Feoktistova, M., Siegmund, D., . . . Leverkus, M. (2011). Cellular FLICE-inhibitory protein (cFLIP) isoforms block CD95- and TRAIL death receptor-

- induced gene induction irrespective of processing of caspase-8 or cFLIP in the death-inducing signaling complex. *J Biol Chem*, 286(19), 16631-16646. doi: 10.1074/jbc.M110.148585
- Kawai, T., & Akira, S. (2010). The role of pattern-recognition receptors in innate immunity: update on Toll-like receptors. *Nat Immunol*, 11(5), 373-384. doi: 10.1038/ni.1863
- Kawai, T., & Akira, S. (2011). Toll-like receptors and their crosstalk with other innate receptors in infection and immunity. *Immunity*, 34(5), 637-650. doi: 10.1016/j.immuni.2011.05.006
- Keenan, K. P., Sharpnack, D. D., Collins, H., Formal, S. B., & O'Brien, A. D. (1986). Morphologic evaluation of the effects of Shiga toxin and E coli Shiga-like toxin on the rabbit intestine. *Am J Pathol*, 125(1), 69-80.
- Kelliher, M. A., Grimm, S., Ishida, Y., Kuo, F., Stanger, B. Z., & Leder, P. (1998). The death domain kinase RIP mediates the TNF-induced NF-kappaB signal. *Immunity*, 8(3), 297-303.
- Kerr, J. F., Wyllie, A. H., & Currie, A. R. (1972). Apoptosis: a basic biological phenomenon with wide-ranging implications in tissue kinetics. *Br J Cancer*, 26(4), 239-257.
- Kim, J. W., Choi, E. J., & Joe, C. O. (2000). Activation of death-inducing signaling complex (DISC) by pro-apoptotic C-terminal fragment of RIP. *Oncogene*, 19(39), 4491-4499. doi: 10.1038/sj.onc.1203796
- Kim, J. Y., Morgan, M., Kim, D. G., Lee, J. Y., Bai, L., Lin, Y., . . . Kim, Y. S. (2011). TNFalpha induced noncanonical NF-kappaB activation is attenuated by RIP1 through stabilization of TRAF2. *J Cell Sci*, 124(Pt 4), 647-656. doi: 10.1242/jcs.075770
- Kim, Y. S., & Ho, S. B. (2010). Intestinal goblet cells and mucins in health and disease: recent insights and progress. *Curr Gastroenterol Rep*, 12(5), 319-330. doi: 10.1007/s11894-010-0131-2
- Klose, C. S., Kiss, E. A., Schwierzeck, V., Ebert, K., Hoyler, T., d'Hargues, Y., . . . Diefenbach, A. (2013). A T-bet gradient controls the fate and function of CCR6-RORgammat+ innate lymphoid cells. *Nature*, 494(7436), 261-265. doi: 10.1038/nature11813
- Komatsu, M., Kobayashi, D., Saito, K., Furuya, D., Yagihashi, A., Araake, H., . . . Watanabe, N. (2001). Tumor necrosis factor-alpha in serum of patients with inflammatory bowel disease as measured by a highly sensitive immuno-PCR. *Clin Chem*, 47(7), 1297-1301.
- Kono, H., & Rock, K. L. (2008). How dying cells alert the immune system to danger. *Nat Rev Immunol*, 8(4), 279-289. doi: 10.1038/nri2215
- Kontoyiannis, D., Pasparakis, M., Pizarro, T. T., Cominelli, F., & Kollias, G. (1999). Impaired on/off regulation of TNF biosynthesis in mice lacking TNF AU-rich elements: implications for joint and gut-associated immunopathologies. *Immunity*, 10(3), 387-398.
- Kreuz, S., Siegmund, D., Rumpf, J. J., Samel, D., Leverkus, M., Janssen, O., . . . Wajant, H. (2004). NFkappaB activation by Fas is mediated through FADD, caspase-8, and RIP and is inhibited by FLIP. *J Cell Biol*, 166(3), 369-380. doi: 10.1083/jcb.200401036
- Krysko, D. V., Vanden Berghe, T., D'Herde, K., & Vandenabeele, P. (2008). Apoptosis and necrosis: detection, discrimination and phagocytosis. *Methods*, 44(3), 205-221. doi: 10.1016/j.ymeth.2007.12.001

- Kumari, S., Redouane, Y., Lopez-Mosqueda, J., Shiraishi, R., Romanowska, M., Lutzmayer, S., . . . Ikeda, F. (2014). Sharpin prevents skin inflammation by inhibiting TNFR1-induced keratinocyte apoptosis. *Elife*, 3. doi: 10.7554/eLife.03422
- Lamkanfi, M., & Dixit, V. M. (2010). Manipulation of host cell death pathways during microbial infections. *Cell Host Microbe*, 8(1), 44-54. doi: 10.1016/j.chom.2010.06.007
- Lamothe, B., Lai, Y., Xie, M., Schneider, M. D., & Darnay, B. G. (2013). TAK1 is essential for osteoclast differentiation and is an important modulator of cell death by apoptosis and necroptosis. *Mol Cell Biol*, 33(3), 582-595. doi: 10.1128/MCB.01225-12
- Laster. (1988). <J Immunol-1988-Laster-2629-34.pdf>.
- Lau, K. S., Juchheim, A. M., Cavaliere, K. R., Philips, S. R., Lauffenburger, D. A., & Haigis, K. M. (2011). In vivo systems analysis identifies spatial and temporal aspects of the modulation of TNF-alpha-induced apoptosis and proliferation by MAPKs. *Sci Signal*, 4(165), ra16. doi: 10.1126/scisignal.2001338
- Lavrik, I. N., & Krammer, P. H. (2012). Regulation of CD95/Fas signaling at the DISC. *Cell Death Differ*, 19(1), 36-41. doi: 10.1038/cdd.2011.155
- Leaphart, C. L., Cavallo, J., Gribar, S. C., Cetin, S., Li, J., Branca, M. F., . . . Hackam, D. J. (2007). A critical role for TLR4 in the pathogenesis of necrotizing enterocolitis by modulating intestinal injury and repair. *J Immunol*, 179(7), 4808-4820.
- Lee, T. H., Shank, J., Cusson, N., & Kelliher, M. A. (2004). The kinase activity of Rip1 is not required for tumor necrosis factor-alpha-induced IkkappaB kinase or p38 MAP kinase activation or for the ubiquitination of Rip1 by Traf2. *J Biol Chem*, 279(32), 33185-33191. doi: 10.1074/jbc.M404206200
- Li, H., Kobayashi, M., Blonska, M., You, Y., & Lin, X. (2006). Ubiquitination of RIP is required for tumor necrosis factor alpha-induced NF-kappaB activation. *J Biol Chem*, 281(19), 13636-13643. doi: 10.1074/jbc.M600620200
- Li, J., McQuade, T., Siemer, A. B., Napetschnig, J., Moriwaki, K., Hsiao, Y. S., . . . Wu, H. (2012). The RIP1/RIP3 necrosome forms a functional amyloid signaling complex required for programmed necrosis. *Cell*, 150(2), 339-350. doi: 10.1016/j.cell.2012.06.019
- Li, L., Thomas, R. M., Suzuki, H., De Brabander, J. K., Wang, X., & Harran, P. G. (2004). A small molecule Smac mimic potentiates TRAIL- and TNFalpha-mediated cell death. *Science*, 305(5689), 1471-1474. doi: 10.1126/science.1098231
- Li, S., Zhang, L., Yao, Q., Li, L., Dong, N., Rong, J., . . . Shao, F. (2013). Pathogen blocks host death receptor signalling by arginine GlcNAcylation of death domains. *Nature*, 501(7466), 242-246. doi: 10.1038/nature12436
- Lin, Y., Devin, A., Rodriguez, Y., & Liu, Z. G. (1999). Cleavage of the death domain kinase RIP by caspase-8 prompts TNF-induced apoptosis. *Genes Dev*, 13(19), 2514-2526.
- Lin, Y., Yang, Q., Wang, X., & Liu, Z. G. (2006). The essential role of the death domain kinase receptor-interacting protein in insulin growth

- factor-I-induced c-Jun N-terminal kinase activation. *J Biol Chem*, 281(33), 23525-23532. doi: 10.1074/jbc.M601487200
- Luthi, A. U., Cullen, S. P., McNeela, E. A., Duriez, P. J., Afonina, I. S., Sheridan, C., . . . Martin, S. J. (2009). Suppression of interleukin-33 bioactivity through proteolysis by apoptotic caspases. *Immunity*, 31(1), 84-98. doi: 10.1016/j.immuni.2009.05.007
- Ma, Y., Temkin, V., Liu, H., & Pope, R. M. (2005). NF-kappaB protects macrophages from lipopolysaccharide-induced cell death: the role of caspase 8 and receptor-interacting protein. *J Biol Chem*, 280(51), 41827-41834. doi: 10.1074/jbc.M510849200
- MacDonald, T. T., Hutchings, P., Choy, M. Y., Murch, S., & Cooke, A. (1990). Tumour necrosis factor-alpha and interferon-gamma production measured at the single cell level in normal and inflamed human intestine. *Clin Exp Immunol*, 81(2), 301-305.
- Mack, C., Sickmann, A., Lembo, D., & Brune, W. (2008). Inhibition of proinflammatory and innate immune signaling pathways by a cytomegalovirus RIP1-interacting protein. *Proc Natl Acad Sci U S A*, 105(8), 3094-3099. doi: 10.1073/pnas.0800168105
- Madison, B. B., Dunbar, L., Qiao, X. T., Braunstein, K., Braunstein, E., & Gumucio, D. L. (2002). Cis elements of the villin gene control expression in restricted domains of the vertical (crypt) and horizontal (duodenum, cecum) axes of the intestine. *J Biol Chem*, 277(36), 33275-33283. doi: 10.1074/jbc.M204935200
- Madrigal, A. G., Barth, K., Papadopoulos, G., & Genco, C. A. (2012). Pathogen-mediated proteolysis of the cell death regulator RIPK1 and the host defense modulator RIPK2 in human aortic endothelial cells. *PLoS Pathog*, 8(6), e1002723. doi: 10.1371/journal.ppat.1002723
- Mahoney, D. J., Cheung, H. H., Mrad, R. L., Plenchette, S., Simard, C., Enwere, E., . . . Korneluk, R. G. (2008). Both cIAP1 and cIAP2 regulate TNFalpha-mediated NF-kappaB activation. *Proc Natl Acad Sci U S A*, 105(33), 11778-11783. doi: 10.1073/pnas.0711122105
- Maloy, K. J., & Powrie, F. (2011). Intestinal homeostasis and its breakdown in inflammatory bowel disease. *Nature*, 474(7351), 298-306. doi: 10.1038/nature10208
- Marchiando, A. M., Shen, L., Graham, W. V., Edelblum, K. L., Duckworth, C. A., Guan, Y., . . . Watson, A. J. (2011). The epithelial barrier is maintained by in vivo tight junction expansion during pathologic intestinal epithelial shedding. *Gastroenterology*, 140(4), 1208-1218 e1201-1202. doi: 10.1053/j.gastro.2011.01.004
- Marchiando, A. M., Shen, L., Graham, W. V., Weber, C. R., Schwarz, B. T., Austin, J. R., 2nd, . . . Turner, J. R. (2010). Caveolin-1-dependent occludin endocytosis is required for TNF-induced tight junction regulation in vivo. *J Cell Biol*, 189(1), 111-126. doi: 10.1083/jcb.200902153
- Martinon, F., Holler, N., Richard, C., & Tschopp, J. (2000). Activation of a pro-apoptotic amplification loop through inhibition of NF-kappaB-dependent survival signals by caspase-mediated inactivation of RIP. *FEBS Lett*, 468(2-3), 134-136.
- Mc Guire, C., Volckaert, T., Wolke, U., Sze, M., de Rycke, R., Waisman, A., . . . van Loo, G. (2010). Oligodendrocyte-specific FADD deletion protects

- mice from autoimmune-mediated demyelination. *J Immunol*, 185(12), 7646-7653. doi: 10.4049/jimmunol.1000930
- McAllister, C. S., Lakhdari, O., Pineton de Chambrun, G., Gareau, M. G., Broquet, A., Lee, G. H., . . . Kagnoff, M. F. (2013). TLR3, TRIF, and caspase 8 determine double-stranded RNA-induced epithelial cell death and survival in vivo. *J Immunol*, 190(1), 418-427. doi: 10.4049/jimmunol.1202756
- McComb, S., Cessford, E., Alturki, N. A., Joseph, J., Shutinoski, B., Startek, J. B., . . . Sad, S. (2014). Type-I interferon signaling through ISGF3 complex is required for sustained Rip3 activation and necroptosis in macrophages. *Proc Natl Acad Sci U S A*, 111(31), E3206-3213. doi: 10.1073/pnas.1407068111
- McQuade, T., Cho, Y., & Chan, F. K. (2013). Positive and negative phosphorylation regulates RIP1- and RIP3-induced programmed necrosis. *Biochem J*, 456(3), 409-415. doi: 10.1042/BJ20130860
- Medema, J. P., Scaffidi, C., Kischkel, F. C., Shevchenko, A., Mann, M., Krammer, P. H., & Peter, M. E. (1997). FLICE is activated by association with the CD95 death-inducing signaling complex (DISC). *EMBO J*, 16(10), 2794-2804. doi: 10.1093/emboj/16.10.2794
- Medema, J. P., Toes, R. E., Scaffidi, C., Zheng, T. S., Flavell, R. A., Melief, C. J., . . . Krammer, P. H. (1997). Cleavage of FLICE (caspase-8) by granzyme B during cytotoxic T lymphocyte-induced apoptosis. *Eur J Immunol*, 27(12), 3492-3498. doi: 10.1002/eji.1830271250
- Meylan, E., Burns, K., Hofmann, K., Blancheteau, V., Martinon, F., Kelliher, M., & Tschopp, J. (2004). RIP1 is an essential mediator of Toll-like receptor 3-induced NF-kappa B activation. *Nat Immunol*, 5(5), 503-507. doi: 10.1038/ni1061
- Micheau, O., & Tschopp, J. (2003). Induction of TNF Receptor I-Mediated Apoptosis via Two Sequential Signaling Complexes. *Cell*, 114(2), 181-190. doi: 10.1016/s0092-8674(03)00521-x
- Mollah, S., Wertz, I. E., Phung, Q., Arnott, D., Dixit, V. M., & Lill, J. R. (2007). Targeted mass spectrometric strategy for global mapping of ubiquitination on proteins. *Rapid Commun Mass Spectrom*, 21(20), 3357-3364. doi: 10.1002/rcm.3227
- Moquin, D. M., McQuade, T., & Chan, F. K. (2013). CYLD deubiquitinates RIP1 in the TNFalpha-induced necrosome to facilitate kinase activation and programmed necrosis. *PLoS One*, 8(10), e76841. doi: 10.1371/journal.pone.0076841
- Moulin, M., Anderton, H., Voss, A. K., Thomas, T., Wong, W. W., Bankovacki, A., . . . Vaux, D. L. (2012). IAPs limit activation of RIP kinases by TNF receptor 1 during development. *EMBO J*, 31(7), 1679-1691. doi: 10.1038/emboj.2012.18
- Mowat, A. M., & Agace, W. W. (2014). Regional specialization within the intestinal immune system. *Nat Rev Immunol*, 14(10), 667-685. doi: 10.1038/nri3738
- Mukherjee, S., Vaishnava, S., & Hooper, L. V. (2008). Multi-layered regulation of intestinal antimicrobial defense. *Cell Mol Life Sci*, 65(19), 3019-3027. doi: 10.1007/s00018-008-8182-3
- Murphy, J. M., Czabotar, P. E., Hildebrand, J. M., Lucet, I. S., Zhang, J. G., Alvarez-Diaz, S., . . . Alexander, W. S. (2013). The pseudokinase

- MLKL mediates necroptosis via a molecular switch mechanism. *Immunity*, 39(3), 443-453. doi: 10.1016/j.immuni.2013.06.018
- Muzio, M., Chinnaiyan, A. M., Kischkel, F. C., O'Rourke, K., Shevchenko, A., Ni, J., . . . Dixit, V. M. (1996). FLICE, a novel FADD-homologous ICE/CED-3-like protease, is recruited to the CD95 (Fas/APO-1) death-inducing signaling complex. *Cell*, 85(6), 817-827.
- Muzio, M., Stockwell, B. R., Stennicke, H. R., Salvesen, G. S., & Dixit, V. M. (1998). An induced proximity model for caspase-8 activation. *J Biol Chem*, 273(5), 2926-2930.
- Nagata, S., Hanayama, R., & Kawane, K. (2010). Autoimmunity and the clearance of dead cells. *Cell*, 140(5), 619-630. doi: 10.1016/j.cell.2010.02.014
- Nazli, A., Chan, O., Dobson-Belaire, W. N., Ouellet, M., Tremblay, M. J., Gray-Owen, S. D., . . . Kaushic, C. (2010). Exposure to HIV-1 directly impairs mucosal epithelial barrier integrity allowing microbial translocation. *PLoS Pathog*, 6(4), e1000852. doi: 10.1371/journal.ppat.1000852
- Nenci, A., Becker, C., Wullaert, A., Gareus, R., van Loo, G., Danese, S., . . . Pasparakis, M. (2007). Epithelial NEMO links innate immunity to chronic intestinal inflammation. *Nature*, 446(7135), 557-561. doi: 10.1038/nature05698
- Neumann, L., Pforr, C., Beaudouin, J., Pappa, A., Fricker, N., Krammer, P. H., . . . Eils, R. (2010). Dynamics within the CD95 death-inducing signaling complex decide life and death of cells. *Mol Syst Biol*, 6, 352. doi: 10.1038/msb.2010.6
- Newton, K., Dugger, D. L., Wickliffe, K. E., Kapoor, N., de Almagro, M. C., Vucic, D., . . . Dixit, V. M. (2014). Activity of protein kinase RIPK3 determines whether cells die by necroptosis or apoptosis. *Science*, 343(6177), 1357-1360. doi: 10.1126/science.1249361
- Newton, K., Sun, X., & Dixit, V. M. (2004). Kinase RIP3 Is Dispensable for Normal NF- κ Bs, Signaling by the B-Cell and T-Cell Receptors, Tumor Necrosis Factor Receptor 1, and Toll-Like Receptors 2 and 4. *Molecular and Cellular Biology*, 24(4), 1464-1469. doi: 10.1128/mcb.24.4.1464-1469.2004
- O'Donnell, M. A., Legarda-Addison, D., Skountzos, P., Yeh, W. C., & Ting, A. T. (2007). Ubiquitination of RIP1 regulates an NF-kappaB-independent cell-death switch in TNF signaling. *Curr Biol*, 17(5), 418-424. doi: 10.1016/j.cub.2007.01.027
- O'Donnell, M. A., Perez-Jimenez, E., Oberst, A., Ng, A., Massoumi, R., Xavier, R., . . . Ting, A. T. (2011). Caspase 8 inhibits programmed necrosis by processing CYLD. *Nat Cell Biol*, 13(12), 1437-1442. doi: 10.1038/ncb2362
- Obeid, M., Tesniere, A., Ghiringhelli, F., Fimia, G. M., Apetoh, L., Perfettini, J. L., . . . Kroemer, G. (2007). Calreticulin exposure dictates the immunogenicity of cancer cell death. *Nat Med*, 13(1), 54-61. doi: 10.1038/nm1523
- Oberst, A., Dillon, C. P., Weinlich, R., McCormick, L. L., Fitzgerald, P., Pop, C., . . . Green, D. R. (2011). Catalytic activity of the caspase-8-FLIP(L) complex inhibits RIPK3-dependent necrosis. *Nature*, 471(7338), 363-367. doi: 10.1038/nature09852

- Ofengeim, D., & Yuan, J. (2013). Regulation of RIP1 kinase signalling at the crossroads of inflammation and cell death. *Nat Rev Mol Cell Biol*, *14*(11), 727-736. doi: 10.1038/nrm3683
- Orozco, S., Yatim, N., Werner, M. R., Tran, H., Gunja, S. Y., Tait, S. W., . . . Oberst, A. (2014). RIPK1 both positively and negatively regulates RIPK3 oligomerization and necroptosis. *Cell Death Differ*, *21*(10), 1511-1521. doi: 10.1038/cdd.2014.76
- Oshiumi, H., Matsumoto, M., Funami, K., Akazawa, T., & Seya, T. (2003). TICAM-1, an adaptor molecule that participates in Toll-like receptor 3-mediated interferon-beta induction. *Nat Immunol*, *4*(2), 161-167. doi: 10.1038/ni886
- Palmer, G., & Gabay, C. (2011). Interleukin-33 biology with potential insights into human diseases. *Nat Rev Rheumatol*, *7*(6), 321-329. doi: 10.1038/nrrheum.2011.53
- Park, H. H., Logette, E., Raunser, S., Cuenin, S., Walz, T., Tschopp, J., & Wu, H. (2007). Death domain assembly mechanism revealed by crystal structure of the oligomeric PIDDosome core complex. *Cell*, *128*(3), 533-546. doi: 10.1016/j.cell.2007.01.019
- Pasparakis, M., & Vandenabeele, P. (2015). Necroptosis and its role in inflammation. *Nature*, *517*(7534), 311-320. doi: 10.1038/nature14191
- Pearson, J. S., Giogha, C., Ong, S. Y., Kennedy, C. L., Kelly, M., Robinson, K. S., . . . Hartland, E. L. (2013). A type III effector antagonizes death receptor signalling during bacterial gut infection. *Nature*, *501*(7466), 247-251. doi: 10.1038/nature12524
- Petersen, S. L., Peyton, M., Minna, J. D., & Wang, X. (2010). Overcoming cancer cell resistance to Smac mimetic induced apoptosis by modulating cIAP-2 expression. *Proc Natl Acad Sci U S A*, *107*(26), 11936-11941. doi: 10.1073/pnas.1005667107
- Petersen, S. L., Wang, L., Yalcin-Chin, A., Li, L., Peyton, M., Minna, J., . . . Wang, X. (2007). Autocrine TNFalpha signaling renders human cancer cells susceptible to Smac-mimetic-induced apoptosis. *Cancer Cell*, *12*(5), 445-456. doi: 10.1016/j.ccr.2007.08.029
- Peterson, L. W., & Artis, D. (2014). Intestinal epithelial cells: regulators of barrier function and immune homeostasis. *Nat Rev Immunol*, *14*(3), 141-153. doi: 10.1038/nri3608
- Pfeffer, K., Matsuyama, T., Kundig, T. M., Wakeham, A., Kishihara, K., Shahinian, A., . . . Mak, T. W. (1993). Mice deficient for the 55 kd tumor necrosis factor receptor are resistant to endotoxic shock, yet succumb to *L. monocytogenes* infection. *Cell*, *73*(3), 457-467.
- Philip, N. H., Dillon, C. P., Snyder, A. G., Fitzgerald, P., Wynosky-Dolfi, M. A., Zwack, E. E., . . . Brodsky, I. E. (2014). Caspase-8 mediates caspase-1 processing and innate immune defense in response to bacterial blockade of NF-kappaB and MAPK signaling. *Proc Natl Acad Sci U S A*, *111*(20), 7385-7390. doi: 10.1073/pnas.1403252111
- Piao, J. H., Hasegawa, M., Heissig, B., Hattori, K., Takeda, K., Iwakura, Y., . . . Nakano, H. (2011). Tumor necrosis factor receptor-associated factor (TRAF) 2 controls homeostasis of the colon to prevent spontaneous development of murine inflammatory bowel disease. *J Biol Chem*, *286*(20), 17879-17888. doi: 10.1074/jbc.M111.221853

- Piguet, P. F., Vesin, C., Guo, J., Donati, Y., & Barazzone, C. (1998). TNF-induced enterocyte apoptosis in mice is mediated by the TNF receptor 1 and does not require p53. *Eur J Immunol*, *28*(11), 3499-3505. doi: 10.1002/(SICI)1521-4141(199811)28:11<3499::AID-IMMU3499>3.0.CO;2-Q
- Pobezinskaya, Y. L., Kim, Y. S., Choksi, S., Morgan, M. J., Li, T., Liu, C., & Liu, Z. (2008). The function of TRADD in signaling through tumor necrosis factor receptor 1 and TRIF-dependent Toll-like receptors. *Nat Immunol*, *9*(9), 1047-1054. doi: 10.1038/ni.1639
- Poltorak, A., He, X., Smirnova, I., Liu, M. Y., Van Huffel, C., Du, X., . . . Beutler, B. (1998). Defective LPS signaling in C3H/HeJ and C57BL/10ScCr mice: mutations in Tlr4 gene. *Science*, *282*(5396), 2085-2088.
- Polykratis, A., Hermance, N., Zelic, M., Roderick, J., Kim, C., Van, T. M., . . . Kelliher, M. A. (2014). Cutting edge: RIPK1 Kinase inactive mice are viable and protected from TNF-induced necroptosis in vivo. *J Immunol*, *193*(4), 1539-1543. doi: 10.4049/jimmunol.1400590
- Poon, I. K., Lucas, C. D., Rossi, A. G., & Ravichandran, K. S. (2014). Apoptotic cell clearance: basic biology and therapeutic potential. *Nat Rev Immunol*, *14*(3), 166-180. doi: 10.1038/nri3607
- Pop, C., Oberst, A., Drag, M., Van Raam, B. J., Riedl, S. J., Green, D. R., & Salvesen, G. S. (2011). FLIP(L) induces caspase 8 activity in the absence of interdomain caspase 8 cleavage and alters substrate specificity. *Biochem J*, *433*(3), 447-457. doi: 10.1042/BJ20101738
- Pott, J., & Hornef, M. (2012). Innate immune signalling at the intestinal epithelium in homeostasis and disease. *EMBO Rep*, *13*(8), 684-698. doi: 10.1038/embor.2012.96
- Qureshi, S. T., Lariviere, L., Leveque, G., Clermont, S., Moore, K. J., Gros, P., & Malo, D. (1999). Endotoxin-tolerant mice have mutations in Toll-like receptor 4 (Tlr4). *J Exp Med*, *189*(4), 615-625.
- Rajput, A., Kovalenko, A., Bogdanov, K., Yang, S. H., Kang, T. B., Kim, J. C., . . . Wallach, D. (2011). RIG-I RNA helicase activation of IRF3 transcription factor is negatively regulated by caspase-8-mediated cleavage of the RIP1 protein. *Immunity*, *34*(3), 340-351. doi: 10.1016/j.immuni.2010.12.018
- Rakoff-Nahoum, S., Hao, L., & Medzhitov, R. (2006). Role of toll-like receptors in spontaneous commensal-dependent colitis. *Immunity*, *25*(2), 319-329. doi: 10.1016/j.immuni.2006.06.010
- Rakoff-Nahoum, S., Paglino, J., Eslami-Varzaneh, F., Edberg, S., & Medzhitov, R. (2004). Recognition of commensal microflora by toll-like receptors is required for intestinal homeostasis. *Cell*, *118*(2), 229-241. doi: 10.1016/j.cell.2004.07.002
- Ramnarain, D. B., Paulmurugan, R., Park, S., Mickey, B. E., Asaithamby, A., Saha, D., . . . Habib, A. A. (2008). RIP1 links inflammatory and growth factor signaling pathways by regulating expression of the EGFR. *Cell Death Differ*, *15*(2), 344-353. doi: 10.1038/sj.cdd.4402268
- Rebsamen, M., Heinz, L. X., Meylan, E., Michallet, M. C., Schroder, K., Hofmann, K., . . . Tschopp, J. (2009). DAI/ZBP1 recruits RIP1 and RIP3 through RIP homotypic interaction motifs to activate NF-kappaB. *EMBO Rep*, *10*(8), 916-922. doi: 10.1038/embor.2009.109

- Rebsamen, M., Meylan, E., Curran, J., & Tschopp, J. (2008). The antiviral adaptor proteins Cardif and Trif are processed and inactivated by caspases. *Cell Death Differ*, *15*(11), 1804-1811. doi: 10.1038/cdd.2008.119
- Reimund, J. M., Wittersheim, C., Dumont, S., Muller, C. D., Baumann, R., Poindron, P., & Duclos, B. (1996). Mucosal inflammatory cytokine production by intestinal biopsies in patients with ulcerative colitis and Crohn's disease. *J Clin Immunol*, *16*(3), 144-150.
- Rickard, J. A., O'Donnell, J. A., Evans, J. M., Lalaoui, N., Poh, A. R., Rogers, T., . . . Silke, J. (2014). RIPK1 regulates RIPK3-MLKL-driven systemic inflammation and emergency hematopoiesis. *Cell*, *157*(5), 1175-1188. doi: 10.1016/j.cell.2014.04.019
- Rioux, J. D., Silverberg, M. S., Daly, M. J., Steinhart, A. H., McLeod, R. S., Griffiths, A. M., . . . Siminovitch, K. A. (2000). Genomewide search in Canadian families with inflammatory bowel disease reveals two novel susceptibility loci. *Am J Hum Genet*, *66*(6), 1863-1870. doi: 10.1086/302913
- Robinson, N., McComb, S., Mulligan, R., Dudani, R., Krishnan, L., & Sad, S. (2012). Type I interferon induces necroptosis in macrophages during infection with *Salmonella enterica* serovar Typhimurium. *Nat Immunol*, *13*(10), 954-962. doi: 10.1038/ni.2397
- Roda, G., Sartini, A., Zambon, E., Calafiore, A., Marocchi, M., Caponi, A., . . . Roda, E. (2010). Intestinal epithelial cells in inflammatory bowel diseases. *World J Gastroenterol*, *16*(34), 4264-4271.
- Roderick, J. E., Hermance, N., Zelic, M., Simmons, M. J., Polykratis, A., Pasparakis, M., & Kelliher, M. A. (2014). Hematopoietic RIPK1 deficiency results in bone marrow failure caused by apoptosis and RIPK3-mediated necroptosis. *Proc Natl Acad Sci U S A*, *111*(40), 14436-14441. doi: 10.1073/pnas.1409389111
- Rothe, M., Pan, M. G., Henzel, W. J., Ayres, T. M., & Goeddel, D. V. (1995). The TNFR2-TRAF signaling complex contains two novel proteins related to baculoviral inhibitor of apoptosis proteins. *Cell*, *83*(7), 1243-1252.
- Roulis, M., Armaka, M., Manoloukos, M., Apostolaki, M., & Kollias, G. (2011). Intestinal epithelial cells as producers but not targets of chronic TNF suffice to cause murine Crohn-like pathology. *Proc Natl Acad Sci U S A*, *108*(13), 5396-5401. doi: 10.1073/pnas.1007811108
- Ruckdeschel, K., Pfaffinger, G., Haase, R., Sing, A., Weighardt, H., Hacker, G., . . . Heesemann, J. (2004). Signaling of apoptosis through TLRs critically involves toll/IL-1 receptor domain-containing adapter inducing IFN-beta, but not MyD88, in bacteria-infected murine macrophages. *J Immunol*, *173*(5), 3320-3328.
- Sakamaki, K., Inoue, T., Asano, M., Sudo, K., Kazama, H., Sakagami, J., . . . Yonehara, S. (2002). Ex vivo whole-embryo culture of caspase-8-deficient embryos normalize their aberrant phenotypes in the developing neural tube and heart. *Cell Death Differ*, *9*(11), 1196-1206. doi: 10.1038/sj.cdd.4401090
- Salzman, N. H., Ghosh, D., Huttner, K. M., Paterson, Y., & Bevens, C. L. (2003). Protection against enteric salmonellosis in transgenic mice

- expressing a human intestinal defensin. *Nature*, 422(6931), 522-526. doi: 10.1038/nature01520
- Sanchez-Munoz, F., Dominguez-Lopez, A., & Yamamoto-Furusho, J. K. (2008). Role of cytokines in inflammatory bowel disease. *World J Gastroenterol*, 14(27), 4280-4288.
- Sandborn, W. J., Feagan, B. G., Stoinov, S., Honiball, P. J., Rutgeerts, P., Mason, D., . . . Investigators, P. S. (2007). Certolizumab pegol for the treatment of Crohn's disease. *N Engl J Med*, 357(3), 228-238. doi: 10.1056/NEJMoa067594
- Sandborn, W. J., Hanauer, S. B., Katz, S., Safdi, M., Wolf, D. G., Baerg, R. D., . . . Zinsmeister, A. R. (2001). Etanercept for active Crohn's disease: a randomized, double-blind, placebo-controlled trial. *Gastroenterology*, 121(5), 1088-1094.
- Sasaki, Y., Derudder, E., Hobeika, E., Pelanda, R., Reth, M., Rajewsky, K., & Schmidt-Suppran, M. (2006). Canonical NF-kappaB activity, dispensable for B cell development, replaces BAFF-receptor signals and promotes B cell proliferation upon activation. *Immunity*, 24(6), 729-739. doi: 10.1016/j.immuni.2006.04.005
- Sato, A., Iizuka, M., Nakagomi, O., Suzuki, M., Horie, Y., Konno, S., . . . Watanabe, S. (2006). Rotavirus double-stranded RNA induces apoptosis and diminishes wound repair in rat intestinal epithelial cells. *J Gastroenterol Hepatol*, 21(3), 521-530. doi: 10.1111/j.1440-1746.2005.03977.x
- Sato, T., Vries, R. G., Snippert, H. J., van de Wetering, M., Barker, N., Stange, D. E., . . . Clevers, H. (2009). Single Lgr5 stem cells build crypt-villus structures in vitro without a mesenchymal niche. *Nature*, 459(7244), 262-265. doi: 10.1038/nature07935
- Scaffidi, C., Kirchhoff, S., Krammer, P. H., & Peter, M. E. (1999). Apoptosis signaling in lymphocytes. *Curr Opin Immunol*, 11(3), 277-285.
- Seymour, R. E., Hasham, M. G., Cox, G. A., Shultz, L. D., Hogenesch, H., Roopenian, D. C., & Sundberg, J. P. (2007). Spontaneous mutations in the mouse Sharpin gene result in multiorgan inflammation, immune system dysregulation and dermatitis. *Genes Immun*, 8(5), 416-421. doi: 10.1038/sj.gene.6364403
- Shibahara, T., Sato, N., Waguri, S., Iwanaga, T., Nakahara, A., Fukutomi, H., & Uchiyama, Y. (1995). The fate of effete epithelial cells at the villus tips of the human small intestine. *Arch Histol Cytol*, 58(2), 205-219.
- Shu, H. B., Takeuchi, M., & Goeddel, D. V. (1996). The tumor necrosis factor receptor 2 signal transducers TRAF2 and c-IAP1 are components of the tumor necrosis factor receptor 1 signaling complex. *Proc Natl Acad Sci U S A*, 93(24), 13973-13978.
- Silke, J., & Hartland, E. L. (2013). Masters, marionettes and modulators: intersection of pathogen virulence factors and mammalian death receptor signaling. *Curr Opin Immunol*, 25(4), 436-440. doi: 10.1016/j.coi.2013.05.011
- Sodhi, C. P., Shi, X. H., Richardson, W. M., Grant, Z. S., Shapiro, R. A., Prindle, T., Jr., . . . Hackam, D. J. (2010). Toll-like receptor-4 inhibits enterocyte proliferation via impaired beta-catenin signaling in necrotizing enterocolitis. *Gastroenterology*, 138(1), 185-196. doi: 10.1053/j.gastro.2009.09.045

- Sprick, M. R., Rieser, E., Stahl, H., Grosse-Wilde, A., Weigand, M. A., & Walczak, H. (2002). Caspase-10 is recruited to and activated at the native TRAIL and CD95 death-inducing signalling complexes in a FADD-dependent manner but can not functionally substitute caspase-8. *EMBO J*, *21*(17), 4520-4530.
- Stanger, B. Z., Leder, P., Lee, T. H., Kim, E., & Seed, B. (1995). RIP: a novel protein containing a death domain that interacts with Fas/APO-1 (CD95) in yeast and causes cell death. *Cell*, *81*(4), 513-523.
- Stark, G. R., Kerr, I. M., Williams, B. R., Silverman, R. H., & Schreiber, R. D. (1998). How cells respond to interferons. *Annu Rev Biochem*, *67*, 227-264. doi: 10.1146/annurev.biochem.67.1.227
- Steinbrecher, K. A., Harmel-Laws, E., Sitcheran, R., & Baldwin, A. S. (2008). Loss of epithelial RelA results in deregulated intestinal proliferative/apoptotic homeostasis and susceptibility to inflammation. *J Immunol*, *180*(4), 2588-2599.
- Strater, J., & Moller, P. (2000). Expression and function of death receptors and their natural ligands in the intestine. *Ann N Y Acad Sci*, *915*, 162-170.
- Su, L., Quade, B., Wang, H., Sun, L., Wang, X., & Rizo, J. (2014). A plug release mechanism for membrane permeation by MLKL. *Structure*, *22*(10), 1489-1500. doi: 10.1016/j.str.2014.07.014
- Sun, L., Wang, H., Wang, Z., He, S., Chen, S., Liao, D., . . . Wang, X. (2012). Mixed lineage kinase domain-like protein mediates necrosis signaling downstream of RIP3 kinase. *Cell*, *148*(1-2), 213-227. doi: 10.1016/j.cell.2011.11.031
- Sun, X., Yin, J., Starovasnik, M. A., Fairbrother, W. J., & Dixit, V. M. (2002). Identification of a novel homotypic interaction motif required for the phosphorylation of receptor-interacting protein (RIP) by RIP3. *J Biol Chem*, *277*(11), 9505-9511. doi: 10.1074/jbc.M109488200
- Tada, K., Okazaki, T., Sakon, S., Kobayashi, T., Kurosawa, K., Yamaoka, S., . . . Nakano, H. (2001). Critical roles of TRAF2 and TRAF5 in tumor necrosis factor-induced NF-kappa B activation and protection from cell death. *J Biol Chem*, *276*(39), 36530-36534. doi: 10.1074/jbc.M104837200
- Takahashi, N., Vereecke, L., Bertrand, M. J., Duprez, L., Berger, S. B., Divert, T., . . . Vandenabeele, P. (2014). RIPK1 ensures intestinal homeostasis by protecting the epithelium against apoptosis. *Nature*, *513*(7516), 95-99. doi: 10.1038/nature13706
- Takeuchi, O., & Akira, S. (2010). Pattern recognition receptors and inflammation. *Cell*, *140*(6), 805-820. doi: 10.1016/j.cell.2010.01.022
- Tanaka, H., Takechi, M., Kiyonari, H., Shioi, G., Tamura, A., & Tsukita, S. (2015). Intestinal deletion of Claudin-7 enhances paracellular organic solute flux and initiates colonic inflammation in mice. *Gut*. doi: 10.1136/gutjnl-2014-308419
- Taylor, C. T., Dzus, A. L., & Colgan, S. P. (1998). Autocrine regulation of epithelial permeability by hypoxia: role for polarized release of tumor necrosis factor alpha. *Gastroenterology*, *114*(4), 657-668.
- Tejedor Cerdana, M. A., Velasco Guardado, A., Fernandez Prodomingo, A., Concepcion Pinero Perez, M. C., Calderon, R., Prieto Bermejo, A. B., .

- . . . Rodriguez Perez, A. (2011). Cytomegalovirus ileitis in an immunocompetent patient. *Rev Esp Enferm Dig*, 103(3), 154-156.
- Tenev, T., Bianchi, K., Darding, M., Broemer, M., Langlais, C., Wallberg, F., . . . Meier, P. (2011). The Ripoptosome, a signaling platform that assembles in response to genotoxic stress and loss of IAPs. *Mol Cell*, 43(3), 432-448. doi: 10.1016/j.molcel.2011.06.006
- Thapa, R. J., Basagoudanavar, S. H., Nogusa, S., Irrinki, K., Mallilankaraman, K., Slifker, M. J., . . . Balachandran, S. (2011). NF-kappaB protects cells from gamma interferon-induced RIP1-dependent necroptosis. *Mol Cell Biol*, 31(14), 2934-2946. doi: 10.1128/MCB.05445-11
- Thapa, R. J., Nogusa, S., Chen, P., Maki, J. L., Lerro, A., Andrade, M., . . . Balachandran, S. (2013). Interferon-induced RIP1/RIP3-mediated necrosis requires PKR and is licensed by FADD and caspases. *Proc Natl Acad Sci U S A*, 110(33), E3109-3118. doi: 10.1073/pnas.1301218110
- Tinel, A., Janssens, S., Lippens, S., Cuenin, S., Logette, E., Jaccard, B., . . . Tschopp, J. (2007). Autoproteolysis of PIDD marks the bifurcation between pro-death caspase-2 and pro-survival NF-kappaB pathway. *EMBO J*, 26(1), 197-208. doi: 10.1038/sj.emboj.7601473
- Ting, A. T., Pimentel-Muinos, F. X., & Seed, B. (1996). RIP mediates tumor necrosis factor receptor 1 activation of NF-kappaB but not Fas/APO-1-initiated apoptosis. *EMBO J*, 15(22), 6189-6196.
- Tokunaga, F., Nakagawa, T., Nakahara, M., Saeki, Y., Taniguchi, M., Sakata, S., . . . Iwai, K. (2011). SHARPIN is a component of the NF-kappaB-activating linear ubiquitin chain assembly complex. *Nature*, 471(7340), 633-636. doi: 10.1038/nature09815
- Tokunaga, F., Sakata, S., Saeki, Y., Satomi, Y., Kirisako, T., Kamei, K., . . . Iwai, K. (2009). Involvement of linear polyubiquitylation of NEMO in NF-kappaB activation. *Nat Cell Biol*, 11(2), 123-132. doi: 10.1038/ncb1821
- Ukena, S. N., Singh, A., Dringenberg, U., Engelhardt, R., Seidler, U., Hansen, W., . . . Westendorf, A. M. (2007). Probiotic *Escherichia coli* Nissle 1917 inhibits leaky gut by enhancing mucosal integrity. *PLoS One*, 2(12), e1308. doi: 10.1371/journal.pone.0001308
- Upton, J. W., Kaiser, W. J., & Mocarski, E. S. (2008). Cytomegalovirus M45 cell death suppression requires receptor-interacting protein (RIP) homotypic interaction motif (RHIM)-dependent interaction with RIP1. *J Biol Chem*, 283(25), 16966-16970. doi: 10.1074/jbc.C800051200
- Upton, J. W., Kaiser, W. J., & Mocarski, E. S. (2010). Virus inhibition of RIP3-dependent necrosis. *Cell Host Microbe*, 7(4), 302-313. doi: 10.1016/j.chom.2010.03.006
- Upton, J. W., Kaiser, W. J., & Mocarski, E. S. (2012). DAI/ZBP1/DLM-1 complexes with RIP3 to mediate virus-induced programmed necrosis that is targeted by murine cytomegalovirus vIRA. *Cell Host Microbe*, 11(3), 290-297. doi: 10.1016/j.chom.2012.01.016
- Vallabhapurapu, S., Matsuzawa, A., Zhang, W., Tseng, P. H., Keats, J. J., Wang, H., . . . Karin, M. (2008). Nonredundant and complementary functions of TRAF2 and TRAF3 in a ubiquitination cascade that activates NIK-dependent alternative NF-kappaB signaling. *Nat Immunol*, 9(12), 1364-1370. doi: 10.1038/ni.1678

- van der Flier, L. G., & Clevers, H. (2009). Stem cells, self-renewal, and differentiation in the intestinal epithelium. *Annu Rev Physiol*, *71*, 241-260. doi: 10.1146/annurev.physiol.010908.163145
- Vanden Berghe, T., Linkermann, A., Jouan-Lanhouet, S., Walczak, H., & Vandenabeele, P. (2014). Regulated necrosis: the expanding network of non-apoptotic cell death pathways. *Nat Rev Mol Cell Biol*, *15*(2), 135-147. doi: 10.1038/nrm3737
- Vanden Berghe, T., Vanlangenakker, N., Parthoens, E., Deckers, W., Devos, M., Festjens, N., . . . Vandenabeele, P. (2010). Necroptosis, necrosis and secondary necrosis converge on similar cellular disintegration features. *Cell Death Differ*, *17*(6), 922-930. doi: 10.1038/cdd.2009.184
- Vandenabeele, P., Declercq, W., Van Herreweghe, F., & Vanden Berghe, T. (2010). The role of the kinases RIP1 and RIP3 in TNF-induced necrosis. *Sci Signal*, *3*(115), re4. doi: 10.1126/scisignal.3115re4
- Varfolomeev, E., Blankenship, J. W., Wayson, S. M., Fedorova, A. V., Kayagaki, N., Garg, P., . . . Vucic, D. (2007). IAP antagonists induce autoubiquitination of c-IAPs, NF-kappaB activation, and TNFalpha-dependent apoptosis. *Cell*, *131*(4), 669-681. doi: 10.1016/j.cell.2007.10.030
- Varfolomeev, E., Maecker, H., Sharp, D., Lawrence, D., Renz, M., Vucic, D., & Ashkenazi, A. (2005). Molecular determinants of kinase pathway activation by Apo2 ligand/tumor necrosis factor-related apoptosis-inducing ligand. *J Biol Chem*, *280*(49), 40599-40608. doi: 10.1074/jbc.M509560200
- Varfolomeev, E. E., Schuchmann, M., Luria, V., Chiannikulchai, N., Beckmann, J. S., Mett, I. L., . . . Wallach, D. (1998). Targeted disruption of the mouse Caspase 8 gene ablates cell death induction by the TNF receptors, Fas/Apo1, and DR3 and is lethal prenatally. *Immunity*, *9*(2), 267-276.
- Vazquez-Torres, A., Vallance, B. A., Bergman, M. A., Finlay, B. B., Cookson, B. T., Jones-Carson, J., & Fang, F. C. (2004). Toll-like receptor 4 dependence of innate and adaptive immunity to Salmonella: importance of the Kupffer cell network. *J Immunol*, *172*(10), 6202-6208.
- Vereecke, L., Beyaert, R., & van Loo, G. (2011). Enterocyte death and intestinal barrier maintenance in homeostasis and disease. *Trends Mol Med*, *17*(10), 584-593. doi: 10.1016/j.molmed.2011.05.011
- Vince, J. E., Pantaki, D., Feltham, R., Mace, P. D., Cordier, S. M., Schmukle, A. C., . . . Silke, J. (2009). TRAF2 must bind to cellular inhibitors of apoptosis for tumor necrosis factor (tnf) to efficiently activate nf-kappaB and to prevent tnf-induced apoptosis. *J Biol Chem*, *284*(51), 35906-35915. doi: 10.1074/jbc.M109.072256
- Vince, J. E., Wong, W. W., Khan, N., Feltham, R., Chau, D., Ahmed, A. U., . . . Silke, J. (2007). IAP antagonists target cIAP1 to induce TNFalpha-dependent apoptosis. *Cell*, *131*(4), 682-693. doi: 10.1016/j.cell.2007.10.037
- Vlantis, K., Wullaert, A., Sasaki, Y., Schmidt-Supprian, M., Rajewsky, K., Roskams, T., & Pasparakis, M. (2011). Constitutive IKK2 activation in intestinal epithelial cells induces intestinal tumors in mice. *J Clin Invest*, *121*(7), 2781-2793. doi: 10.1172/JCI45349

- Wachter, T., Sprick, M., Hausmann, D., Kerstan, A., McPherson, K., Stassi, G., . . . Leverkus, M. (2004). cFLIPL inhibits tumor necrosis factor-related apoptosis-inducing ligand-mediated NF-kappaB activation at the death-inducing signaling complex in human keratinocytes. *J Biol Chem*, 279(51), 52824-52834. doi: 10.1074/jbc.M409554200
- Wada, Y., Mori, K., & Iwanaga, T. (1997). Apoptosis of enterocytes induced by inoculation of a strain of attaching and effacing Escherichia coli and verotoxin. *J Vet Med Sci*, 59(9), 815-818.
- Wagner, S., Beil, W., Westermann, J., Logan, R. P., Bock, C. T., Trautwein, C., . . . Manns, M. P. (1997). Regulation of gastric epithelial cell growth by Helicobacter pylori: offence for a major role of apoptosis. *Gastroenterology*, 113(6), 1836-1847.
- Wajant, H. (2003). Death receptors. *Essays Biochem*, 39, 53-71.
- Wang, H., Sun, L., Su, L., Rizo, J., Liu, L., Wang, L. F., . . . Wang, X. (2014). Mixed lineage kinase domain-like protein MLKL causes necrotic membrane disruption upon phosphorylation by RIP3. *Mol Cell*, 54(1), 133-146. doi: 10.1016/j.molcel.2014.03.003
- Wang, L., Du, F., & Wang, X. (2008). TNF-alpha induces two distinct caspase-8 activation pathways. *Cell*, 133(4), 693-703. doi: 10.1016/j.cell.2008.03.036
- Weinlich, R., & Green, D. R. (2014). The two faces of receptor interacting protein kinase-1. *Mol Cell*, 56(4), 469-480. doi: 10.1016/j.molcel.2014.11.001
- Weiss, D. S., Raupach, B., Takeda, K., Akira, S., & Zychlinsky, A. (2004). Toll-like receptors are temporally involved in host defense. *J Immunol*, 172(7), 4463-4469.
- Welz, P. S., Wullaert, A., Vlantis, K., Kondylis, V., Fernandez-Majada, V., Ermolaeva, M., . . . Pasparakis, M. (2011). FADD prevents RIP3-mediated epithelial cell necrosis and chronic intestinal inflammation. *Nature*, 477(7364), 330-334. doi: 10.1038/nature10273
- Weng, D., Marty-Roix, R., Ganesan, S., Proulx, M. K., Vladimer, G. I., Kaiser, W. J., . . . Lien, E. (2014). Caspase-8 and RIP kinases regulate bacteria-induced innate immune responses and cell death. *Proc Natl Acad Sci U S A*, 111(20), 7391-7396. doi: 10.1073/pnas.1403477111
- Wertz, I. E., & Dixit, V. M. (2008). Ubiquitin-mediated regulation of TNFR1 signaling. *Cytokine Growth Factor Rev*, 19(3-4), 313-324. doi: 10.1016/j.cytogfr.2008.04.014
- Williams, J. M., Duckworth, C. A., Watson, A. J., Frey, M. R., Miguel, J. C., Burkitt, M. D., . . . Pritchard, D. M. (2013). A mouse model of pathological small intestinal epithelial cell apoptosis and shedding induced by systemic administration of lipopolysaccharide. *Dis Model Mech*, 6(6), 1388-1399. doi: 10.1242/dmm.013284
- Wilson, N. S., Dixit, V., & Ashkenazi, A. (2009). Death receptor signal transducers: nodes of coordination in immune signaling networks. *Nat Immunol*, 10(4), 348-355. doi: 10.1038/ni.1714
- Wittkopf, N., Gunther, C., Martini, E., He, G., Amann, K., He, Y. W., . . . Becker, C. (2013). Cellular FLICE-like inhibitory protein secures intestinal epithelial cell survival and immune homeostasis by regulating caspase-8. *Gastroenterology*, 145(6), 1369-1379. doi: 10.1053/j.gastro.2013.08.059

- Wong, W. W., Gentle, I. E., Nachbur, U., Anderton, H., Vaux, D. L., & Silke, J. (2010). RIPK1 is not essential for TNFR1-induced activation of NF-kappaB. *Cell Death Differ*, *17*(3), 482-487. doi: 10.1038/cdd.2009.178
- Wright, A., Reiley, W. W., Chang, M., Jin, W., Lee, A. J., Zhang, M., & Sun, S. C. (2007). Regulation of early wave of germ cell apoptosis and spermatogenesis by deubiquitinating enzyme CYLD. *Dev Cell*, *13*(5), 705-716. doi: 10.1016/j.devcel.2007.09.007
- Wu, X. N., Yang, Z. H., Wang, X. K., Zhang, Y., Wan, H., Song, Y., . . . Han, J. (2014). Distinct roles of RIP1-RIP3 hetero- and RIP3-RIP3 homo-interaction in mediating necroptosis. *Cell Death Differ*, *21*(11), 1709-1720. doi: 10.1038/cdd.2014.77
- Xie, T., Peng, W., Yan, C., Wu, J., Gong, X., & Shi, Y. (2013). Structural insights into RIP3-mediated necroptotic signaling. *Cell Rep*, *5*(1), 70-78. doi: 10.1016/j.celrep.2013.08.044
- Xu, M., Skaug, B., Zeng, W., & Chen, Z. J. (2009). A ubiquitin replacement strategy in human cells reveals distinct mechanisms of IKK activation by TNFalpha and IL-1beta. *Mol Cell*, *36*(2), 302-314. doi: 10.1016/j.molcel.2009.10.002
- Yamamoto, M., Sato, S., Hemmi, H., Hoshino, K., Kaisho, T., Sanjo, H., . . . Akira, S. (2003). Role of adaptor TRIF in the MyD88-independent toll-like receptor signaling pathway. *Science*, *301*(5633), 640-643. doi: 10.1126/science.1087262
- Yamamoto, M., Sato, S., Hemmi, H., Sanjo, H., Uematsu, S., Kaisho, T., . . . Akira, S. (2002). Essential role for TIRAP in activation of the signalling cascade shared by TLR2 and TLR4. *Nature*, *420*(6913), 324-329. doi: 10.1038/nature01182
- Yamamoto, M., Sato, S., Mori, K., Hoshino, K., Takeuchi, O., Takeda, K., & Akira, S. (2002). Cutting edge: a novel Toll/IL-1 receptor domain-containing adapter that preferentially activates the IFN-beta promoter in the Toll-like receptor signaling. *J Immunol*, *169*(12), 6668-6672.
- Yeh, W. C., de la Pompa, J. L., McCurrach, M. E., Shu, H. B., Elia, A. J., Shahinian, A., . . . Mak, T. W. (1998). FADD: essential for embryo development and signaling from some, but not all, inducers of apoptosis. *Science*, *279*(5358), 1954-1958.
- Yeh, W. C., Shahinian, A., Speiser, D., Kraunus, J., Billia, F., Wakeham, A., . . . Mak, T. W. (1997). Early lethality, functional NF-kappaB activation, and increased sensitivity to TNF-induced cell death in TRAF2-deficient mice. *Immunity*, *7*(5), 715-725.
- Zachrisson, K., Neopikhanov, V., Samali, A., & Uribe, A. (2001). Interleukin-1, interleukin-8, tumour necrosis factor alpha and interferon gamma stimulate DNA synthesis but have no effect on apoptosis in small-intestinal cell lines. *Eur J Gastroenterol Hepatol*, *13*(5), 551-559.
- Zarnegar, B. J., Wang, Y., Mahoney, D. J., Dempsey, P. W., Cheung, H. H., He, J., . . . Cheng, G. (2008). Noncanonical NF-kappaB activation requires coordinated assembly of a regulatory complex of the adaptors cIAP1, cIAP2, TRAF2 and TRAF3 and the kinase NIK. *Nat Immunol*, *9*(12), 1371-1378. doi: 10.1038/ni.1676
- Zhang, D., Lin, J., & Han, J. (2010). Receptor-interacting protein (RIP) kinase family. *Cell Mol Immunol*, *7*(4), 243-249. doi: 10.1038/cmi.2010.10

- Zhang, D. W., Shao, J., Lin, J., Zhang, N., Lu, B. J., Lin, S. C., . . . Han, J. (2009). RIP3, an energy metabolism regulator that switches TNF-induced cell death from apoptosis to necrosis. *Science*, *325*(5938), 332-336. doi: 10.1126/science.1172308
- Zhang, H., Zhou, X., McQuade, T., Li, J., Chan, F. K., & Zhang, J. (2011). Functional complementation between FADD and RIP1 in embryos and lymphocytes. *Nature*, *471*(7338), 373-376. doi: 10.1038/nature09878
- Zhang, J., Cado, D., Chen, A., Kabra, N. H., & Winoto, A. (1998). Fas-mediated apoptosis and activation-induced T-cell proliferation are defective in mice lacking FADD/Mort1. *Nature*, *392*(6673), 296-300. doi: 10.1038/32681
- Zhang, L., Blackwell, K., Shi, Z., & Habelhah, H. (2010). The RING domain of TRAF2 plays an essential role in the inhibition of TNF α -induced cell death but not in the activation of NF- κ B. *J Mol Biol*, *396*(3), 528-539. doi: 10.1016/j.jmb.2010.01.008
- Zhang, X. D., Franco, A. V., Nguyen, T., Gray, C. P., & Hersey, P. (2000). Differential localization and regulation of death and decoy receptors for TNF-related apoptosis-inducing ligand (TRAIL) in human melanoma cells. *J Immunol*, *164*(8), 3961-3970.
- Zheng, L., Bidere, N., Staudt, D., Cubre, A., Orenstein, J., Chan, F. K., & Lenardo, M. (2006). Competitive control of independent programs of tumor necrosis factor receptor-induced cell death by TRADD and RIP1. *Mol Cell Biol*, *26*(9), 3505-3513. doi: 10.1128/MCB.26.9.3505-3513.2006
- Zhou, R., Wei, H., Sun, R., & Tian, Z. (2007). Recognition of Double-Stranded RNA by TLR3 Induces Severe Small Intestinal Injury in Mice. *The Journal of Immunology*, *178*(7), 4548-4556. doi: 10.4049/jimmunol.178.7.4548
- Zhou, W., & Yuan, J. (2014). Necroptosis in health and diseases. *Semin Cell Dev Biol*, *35*, 14-23. doi: 10.1016/j.semcdb.2014.07.013

Acknowledgement

First of all I would like to thank Prof. Manolis Pasparakis for giving me the opportunity to do my PhD work in his Lab and giving such an interesting project trustworthy in my hands. I am very thankful for his scientific guidance and his sustained interest in the progress of my work.

I want to express my deep gratitude to Katerina Vlantis for her supervision and support whenever needed, numerous helpful scientific discussions and her constructive comments for this manuscript. I highly appreciate her contribution and exceptional commitment during the preparation and revision of our publication. A special thank goes to Chun Kim for many inspiring discussions, his outstanding contribution to our publication and his personal support. Furthermore I want to thank Katerina Vlantis, Vanesa Fernández-Majada, Christina Eftychi, Robin Schwarzer and Patrick Welz for the supportive and unique environment within the “Gut-Lab” that helped me through up and downs. Moreover, I want to express my thankfulness to all collaborators that contributed to this work, with special thanks to the Michelle Kelliher Lab and Apostolos Polykratis for generating the mouse and the fruitful discussions.

I deeply appreciate the invaluable help provided by the team of our excellent technical assistants. I am thankful to Daniela Beier, Elza Mahlberg and Edeltraud Stade for patiently cutting countless sections. Many thanks to Jennifer Buchholz, Brigitte Hülser and Bianca Wolf for countless genotyping PCRs during the last for 4 years. Thanks to Claudia Uthoff-Hachenberg for her aplomb and help in all kind of problems and situations that came along. I also want to thank Dr. Hafner, Silke Röpke and Johannes Winkler for their help with administrative, bureaucratic and other issues that arose. My grateful thanks to all former and current Lab-members for the nice hours and the valuable experiences in- and outside the Lab.

Ein großer Dank geht an meine Familie und Freunde für die immerwährende Unterstützung in guten und schweren Zeiten. Ohne euch wäre diese Arbeit nicht möglich gewesen. Danke, dass Ihr niemals den Glauben an mich verloren habt!

Teilpublikation

Teile dieser Doktorarbeit wurden in folgender Publikation veröffentlicht:

Dannappel M.*, Vlantis K.*, Kumari S.*, Polykratis A.*, Kim C., Wachsmuth L., Eftychi C., Lin J., Corona T., Hermance N., Zelic M., Kirsch P, Basic M., Bleich A., Kelliher M. & Pasparakis M., (2014). RIPK1 maintains epithelial homeostasis by inhibiting apoptosis and necroptosis, Nature 513(7516):90-4

LETTER

doi:10.1038/nature13608

RIPK1 maintains epithelial homeostasis by inhibiting apoptosis and necroptosis

Marius Dannappel^{1*}, Katerina Vlantis^{1*}, Snehlata Kumari^{1*}, Apostolos Polykratis^{1*}, Chun Kim¹, Laurens Wachsmuth¹, Christina Eftychi¹, Juan Lin¹, Teresa Corona¹, Nicole Hermance², Matija Zelic², Petra Kirsch³, Marijana Basic⁴, Andre Bleich⁴, Michelle Kelliher^{2,§} & Manolis Pasparakis^{1,§}

Necroptosis has emerged as an important pathway of programmed cell death in embryonic development, tissue homeostasis, immunity and inflammation^{1–6}. RIPK1 is implicated in inflammatory and cell death signalling^{9–13} and its kinase activity is believed to drive RIPK3-mediated necroptosis^{14,15}. Here we show that kinase-independent scaffolding RIPK1 functions regulate homeostasis and prevent inflammation in barrier tissues by inhibiting epithelial cell apoptosis and necroptosis. Intestinal epithelial cell (IEC)-specific RIPK1 knockout caused IEC apoptosis, villus atrophy, loss of goblet and Paneth cells and premature death in mice. This pathology developed independently of the microbiota and of MyD88 signalling but was partly rescued by TNFR1 (also known as TNFRSF1A) deficiency. Epithelial FADD ablation inhibited IEC apoptosis and prevented the premature death of mice with IEC-specific RIPK1 knockout. However, mice lacking both RIPK1 and FADD in IECs displayed RIPK3-dependent IEC necroptosis, Paneth cell loss and focal erosive inflammatory lesions in the colon. Moreover, a RIPK1 kinase inactive knock-in delayed but did not prevent inflammation caused by FADD deficiency in IECs or keratinocytes, showing that RIPK3-dependent necroptosis of FADD-deficient epithelial cells only partly requires RIPK1 kinase activity. Epidermis-specific RIPK1 knockout triggered keratinocyte apoptosis and necroptosis and caused severe skin inflammation that was prevented by RIPK3 but not FADD deficiency. These findings revealed that RIPK1 inhibits RIPK3-mediated necroptosis in keratinocytes *in vivo* and identified necroptosis as a more potent trigger of inflammation compared with apoptosis. Therefore, RIPK1 is a master regulator of epithelial cell survival, homeostasis and inflammation in the intestine and the skin.

Mice lacking RIPK1 die perinatally, exhibiting apoptosis in multiple tissues including the intestine⁹ (Extended Data Fig. 1a). We generated mice with IEC-specific knockout of RIPK1 (RIPK1^{IEC-KO}) (Fig. 1a and Extended Data Fig. 1b–d) and found that they showed reduced body weight and died within the first 4 weeks of life (Fig. 1b, c). Intestinal sections from 3-week-old RIPK1^{IEC-KO} mice revealed pronounced villus atrophy and Paneth cell loss in the ileum, as well as reduced numbers of goblet cells and differentiated enterocytes, crypt elongation and IEC hyperproliferation in both the ileum and colon (Fig. 1d and Extended Data Fig. 1e, f). RIPK1^{IEC-KO} intestines contained highly increased numbers of cleaved caspase-3-positive (CC3⁺) apoptotic IECs, but did not show signs of epithelial erosion, suggesting that the epithelial barrier remained largely intact (Fig. 1d and Extended Data Fig. 1e, f). Messenger RNA levels of *Tnf*, *Il1b*, *Ccl5* and *Cxcl1* and leukocyte numbers were moderately increased in the ileum and colon of RIPK1^{IEC-KO} mice (Fig. 1e, f and Extended Data Fig. 2), indicating the presence of a mild inflammatory response. Newborn RIPK1^{IEC-KO} mice showed only a few apoptotic IECs, while 7-day-old mice showed increased numbers of apoptotic IECs, loss of goblet cells, elongated hyperproliferative crypts

and increased immune cell infiltration concomitant with moderately increased expression of tumour necrosis factor (TNF) and interleukin (IL)-1 β (Extended Data Fig. 3). Tamoxifen-inducible ablation of RIPK1 in IECs of adult mice (RIPK1^{tamIEC-KO}) caused rapid weight loss and death of the animals (Extended Data Fig. 4a–d) due to extensive IEC apoptosis resulting in severe intestinal pathology (Extended Data Fig. 4e–j). Collectively, these results revealed that epithelial-cell-intrinsic RIPK1 is essential for IEC survival and the maintenance of intestinal tissue structure and homeostasis.

The luminal microbiota regulates intestinal homeostasis and contributes to inflammation both in human inflammatory bowel disease and in mouse models^{16,17}. Antibiotic treatment briefly delayed but did not prevent severe intestinal pathology, weight loss and death of mice with inducible or constitutive IEC-specific RIPK1 knockout (Extended Data Fig. 4c–e, j–l). Moreover, RIPK1^{IEC-KO} mice raised under germ-free conditions developed similar intestinal pathology, although some of the mice survived up to the age of 5 weeks, indicating that the microbiota contributes to disease severity (Fig. 1g–j). In addition, MyD88 deficiency did not prevent intestinal pathology in RIPK1^{IEC-KO} mice (Fig. 2a, b, d and Extended Data Fig. 5a–c). Therefore, epithelial cell death and intestinal pathology in RIPK1^{IEC-KO} mice develop independently of the microbiota and of MyD88-dependent TLR signalling. RIPK1^{IEC-KO}/*Tnfr1*^{-/-} mice were partially protected from severe wasting, with approximately 50% of the mice surviving to at least 3 months of age, and showed reduced IEC apoptosis and ameliorated intestinal pathology (Fig. 2a–e and Extended Data Fig. 5a–c). Thus, IEC death and intestinal pathology in RIPK1^{IEC-KO} mice is induced mainly by TNFR1 signalling but TNFR1-independent pathways also contribute.

Epithelial FADD deficiency inhibited IEC apoptosis and villus atrophy and prevented the severe wasting and premature death of RIPK1^{IEC-KO} mice (Fig. 2f–h), suggesting an important pathogenic role of FADD-dependent apoptosis. However, RIPK1^{IEC-KO}/FADD^{IEC-KO} intestines contained increased numbers of CC3⁺ dying IECs and showed Paneth cell loss in the ileum and signs of colitis affecting primarily the distal colon (Fig. 2f, i, j and Extended Data Fig. 6). In contrast with RIPK1^{IEC-KO} mice, in which the distal colon was only mildly affected and that did not show epithelial erosions (0 of 18 mice analysed), histological examination of Swiss roll sections revealed focal epithelial erosions in the distal colon of RIPK1^{IEC-KO}/FADD^{IEC-KO} mice (8 of 14 mice) and RIPK1^{IEC-KO} mice with heterozygous epithelial FADD deficiency (FADD^{hetIEC-KO}) (5 of 6 mice) at the age of 3 weeks (Extended Data Fig. 6). Adult RIPK1^{IEC-KO}/FADD^{IEC-KO} mice displayed villus shortening, loss of goblet and Paneth cells and crypt elongation in the small intestine, as well as focal inflammatory erosive lesions and crypt abscess formation in the distal colon in 5 of 7 mice examined (Extended Data Fig. 7a). Therefore, although epithelial FADD deficiency strongly reduced the number of apoptotic

¹Institute for Genetics, Centre for Molecular Medicine (CMMC), and Cologne Excellence Cluster on Cellular Stress Responses in Aging-Associated Diseases (CECAD), University of Cologne, 50931 Cologne, Germany. ²Department of Cancer Biology, University of Massachusetts Medical School, Worcester, Massachusetts 01605, USA. ³Tierforschungszentrum, University of Ulm, Albert-Einstein-Allee 11, D-89081 Ulm, Germany. ⁴Institute for Laboratory Animal Science, Hannover Medical School, D-30625 Hannover, Germany.

*These authors contributed equally to this work.
[§]These authors jointly supervised this work.

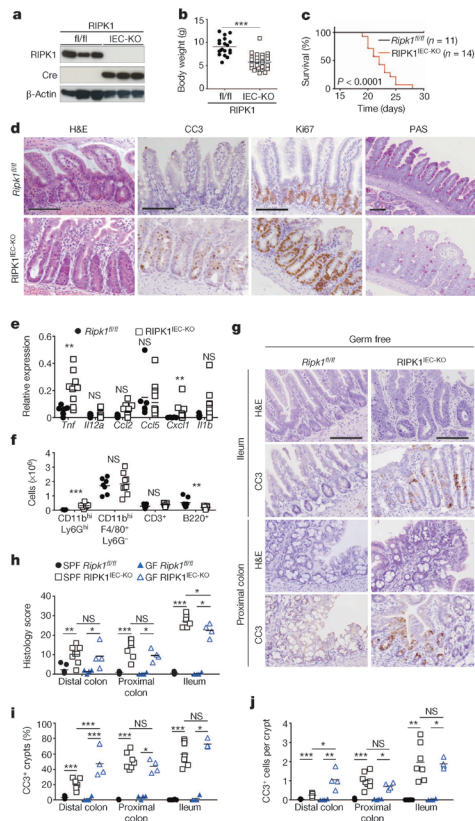


Figure 1 | Epithelial RIPK1 ablation causes microbiota-independent intestinal pathology. **a**, Immunoblot of small intestine IECs from *Ripk1^{fl/fl}* (*fl/fl*) and *RIPK1^{IEC-KO}* (*IEC-KO*) mice. **b**, **c**, Body weight (**b**) and Kaplan-Meier survival curve (**c**) of *Ripk1^{fl/fl}* and *RIPK1^{IEC-KO}* mice. **d**, Representative images of ileal sections from *Ripk1^{fl/fl}* and *RIPK1^{IEC-KO}* mice stained as indicated. H&E, haematoxylin and eosin. **e**, **f**, Quantitative polymerase chain reaction with reverse transcription (qRT-PCR) of cytokine and chemokine expression (**e**) and fluorescence-activated cell sorting (FACS) of lamina propria leukocytes (**f**) in the small intestine of *Ripk1^{fl/fl}* and *RIPK1^{IEC-KO}* mice. **g**, Representative images of H&E- or CC3-stained intestinal sections from germ-free *Ripk1^{fl/fl}* and *RIPK1^{IEC-KO}* mice. **h**–**j**, Quantification of histological pathology score (**h**), crypts containing CC3⁺ cells (**i**) and CC3⁺ cells per crypt (**j**) in intestinal sections of the indicated mice. GF, germ free; SPF, specific pathogen free. Scale bars, 100 μ m. * $P \leq 0.05$, ** $P \leq 0.01$, *** $P \leq 0.005$; NS, not significant.

epithelial cells and prevented wasting and premature death of *RIPK1^{IEC-KO}* mice, it did not normalize but rather altered their intestinal pathology, with *RIPK1^{IEC-KO}/FADD^{IEC-KO}* animals resembling the phenotype of *FADD^{IEC-KO}* mice⁵.

We reasoned that RIPK3-dependent necroptosis could induce the death of IECs in *RIPK1^{IEC-KO}/FADD^{IEC-KO}* mice, as in *FADD^{IEC-KO}* mice⁵. Indeed, triple-deficient *RIPK1^{IEC-KO}/FADD^{IEC-KO}/Ripk3^{-/-}* mice did not show macroscopic or histological signs of intestinal pathology, although they displayed slightly increased mRNA levels of *Tnf*, *Il1b*, *Cd5*

and *Il10* in the colon (Fig. 2f–k and Extended Data Figs 5d, e, 6, 7a, b). In contrast, RIPK3 deficiency alone did not prevent wasting, early lethality, IEC apoptosis or intestinal pathology in *RIPK1^{IEC-KO}* mice (Fig. 2f–j and Extended Data Figs 5d, e, 6, 7b). Therefore, RIPK3-dependent necroptosis does not constitute a primary pathway inducing IEC death and intestinal pathology in *RIPK1^{IEC-KO}* mice, but becomes functionally important when FADD ablation inhibits apoptosis and sensitizes RIPK1-deficient IECs to necroptosis. These results suggested that RIPK3 induces RIPK1-independent necroptosis in FADD-deficient IECs, which is surprising as RIPK1 kinase activity is considered essential for RIPK3-mediated necroptosis, at least downstream of TNFR1 (refs 14, 15), which is the major driver of epithelial cell necroptosis in the colon of *FADD^{IEC-KO}* mice⁵. To address specifically the role of RIPK1 kinase activity, we crossed *FADD^{IEC-KO}* mice with knock-in mice expressing kinase-inactive RIPK1 (*RIPK1* (D138N)) and found that lack of RIPK1 kinase activity did not prevent IEC necroptosis and intestinal inflammation in *FADD^{IEC-KO}* mice (Fig. 2l and Extended Data Fig. 7c, d). Therefore, RIPK1 deficiency or loss of its kinase activity only partly inhibited RIPK3-dependent necroptosis of FADD-deficient IECs, providing genetic evidence that both RIPK1-dependent and RIPK1-independent pathways drive RIPK3-mediated necroptosis and intestinal inflammation in *FADD^{IEC-KO}* mice.

As shown previously^{9,18}, RIPK1 deficiency but not loss of its kinase activity partially inhibited TNF-mediated NF- κ B activation in mouse embryonic fibroblasts (MEFs) (Extended Data Fig. 8a), suggesting that loss of RIPK1 scaffolding function might trigger epithelial cell apoptosis by inhibiting NF- κ B. However, NF- κ B inhibition in the intestinal epithelium did not phenocopy the intestinal pathology of *RIPK1^{IEC-KO}* mice^{19–21}. Moreover, sustained NF- κ B activation in RIPK1-deficient epithelial cells by expression of a constitutively active *Ikk2* transgene^{22,23} did not prevent IEC death and rather aggravated the intestinal pathology of *RIPK1^{IEC-KO}* mice, suggesting that RIPK1 deficiency does not sensitize IECs to apoptosis by inhibiting NF- κ B (Extended Data Fig. 8b–d).

RIPK1-deficient IECs did not show reduced mRNA expression of pro-survival genes, but expressed reduced amounts of cIAP1 (also known as BIRC2) and TRAF2 proteins (Fig. 3a, b), suggesting that RIPK1 might control their stability. Indeed, consistent with previous reports^{24,25}, we found that TNF stimulation induced rapid degradation of TRADD, cIAP1, TRAF2 and c-FLIP (also known as CFLAR), but not of TRAF6, in *RIPK1*-deficient but not in *RIPK1*(D138N) primary MEFs (Fig. 3c), suggesting that lack of the RIPK1 scaffolding function triggers degradation of proteins recruited to the TNFR1 signalling complex. We then sought to address whether RIPK1-deficient intestinal epithelial cells show similar responses. However, small intestinal crypts from *RIPK1^{IEC-KO}* mice died shortly after isolation and failed to form organoids (data not shown). Nevertheless, tamoxifen-inducible RIPK1 deletion resulted in reduced expression of cIAP1, TRAF2 and c-FLIP proteins and caused rapid organoid death (Fig. 3d–f), suggesting that loss of pro-survival protein expression contributes to death of *RIPK1*-deficient IECs. Interestingly, TRAF2-deficient mice develop a similar intestinal phenotype and early lethality that was not prevented by antibiotic treatment and was only partially rescued by TNFR1 deficiency, suggesting that loss of TRAF2 could contribute to the intestinal pathology of *RIPK1^{IEC-KO}* mice²⁶.

SMAC (also known as DIABLO) mimetic-compound-mediated cIAP1/2 degradation induced activation of both non-canonical and canonical NF- κ B and the expression of TNF and other cytokines^{27,28}, suggesting that loss of cIAP proteins could trigger the expression of TNF and other cytokines by *RIPK1*-deficient IECs that could act in an autocrine fashion to induce their death. Indeed, *RIPK1*-deficient primary IECs showed increased NF- κ B activation and expressed elevated levels of TNF, while tamoxifen-inducible deletion of *RIPK1* upregulated TNF expression in organoids (Fig. 3g–j). Moreover, intestinal crypts from *RIPK1^{IEC-KO}/Tnfr1^{-/-}* mice did not die rapidly, as did crypts from *RIPK1^{IEC-KO}* mice, and although they did not grow as well as control organoids they could be maintained for a short period in culture (Fig. 3k), consistent with a role of autocrine TNF production in triggering the death of *RIPK1*-deficient IECs. *RIPK1*/TNFR1 double-deficient organoids were more sensitive to

RESEARCH LETTER

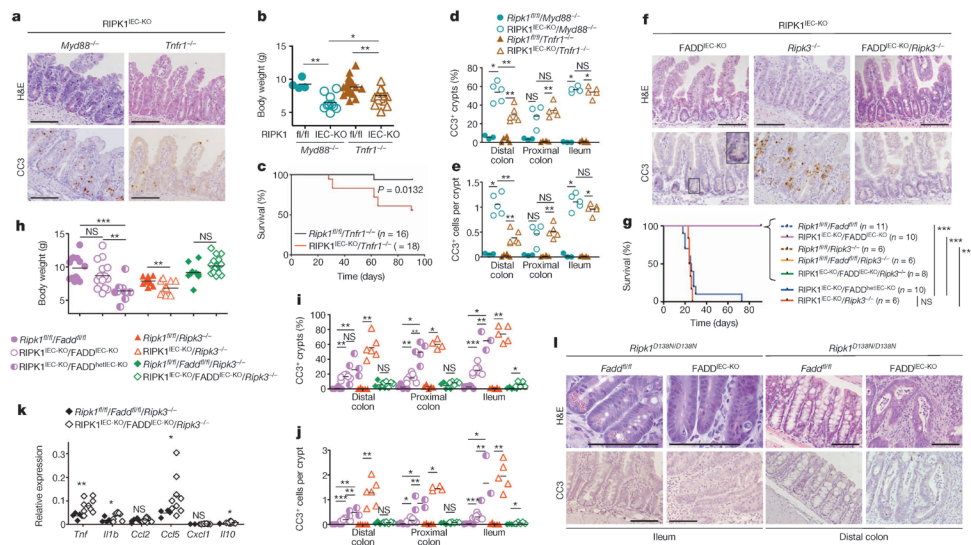


Figure 2 | Death of RIPK1-deficient IECs depends on FADD and RIPK3.

a, Representative images of H&E- or CC3-stained ileal sections from the indicated mice. **b, c**, Body weight (**b**) and Kaplan–Meier survival curve (**c**) of the indicated mice. **d, e**, Quantification of crypts containing CC3⁺ cells (**d**) and CC3⁺ cell numbers per crypt (**e**) in intestinal sections of the indicated mice. **f**, Representative images of ileal sections from the indicated mice. Arrow depicts CC3⁺ dying IEC. **g, h**, Kaplan–Meier survival curve (**g**) and body weight (**h**) of

mice with the indicated genotypes. **i, j**, Quantification of crypts containing CC3⁺ cells (**i**) and CC3⁺ cell numbers per crypt (**j**) in intestinal sections of the indicated mice. **k**, qRT-PCR analysis of cytokine expression in the small intestine of the indicated mice. **l**, Representative images of intestinal sections from 4-month-old mice with the indicated genotypes. Scale bars, 100 μ m. * $P \leq 0.05$, ** $P \leq 0.01$, *** $P \leq 0.005$; NS, not significant.

death induced by polyinosinic:polycytidylic acid (poly(I:C)), interferon (IFN)- β and IFN- γ (Fig. 3k), indicating that TIR-domain-containing adapter-inducing interferon- β (TRIF)- and IFN-dependent pathways also contribute to the death of RIPK1-deficient IECs. However, IEC-specific ablation of TRIF did not considerably ameliorate intestinal pathology in RIPK1^{IEC-KO} mice (Extended Data Fig. 8e–h), suggesting that TRIF-mediated signalling is not a major driver of IEC apoptosis but could contribute in a redundant fashion together with TNFR1 and IFN signalling. Together, these findings suggest that RIPK1 deficiency results in degradation of cIAP proteins and TRAF2, triggering NF- κ B-mediated expression of TNF and other cytokines that act in a partly redundant fashion to induce the death of RIPK1-deficient IECs. The mild upregulation of *Tnf* in the colon of RIPK1^{IEC-KO}/FADD^{IEC-KO}/Ripk3^{-/-} mice (Fig. 2k) is compatible with this epithelial cell death independent mechanism inducing *Tnf* expression, which also provides a microbiota-independent trigger of IEC death in RIPK1^{IEC-KO} mice.

To investigate the function of RIPK1 in the epidermis, we generated mice with keratinocyte-specific RIPK1 deficiency (RIPK1^{E-KO} mice) (Extended Data Fig. 9a). RIPK1^{E-KO} mice progressively developed severe inflammatory skin lesions starting at around 1 week of age, characterized by epidermal thickening, increased keratin 14 (K14; also known as KRT14) and reduced K10 expression and upregulation of K6 in the interfollicular epidermis, as well as infiltration of Gr-1-positive cells and increased inflammatory cytokine and chemokine expression (Fig. 4a–c and Extended Data Fig. 9a, b). Histological analysis revealed the presence of CC3⁺ but also CC3⁻ dying keratinocytes, identified by their pyknotic nuclei and eosinophilic cytoplasm in the epidermis of RIPK1^{E-KO} mice (Fig. 4d and Extended Data Fig. 9d). To address the role of FADD-mediated apoptosis, we generated FADD^{E-KO}/RIPK1^{E-KO} mice and found that they did not show early postnatal skin inflammation and death, as did FADD^{E-KO}

mice⁴, but developed severe inflammatory skin lesions later, similarly to RIPK1^{E-KO} mice (Fig. 4a–c and Extended Data Fig. 9c, d). Importantly, FADD^{E-KO}/Ripk1^{D138N/D138N} mice showed a similar skin phenotype to FADD^{E-KO}/RIPK1^{E-KO} mice (Fig. 4a, b). Therefore, lack of RIPK1 or its kinase activity delayed but could not prevent keratinocyte necroptosis and inflammation caused by FADD deficiency. Additional deficiency in RIPK3 fully prevented skin inflammation in RIPK1^{E-KO}/FADD^{E-KO}/Ripk3^{-/-} mice (Fig. 4a–c and Extended Data Fig. 9e, g), showing that RIPK1-independent RIPK3-dependent keratinocyte necroptosis drives skin inflammation.

Surprisingly, RIPK1^{E-KO}/Ripk3^{-/-} mice did not develop skin inflammation and their epidermis contained strongly reduced numbers of CC3⁺ but similar numbers of CC3⁻ keratinocytes compared with RIPK1^{E-KO} mice (Fig. 4a–d and Extended Data Fig. 9d, e, g), showing that RIPK3-mediated necroptosis of RIPK1-deficient keratinocytes causes the inflammatory skin lesions. CRISPR/Cas9-mediated knockout of MLKL also prevented skin inflammation in RIPK1^{E-KO} mice, further supporting an essential role of RIPK3/MLKL-dependent necroptosis in this model (Extended Data Fig. 10). Therefore, at least in the context of keratinocyte-specific RIPK1 deficiency, necroptosis of keratinocytes triggers skin inflammation but apoptosis does not, highlighting the different immune regulatory properties of these programmed cell death pathways in a disease-relevant *in vivo* experimental setting. Considering that *Ripk1*^{D138N/D138N} mice did not develop skin lesions (Fig. 4a), these results show that RIPK1 acts through a kinase-independent scaffolding function to restrain RIPK3-mediated necroptosis in keratinocytes and prevent skin inflammation.

RIPK1^{E-KO}/Tnfr1^{-/-} mice showed largely normal skin until postnatal day (P)28, but developed patchy inflammatory skin lesions by the age of 7–8 weeks (Fig. 4a–d and Extended Data Fig. 9d, e, g). Therefore, TNFR1 critically contributes but is not the only trigger of keratinocyte necroptosis

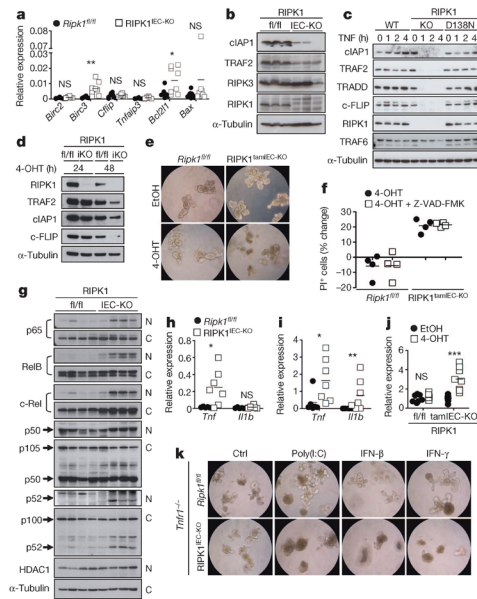


Figure 3 RIPK1 prevents the degradation of pro-survival proteins. **a, b**, qRT-PCR of pro-survival genes (**a**) and immunoblot of the indicated proteins (**b**) in small intestine IECs from *Ripk1^{fl/fl}* (*fl/fl*) and RIPK1^{IEC-KO} (IEC-KO) mice. **c**, Immunoblot of wild-type (WT), *Ripk1^{-/-}* (KO) and *Ripk1^{D138N/D138N}* (D138N) MEFs stimulated with 10 ng ml⁻¹ recombinant murine TNF. **d**, Immunoblot of small intestine organoids from *Ripk1^{fl/fl}* (*fl/fl*) and RIPK1^{tamIEC-KO} (iKO) mice treated with 4-hydroxytamoxifen (4-OHT) for 24 or 48 h. **e**, *Ripk1^{fl/fl}* and RIPK1^{tamIEC-KO} organoids were treated with vehicle (ethanol; EtOH) or 4-OHT for 20 h and photographed 48 h later. Original magnification, ×400. **f**, FACS quantification of propidium iodide (PI)⁺ cells in organoids 43 h after treatment with 4-OHT in the presence or absence of z-VAD-FMK. **g**, Immunoblot of cytoplasmic (C) and nuclear (N) proteins from small intestine IECs of four *Ripk1^{fl/fl}* and four RIPK1^{IEC-KO} mice with the indicated antibodies. **h, i**, qRT-PCR of *Tnf* and *Il1b* expression in IECs from small intestine (**h**) or colon (**i**) of *Ripk1^{fl/fl}* and RIPK1^{IEC-KO} mice. **j**, qRT-PCR of *Tnf* expression in small intestine organoids from *Ripk1^{fl/fl}* and RIPK1^{IEC-KO} mice 30 h after treatment with EtOH or 4-OHT. **k**, Representative images of *Ripk1^{fl/fl}*/*Tnfr1^{-/-}* and RIPK1^{IEC-KO}/*Tnfr1^{-/-}* organoids 16 h after treatment with 100 μg ml⁻¹ poly(I:C), 1,000 U ml⁻¹ IFN-β and 1,000 U ml⁻¹ IFN-γ. Original magnification, ×400. Ctrl, control. Representative data are shown of four (**e, f, k**), three (**c**) or two (**d, j**) independent experiments. **P* ≤ 0.05, ***P* ≤ 0.01, ****P* ≤ 0.005; NS, not significant.

and inflammation in RIPK1^{E-KO} mice. Keratinocyte-specific TRIF ablation also mildly ameliorated skin lesion development in RIPK1^{E-KO} mice (Fig. 4a, b and Extended Data Fig. 9e). Collectively, these results showed that TNFR1- and TRIF-mediated signalling contribute to RIPK3-dependent keratinocyte necroptosis and skin inflammation in RIPK1^{E-KO} mice.

cIAP1 was expressed at very low levels at steady state and was undetectable after TNF stimulation in RIPK1-deficient primary keratinocytes (Fig. 4e), similar to our findings in IECs. Moreover, RIPK1-deficient primary keratinocytes were highly sensitive to TNF-induced death that was inhibited by the caspase inhibitor z-VAD-FMK, demonstrating that *in vitro* these cells died primarily by apoptosis and were resistant to necroptosis even though they expressed RIPK3 (Fig. 4f, g). This result

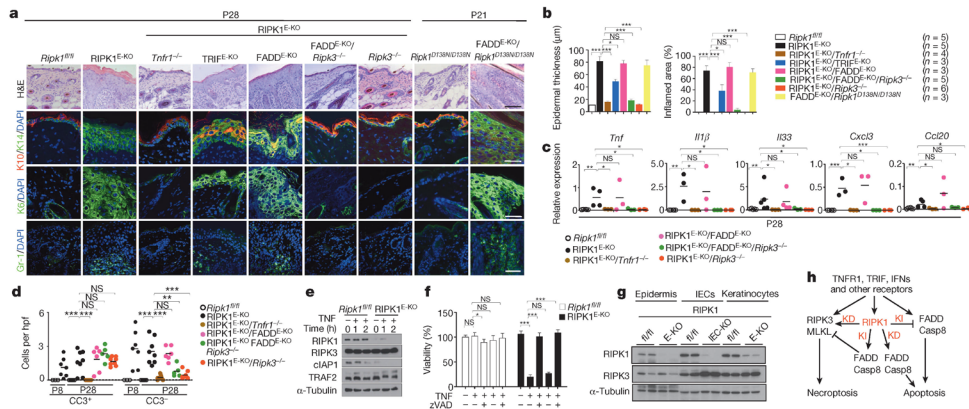


Figure 4 RIPK1 ablation causes keratinocyte necroptosis and skin inflammation. **a**, Representative images of skin sections from the indicated mice stained with H&E or the indicated antibodies. Nuclei stained with 4',6-diamidino-2-phenylindole (DAPI). Scale bars, 100 μm (H&E); 50 μm (immunostainings). **b**, Microscopic quantification of epidermal thickness and inflamed skin area in the indicated mice. Error bars represent mean values ± standard error of the mean (s.e.m.). **c**, qRT-PCR of cytokine and chemokine expression in total skin from the indicated mice. **d**, Quantification of CC3⁺ and CC3⁻ dying cells per high power field (hpf) in skin sections from the indicated mice. **e**, Immunoblot of primary keratinocytes stimulated with

20 ng ml⁻¹ recombinant murine TNF for the indicated time points. **f**, Quantification of cell viability in primary keratinocytes treated with 50 ng ml⁻¹ recombinant murine TNF in the presence or absence of z-VAD-FMK (zVAD; 20 μM) and necrostatin-1 (Nec; 30 μM). Mean values ± s.e.m. from biological triplicates (*n* = 3) are shown. **g**, Immunoblot of protein extracts from P4 epidermis, IECs or keratinocytes from mice of the indicated genotypes. **h**, Schematic model of the kinase-dependent (KD) and -independent (KI) functions of RIPK1 in apoptosis and necroptosis. Representative data of three independent experiments are shown in **e, f**. **P* ≤ 0.05, ***P* ≤ 0.01, ****P* ≤ 0.005; NS, not significant.

RESEARCH LETTER

is surprising considering that RIPK1 deficiency *in vivo* triggers skin inflammation by sensitizing keratinocytes to RIPK3-dependent necroptosis, and suggests that mechanisms related to keratinocyte differentiation and the *in vivo* tissue context could determine the sensitivity of keratinocytes to apoptosis and necroptosis.

Collectively, our results revealed a novel kinase-independent scaffolding function of RIPK1 as an inhibitor of epithelial cell apoptosis and necroptosis *in vivo* that is essential for the maintenance of physiological tissue homeostasis in the intestine and the skin. The mechanisms determining whether RIPK1 deficiency sensitizes epithelial cells to apoptosis or necroptosis remain unclear and do not seem to depend on differential expression of RIPK3 (Fig. 4g). Our experiments also showed that necroptosis of FADD-deficient IECs and keratinocytes only partly depends on RIPK1 kinase activity, demonstrating that both RIPK1-dependent and -independent pathways drive RIPK3-mediated necroptosis. Therefore, RIPK1 is a central regulator of cell death that has the capacity to either inhibit or induce apoptosis and necroptosis (Fig. 4h). Considering its key role as a molecular hub integrating and decoding multiple ubiquitination (K63, K48, linear) signals to determine cellular responses to stimuli that are derived (for example, lipopolysaccharide, double-stranded RNA) or induced (for example, TNF, IFNs) by microbes and are capable of triggering both inflammation and cell death, RIPK1 emerges as a key regulator of immunity and homeostasis in barrier tissues.

Note added in proof An accompanying paper (Takahashi, N. *et al.*, *Nature* <http://dx.doi.org/10.1038/nature13706>) reports similar results on the role of RIPK1 in preventing IEC apoptosis, with some differences on the effect of antibiotic treatment and MYD88 deficiency on the intestinal pathology of RIPK1^{IEC-KO} mice.

Online Content Methods, along with any additional Extended Data display items and Source Data, are available in the online version of the paper; references unique to these sections appear only in the online paper.

Received 20 December 2013; accepted 25 June 2014.

Published online 17 August 2014.

- Oberst, A. *et al.* Catalytic activity of the caspase-8-FLIP_L complex inhibits RIPK3-dependent necrosis. *Nature* **471**, 363–367 (2011).
- Kaiser, W. J. *et al.* RIP3 mediates the embryonic lethality of caspase-8-deficient mice. *Nature* **471**, 368–372 (2011).
- Zhang, H. *et al.* Functional complementation between FADD and RIP1 in embryos and lymphocytes. *Nature* **471**, 373–376 (2011).
- Bonnet, M. C. *et al.* The adaptor protein FADD protects epidermal keratinocytes from necroptosis *in vivo* and prevents skin inflammation. *Immunity* **35**, 572–582 (2011).
- Weitz, P. S. *et al.* FADD prevents RIP3-mediated epithelial cell necrosis and chronic intestinal inflammation. *Nature* **477**, 330–334 (2011).
- Dillon, C. P. *et al.* Survival function of the FADD-CASPASE-8-cFLIP(L) complex. *Cell Rep.* **1**, 401–407 (2012).
- Duprez, L. *et al.* RIP kinase-dependent necrosis drives lethal systemic inflammatory response syndrome. *Immunity* **35**, 908–918 (2011).
- Upton, J. W., Kaiser, W. J. & Mocsarski, E. S. Virus inhibition of RIP3-dependent necrosis. *Cell Host Microbe* **7**, 302–313 (2010).
- Kelliher, M. A. *et al.* The death domain kinase RIP mediates the TNF-induced NF- κ B signal. *Immunity* **8**, 297–303 (1998).
- Cusson-Hernance, N., Khurana, S., Lee, T. H., Fitzgerald, K. A. & Kelliher, M. A. Rip1 mediates the Trif-dependent toll-like receptor 3- and 4-induced NF- κ B activation but does not contribute to interferon regulatory factor 3 activation. *J. Biol. Chem.* **280**, 36560–36566 (2005).
- Meylan, E. *et al.* RIP1 is an essential mediator of Toll-like receptor 3-induced NF- κ B activation. *Nature Immunol.* **5**, 503–507 (2004).
- Kawai, T. *et al.* IPS-1, an adaptor triggering RIG-I- and Mda5-mediated type I interferon induction. *Nature Immunol.* **6**, 981–988 (2005).
- Rajput, A. *et al.* RIG-I RNA helicase activation of IRF3 transcription factor is negatively regulated by caspase-8-mediated cleavage of the RIP1 protein. *Immunity* **34**, 340–351 (2011).
- Christofferson, D. E., Li, Y. & Yuan, J. Control of life-or-death decisions by RIP1 kinase. *Annu. Rev. Physiol.* **76**, 129–150 (2014).
- Vanden Berghe, T., Linkermann, A., Jouan-Lanhouet, S., Walczak, H. & Vandenabeele, P. Regulated necrosis: the expanding network of non-apoptotic cell death pathways. *Nature Rev. Mol. Cell Biol.* **15**, 135–147 (2014).
- Hill, D. A. & Artis, D. Intestinal bacteria and the regulation of immune cell homeostasis. *Annu. Rev. Immunol.* **28**, 623–667 (2010).
- Kaser, A., Zeissig, S. & Blumberg, R. S. Inflammatory bowel disease. *Annu. Rev. Immunol.* **28**, 573–621 (2010).
- Lee, T. H., Shank, J., Cusson, N. & Kelliher, M. A. The kinase activity of Rip1 is not required for tumor necrosis factor- α -induced κ B kinase or p38 MAP kinase activation or for the ubiquitination of Rip1 by Traf2. *J. Biol. Chem.* **279**, 33185–33191 (2004).
- Greter, F. R. *et al.* IKK β links inflammation and tumorigenesis in a mouse model of colitis-associated cancer. *Cell* **118**, 285–296 (2004).
- Nenci, A. *et al.* Epithelial NEMO links innate immunity to chronic intestinal inflammation. *Nature* **446**, 557–561 (2007).
- Steinbrecher, K. A., Harmel-Laws, E., Sticheran, R. & Baldwin, A. S. Loss of epithelial RelA results in deregulated intestinal proliferative/apoptotic homeostasis and susceptibility to inflammation. *J. Immunol.* **180**, 2588–2599 (2008).
- Sasaki, Y. *et al.* Canonical NF- κ B activity, dispensable for B cell development, replaces BAFF-receptor signals and promotes B cell proliferation upon activation. *Immunity* **24**, 729–739 (2006).
- Vlantis, K. *et al.* Constitutive IKK2 activation in intestinal epithelial cells induces intestinal tumors in mice. *J. Clin. Invest.* **121**, 2781–2793 (2011).
- Gentile, I. E. *et al.* In TNF-stimulated cells, RIPK1 promotes cell survival by stabilizing TRAF2 and cIAP1, which limits induction of non-canonical NF- κ B and activation of caspase-8. *J. Biol. Chem.* **286**, 13282–13291 (2011).
- Kim, J. Y. *et al.* TNF α -induced noncanonical NF- κ B activation is attenuated by RIP1 through stabilization of TRAF2. *J. Cell Sci.* **124**, 647–656 (2011).
- Piao, J. H. *et al.* Tumor necrosis factor receptor-associated factor (TRAF) 2 controls homeostasis of the colon to prevent spontaneous development of murine inflammatory bowel disease. *J. Biol. Chem.* **286**, 17879–17888 (2011).
- Varfolomeev, E. *et al.* IAP antagonists induce auto-ubiquitination of c-IAPs, NF- κ B activation, and TNF α -dependent apoptosis. *Cell* **131**, 669–681 (2007).
- Vince, J. E. *et al.* IAP antagonists target cIAP1 to induce TNF α -dependent apoptosis. *Cell* **131**, 682–693 (2007).

Acknowledgements We are grateful to V. Dixit for *Ripk3*^{-/-}, D. Gumucio for Villin-Cre and S. Robine for Villin-CreER^{fl} mice. We thank C. Uthoff-Hachenberg, J. Buchholz, E. Mahlberg, B. Kühnel, B. Hülser, P. Janowski, S. Assenmacher and P. Scholl for technical assistance. M.P. acknowledges funding from the European Research Council (2012-ADG_20120314), the German Research Council (DFG; SF8670, SF8829, SP11656), the European Commission (grants 223404 (Masterswitch) and 223151 (InfiaCare)), the Deutsche Krebshilfe, the Else Kröner-Fresenius-Stiftung and the Helmholtz Alliance (PCCC). Research reported in this publication was also supported by the National Institute of Allergy and Infectious Diseases division of the National Institutes of Health under award R01AI075118 to M.K.

Author Contributions M.D. together with K.V. performed and analysed the experiments related to the intestine and S.K. performed and analysed the experiments related to the skin. N.H. and M.K. designed and generated the targeting constructs for the *Ripk1*^{fl/fl} and *Ripk1*^{D138N/D138N} mice. A.P. performed the gene targeting in embryonic stem cells and generated the *Ripk1*^{fl/fl}, *Ripk1*^{D138N/D138N} and *Trif*^{fl/fl} mice. M.Z. contributed to the analysis of intestines from *Ripk1*^{-/-} neonates. C.K. and J.L. performed biochemical analysis of RIPK1-deficient MEFs, IECs and keratinocytes. C.E. performed FACS analysis of intestinal immune cells. T.C. performed qRT-PCR analysis. L.W. designed and tested the short guiding RNAs for CRISPR/Cas9-mediated targeting of *Mki1*. P.K., M.B. and A.B. generated germ-free RIPK1^{IEC-KO} mice. M.P. coordinated the project and together with K.V., M.D. and S.K. wrote the paper.

Author Information Reprints and permissions information is available at www.nature.com/reprints. The authors declare no competing financial interests. Readers are welcome to comment on the online version of the paper. Correspondence and requests for materials should be addressed to M.P. (pasparakis@uni-koeln.de).

METHODS

Mice. *Ripk1^{fl/fl}*, *Ripk1^{D138N/D138N}* (ref. 29), *Tyrr^{fl/fl}*, *Fadd^{fl/fl}* (ref. 30), FADD-IRES-eGFP^{fl/fl} (ref. 4) and *R26-Stop^{fl}/Ikk2ca²* mice expressing a constitutively active *Ikk2* (*Ikk2ca*) transgene were generated by gene targeting in C57BL/6 embryonic stem (ES) cells. *FLPe-Deleter^{fl}* mice were used to delete the FRT-flanked neo cassette and *Cre-Deleter^{fl}* mice were employed to delete the RIPK1 floxed sequences in the germ line and generate *Ripk1^{-/-}* mice and MEFs. *Villin-Cre^{fl}*, *VillinCreER^{fl}* (ref. 34), *K14-Cre^{fl}*, *Tyrr^{fl}* (ref. 36), *Myd88^{-/-}* (ref. 37) and *Ripk3^{-/-}* (ref. 38) mice were backcrossed for at least ten generations into the C57BL/6 genetic background. Mice were maintained at the SPF animal facilities of the Institute for Genetics, University of Cologne, and of the University of Massachusetts Medical School and kept under a 12 h light cycle, and given a regular chow diet (Harlan diet no. 2918 or ProLab Isoport RMH3000 5P76) *ad libitum*. Germ-free mice were produced at the gnotobiotic facilities of the University of Ulm and of the Hannover Medical School. All animal procedures were conducted in accordance with European, national and institutional guidelines and protocols were approved by local government authorities (Landesamt für Natur, Umwelt und Verbraucherschutz Nordrhein-Westfalen, Germany). Animals requiring medical attention were provided with appropriate care and excluded from the experiments described. No other exclusion criteria existed. For antibiotic treatment of RIPK1^{IEC-KO} mice one of two different broad spectrum antibiotic mixtures was added to the drinking water starting from embryonic day (E)17.5: 1 g l⁻¹ ampicillin (ICN Biomedicals), 1 g l⁻¹ neomycin (Sigma), 0.5 g l⁻¹ Meronem (AstraZeneca) and 0.5 g l⁻¹ ciprofloxacin (Fluka) or 1 g l⁻¹ ampicillin (ICN Biomedicals), 1 g l⁻¹ metronidazole (Sigma), 0.5 g l⁻¹ vancomycin (Eberth) and 0.2 g l⁻¹ ciprofloxacin (Fluka). In *VillinCreER^{fl}/Ripk1^{fl/fl}* mice a modified version of the first protocol was employed, where Meronem was replaced by 0.5 g l⁻¹ vancomycin (Eberth). As neither the overall physiological response nor tissue pathology differed between the two regimens, mouse groups receiving either antibiotic mixture were analysed together and data from individual experiments were pooled. *VillinCreER^{fl}* recombinase activity was induced by three daily intraperitoneal administrations of 1 mg tamoxifen. Littermates not carrying the *Villin-Cre*, *Villin-CreER^{fl}* and *K14-Cre* transgenes were used as controls in all experiments. Mice of the indicated genotype were assigned at random to groups. Mouse studies were performed in a blinded fashion. Unless otherwise indicated, mice were analysed at 3 weeks of age. Groups included male and female animals.

Targeting of the *Mkl1* gene in zygotes from RIPK1^{IEC-KO} mice. Fertilized oocytes obtained from breedings of *K14-Cre*, *Ripk1^{fl/fl}* males with *Ripk1^{fl/fl}* females were microinjected with *Mkl1* short guiding (sgRNA) and *Cas9* mRNA. sgRNA and truncated sgRNA were prepared by *in vitro* transcription of T7-promoter and sgRNA targeting sequence containing PCR products. These sgRNA templates were generated using a long sgRNA forward primer containing the T7 promoter (5'-TTAATACGA CTCACTATAGG-3') used for *in vitro* transcription, 20 bp sgRNA (5'-CGTCTAGG AAACCGTGTGCA-3') or 18 bp sgRNA_TRUNC³⁹ (5'-TCTAGGAACCGTGTG CA-3') targeting sequence and 20 bp homology to the px330 template (5'-GTTTGA GAGCTAGAAATAGC-3'; Zhang laboratory, Addgene plasmid 42230). The forward primer for MLKL sgRNA is 5'-TTAATACGACTCACTATAGGCGTCTAGGAA ACGGTGTGACGTTTATAGAGCTAGAAATAGC-3' and the forward primer for MLKL sgRNA_TRUNC is 5'-TTAATACGACTCACTATAGGCTAGGAAACCGTGTGACGTTTATAGAGCTAGAAATAGC-3'. The long forward primers were used together with sgRNA_rev (5'-AAAAAGCAGCGACTCGGTGCC-3') to amplify the chimaeric sgRNA template from px330. The resulting 121 bp or 119 bp PCR product (MLKL sgRNA or MLKL sgRNA_TRUNC) was used for *in vitro* transcription using the T7 High Yield *in vitro* transcription kit (NEB) and sgRNA was purified using RNA isolation columns (Macherey Nagel). Fertilized oocytes were injected at 0.5 days post-coitum (dpc) with 100 ng μ l⁻¹ *Cas9* mRNA (TriLink) together with 50 ng μ l⁻¹ sgRNA and the surviving two-cell-stage embryos were transferred the next day to foster mothers. Progeny was genotyped using the following primers: typing_fwd, 5'-GTCTGACAGCGTGGAGGTAT-3'; typing_rev, 5'-CCAGACGT CTCTCAGCTTC-3', and the T7 endonuclease I assay. Briefly, PCR product was boiled for 10 min at 98 °C and annealed by slowly cooling down to room temperature. The reaction was subsequently incubated with T7 endonuclease I (NEB) and analysed on a 2% agarose gel. Appearance of additional bands indicated mutations at the *Mkl1* locus. Additionally the PCR product was subjected to *Apa*I restriction (NEB) with a lack of cleavage indicating the presence of a mutation. Mutations in the *Mkl1* locus were identified by sequencing the PCR product (GATC-Biotech).

IEC isolation and immunoblotting. IECs were isolated by sequential incubation of intestinal tissue in 1 mM dithiothreitol (DTT) and 1.5 mM EDTA solutions as described previously⁴⁰. Cell lysates from IECs and keratinocytes were prepared as described^{41,42}. Lysis buffer was supplemented with protease and phosphatase inhibitor tablets (Roche). Cell lysates were separated on SDS-PAGE and transferred to PVDF membranes (IPVH0010, Millipore). Membranes were probed with primary antibodies against the following proteins: RIPK1 (610459, BD Biosciences), RIPK3 (ADI-905-242-100), cIAP1 (ALX-803-335-C100, Enzo), IkB α (sc-371), TRAF2 (sc-876),

TRAF3 (sc-949), TRADD (sc-7868), p65 (sc-372), c-Rel (sc-71), HDAC1 (sc-7872), β -actin (sc-1616, SantaCruz), phospho-p65 (3033), JNK (9252), RelB (4922), phospho-p38 (9211), p38 (8690), phospho-ERK (9101), ERK (9102, Cell Signaling), phospho-JNK (44-682G, Invitrogen), p100/52 (NR1495), p105/50 (NR1157, NCI BRB), α -tubulin (T6074, Sigma), TRAF6 (597, MBL), c-FLIP (AG-208-0005-C100, Adipogen), followed by secondary HRP-coupled antibodies (GE Healthcare and Jackson ImmuneResearch) and developed with chemiluminescent detection substrate (GE Healthcare and Thermo Scientific).

Isolation of lamina propria cells and flow cytometry. Colon and small intestine lamina propria cells were isolated using a modified version of a previously described protocol⁴³. In brief, after removal of Peyer's patches, small intestine and colon tissues were incubated at 37 °C in HBSS containing 4% FCS, 10 mM HEPES and 5 mM EDTA. The remaining tissue was cut into small pieces and digested in HBSS containing 4% FCS, 10 mM HEPES, Dispase II (0.15 mg ml⁻¹; Roche), Collagenase D (0.4 mg ml⁻¹; Roche) and DNase I (0.5 mg ml⁻¹; Sigma-Aldrich). The isolated cells were purified by Percoll gradient centrifugation (GE Healthcare Life Sciences). Single-cell suspensions were preincubated with CD16/CD32 antibody (BD Biosciences) for Fc-receptor blocking and subsequently stained with the following fluorescently labelled antibodies: CD3e (145-2C11), CD11b (M1/70), CD45.2 (104), Ly6G (1A8), B220 (RA3-6B2), F4/80 (BM8) (BD Biosciences or eBioscience). Experiments were acquired on a BD FACS Canto I (BD Biosciences) interfaced to FACSDiva software (BD), and analysed with FlowJo software (Tree Star).

Histology. Intestinal tissues were fixed in 4% paraformaldehyde, skin sections in 10% formalin and embedded in paraffin and cut in 3–5 μ m sections. Paraffin sections were rehydrated and heat-induced antigen retrieval was performed in citrate buffer, TRIS buffer or by proteinase K treatment. Primary antibodies for immunohistochemistry were anti-CD45 (550566, eBioscience), anti-Gr-1 (551459, BD Biosciences) and MCAT1GGA, Serotec, anti-F4/80 (clone A3-1, homemade), anti-B220 (clone RA3 6B2, homemade), anti-CD3 (ab5690, Abcam), anti-active caspase-3 (9661, Cell signalling and AF835, R&D Systems), anti-Ki67 (M724901, Dako), anti-human lysozyme (A0099, Dako). Biotinylated secondary antibodies were purchased from Perkin Elmer and Dako. Stainings were visualized with ABC Kit Vectastain Elite (Vector Laboratories) or Streptavidin-HRP (Millipore) and DAB substrate (DAKO and Vector Laboratories). Incubation times with DAB substrate were equal for all samples. Periodic acid–Schiff (PAS) reaction was performed according to standard protocols. Endogenous alkaline phosphatase activity was visualized using Vector Red Alkaline Phosphatase Substrate Kit according to the manufacturer's instructions (SK-5100, Vector Laboratories). Immunostainings on skin sections were performed as previously described⁴². Gr-1 staining was performed on cryo-sections. For assessment of intestinal pathology, H&E-stained intestinal sections were subjected blindly to a semiquantitative composite histological pathology scoring system as described previously⁴⁴. Microscopic quantification of epidermal thickness was performed by measurement of epidermal thickness in four different back skin areas for each mouse. In each field, four measurements were performed. The percentage of the inflamed area was determined by measuring the cumulative number of the inflamed areas in relation to the total area of one section from back skin of each mouse. The number of CC3⁺ and CC3⁻ dying cells was determined on the same skin section by staining with anti-CC3 antibodies and counterstaining with H&E. Dying CC3⁻ keratinocytes were identified by their pyknotic nuclei and eosinophilic cytoplasm.

Near native imaging. Sections for imaging of mCherry at near native conditions were prepared as described⁴⁵. Briefly, the intestine was dissected, thoroughly rinsed and fixed in 4% PFA for 20 min at room temperature. Tissue was embedded in 4% low melting agarose and sectioned with a vibrating blade microtome (Leica) at 150 μ m. Permeabilization and staining were performed in PBS supplemented with 1% (wt/vol) BSA, 1% (vol/vol) dimethylsulphoxide (DMSO) and 2% (vol/vol) Triton X-100. Paneth cells were visualized with anti-lysozyme antibody and goat anti-rabbit IgG Alexa-488 (Molecular Probes, A11008). Images of fluorescent stainings were acquired with a Zeiss Meta 510 confocal laser-scanning microscope.

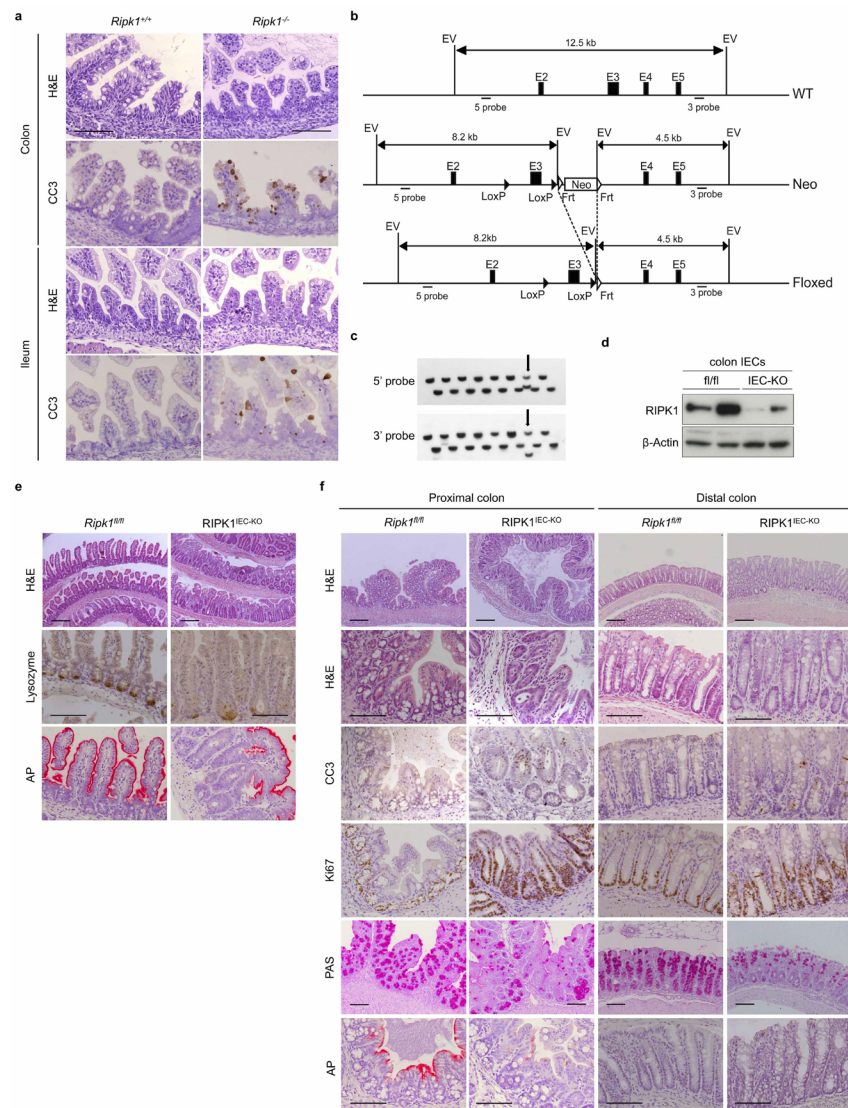
Isolation and culture of primary murine keratinocytes. Isolation and culture of primary murine keratinocytes was performed as described previously⁴⁶.

Isolation and culture of intestinal organoids. Small intestinal crypts were isolated and grown to organoids as described previously⁴⁷. Deletion of RIPK1 in organoid cultures from RIPK1^{tm/IEC-KO} mice was induced by addition of 100 nM 4-OH-tamoxifen (4-OHT) to the culture medium for 20–24 h. Cell death of organoid cultures was determined by quantification of propidium iodide (PI)-positive cells by flow cytometry acquired on a FACSCalibur, BD. For qRT-PCR analysis organoids were harvested 36 h after 4-OHT removal. For each genotype, organoids from two different mice were enrolled, seeded out in quadruplicates and processed independently.

qRT-PCR. Total RNA was extracted with Trizol Reagent (Life Technologies) and RNeasy Columns (Qiagen) and cDNA was prepared with Superscript III cDNA-synthesis Kit (Life Technologies). qRT-PCR was performed with TaqMan probes (Life Technologies) with TATA-box-binding protein as reference gene for intestinal

RESEARCH LETTER

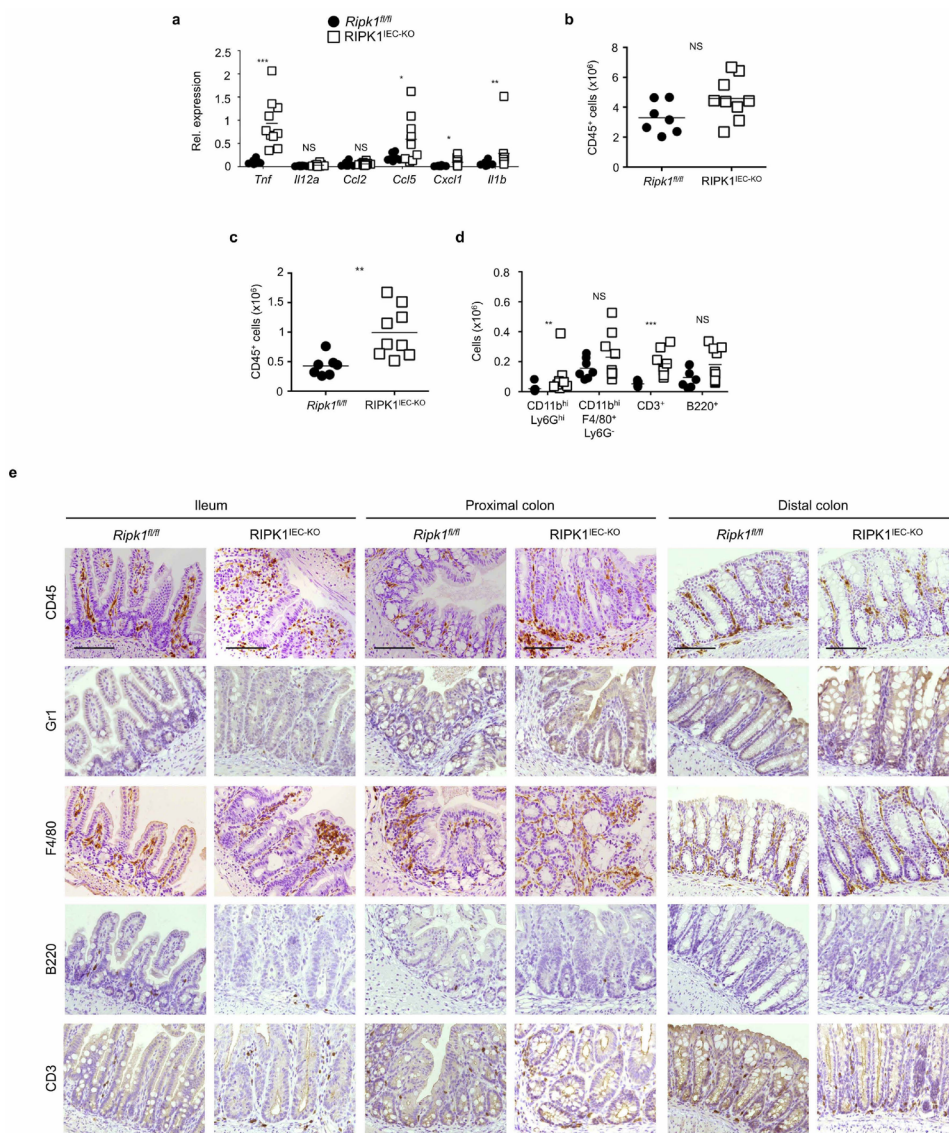
- samples and HRPT for skin tissue. Data were analysed according to the ACT method. Primer sequences are available upon request.
- Statistics.** Data shown in column graphs represent the mean \pm s.d. or \pm s.e.m., as indicated in the figure legends. To determine the group size necessary for adequate statistical power, power analysis was performed using preliminary data sets. When data fulfilled the criteria for Gaussian distribution, unpaired Student's *t*-tests were performed; otherwise the nonparametric Mann-Whitney test was chosen. For the keratinocyte viability assay, a paired Student's *t*-test was performed. **P* \leq 0.05, ***P* \leq 0.01, ****P* \leq 0.005. Statistical analysis was performed with Prism6, GraphPad or Excel, Microsoft software.
29. Polykratis, A. *et al.* Cutting edge: RIPK1 kinase inactive mice are viable and protected from TNF-induced necroptosis *in vivo*. *J. Immunol.* <http://dx.doi.org/10.4049/jimmunol.1400590> (2014).
 30. Mc Guire, C. *et al.* Oligodendrocyte-specific FADD deletion protects mice from autoimmune-mediated demyelination. *J. Immunol.* **185**, 7646–7653 (2010).
 31. Rodríguez, C. I. *et al.* High-efficiency deleter mice show that FLPe is an alternative to Cre-loxP. *Nature Genet.* **25**, 139–140 (2000).
 32. Schwenk, F., Baron, U. & Rajewsky, K. A cre-transgenic mouse strain for the ubiquitous deletion of loxP-flanked gene segments including deletion in germ cells. *Nucleic Acids Res.* **23**, 5080–5081 (1995).
 33. Madison, B. B. *et al.* Cis elements of the villin gene control expression in restricted domains of the vertical (crypt) and horizontal (duodenum, cecum) axes of the intestine. *J. Biol. Chem.* **277**, 33275–33283 (2002).
 34. El Marjou, F. *et al.* Tissue-specific and inducible Cre-mediated recombination in the gut epithelium. *Genesis* **39**, 186–193 (2004).
 35. Hafner, M. *et al.* Keratin 14 Cre transgenic mice authenticate keratin 14 as an oocyte-expressed protein. *Genesis* **38**, 176–181 (2004).
 36. Pfeffer, K. *et al.* Mice deficient for the 55 kd tumor necrosis factor receptor are resistant to endotoxic shock, yet succumb to *L. monocytogenes* infection. *Cell* **73**, 457–467 (1993).
 37. Adachi, O. *et al.* Targeted disruption of the *MyD88* gene results in loss of IL-1- and IL-18-mediated function. *Immunity* **9**, 143–150 (1998).
 38. Newton, K., Sun, X. & Dixit, V. M. Kinase RIP3 is dispensable for normal NF- κ Bs, signaling by the B-cell and T-cell receptors, tumor necrosis factor receptor 1, and Toll-like receptors 2 and 4. *Mol. Cell. Biol.* **24**, 1464–1469 (2004).
 39. Fu, Y., Sander, J. D., Reyon, D., Cascio, V. M. & Joung, J. K. Improving CRISPR-Cas nuclease specificity using truncated guide RNAs. *Nature Biotechnol.* **32**, 279–284 (2014).
 40. Ukena, S. N. *et al.* Probiotic *Escherichia coli* Nissle 1917 inhibits leaky gut by enhancing mucosal integrity. *PLoS ONE* **2**, e1308 (2007).
 41. Schmidt-Suppran, M. *et al.* NEMO/IKK γ -deficient mice model incontinentia pigmenti. *Mol. Cell* **5**, 981–992 (2000).
 42. Kumari, S. *et al.* Tumor necrosis factor receptor signaling in keratinocytes triggers interleukin-24-dependent psoriasis-like skin inflammation in mice. *Immunity* **39**, 899–911 (2013).
 43. Klose, C. S. *et al.* A T-bet gradient controls the fate and function of CCR6⁺ ROR γ ⁺ innate lymphoid cells. *Nature* **494**, 261–265 (2013).
 44. Adolph, T. E. *et al.* Paneth cells as a site of origin for intestinal inflammation. *Nature* **503**, 272–276 (2013).
 45. Snippert, H. J., Schepers, A. G., Delconte, G., Siersema, P. D. & Clevers, H. Slide preparation for single-cell-resolution imaging of fluorescent proteins in their three-dimensional near-native environment. *Nature Protocols* **6**, 1221–1228 (2011).
 46. Tscharrntke, M. *et al.* Impaired epidermal wound healing *in vivo* upon inhibition or deletion of Rac1. *J. Cell Sci.* **120**, 1480–1490 (2007).
 47. Sato, T. *et al.* Single Lgr5 stem cells build crypt-villus structures *in vitro* without a mesenchymal niche. *Nature* **459**, 262–265 (2009).



Extended Data Figure 1 | Intestinal pathology in *Ripk1*^{-/-} and *RIPK1*^{IEC-KO} mice. **a**, Representative images of colonic and ileal sections from newborn *Ripk1*^{+/+} and *Ripk1*^{-/-} mice stained with H&E or immunostained for CC3. **b**, Targeting strategy for the generation of mice with *loxP*-flanked (floxed (fl)) *Ripk1* alleles. Exon 3 of the *Ripk1* gene was flanked with *loxP* sites and an FRT-flanked neomycin (Neo) selectable cassette was introduced after the 3' *loxP* site. The Neo cassette was excised by crossing the *Ripk1*^{neoFloxed} mice with Flp-deleter mice. **c**, Representative Southern blots depicting the identification of correctly targeted embryonic stem (ES) cell clones by using

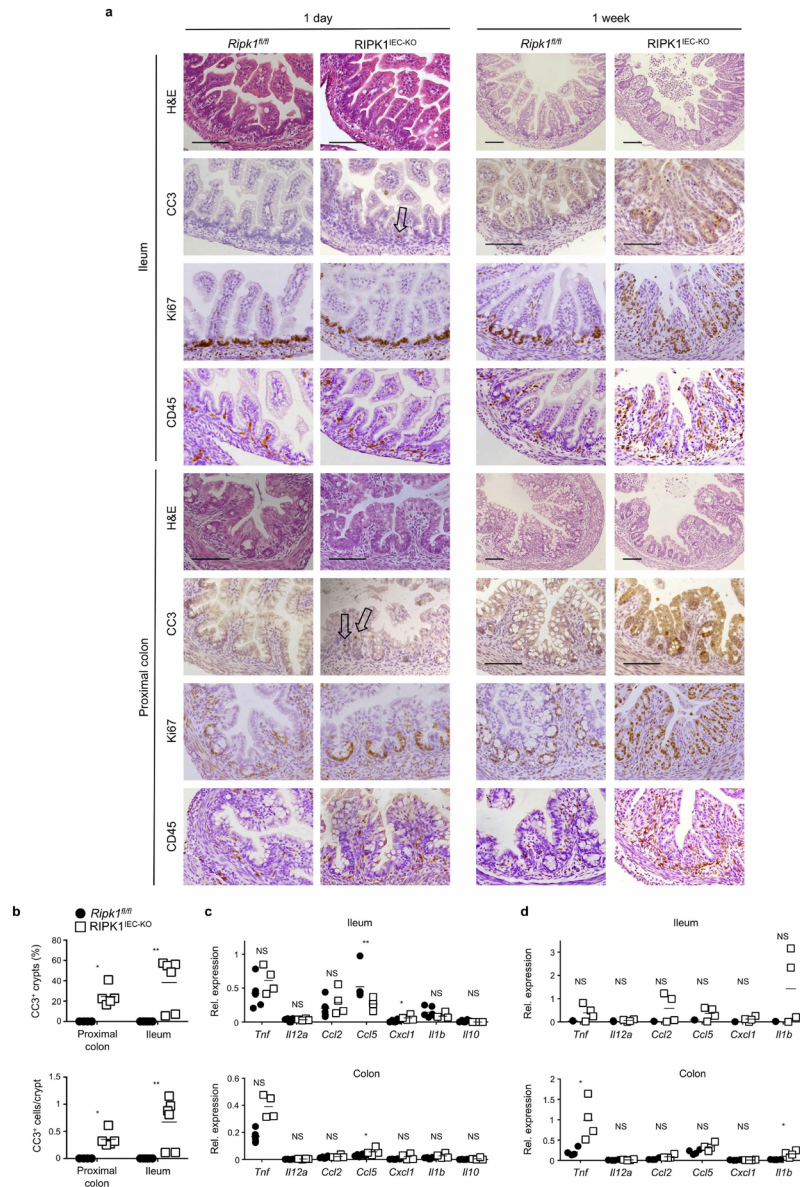
5' and 3' external probes. Arrows indicate a correctly targeted ES cell clone. Screening for the *loxP* site in intron 2 was performed by PCR (data not shown). Double combs allowing loading samples at two levels were used to maximize loading capacity of the gels for screening ES clones in 96-well plates. **d**, Immunoblot of colon IEC protein extracts from *Ripk1*^{fl/fl} and *RIPK1*^{IEC-KO} mice. **e, f**, Representative images of ileal (**e**) or colon (**f**) sections from *Ripk1*^{fl/fl} and *RIPK1*^{IEC-KO} mice stained with H&E, PAS or alkaline phosphatase (AP), or immunostained against lysozyme, CC3 or Ki67. Scale bars, 100 μ m.

RESEARCH LETTER



Extended Data Figure 2 | Mild intestinal inflammation in RIPK1^{IEC-KO} mice. **a**, qRT-PCR analysis of cytokine and chemokine expression in colon tissue from *Ripk1^{fl/fl}* and RIPK1^{IEC-KO} mice. **b-d**, FACS analysis of lamina propria leukocytes in the small intestine (**b**) and colon (**c, d**) of *Ripk1^{fl/fl}* and

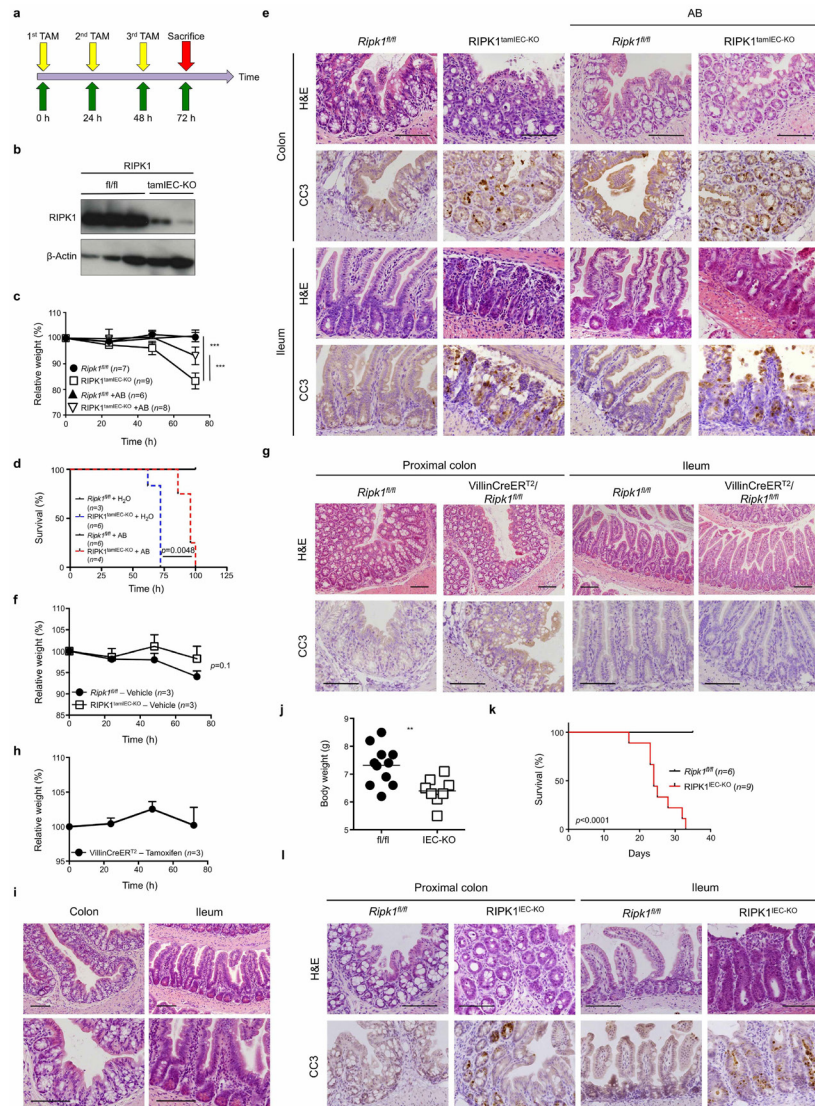
RIPK1^{IEC-KO} mice. **e**, Representative images from intestinal sections from *Ripk1^{fl/fl}* and RIPK1^{IEC-KO} mice immunostained with the indicated antibodies. Scale bars, 100 μ m. * $P \leq 0.05$, ** $P \leq 0.01$, *** $P \leq 0.005$; NS, not significant.



Extended Data Figure 3 | Assessment of intestinal pathology in newborn and 1-week-old RIPK1^{IEC-KO} mice. **a**, Representative images of intestinal sections from *Ripk1^{fl/fl}* and RIPK1^{IEC-KO} mice stained with H&E or immunostained with the indicated antibodies. Arrows indicate sparse CC3⁺ IECs in sections from 1-day-old animals. Scale bars, 100 μm. **b**, Quantification

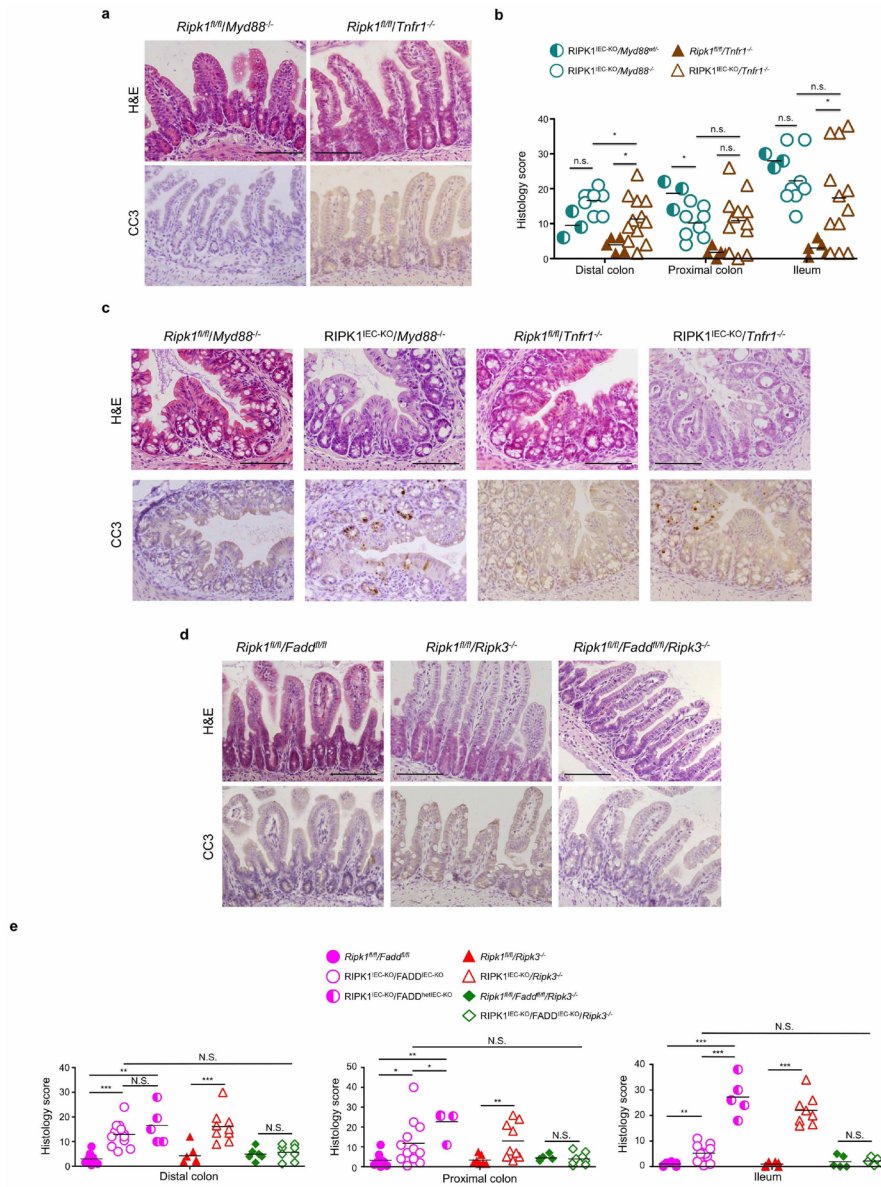
of crypts containing CC3⁺ cells and the number of CC3⁺ cells per crypt in intestinal sections of 1-week-old *Ripk1^{fl/fl}* and RIPK1^{IEC-KO} mice. **c**, **d**, qRT-PCR analysis of cytokine and chemokine expression in small intestinal and colon tissue from 1-day-old (**c**) and 1-week-old (**d**) *Ripk1^{fl/fl}* and RIPK1^{IEC-KO} mice. **p* ≤ 0.05, ***p* ≤ 0.01, ****p* ≤ 0.005; NS, not significant.

RESEARCH LETTER



Extended Data Figure 4 | Antibiotic treatment does not prevent intestinal pathology in $RIPK1^{IEC-KO}$ and $RIPK1^{tamIEC-KO}$ mice. **a**, Experimental outline of tamoxifen injections (TAM; 1 mg, intraperitoneally). **b**, Immunoblot of small intestine IEC protein extracts from tamoxifen-treated $Ripk1^{fl/fl}$ and $RIPK1^{tamIEC-KO}$ mice. **c–e**, Body weight change (**c**), Kaplan–Meier survival curve (**d**) and representative images of H&E- and CC3-stained intestinal sections (**e**) of tamoxifen-treated $Ripk1^{fl/fl}$ and $RIPK1^{tamIEC-KO}$ mice receiving antibiotics (+AB) or normal drinking water starting 4 weeks before tamoxifen administration. **f, g**, Body weight change (**f**) and representative images of

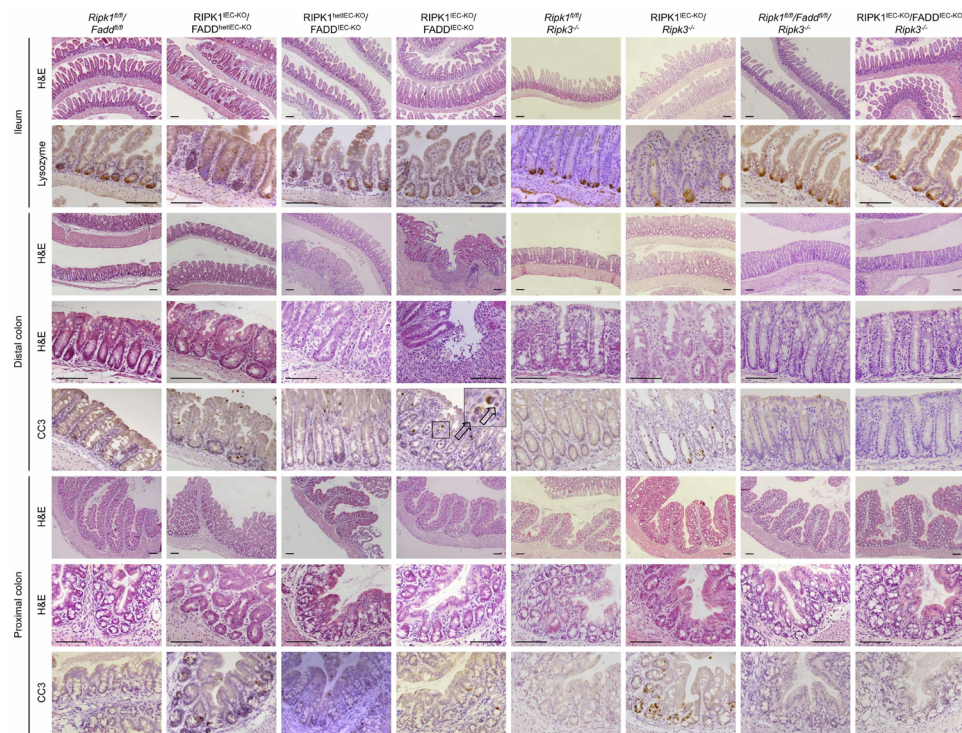
H&E- and CC3-stained intestinal sections (**g**) in vehicle-injected $Ripk1^{fl/fl}$ and $RIPK1^{tamIEC-KO}$ mice. **h, i**, Body weight changes (**h**) and representative images of H&E-stained intestinal sections (**i**) of tamoxifen-injected VillinCreER¹² mice ($n = 3$). **j–l**, Body weight (**j**), Kaplan–Meier survival curve (**k**) and representative images of H&E- and CC3-stained intestinal sections (**l**) of $Ripk1^{fl/fl}$ and $RIPK1^{IEC-KO}$ mice treated with antibiotics from E17.5 to 3 weeks of age. Scale bars, 100 μ m. Error bars represent mean values \pm s.d. * $P \leq 0.05$, ** $P \leq 0.01$, *** $P \leq 0.005$; NS, not significant.



Extended Data Figure 5 | Role of MyD88, TNFR1, FADD and RIPK3 in the intestinal pathology of RIPK1^{IEC-KO} mice. a, Representative images of ileal sections from the indicated mice as controls for the mice shown in Fig. 2a. b, Quantification of histological pathology score of the indicated mice. c, Representative images of H&E- or CC3-stained colon sections from the

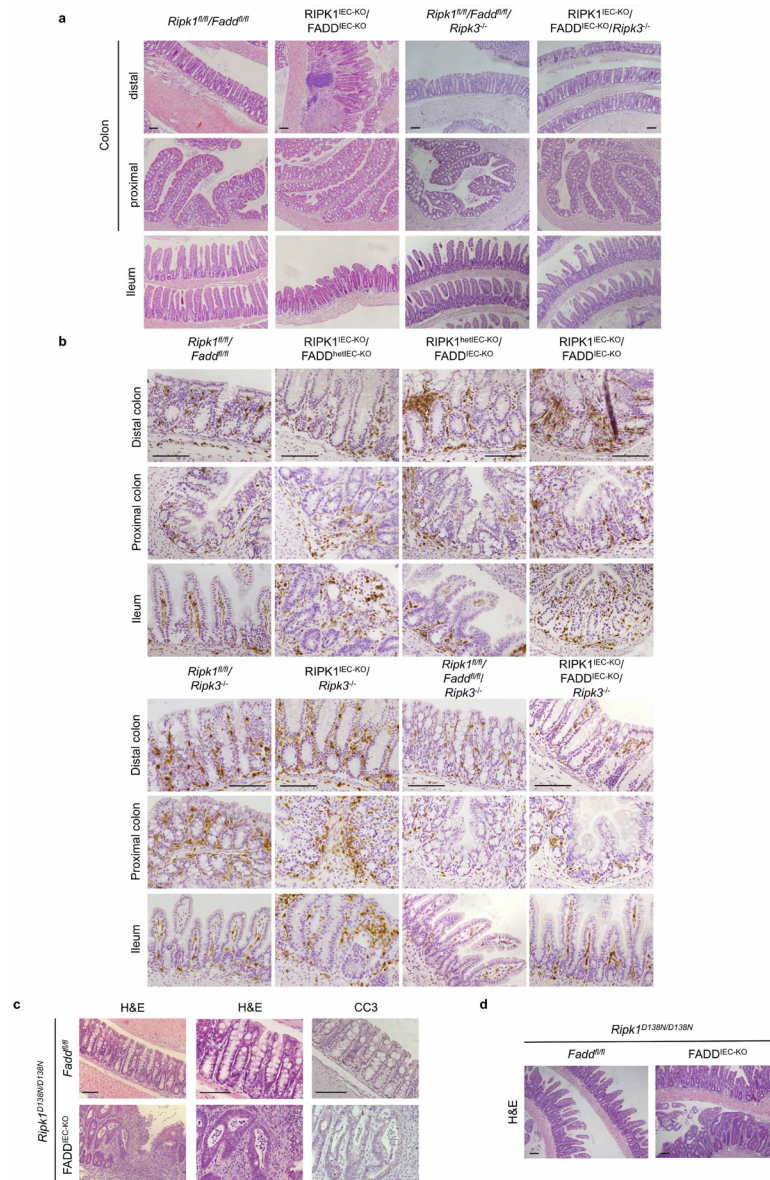
indicated mice. d, Representative images of H&E- or CC3-stained ileal sections from the indicated mice. Scale bars, 100 μ m. e, Quantification of histological pathology score of the indicated mice. * $P \leq 0.05$, ** $P \leq 0.01$, *** $P \leq 0.005$; NS, not significant.

RESEARCH LETTER



Extended Data Figure 6 | Epithelial-specific FADD deficiency reduces IEC apoptosis, ameliorates crypt atrophy but triggers erosive lesions in the colon of RIPK1^{IEC-KO} mice. Representative images of ileal and colonic sections from

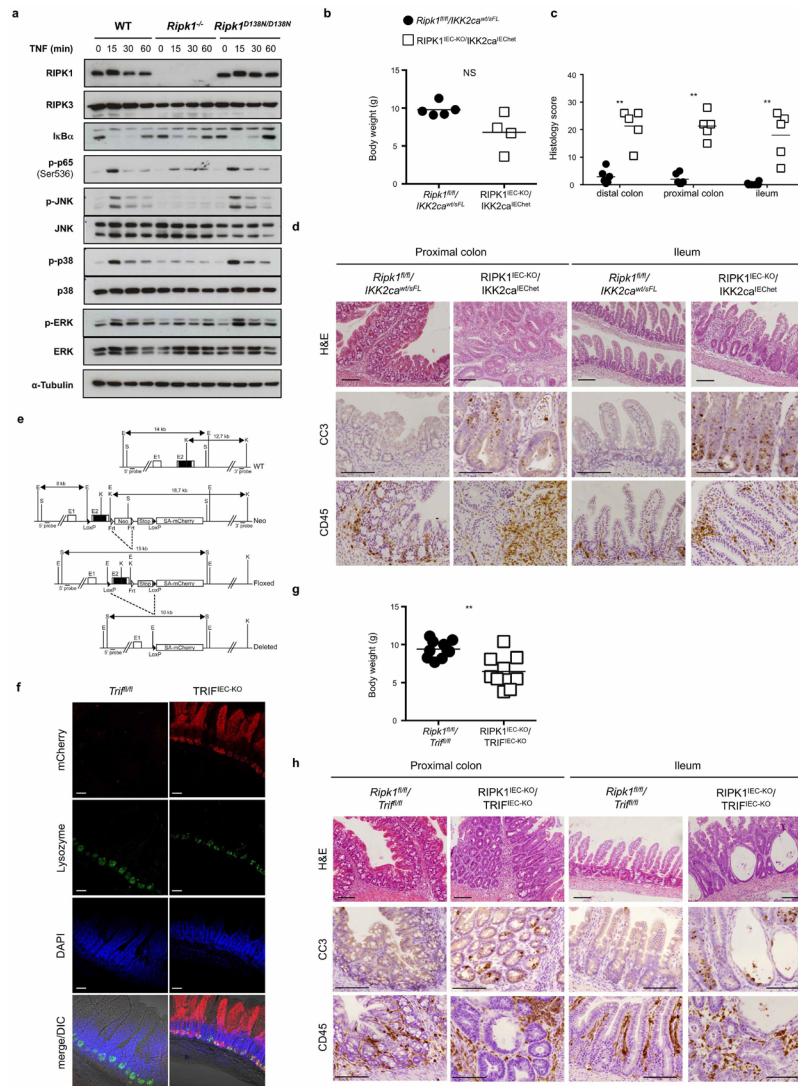
the indicated mice stained with H&E or immunostained against lysozyme or CC3. Scale bars, 100 μ m.



Extended Data Figure 7 | FADD and RIPK3 deficiency restores intestinal homeostasis in *RIPK1^{IEC-KO}* mice and IEC necroptosis in *FADD^{IEC-KO}* mice occurs in the absence of RIPK1 kinase activity. **a, Representative images of H&E-stained colonic and ileal sections of adult mice with the indicated genotypes. **b**, Representative images of colonic and ileal sections of mice with**

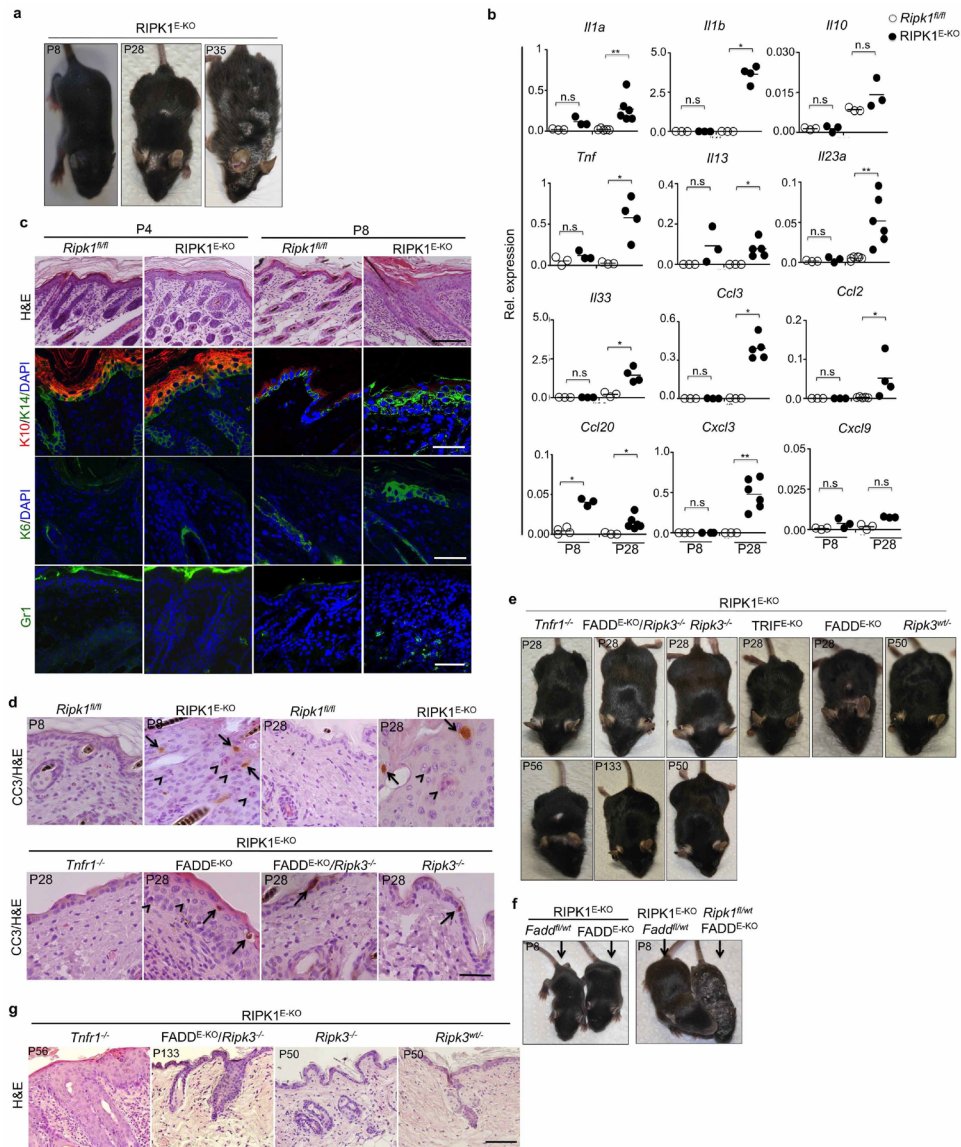
the indicated genotypes immunostained for CD45. **c, d**, Representative images of colonic (**c**) and ileal (**d**) sections of adult *Fadd^{fl/fl}/Ripk1^{D138N/D138N}* and *FADD^{IEC-KO}/Ripk1^{D138N/D138N}* mice stained with H&E or immunostained against CC3. Scale bars, 100 μ m.

RESEARCH LETTER



Extended Data Figure 8 | Assessment of the role of NF- κ B and TRIF signalling in RIPK1^{IEC-KO} mice. **a**, Immunoblot analysis of protein extracts from wild-type (WT), *Ripk1*^{-/-} and *Ripk1*^{D138N/D138N} MEFs after stimulation with 10 ng ml⁻¹ recombinant murine TNF for the indicated time points. Data are representative of five independent experiments. **b–d**, Body weight (**b**), quantification of histological pathology score (**c**) and representative H&E-, CC3- or CD45-stained intestinal sections (**d**) of mice with the indicated genotypes. **e**, Targeting strategy used for the generation of *Trif*^{fl/fl} mice. Exon 2 of the *Trif* gene was flanked with *loxP* sites. FRT-flanked neo and a stop cassette were placed upstream of the 3' *loxP* site. A splice acceptor (SA)-mCherry

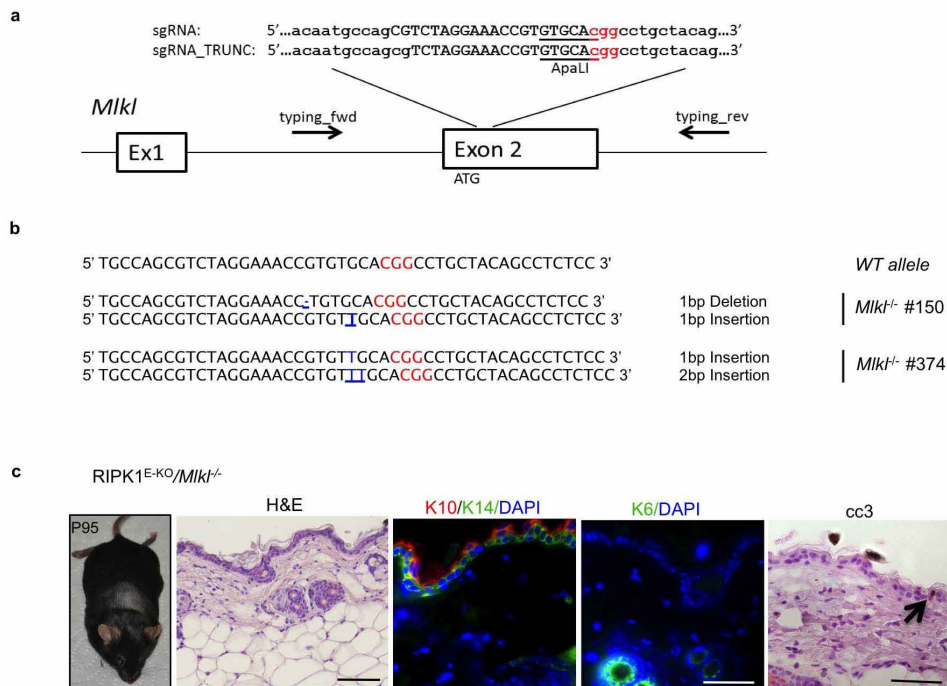
cassette was introduced downstream of the 3' *loxP* site. Cre-mediated recombination removes the *Trif* coding sequences and the stop cassette inducing the expression of mCherry by the *Trif* locus. The FRT-flanked neo was excised by crossing *Trif*^{neoFlxneo} mice with Flp-Deleter mice. **f**, Confocal microscopy images of near native small intestinal sections of *Trif*^{fl/fl} and TRIF^{IEC-KO} mice stained with anti-lysozyme and DAPI. **g**, **h**, Body weight (**g**) and representative images of H&E-, CC3- or CD45-stained intestinal sections (**h**) of the indicated mice. Scale bars, 100 μ m. * $P \leq 0.05$, ** $P \leq 0.01$, *** $P \leq 0.005$; NS, not significant.



Extended Data Figure 9 | Skin inflammation in RIPK1^{E-KO} mice is dependent on RIPK3-mediated necroptosis. **a**, Representative macroscopic images of RIPK1^{E-KO} mice. **b**, qRT-PCR analysis of pro-inflammatory cytokines and chemokines on total skin mRNA from *Ripk1^{fl/fl}* and RIPK1^{E-KO} mice. **c**, **d**, Representative images of skin sections from the indicated mice stained as indicated. In **d**, arrows point to CC3⁺ cells and arrowheads depict

CC3⁺ dying cells identified by their pyknotic nuclei and eosinophilic cytoplasm. Scale bars, 100 μ m in H&E stained; 50 μ m in immunostained sections. **e-g**, Representative macroscopic pictures (**e**, **f**) and H&E-stained skin sections (**g**) of the indicated mice. Scale bars, 100 μ m. * $P \leq 0.05$, ** $P \leq 0.01$, *** $P \leq 0.005$; NS, not significant.

RESEARCH LETTER



Extended Data Figure 10 | CRISPR/Cas9-mediated knockout of MLKL prevents skin inflammation in RIPK1^{E-KO} mice. **a**, Schematic depiction of the *Mkl1* locus. The sequence targeted by the small guide RNAs (sgRNA and truncated TRUNC_sgRNA) is indicated by capital letters. The position of the ATG and the binding sites of the primers used for genotyping and sequencing are indicated. The sgRNAs were designed to target a sequence containing an ApaLI restriction site that is used for RFLP analysis (underlined). The protospacer-adjacent motif (PAM) sequence is depicted in red. **b**, Sequences of the wild-type (WT) *Mkl1* locus and of the targeted *Mkl1* alleles of the two

obtained RIPK1^{E-KO}/*Mkl1*^{-/-} mice. Mouse #150 carries one allele with one base pair (bp) deletion and one allele with one bp insertion. Mouse #374 carries one allele with one bp insertion and one allele with two bp insertions. All mutations cause frameshift and ablate MLKL protein expression. Mouse #150 was obtained using the full-length MLKL-sgRNA and mouse #374 was obtained using the truncated MLKL-sgRNA_TRUNC. **c**, Macroscopic appearance and histological images of skin sections from RIPK1^{E-KO}/*Mkl1*^{-/-} mouse #150 at the age of P95. Scale bars, 100 μ m (H&E); 50 μ m (keratins and CC3).

Erklärung:

Ich versichere, dass ich die von mir vorgelegte Dissertation selbständig angefertigt, die benutzten Quellen und Hilfsmittel vollständig angegeben und die Stellen der Arbeit – einschließlich Tabellen, Karten und Abbildungen –, die anderen Werken im Wortlaut oder Sinn nach entnommen sind, in jedem Einzelfall als Entlehnung kenntlich gemacht habe; dass diese Dissertation noch keiner anderen Fakultät oder Universität zur Prüfung vorgelegen hat; dass sie – abgesehen von unten angegebenen Teilpublikation – noch nicht veröffentlicht worden ist sowie, dass ich eine solche Veröffentlichung vor Abschluss des Promotionsverfahrens nicht vornehmen werde. Die Bestimmungen der Promotionsordnung sind mir bekannt. Die von mir vorgelegte Dissertation ist von Prof. Dr. Manolis Pasparakis betreut worden.

Datum

Marius Volker Dannappel

Curriculum Vitae

Curriculum Vitae



Personal Details

Name: Marius Volker Dannappel
Date of birth: January, 24th 1985
Place of birth: Bergisch Gladbach
Nationality: German
Current address: Dillenburgerstraße 1
51105 Cologne
Phone: +49 175 4457819
Marital status: single
E-Mail: MariusDannappel@googlemail.de
dannappm@uni-koeln.de

Education

Since 11/2011 University of Cologne,
Cologne Excellence Cluster on Cellular Stress
Responses in Aging-Associated Diseases
(CECAD) & Institute for Genetics

Graduate student (PhD)
in the lab of Prof. Dr. Manolis Pasparakis

Research focus:
Regulation of cell death and inflammation

10/2009 – 12/2011 University of Cologne, Germany
Biological Science

Major fields of study:
(Mouse-) genetics and neurobiology

Master-thesis:
Super-resolution microscopy (dSTORM) of
proteins in different cell lines (Grade: 1.3)

Degree: Master of Science (Grade: 1.8)

Education (continued)

10/2005 – 08/2009 Germany	University of Applied Science, Rheinbach, Applied Biology Major fields of study: Genetics, immunology, microbiology, clinical research Bachelor-thesis: Influence of haematocrit on variability on the accuracy of Self-Monitoring blood glucose (SMBG) devices (Grade: 1.7) Degree: Bachelor of Science (Grade 2.2)
08/1995 – 06/ 2004	Gymnasium Herkenrath (High School) General Qualification for University Entrance

Work Experience

- Since 11/2011
- University of Cologne, Germany
Cologne Excellence Cluster on Cellular Stress Responses in Aging-Associated Diseases (CECAD) & Institute for Genetics
- Graduate student
- Mouse colony management
 - Handling of mice, intraperitoneal injections, *in vivo* colon endoscopy of mice, dissection of mouse tissues
 - Histology, tissue sectioning, immunofluorescence (IF) and immunohistochemistry (IHC) stainings
 - FACS
 - Molecular biology, e.g. DNA and RNA extraction, PCR, qRT-PCR, protein extraction, western blot
 - Cell culture of mammalian cells, small intestinal organoid culture, transfection, cell death assays
 - Cloning
 - Experimental design and organisation
 - Student teaching
- 05/2011 – 11/2011
- Forschungszentrum Jülich, Germany
- Master student
- Developing IF staining protocols suitable for super-resolution imaging
 - Antibody conjugation
 - Establishment and optimisation of dSTORM – direct stochastic optical reconstruction microscopy in the Forschungszentrum Jülich
- 10/2008 – 01/2009
(ikfe),
- Instiut für klinische Forschung und Entwicklung
Mainz, Germany
(now clinlogix)
- Bachelor student
- Study design and conduction
 - Assisting supervising CRA – Clinical Research Associate
 - Assistance in clinical monitoring

Publication

- 08/2014 **Dannappel M.***, Vlantis K.*, Kumari S.*, Polykratis A.*, Kim C., Wachsmuth L., Eftychi C., Lin J., Corona T., Hermance N., Zelic M., Kirsch P., Basic M., Bleich A., Kelliher M. & Pasparakis M., (2014) RIPK1 maintains epithelial homeostasis by inhibiting apoptosis and necroptosis, **Nature** 513(7516):90-4
*shared first authorship

Poster

- 10/2014 RIPK1 controls intestinal homeostasis by preventing epithelial cell apoptosis and necroptosis
Dannappel M., Vlantis K., Polykratis A., Kim C., Corona T., Hermance N., Zelic M., Kirsch P., Basic M., Bleich A., Kelliher M. & Pasparakis M., (2014) Keystone Symposia Conference – Cell Death Signaling in Cancer and the Immune System Guarua – Sao Paulo, Brasil, Poster 1049
- 05/2009 Laboruntersuchung zum Einfluss des Hämatokrit auf die Ergebnisse von Blutzuckermessgeräten zur Patientenselbsttestung;
Musholt P.B., **Dannappel M.**, Schneider M., Borig J., Forst T., Pfützner A., (2009) Diabetologie & Stoffwechsel 4:S33-34, Georg Thieme Verlag KG Stuttgart, ISSN 1861-9002, Poster 90

Extra qualifications & seminars

03/2012	Institute seminar in the Forschungszentrum Jülich “(d)STORM super-resolution microscopy on tubulin fibers and membrane proteins”
11/2008	Attended seminar “Klinische Prüfung nach AMG and GCP”; ikfe, Mainz, Germany
Summer semester 2008	Attended seminars “Applied Clinical Research, Good Clinical Practise”
Summer semester 2007	Attended seminars “Qualitätssicherung in der Analytik (GLP – Good Laboratory Practise)” (Grade: 2.0)

Extra curricular activities

2001 – 2008	Group Leader in a youth organisation (KJG – Katholische Junge Gemeinde Herkenrath)
	fund raising, organisation and realization of leisure time excursions and weekends

Languages and abilities

Languages:	German (Mother tongue) English, fluent in spoken and written French, basics
Computer applications:	Microsoft Office Adobe Photoshop Prism Graph Pad
Interests:	Football, Jogging, Travel, Poker, Reading